NNT : 2024AIXM0075

THÈSE DE DOCTORAT

Soutenue à Aix-Marseille Université
Le 22 mars 2024 par

Ousmane DAO

Étude de l'interaction entre l'état énergétique cellulaire et le stockage du carbone chez la microalgue *Chlamydomonas reinhardtii*

Discipline
Biologie-Santé

Spécialité
Biologie végétale

École doctorale
ED62- SCIENCES DE LA VIE ET DE LA SANTE

Laboratoire
UMR 7265 – Institute de Biosciences et Biotechnologies d'Aix-Marseille (BIAM)

Composition du jury

Matteo Ballottari Université de Verona	Rapporteur
Gilles Curien CEA de Grenoble	Rapporteur
Pierre Crozet IBPC, Sorbonne Université	Examinateur
Gilles Peltier CEA de Cadarache, BIAM, AMU	Examinateur
Stefano Caffarri BIAM, AMU	Président du jury
Yonghua Li-Beisson CEA de Cadarache, BIAM, AMU	Directrice de thèse
Hélène Launay BIP, CNRS, AMU	Invitée
Jean François Sassi CEA de Cadarache	Invité

Affidavit

Je soussigné, Ousmane DAO, déclare par la présente que le travail présenté dans ce manuscrit est mon propre travail, réalisé sous la direction scientifique de Yonghua Li-Beisson, dans le respect des principes d'honnêteté, d'intégrité et de responsabilité inhérents à la mission de recherche. Les travaux de recherche et la rédaction de ce manuscrit ont été réalisés dans le respect à la fois de la charte nationale de déontologie des métiers de la recherche et de la charte d'Aix-Marseille Université relative à la lutte contre le plagiat.

Ce travail n'a pas été précédemment soumis en France ou à l'étranger dans une version identique ou similaire à un organisme examinateur.

Fait à Cadarache, le 10 janvier 2024.



Cette œuvre est mise à disposition selon les termes de la Licence Creative Commons Attribution - Pas d'Utilisation Commerciale - Pas de Modification 4.0 International.

Liste de publications et/ou brevets et participation aux conférences

1) Liste des publications et/ou brevet [1] réalisées dans le cadre du projet de thèse :

    1. Ousmane Dao, Saleh Alseekh, Adrien Burlacot, Marie Bertrand, Pascaline Auroy, Phuong-Chi Nguyen, Bertrand Légeret, Anja Krieger-Liszkay, Alisdair R Fernie, Andreas P.M. Weber, Gilles Peltier, Yonghua Li-Beisson (In prep). Role of malate shuttle in photosynthetic acclimation of Chlamydomonas to environmental fluctuations.
    2. Gilles Peltier, Carolyne Stoffel, Justin Findinier, Sai Kiran Madireddi, Ousmane Dao, Virginie Epting, Amelie Morin, Arthur Grossman, Yonghua Li-Beisson, Adrien Burlacot (2024). Alternative electron pathways of photosynthesis power green algal CO2 capture. The plant Cell 10.1093/plcell/koae143
    3. Ousmane Dao, Adrien Burlacot, Marie Bertrand, Pascaline Auroy, Gilles Peltier, Yonghua Li-Beisson (2023). Cyclic and pseudo-cyclic electron pathways play antagonistic roles during nitrogen deficiency in Chlamydomonas reinhardtii. BioRxiv 10.1101/2023.01.18.524499
    4. Adrien Burlacot, Ousmane Dao, Pascaline Auroy, Stéphan Cuiné, Yonghua Li-Beisson, Gilles Peltier (2022). Alternative photosynthesis pathways drive the algal CO2-concentrating mechanism. Nature 10.1038/s41586-022-04662-9
    5. Ousmane Dao, Franziska Kuhnert, Andreas PM Weber, Gilles Peltier, Yonghua Li-Beisson (2021). Physiological functions of malate shuttles in plants and algae. Trends in Plant Science. doi: 10.1016/j.tplants.2021.11.007

2) Participation aux conférences[2] et écoles d'été au cours de la période de thèse :
    1. October 2023 (Oral) – "The crosstalk between Photorespiration and the CO2-concentrating mechanism in microalgae" at the 22nd Congress of French Bioenergetics Group Bédoin-Vaucluse, France.
    2. June 2023 (Oral) – "Deciphering the role of the chloroplast dicarboxylate transporter LCI20 during photorespiration in Chlamydomonas" at the 20th International Conference on the Cell and Molecular Biology of Chlamydomonas organized by Princeton University, New Jersey, USA.
    3. June 2022 (Oral) – "The regulation of photosynthetic electron flow during N starvation in microalgae" at the "Photosynthesis Symposium 2022" organized by SFPHI in Gif sur Yvette, France.
    4. Mai 2022 (Oral) – "The regulation of photosynthetic electron flow during N starvation in microalgae" at the XXVI International School of Pure and

[1] Cette liste comprend les articles publiés, les articles soumis à publication et les articles en préparation ainsi que les livres, chapitres de livre et/ou toutes formes de valorisation des résultats des travaux propres à la discipline du projet de thèse. La référence aux publications doit suivre les règles standards de bibliographie et doit être conforme à la charte des publications d'AMU.

[2] Le terme « conférence » est générique. Il désigne à la fois « conférence », « congrès », « workshop », « colloques », « rencontres nationales et/ou internationales » … etc.

Applied Biophysics on Molecular and Biophysical Bases of Photosynthesis in Venice, Italy.

5. December 2021 (Oral) – "Photosynthetic adaptation to nutrient shortage in microalgae" at the 04th IRN France-Japan Frontiers in Plant Biology - Webinars 2021 on Photosynthesis and metabolism.
6. August 2021 (poster) – "Alternative electron pathways of photosynthesis affect carbon storage during N deprivation in Chlamydomonas" at the 19th International Conference on the Cell and Molecular Biology of Chlamydomonas, France.

Résumé

Les microalgues représentent la moitié de la fixation photosynthétique du CO2 sur terre et sont très prometteuses pour les applications biotechnologiques grâce à leur capacité à accumuler de grandes quantités d'amidon et de triacylglycérols (TAG). Cependant, les fluctuations environnementales telles que la limitation en azote (N) ou CO_2 affectent fortement la photosynthèse, et donc la production de biomasse et de réserves de carbone. Par conséquent, la compréhension des mécanismes moléculaires qui régulent la production et la canalisation de l'énergie photosynthétique vers les réserves de carbone dans un environnement fluctuant chez les microalgues est essentielle pour leur domestication. Dans la première partie de cette thèse, nous avons exploré la régulation de la photosynthèse chez Chlamydomonas, une microalgue verte modèle, en réponse à la privation d'azote (chapitre 1). Le deficit en azote est souvent rencontré dans la nature et conduit à un arrêt de la croissance, à une dinimution de l'efficacité photosynthétique et à un stockage massif de carbone. Les mécanismes par lesquels la photosynthèse est régulée étaient largement inconnus. Nous avons montré que le flux cyclique d'électrons contrôlé par le Proton Gradient Regulator-like 1 (PGRL1) contribue à la diminution de l'efficacité photosynthétique pendant la carence en azote. En l'absence de PGRL1, les cellules présentent une photosynthèse soutenue et une suraccumulation de TAG grâce aux protéines Flavodiiron (FLV). Nous avons donc proposé une stratégie pour améliorer la production de biomasse et de TAG pour des applications biotechnologiques. Dans la deuxième partie de cette thèse, nous avons exploré le rôle de la communication redox inter-organelles via la navette malate dans l'adaptation de Chlamydomonas aux fluctuations environnementales (Chapitres 2 et 3). Nous avons démontré le rôle essentiel du transporteur chloroplastique de malate, Low-CO2 Inducible 20 (LCI20), lors de la fluctuation des sources de carbone (CO_2 et/ou acetate). En mesurant la sécrétion de glycolate et en surveillant la croissance sous différents rapports CO_2/O_2, nous avons découvert que LCI20 joue un rôle dans la photorespiration qui a été récemment sous-estimé chez les microalgues en raison de la présence de mécanismes de concentration de CO_2. Nous discutons de la pertinence physiologique des mécanismes de navette du malate chez les microalgues pendant la colonisation de niches écologiques contrastées.

Mots clés : *Chlamydomonas reinhardtii*, Microalgue, Photosynthèse, Photorespiration, Communications redox, Stockage de carbone, Régulation photosynthétique

Abstract

Microalgae account for half of photosynthetic CO_2 fixation on earth and hold great promise for biotechnological applications thanks to their capacity in accumulating large amount of starch and triacylglycerols (TAGs). However, environmental fluctuations such as nitrogen (N) or CO_2 limitation strongly affect photosynthesis, therefore biomass and carbon reserves production. Therefore, understanding the molecular mechanisms that regulate the production and chanelling of photosynthetic energy to carbon reserves in a fluctuating environment in microalgae is essential for their domestication. In the first part of this thesis, we explored the regulation of photosynthesis in Chlamydomonas, a model green microalga, in response to N starvation (Chapter 1). N scarcity is often encountered in nature and leads to growth arrest, down-regulation of photosynthesis and massive carbon storage. The mechanisms by which photosynthesis is regulated were largely unknown. We have shown that the cyclic electron flow controlled by the Proton Gradient Regulator-like 1 (PGRL1) contributes to the downregulation of photosynthesis during N deficiency. In the absence of PGRL1, cells exhibit sustained photosynthesis and TAG over accumulation thanks to Flavodiiron (FLV) proteins. We therefore proposed a strategy to improve biomass and TAG production for biotechnological applications. In the second part of this thesis, we explored the role of inter-organelle redox communication via the malate shuttle in the adaptation of Chlamydomonas to fluctuations in carbon sources (CO_2 level or acetate) (Chapters 2 and 3). We have demonstrated the essential role of the chloroplastic malate transporter, Low-CO_2 Inducible 20 (LCI20), during the transition from high to low CO_2 and from photoautotrophy to mixotrophy. By measuring glycolate secretion and monitoring growth under different CO_2/O_2 ratios, we discovered that LCI20 plays a role in photorespiration that has recently been underestimated in microalgae due to the presence of active CO_2 concentration mechanisms. We discuss the physiological relevance of malate shuttle mechanisms in microalgae during colonization of contrasting ecological niches.

Keywords: *Chlamydomonas reinhardtii*, Microalgae, Photosynthesis, Photorespiration, Redox communications, Carbon storage, Photosynthetic regulation

Acknowledgements

First of all, my sincere thanks to the members of the jury for agreeing to evaluate this thesis. I would like to thank Stefano Caffarri for accepting to become president of the jury, Matteo Ballottari and Gilles Curien for agreeing to act as repporters for the defense, and all the members of the jury for their critical reading of this manuscript and their judgment on the quality of this thesis. It is a great pleasure to have Pierre Crozet (my former supervisor) as examiners alongside Hélène Launay. I would also like to thank Hélène Launay, Bernard Genty, Andreas Weber, Dimitris Petroutsos, Ben Field, Claire Remacle and Brigitte Gontero for their advice and suggestions throughout this thesis and especially during my two thesis monitoring committees.

During my PhD, I spent most of my time growing microalgae, but in the end, I realized that it was I who was growing. None of what I achieved in those 4-5 years would have been possible without the unconditional support and help of the following people:

Yonghua Li-Beisson, I cannot thank you enough for trusting me to work on your projects and for being the director of this thesis. You were like a mother to me and I couldn't have expected more from you. Your work ethic, style and organization are simply incredible and have been of crucial importance to me. I wish all students to have a director like you. Thank you for the many times we got excited about unconfirmed results. I'm sure that these moments helped to advance our thinking. Thank you for giving me the freedom to explore various subjects and to attempt risky projects that came to nothing. Outside the professional context, I have greatly appreciated your advice on my personal life and career choices. You are undoubtedly a source of inspiration for me as I pursue my career.

Gilles Peltier for co-supervising this work and for all the stimulating discussions about the results. Every time I entered your office, you were open to discussion and willing to help me. One of the most difficult challenges for me during this thesis has been to explain the results to you and to try to interpret them. Thanks for teaching me photosynthesis and helping to extablish new experimental setups.

Stephan Cuiné, Stephanie Blangy, Marie Bertrand and Pascaline Auroy for their support throughout this work. I know I've asked a lot at one time or another, to the point of upsetting you. I sincerely apologize for having taken advantage of your generosity and kindness. You are the building blocks of this thesis so far.

The entire EBMP team, current and former members, for all the project discussions, not only at lab meetings, but also in your offices. It was a great pleasure and a difficult challenge for me to try to explain photosynthesis to you. I had a great time with you outside the lab.

Adrien Burlacot, you were my inspiration when I started this thesis. One of my greatest goals was to come a little closer to your performance and expertise in the field. So, thank you for your contribution and for teaching me the basics of photosynthesis during the time we spent together in the lab. I wish you all the best for your career.

I would like to thank all the people who have supported me in any way, near or far, whose names I may have forgotten to mention. The entire BIAM Institute, the management and other research teams, for the many times I have benefited from your services in sending sampling to collaborators, missions and discussions in general.

Scientific research is not usually carried out by a single person or in a single laboratory. I have had the privilege of collaborating with scientists from other cities and countries. I would like to thank Michael Hippler, Felix Buchert, Adrien Burlacot, Saleh Alseekh, Alisdair R Fernie, Franziska Kuhnert, Andreas Weber and Anja Krieger-Liszkay for their substantial contributions to my various projects. I hope we can continue to collaborate and do science together in the future. As part of these collaborations, I had the great honor of making a 2-month research visit to Andreas Weber's lab in Dusseldurf, where I met some wonderful people (Emin Dülger). I'd also like to thank Anja Liskay for welcoming me into her lab for a week to learn new techniques. I was also lucky enough to have been mentoring some very competent people like Mathieu Webel during his Master 1 internship and Shiyan Zheng during a sabbatical in the EBMP team.

Pursuing a PhD is a question of dedication and passion. I'd like to thank Jean-Denis Faure, Pierre Crozet, Lionel Gissot, Alia Dellagi and Carine Alix for teaching me the fundamentals of plant science during my master's degree, and for giving me a taste for research. Without them, I would have chosen a different professional career and none of this would have happened.

When I arrived in Aix-en-Provence for this PhD, I was alone and had no friends. Then along the way, I met many beautiful people (Abraham, Tim, Jessi, Poutoum etc.) who eventually became brothers and friends of mine. I couldn't imagine my life in Aix without your presence. With you, I've been able to play football (my favorite activity), go to the gym, travel around Europe, have fun and so on. So, thank you for being in my life and I have only good memories of our relationship.

These days at Cadarache were an opportunity to meet the woman of my life. The one who, despite my bad behavior and constant stress, never ceased to devote herself to my services. I could say that you were my BIAM gift (hahaha). Your company has undoubtedly been the remedy for all my stress and has helped me cope with the difficulties encountered during these years. I feel privileged to have a companion like you. I'll never forget the many times you came to pick me up in Cadarche, driving an hour because I'd finished late. I hope that together we'll have many more wonderful experiences and achievements in both our professional and personal lives.

Finally, I dedicate this thesis to my family and in particular to my parents for their moral support, without which I would surely have given up halfway through. Many thanks to my parents for the education they gave me. Being separated from you for 10 years now is still painful and difficult to live with, but it shows me how important it is to belong to a supportive and wonderful family. Despite this distance, you have been involved in every decision I have made over the last ten years. Your advice will stay with me forever, and I'm truly grateful to belong to this family. I look forward to spending more time with you in the future.



Ousmane DAO

Plant biologist
66 Av Gaston Berger 13100 Aix-en-Provence
+33(0)621528454
ousmanedao17@yahoo.fr



Research Experiences

10/2021 – 12/2021

Visiting researcher, Heinrich Heine University, Düsseldorf - Germany
Project: Characterization of chloroplast malate translocators of Chlamydomonas in the team of Prof. Andreas Weber, Plant biochemistry.

10/2019 – present

PhD student in plant biology, Biosciences and Biotechnologies Institute of Aix-Marseille (BIAM), CEA Cadarache - France
Project: Studying the interaction between cellular energy status and carbon storage in the microalga *Chlamydomonas reinhardtii*.
Acquired expertise: Project management, teamwork, molecular biology and biophysics, biochemistry, microalgal cultivation and crossing, lipid analysis, Confocal microscopy.
Achievement: – Isolated and characterized several Chlamydomonas mutants impaired in photorespiration. – Advanced knowledge Insight into malate shuttle mechanism in Chlamydomonas. – Contributed to the discovery of the energy supply network of the algal CO_2 concentrating mechanism published in Nature. – Deciphering the photosynthetic regulators during nitrogen deficiency.
Supervisor: Yonghua LI-BEISSON, Research director at CEA

01/2019 – 06/2019 (Master 2 level)

Research internship, Institute Jean Pierre Bourgin, INRA Versailles - France
Project: Channeling seed oil metabolism for the targeted synthesis of novel oil in *Camelina Sativa* and N*icotiana benthamiana* using a multiplex CRISPR-Cas9.
Acquired expertise: Agroinfiltration of leaves; GoldenBraid cloning; CRISPR-Cas9 design using CRISPOR; CRISPR assembly; Confocal microscopy; PCR.
Achievement: Obtention of Camelina T1 and T2 generation of CRISPR mutants. Ectopic expression of lipid biosynthesis genes in the leaf of *N. Benthamiana* to increase oil accumulation.
Supervisor: Jean-Denis FAURE, professor at Agroparistech INRA

04/2018 – 08/2019 (Master 1 level)

Research internship, Biology and Physico-Chemical Institute (IBPC), CNRS Paris - France
Project: Validation of a controlled protein secretion system (RUSH) in *Chlamydomonas reinhardtii*.
Acquired expertise: Cultivation of Chlamydomonas; Golden Gate Modular cloning; *In silico* design with Serial Cloner and Genome Compiler; PCR, RT-PCR.
Achievement: Building and validation of a synthetic platform for controlling protein secretion in *Chlamydomonas reinhardtii*.
Supervisor: Pierre CROZET, lecturer at Sorbonne University

Education

2019-present: PhD thesis in Plant Biology, Aix-Marseille university, France
2017-2019: Master in Plant Sciences, Agroparistech, Univ-Paris-Saclay, France
2014-2017: Licence in Microbial Biotechnology, University of Oran Ahmed Ben Bella – Oran- Algeria

Publications

1 - Ousmane Dao, Saleh Alseekh, Adrien Burlacot, Marie Bertrand, Pascaline Auroy, Phuong-Chi Nguyen, Bertrand Légeret, Anja Krieger-Liszkay, Alisdair R Fernie, Andreas Weber, Gilles Peltier, Yonghua Li-Beisson (**In prep**). **Role of malate shuttle in photosynthetic adaptation of Chlamydomonas to environmental fluctuations.**

2 - Gilles Peltier, Carolyne Stoffel, Justin Findinier, Sai Kiran Madireddi, **Ousmane Dao**, Virginie Epting, Amelie Morin, Arthur Grossman, Yonghua Li-Beisson, Adrien Burlacot (**2023**). **Alternative electron pathways of photosynthesis power green algal CO2 capture. The plant Cell** 10.1093/plcell/koae143

3 - Lionel Gissot, Florent Fontaine, Zsolt Kelemen, **Ousmane Dao**, Isabelle Bouchez, Carine Deruyffelaere, Michèle Winkler, Anais Da Costa, Fabienne Pierre, Chouaib Meziadi, Jean-Denis Faure, Marine Froissard (**2023**). **E and M SARS-CoV-2 membrane protein expression and enrichment with plant lipid droplets. Biotechnology Journal** 10.1002/biot.202300512

4 - Ousmane Dao, Adrien Burlacot, Marie Bertrand, Pascaline Auroy, Gilles Peltier, Yonghua Li-Beisson (**2023**). **Cyclic and pseudo-cyclic electron pathways play antagonistic roles during nitrogen deficiency in Chlamydomonas reinhardtii**. **BioRxiv** 10.1101/2023.01.18.524499

5 - Adrien Burlacot, **Ousmane Dao**, Pascaline Auroy, Stéphan Cuiné, Yonghua Li-Beisson, Gilles Peltier (**2022**). **Alternative photosynthesis pathways drive the algal CO_2-concentrating mechanism. Nature** 10.1038/s41586-022-04662-9

6 - Ousmane Dao, Franziska Kuhnert, Andreas PM Weber, Gilles Peltier, Yonghua Li-Beisson (**2021**). **Physiological functions of malate shuttles in plants and algae. Trends in Plant Science**. doi: 10.1016/j.tplants.2021.11.007

7 - IGEM TEAM GO Paris-Saclay 2018 - Briand William, **Dao Ousmane**, Garnier Guillaume, Guegan Raphaël, Marta Britany, Maupu Clémence, Miesch Julie, Papadopoulo Kenn, Radoux Arthur, Rojahn Julie, Zhu Yueying, Mahnaz Sabeti-Azad, Céline Aubry, Arnaud Ferré, Sylvie Lautru, Olivier Namy, Phillipe Bouloc and Stéphanie Bury-Moné *et al.*- (**2018**) **Degradation of the anticancer agent Methotrexate from the hospital wastewater**. ***Med Sci (Paris)* 34, 1111–1114**

Oral and poster communications

October 2023 (Oral) – "The crosstalk between Photorespiration and the CO_2-concentrating mechanism in microalgae" at **the 22nd Congress of French Bioenergetics Group** Bédoin-Vaucluse, France.

June 2023 (Oral) – "Deciphering the role of the chloroplast dicarboxylate transporter LCI20 during photorespiration in Chlamydomonas" at **the 20th International Conference on the Cell and Molecular Biology of Chlamydomonas** organized by Princeton University, New Jersey, USA.

June 2022 (Oral) – "The regulation of photosynthetic electron flow during N starvation in microalgae" at the "**Photosynthesis Symposium 2022**" organized by SFPHI in Gif sur Yvette, France.
Mai 2022 (Oral) – "The regulation of photosynthetic electron flow during N starvation in microalgae" at the **XXVI International School of Pure and Applied Biophysics on Molecular and Biophysical Bases of Photosynthesis** in Venice, Italy.
December 2021 (Oral) – "Photosynthetic adaptation to nutrient shortage in microalgae" at the **04th IRN France-Japan Frontiers in Plant Biology** - Webinars 2021 on Photosynthesis and metabolism.
August 2021 (poster) – "Alternative electron pathways of photosynthesis affect carbon storage during N deprivation in Chlamydomonas" at the **19th International Conference on the Cell and Molecular Biology of Chlamydomonas**, France.
October 2018 (Oral) – "IGEM PARIS SACLAY 2018: METHOTREXIT, A heterogeneous cleaning factory" at the **3rd edition of the EUSynBioS Symposium,** France.

Awards

October 2023 – The best oral presentation award «The crosstalk between Photorespiration and the CO_2-concentrating mechanism in microalgae» at the 22nd Congress of French Bioenergetics Group" Bédoin-Vaucluse, France.
August 2021 – The best poster award "Alternative electron pathways of photosynthesis affect carbon storage during N deprivation in Chlamydomonas" at the 19th International Conference on the Cell and Molecular Biology of Chlamydomonas
October 2019 -- CEA international PhD studentship, FRANCE
October 2018 -- Gold medal in the international Genetically Engineered Machine (iGEM 2018) competition in Boston, USA.
June 2017-- Best student award in the Microbial Biotechnology major at the University of Oran Ahmed Ben Bella, Algeria
September **2014** --Winner of the Malian scholarship in Algeria 2014-2017

Outreach activities

2017-2018 Member of the iGEM team GO-Paris-Saclay
2020-present Member of the Malian Young Researchers Association (MYRA)

Table of content

Affidavit **2**

Liste de publications et/ou brevets et participation aux conférences **3**

Résumé **5**

Abstract **6**

Acknowledgements **7**

Curriculum vitæ **9**

Table of content **12**

List of Abbreviations **14**

I. General introduction **16**

1. Microalgae **17**

2. The use of *Chlamydomonas reinhardtii* as a model **17**

3. Photosynthetic energy production and electron management **18**

3.1. Cyclic electron flow (CEF) 20

3.2. Pseudo-cyclic electron flow (PCEF or pseudo-CEF) 21

3.3. Energetic exchanges between chloroplast and mitochondria 22

3.4. Photorespiration in microalgae: an evolutionary remnant or a necessity? 23

3.5. Starch and TAG as energy and carbon sinks 26

4. Physiological functions of malate shuttles in plants and algae (TIPS doi: 10.1016/j.tplants.2021.11.007) **28**

II. Objectives of this PhD thesis **43**

III. Results **46**

Chapter 1: Photosynthetic regulation during phototrophic nitrogen limitation **47**

Foreword 47

Cyclic and pseudo-cyclic electron pathways play antagonistic roles during nitrogen deficiency in *Chlamydomonas reinhardtii* (BioRxiv DOI: 10.1101/2023.01.18.524499) 48

Conclusion 65

Chapter 2: Identification and mapping of mutants potentially involved in energy trafficking **66**

Chapter 3. Role of malate shuttle in photosynthetic adaptation of Chlamydomonas to environmental fluctuations **71**

Foreword 71

Role of malate shuttle in photosynthetic acclimation of Chlamydomonas to environmental fluctuations. (In prep) 72

Conclusion 90

Chapter 4. The energization of the CO_2 concentrating mechanism in *Chlamydomonas reinhardtii* 91

Foreword 91

Alternative photosynthesis pathways drive the algal CO_2-concentrating mechanism. (Nature DOI: 10.1038/s41586-022-04662-9) 92

Conclusion 100

IV. General conclusion and perspectives 101

V. Annex: 106

Annex 1: Alternative electron pathways of photosynthesis power green algal CO2 capture. (The plant Cell 10.1093/plcell/koae143) 107

Annex 2: Supporting information of Chapter 1 139

Annex 3: Supporting information of Chapter 3 148

Annex 4: Supporting information of Chapter 4 152

References 168

List of Abbreviations

AAA: ADP/ATP translocase

ADP: adenosine diphosphate

AOX: Alternative oxidase

ATP: adenosine triphosphate

Chl: Chlorophyll

DNA: Deoxyribonucleic Acid

CBB: Calvin-Benson-Bassham cycle

CCM: CO_2 concentration mechanism

CEF: Cyclic electron flow

Ci: Total dissolved inorganic carbon

CLiP: Chlamydomonas library project

CoA: Coenzyme A

COX: Cytochrome oxidase

CRISPR: Clustered regularly interspaced short palindromic repeats

cyt b6/f: Cytochrome b6/f

DCMU: 3-(3,4-dichlorophenyl)-1,1-dimethylurea

e^-: electron

FLV: Flavodiiron protein

FNR: Ferredoxin NADPH oxydo-reductase

LCI20: Low-CO_2 inducible 20

M: Molar

MDH: Malate dehydrogenase

mETC: Mitochondrial electron transport chain

MIMS: Membrane inlet mass spectrometry

MM: Minimal medium

mol: International system base unit of amount of substance

mt: Mating type

N: Nitrogen

NAD(P)H: Nicotinamide adenine dinucleotide (phosphate) reduced

$NAD(P)^+$: Nicotinamide adenine dinucleotide (phosphate) oxidized

NPQ: Non-photochemical quenching

OAA: oxaloacetate

OMT: Oxoglutarate/malate translocator

PAM: Pulse-amplitude modulated fluorimeter

bp: Base pair

Pc: Plastocyanin

PCR: Polymerase chain reaction

PET: Photosynthetic electron transfer

PGRL1: Proton gradient regulator like 1

PGR5: Proton gradient regulator 5

pmf : Proton motive force

PQ: Plastoquinone

PQH_2: Reduced plastoquinone

PSI: Photosystem I

PSII: Photosystem II

PTOX: plastoquinone terminal oxidase

Q_A: Quinone A of PSII

qE: Energy dependent NPQ

Rubisco: Ribulose-1,5-bisphosphate carboxylase/oxygenase

ROS: Reactive oxygen species

SDS: Sodium dodecyl sulfate

TAP: Tris acetate phosphate medium

TAG: Triacylglycerol

TCA, tricarboxylic acid cycle

WT: Wild type

I. General introduction

1. Microalgae

The increase in atmospheric concentration of carbon dioxide (CO_2), a major component of greenhouse gases, causes serious environmental concern affecting the global carbon cycle and temperature (Wuebbles and Jain, 2001). To reach the goals of the Paris agreement (Ourbak and Tubiana, 2017), i.e. to hold the increase in global average temperature over a year to "well below" 2°C, the replacement of the fossil fuels by renewable energy sources is a key. Biofuels derived from microalgal biomass (known as the third generation biofuel) are renewable and sustainable energies with no net release of CO_2 (Lee and Lavoie, 2013). This makes microalgae a promising tool to address climate change and energy security.

Microalgae are phylogenetically diverse group of microorganisms found in almost all ecosystems. That means, unlike crops often limited to temperate zones and require fresh water, microalgae can be cultivated in all ecological niches all year round without the need for fresh water. Microalgae are autotrophs and require only sun light, CO_2, water and very small amount of minerals for survival and growth. Their photosynthetic performance (solar-to-biomass energy conversion efficiency) is 10-50 times higher than those of land plants (Costa et al., 2000; Melis, 2009), resulting therefore a theoretical higher biomass production per area compared to land plants (Tiwari and Kiran, 2018). Moreover, many species of microalgae possess a natural capacity to synthesize and accumulate triacylglycerols (TAGs, oil) and starch – the precursors for biofuel and bioplastics, respectively. Moreover, this capacity can be further enhanced by adverse environmental situations such as high light (HL), salt, or nutrient deficiency (Hu et al., 2008).

2. The use of *Chlamydomonas reinhardtii* as a model

Chlamydomonas is a genus of unicellular green algae (Chlorophyta) (Falkowski et al., 2004). The biflagellate unicellular alga *Chlamydomonas reinhardtii* was originally developed as a model to study the molecular basis of eukaryotic cellular processes, in particular those that cannot be investigated in yeast, such as photosynthesis, flagellar function and photoreception (Rochaix, 1995; Pröschold et al., 2005; Salomé and Merchant, 2019) and more recently extended to the study of starch, hydrogen production, and lipid metabolism (Siaut et al., 2011; Godaux et al., 2013; Li-Beisson et al., 2015; Du and Benning, 2016). Photosynthetic mutants of Chlamydomonas are viable because this alga can grow heterotrophically with acetate as a sole carbon source. This feature, together with the fact that Chlamydomonas is haploid during vegetative growth and mutant phenotypes can be readily detectable at the first generation have made Chlamydomonas a prime model for functional genomics study of photosynthesis, cell cycle, lipid/starch metabolism and carbon-concentrating mechanisms (CCM) (Fang et al., 2012; Cross and Umen, 2015; Wang et al., 2015).

In addition, its three genomes (nuclear, plastid and mitochondria) have been sequenced, can be transformed and have lately been shown to accept genome editing by CRISPR/Cas9 (Merchant et al., 2007; Gallaher et al., 2017; Crozet et al., 2018; Schroda, 2019; Picariello et al., 2020). Furthermore, a game changing resource i.e. the creation of a large collection of indexed mutant library for Chlamydomonas (the Chlamydomonas library project – CLIP) (Li et al., 2016) have been made available to public. The landscape of research on Chlamydomonas have never seem to be so promising.

Intro

3. Photosynthetic energy production and electron management

During the primary reactions of photosynthesis, light energy is captured by the light harvesting complex (LHCs) associated to the two photosystems (PS) II and I. Light energy transferred to the reaction center of PSII is used to split water into protons, oxygen and electrons. Electrons are then sequentially transferred from PSII to plastoquinone homolog A (Q_A), plastoquinone (PQ), cytochrome *b6/f* complex (Cyt*b6/f*), plastocyanin (Pc) until the acceptor side of PSI where they are used by the ferredoxin (Fd) and ferredoxin $NADP^+$ reductase (FNR) to reduce $NADP^+$ to NADPH (**Fig. I.1**). Along the electron transport chain, protons are translocated from the stroma to the lumen of thylakoid through the operation of a proton pumping Q-cycle by the Cyt*b6/f* complex (Sacksteder et al., 2000; Cramer et al., 2011). This, together with the protons generated at the luminal side from water splitting, forms the proton gradient (ΔpH) that contributes to generate a proton motive force (*pmf*). The *pmf* drives the synthesis of ATP through ATP synthase. The stepwise flux of electrons from the water splitting to the acceptor side of PSI is called "Linear Electron Flow" (LEF), the major powerhouse of photosynthesis. The net result of LEF reaction is the production of O_2, NADPH and ATP.

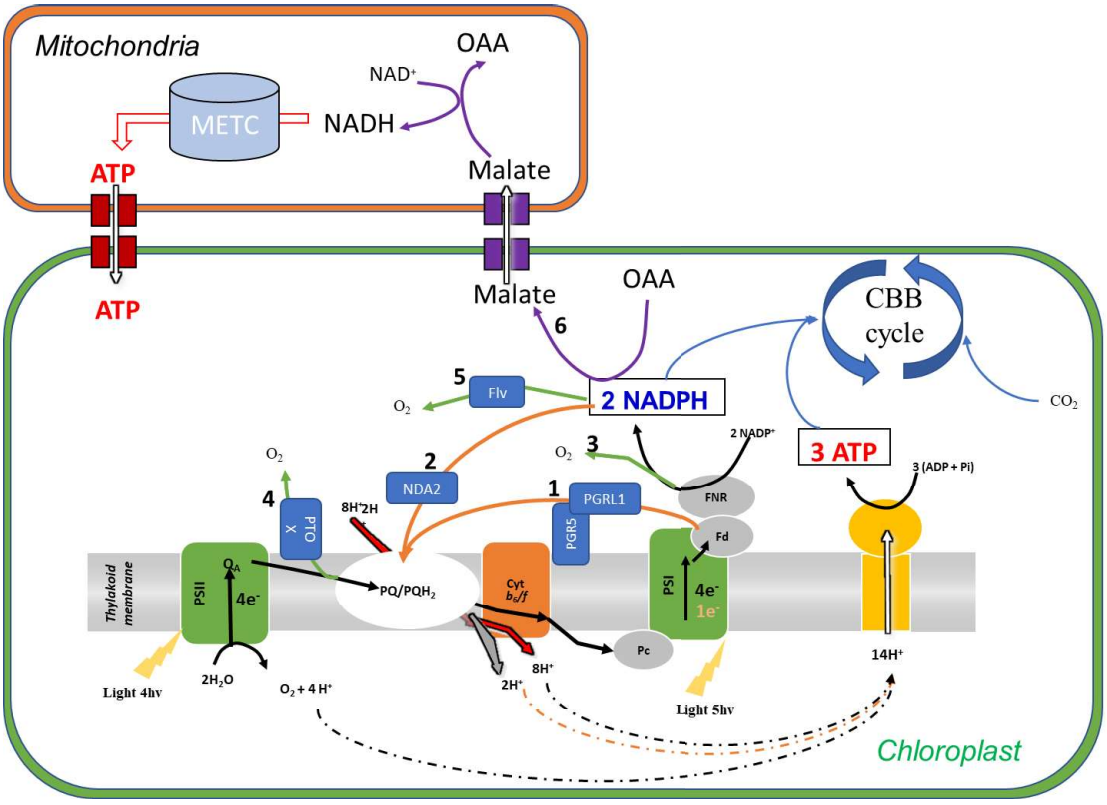

Figure I.1: A schematic representation of photosynthetic linear and alternative electron pathways. Assuming that $14H^+$ are needed to produce 3 ATP and that LEF (dark

arrows) provides only 12 protons from the absorption of 4 quanta by both photosystems, one electron should be recycled through CEF (orange arrows) to translocate two additional H^+ into the lumen. The flux of the recycled electron through PSI requires an additional quantum. The overall $14H^+$ combined with the 4 electrons extracted from two molecules of water give a stoichiometric ratio of 3 ATP/2 NADPH enough to fix one molecule of CO_2 in the CBB. Green arrows correspond to O_2-photoreduction without a net production of NADPH. The chloroplast-mitochondria communication (purple) uses excess NADPH to reduce oxaloacetate (OAA) to malate that is shuttled through malate valve to sustain the mitochondrial electron transport chain (METC) for the synthesis of ATP. The transfer of mitochondrial-derived ATP to chloroplast is likely to operate through a specific but not yet identified ATP translocator.
Abbreviations: ADP, adenosine diphosphate; ATP, adenosine triphosphate; CBB, Calvin Benson Bassham; Fd, ferredoxin; FLV, flavodiiron protein; FNR, ferredoxin-NADP$^+$ reductase; METC, mitochondrial electron transport chain; NAD(P)H, nicotinamide adenine dinucleotide (phosphate); NDA2, NAD(P)H dehydrogenase 2; OAA, oxaloacetate; PC, plastocyanin; PQ/PQH$_2$, plastoquinone/plastoquinol; PTOX, plastoquinone terminal oxidase; PS, photosystem; TCA, tricarboxylic acid cycle; Q_A, quinone A.

ATP and NADPH are universal cellular energy currencies and their ratio is therefore a good indicator of cellular energy status. Theoretically, in one run, LEF produces 2.57 ATP for each 2 NADPH produced (see **Fig. I.1** for detail) (Allen, 2002), which are mostly used to drive the CO_2 fixation through a series of carbon fixation reactions initiated by the rubisco (ribulose 1,5-bisphosphate carboxylase oxygenase) and collectively known as the Calvin Benson Bassham (CBB) cycle. However, ATP/NADPH (2.57/2) produced by the LEF is not sufficient to drive the optimal CO_2 assimilation which requires an ATP/NADPH ratio of 3/2 (Kramer and Evans, 2011). This imbalance is accentuated in natural environment when light, CO_2 or nutrient level fluctuate constantly. For example, under low CO_2 condition, a high level of ATP is required to power the CO_2 concentrating mechanism (CCM) (Burlacot et al., 2022; Burlacot and Peltier, 2023). The imbalance can also be brought about by an over-production of NADPH, e.g. during HL exposure, reductant produced by the photochemical reactions exceeds the utilization capacity of the chloroplast. Excess reductants are potentially harmful because it can lead to photoinhibition, production of reactive oxygen species (ROS) and cell death (Erickson et al., 2015). In addition to the difference in the stoichiometry production and requirement of ATP and NADPH, another issue cells have to manage is that energy production and their usage occur at very different time scales, i.e. photochemical reactions occur at much faster rate (nanosecond-scale) compared to down-stream metabolic reactions (i.e. second- or minute-scale) (Chow, 2003; Neto et al., 2021; Baikie et al., 2023).

Management of the cellular energy level is therefore essential to cell fitness and survival particularly important in a changing environment. This could occur at varying time scales, i.e. short-term or long-term adaptation. Several mechanisms have therefore evolved, which include the chloroplast-located alternative electron pathways, the metabolic interaction with mitochondria, or by modulating sink capacity in terms of starch and fatty acid synthesis (Alric and Johnson, 2017; Burlacot et al., 2019). An overview on short-term electron generation, management and usage is summarized in **Fig. I.1**. Detailed protein components of these pathways will be detailed in below sections.

Intro

3.1. Cyclic electron flow (CEF)

CEF, in contrast to LEF, involves only PSI and recycles electrons from the acceptor side of PSI to cytochrome *b6/f* complex. The cyclic flow of electrons from cytochrome *b6/f* to PSI is coupled to the generation of a *pmf* across thylakoid membranes, which are used by the ATP synthase to produce ATP without net NADPH production, consequently increasing ATP/NADPH ratio. Several pathways of CEF have been characterized in plants and algae: (1) the type I NADPH dehydrogenase complex (NDH)-mediated CEF that uses NADPH as electron donor to reduce the PQ pool. The type I NDH occurs only in cyanobacteria and higher plants but absent in eukaryotic algae (Peltier et al., 2016); (2) the soluble type II NDH (named NDA2), in contrast to the type I NDH which contains several transmembrane domains, is present only in some green algae (e.g. *Chlamydomonas reinhardtii*) and was shown as a NADPH:PQ oxidoreductase able to reduce the PQ pool using electrons from NADPH (Desplats et al., 2009); and (3) the proton gradient regulator 5 (PGR5)/PGR like 1 (PGRL1)-mediated CEF pathway, which is common between plants, algae and cyanobacteria. Both PGR5 and PGRL1 bind to the PSI acceptor side and use the reduced Fd as an electron donor to reduce the PQ pool (DalCorso et al., 2008).

In *Chlamydomonas reinhardtii*, both NDA2 and PGR5/PGRL1 pathways were found to be strongly induced in anaerobic conditions when O_2-photoreduction is limited (Alric, 2014). Importance of the CEF pathway in re-equilibrating ATP/NADPH balance has been further witnessed through the study of *pgrl1* or *pgr5* mutants. For example, the *pgrl1* mutant had lower biomass productivity in fluctuating light, however behaved similarly to WT under steady state, and the authors attributed this to a compensatory mechanism from mitochondria and O_2 photoreduction as supported by immunoblot using antibodies against FLV (Flavodiiron protein) and the use of mitochondria inhibitors (Dang et al., 2014). Another important observation is the HL sensitivity of Chlamydomonas lacking PGR5 suggesting a role of CEF in light energy dissipation (Johnson et al., 2014). Overall, the contribution of CEF to the energy budget of photosynthesis under limiting CO_2 condition was estimated to be ~33% of the photosynthetic electron transfer rate (Lucker and Kramer, 2013). The conditions where the PGR5/PGRL1 pathway is mostly required are likely those when extra protons are needed for either inducing NPQ (qE) or ATP synthesis e.g. HL or low CO_2. Under low CO_2, microalgae induce CCM to accumulate inorganic CO_2 in the pyrenoid near Rubisco. We have recently demonstrated the combined contribution of CEF and pseudo-CEF (see **section 3.2**) to microalgal CCM through fueling the recently discovered inorganic carbon transporters bestrophin under limiting CO_2 condition (Mukherjee et al., 2019; Burlacot et al., 2022). Indeed, the involvement of CEF in photosynthetic control under suboptimal conditions of CO_2 fixation has been pointed out/or suggested in Arabidopsis and Chlamydomonas (Munekage et al., 2002; Dang et al., 2014; Yamamoto and Shikanai, 2019). Taken together, above findings highlight the critical role of CEF in the acclimation of photosynthesis under fluctuating O_2, CO_2 and light availability.

Our recent discoveries of the role of CEF during N deficiency is a new add-on to the list (**Chapter 1** for more information). We have not only shed light on this role of CEF as a key player for downregulating the photosynthetic electron transfer rate during N deficiency but also for a first time discovered that CEF and pseudo-CEF play antagonistic rather than complementary roles under this condition.

3.2. Pseudo-cyclic electron flow (PCEF or pseudo-CEF)

Under conditions where the photosynthetic chain becomes over reduced due to the limitations of the electron acceptor $NADP^+$, electrons arriving at the acceptor side of PSI can be re-routed toward alternative electron acceptors, including molecular O_2, proton and nitric oxide (NO) in Chlamydomonas. Molecular oxygen (O_2) can be used as an electron acceptor when PSI is over reduced (Allen, 1975). Photoreduction of O_2 can occur via two routes, i.e. the non-enzymatic reaction (also known as Mehler reaction) (Mehler, 1951) and the enzymatic reduction of O_2. In the Mehler reaction, the transfer of electrons from PSI acceptor side to O_2 is associated with the generation of superoxide O_2^- that could be converted to H_2O_2 and then to water by the sequential actions of superoxide dismutase (SOD) and catalase (CAT) (Badger et al., 2000). H_2O_2 is cellular messenger and has been shown to play an important role in retrograde signaling or signaling between subcellular compartments (Heyno et al., 2014; Kong et al., 2018).

Several pathways of enzymatic reduction of O_2 are known to occur in the chloroplast. This includes photorespiration mediated by rubisco (Sharkey, 2001; Bauwe et al., 2010; Fernie and Bauwe, 2020), chlororespiration by the plastid terminal oxidase (PTOX) (Peltier and Cournac, 2002) and the reaction catalyzed by FLV (Gerotto et al., 2016; Chaux et al., 2017a). Depending on plants or algal species or the environmental conditions, the contribution of one pathway or another could vary. For example, in C3 plants, the oxygenase activity of rubisco is the major pathway of O_2 photoreduction (Eisenhut et al., 2019). The significance of photorespiration is probably underestimated in green microalgae because of the occurrence of CCM (see **section 3.4** for more details on photorespiration). Chlamydomonas mutants lacking PTOX2, catalyzing the transfer of electrons from the reduced plastoquinone to O_2 producing water, displayed a constitutive reduced state of the plastoquinone pool and were more sensitive to light (Houille-Vernes et al., 2011). In Chlamydomonas, FLV-mediated O_2-photoreduction has also been shown to be a major pathway (Jokel et al., 2015; Chaux et al., 2017a; Saroussi et al., 2019). Homologs of FLV are present in most of the photosynthetic organisms from cyanobacteria to gymnosperm but absent in angiosperm (Yamamoto et al., 2016). FLV significantly contributes to photoprotection (especially during dark-to-light transitions or during acclimation to fluctuating light) by using electrons from ferredoxin to reduce O_2 by doing so relaxing the reducing pressure in the chloroplast meanwhile generating extra proton in the lumen (Gerotto et al., 2016; Chaux et al., 2017a; Saroussi et al., 2019). In Chlamydomonas, under HL, the mutants (*flv*) deficient in FLVs displayed around 30% reduction in the *pmf* and 50% reduction in ΔpH components as compared to the parental WT suggesting a lower acidification of the lumen (Chaux et al., 2017a).

Collectively, the flux of electrons from water splitting in the PSII reaction center to O_2 reduction producing water as final product is known as water-to-water cycle (WWC) also referred as O_2-photoreduction or pseudo-cyclic electron flow (Pseudo-CEF) (Allen, 1975; Allen, 2002). In contrast to CEF that involves only PSI, pseudo-CEF involves both photosystems similar to the LEF. Together with CEF, pseudo-CEF contributes to re-equilibrate ATP/NADPH by providing an alternative electron acceptor thereby allowing the linear electron flow along the photosynthetic chain with ATP generation but without a net synthesis of NADPH. Therefore, CEF and PCEF functionally compensate each other in many conditions by generating extra ATP or H^+ e.g. for CCM or NPQ functioning respectively. However, our recent work revealed an antagonist role between CEF and PCEF during N starvation. We have shown that the CEF constraints the PET rate by activating the photosynthetic control via cytochrome b6f, whereas PCEF promote the PET and favor TAG accumulation (**Chapter 1**).

3.3. Energetic exchanges between chloroplast and mitochondria

Chloroplast and mitochondria are energetic organelles both producing ATP and playing a substantial role in NAD(P)H turnover and O_2 metabolism. Tight coordination of their activities is therefore expected for optimal growth (Raghavendra and Padmasree, 2003; Noguchi and Yoshida, 2008; Van Aken and Whelan, 2012). The energetic exchange between chloroplast and mitochondria could occur at several levels, i.e. NADPH, ATP or intermediates of CBB cycle and through photorespiration. The latter has been well studied in higher plants (Eisenhut et al., 2019), and often considered minimal in algae having a CCM mechanism (Wang et al., 2015). When NADPH production exceeds the consumption by the chloroplast metabolism, to avoid oxidative damage, excess NADPH can also be exported from chloroplast (**Fig. I.1**). For example, Peltier and Thibault (Peltier and Thibault, 1985a) noticed persistent O_2 uptake by mitochondrial respiration in Chlamydomonas under continuous illumination, suggesting that reductant from chloroplast, at least some of it, can be re-routed to drive mitochondrial respiration (O_2 reduction). The occurrence of NAD(P)H trafficking from chloroplast to mitochondria was observed recently by the study of Chlamydomonas mutants defected in PGRL1-mediated CEF (Dang et al., 2014). In the *pgrl1* mutant, inhibition of mitochondrial respiration resulted in an impaired photosynthetic performance under HL and low-carbon condition when the demand for ATP is high. And vice versa, a defect in mitochondrial respiration is also accompanied by an increased rate of CEF (Cardol et al., 2003).

In return, mitochondria can provide ATP to the chloroplast to sustain anabolic reactions. The photoautotrophic growth of Chlamydomonas mutant FUD50, impaired in the chloroplast ATP synthase, could be restored by an additional mutation resulting in a high mitochondrial respiration. Moreover, the photosynthesis of the FUD50su (FUD50 suppressor strain) was sensitive to inhibitors specific to mitochondrial respiration (Lemaire et al., 1988). This observation clearly indicate that mitochondria-derived ATP can compensate the lack of chloroplast ATP synthase, suggesting a flux of ATP from mitochondria to chloroplast but the molecular mechanisms of ATP transport remain unknown.

In parallel, work in the model diatom *Phaeodactylum tricornutum* has shown that the redox exchange [ATP and NAD(P)H] between chloroplast and mitochondria is constitutive and plays a critical role in driving CO_2 fixation (Bailleul et al., 2015). Taken together, current literature support that there occurs an energetic exchange between chloroplast and mitochondria and that this exchange is critical to maintain optimal photosynthesis and CO_2 fixation.

Having said that, cell membranes are not permeable to ATP, $NAD(P)^+$ and NAD(P)H, therefore they are usually transported across the subcellular compartments either directly using specific transporters (known ATP transporters or NAD^+ transporters) (Reiser et al., 2004; Weber and Linka, 2011; van Roermund et al., 2016; Hashida and Kawai-Yamada, 2019), or more often transported as organic compounds such as malate or triose-phosphate through the activity of the malate-oxaloacetate and triose phosphate redox shuttles (Kinoshita et al., 2011; Johnson and Alric, 2013; Zhao et al., 2018; Huang et al., 2023). Despite strong evidence of the occurrence of energy trafficking pathways between the two energetic organelles, thus far, no known molecular players involved in reductant export from chloroplast to mitochondria or in ATP transport from mitochondria to chloroplast are known in algae. Current state of art on the role of malate shuttle and its major components i.e. MDHs and dicarboxylate translocators in plants and algae has been

presented as a review article published in Trends in Plant Science (presented in **section 4**).

Overall, we have recently demonstrated that metabolic interaction between chloroplast and mitochondria are not minor but could play an important role in sustaining CO_2 fixation under steady state condition of photosynthesis (Peltier et al., 2023), where the authors have estimated the contribution of one pathway versus another under contrasting environments (detailed in **Annex 1**).

3.4. Photorespiration in microalgae: an evolutionary remnant or a necessity?

Photorespiration (PR) very likely co-evolved with oxygenic photosynthesis around 3 billion years ago (Fernie and Bauwe, 2020). The CO_2 fixation enzyme rubisco can also react with O_2 producing a harmful metabolite 2-phosphoglycolate (2-PG) and this reaction depends on the stoichiometric ratio of CO_2/O_2 (Fernie and Bauwe, 2020; Bauwe, 2023; Segura Broncano et al., 2023). PR has so far been overlooked in green microalgae having an efficient biophysical CCM that can concentrate up to 1000-fold the atmospheric CO_2 concentration near the catalytic site of rubisco, thereby decreasing its oxygenase activity (Wang et al., 2015). In Chlamydomonas, genes encoding core photorespiratory enzymes i.e. rubisco, phosphoglycolate phosphatase (PGLP), glycolate dehydrogenase (GDH/GYD), glycolate oxidase (GOX), glutamate glyoxylate aminotransferase (GGT), glycine decarboxylase complex (GDC), serine hydroxymethyl transferase (SHMT), serine/alanine glyoxylate aminotransferase (SGAT), hydroxypyruvate reductase (HPR), and glycerate kinase (GLYK) are present in the genome of Chlamydomonas (**Table I.1**) (Merchant et al., 2007; Gallaher et al., 2015).

In the late 80s, Moroney et al. observed that cells grown under high-CO_2 when transferred into air (low-CO_2 level) produced three times more glycolate (with half secreted) compared to cells grown in air (Moroney et al., 1986). Under steady-state air condition, the functioning of CCM might prevent the oxygenation reaction of rubisco whereas during transition from high-CO_2 to air, CCM needs time to be fully activated. Later, Suzuki et al. reported a high-CO_2 requiring Chlamydomonas mutant (designated 18-7F) which is defected in the PGLP catalyzing the conversion of 2-PG to glycolate. Interestingly, at 2% O_2 when PR is suppressed, the photosynthetic performance of air-adapted 18-7F mutant cells was similar to wild-type suggesting that O_2 concentration is key for the high-CO_2 requiring phenotype (Suzuki et al., 1990). Taken together, only rubisco, GDH/GYD, PGLP and HPR1 have been characterized at physiological or molecular level (Suzuki et al., 1990; Mamedov et al., 2001; Nakamura et al., 2011; Aboelmy and Peterhansel, 2014; Shi et al., 2021), the remaining components, subcellular organization of the PR pathway in algae and its physiological function remain hypothetical.

Table 1.1: List of known and putative photorespiratory genes encoded in the genome of Chlamydomonas. Subcellular localizations are based on prediction using PredAlgo unless otherwised precised as Exp: experimental.

Enzyme	Gene ID (V6)	Isoforms	Subcellular localization	Brief description
Rubisco	CreCp.g802313	RBCL	Chloroplast (Exp)	ribulose-bisphosphate carboxylase large subunit (rbcL)

	Cre02.g120100	RBCS1	Chloroplast (Exp)	ribulose-bisphosphate carboxylase small subunit (rbcS)
	Cre02.g120150	RBCS2	Chloroplast (Exp)	ribulose-bisphosphate carboxylase small subunit (rbcS)
PGLP	Cre03.g168700	PGP1	Chloroplast	Phosphoglycolate phosphatase/4-nitrophenylphosphatase
	Cre10.g438100	PGP2	Chloroplast	Phosphoglycolate phosphatase/4-nitrophenylphosphatase
	Cre03.g162601	PGP3	Chloroplast	CDP-diacylglycerol-glycerol-3-phosphate/3-phosphatidyltransferase
GDH	Cre06.g288700	GDH/GYD	Mitochondria	Glycolate dehydrogenase
GYX	Cre03.g171300	GYX1	Peroxisome	Glycolate oxidase
GGT	Cre10.g451950	AAT	Mitochondria	Alanine aminotransferase
	Cre06.g294650	AGT1	Mitochondria/ Peroxisome	Alanine-glyoxylate transaminase
	Cre03.g182800	AGT2	Mitochondria/ Peroxisome	Alanine-glyoxylate transaminase
GDC	Cre12.g534800	GDC-P	Mitochondria	Glycine cleavage system P protein
	Cre06.g253350	GDC-H	Mitochondria	Glycine cleavage system H protein
	Cre03.g193750	GDC-T	Mitochondria	Glycine cleavage system T protein
	Cre18.g749847	DLDH	Mitochondria	Glycine cleavage system L protein, Dihydrolipoyl dehydrogenase
SHMT	Cre16.g664550	SHMT1	Mitochondria	Serine hydroxymethyltransferase
	Cre06.g293950	SHMT2	Mitochondria	Glycine hydroxymethyltransferase / Threonine aldolase
	Cre09.g411900	SHMT3	Mitochondria	Glycine hydroxymethyltransferase / Threonine aldolase
SGAT	Cre01.g005150	SGA1	Mitochondria	Alanine-glyoxylate aminotransferase / Serine-glyoxylate transaminase
HPR	Cre06.g295450	HPR1	Mitochondria (Exp)	Hydroxypyruvate reductase 1
	Cre01.g019100	HPR2	Cytosol	Hydroxypyruvate reductase 2
	Cre02.g087300	HPR3	Cytosol	Hydroxypyruvate reductase 3
	Cre07.g324550	HPR4/LDH1	Chloroplast (Exp)	D-lactate dehydrogenase
	Cre16.g689700	HPR5	Mitochondria (Exp)	Hydroxypyruvate reductase 5
GLYK	Cre12.g542300	GLYK1	Chloroplast	Glycerate kinase

One of the most intriguing questions of PR pathways in Chlamydomonas (**Fig. 1.2**) is the presence of two putative oxidative pathways of glycolate: glycolate dehydrogenase (GDH/GYD) in the mitochondria and glycolate oxidase (GOX) with putative localization in peroxisome (Chauvin et al., 2008). A Chlamydomonas knockout mutant of GDH/GYD reported as High-CO_2 Requiring 89 (HCR89) was shown to secrete twice more glycolate 20 h after transition from high-CO_2 to air and showed no detectable activity of GDH/GYD (Nakamura et al., 2005; Aboelmy and Peterhansel, 2014). Another difference between higher plants and Chlamydomonas is the localization of HPR1 in

mitochondrion instead of peroxisome (**Fig. I.2** and **Table I.1**) (Shi et al., 2021). HPR1-deficient strains when transferred from high-CO_2 to air are compromised in growth and secreted 10 times more glycolate compared to the wild-type 2 d after being transferred into air (Shi et al., 2021). Based on the subcellular localization of HPR1 and GDH/GYD, PR pathways in Chlamydomonas might occur between chloroplast and mitochondria in contrast to higher plants where peroxisome is also involved (Santhanagopalan et al., 2021; Shi et al., 2021). However, Chlamydomonas glycolate oxidase and two alanine-glyoxylate transaminases possessed putative peroxisomal targeting peptides in their sequence, suggesting a possible peroxisome location. Of course, this does not rule out a potential dual targeting (mitochondria and plus peroxisome). Taken together, a complete subcellular localization study will be essential to outline the subcellular locations of the PR pathway in Chlamydomonas.

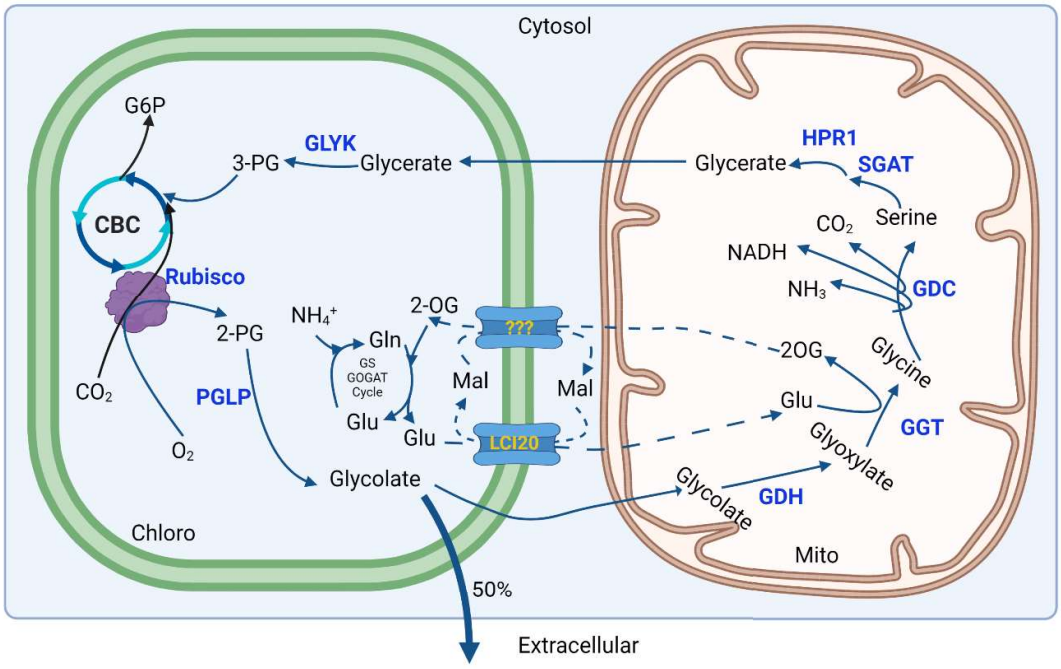

Figure I.2: Speculative and simplified scheme of photorespiratory pathway in Chlamydomonas. Putative or previously characterized enzymes with confirmed demonstrated subcellular location or being predicted by PredAlgo (Tardif et al., 2012). We did not consider the putative localization of GYX in the peroxisome due to absence of experimental evidence so far, but it is not clearly ruled out that peroxisome was not involved photorespiration. PR pathways is shown in blue and it is estimated that half of glycolate is secreted and half recycled into 3-PG. The involvement of the low-carbon inducible 20 LCI20 (homolog of DiT2 in Arabidopsis) is based on knowledge on PR pathways in higher plants and our recent study on LCI20 in Chlamydomonas (for details see results in **Chapter 3**). The same abbreviations used as shown in **Table 1.1**.

The above studies suggest that PR might be at least transiently active in Chlamydomonas during very-low-CO_2 adaptation. Recent transcriptomic studies showed that the expression of 5 genes encoding for SGAT, HPR1, GDC, GDH/GYD and GLYK enzymes increases in response to limiting CO_2 level in a CCM1 dependent manner (Miura

et al., 2004; Yamano et al., 2008; Fang et al., 2012; Santhanagopalan et al., 2021), suggesting that PR and CCM are co-regulated at least at transcriptional level.

In addition to the core enzymes, the PR pathway involves a few auxiliary enzymes and shuttle proteins. In higher plants, considerable research effort has led to the identification of the metabolite transporters that are needed for PR (Somerville and Ogren, 1983; Weber et al., 1995; Taniguchi et al., 2002; Renné et al., 2003; Weber and Linka, 2011; Schlüter and Weber, 2020). Homolog of known Arabidopsis chloroplast dicarboxylate transporter 1 and 2 (DiT1, DiT2) and mitochondrial glutamate transporter (BOU) important for PR (Renné et al., 2003; Schneidereit et al., 2006; Eisenhut et al., 2013; Porcelli et al., 2018) could be found encoded by the Chlamydomonas genome annotated as 2-oxoglutarate malate translocator and low-carbon inducible 20 (OMT1/OMT2 and LCI20, respectively) and carnitine/acylcarnitine transporter (CCP1/2) (Pollock et al., 2004; Merchant et al., 2007; Blaby et al., 2015; Gallaher et al., 2015; Atkinson et al., 2016). The expression of LCI20 and CCP1/2 is also responsive to CO_2 in a CCM1-dependent manner and strongly induced after transition from high to low-CO_2 suggesting that LCI20 could play a role in PR (Miura et al., 2004; Pollock et al., 2004; Yamano et al., 2008). In **Chapter 3** we reporte detailed functional characterization of the role of LCI20 in the photorespiration.

Photorespiration is at the crossroad of carbon, nitrogen and energy metabolism. It has long been debated about the physiological reason/evolutionary emergence of photorespiration: on one hand, the main purpose of photorespiratory pathways is considered to remove the toxic 2-PG and recycle the carbon back into the chloroplast for CBB cycle as efficiently as possible (Fernie and Bauwe, 2020; Bauwe, 2023; Segura Broncano et al., 2023). It is estimated that 25% of photosynthetically fixed carbon and 30% of energy produced are lost during PR. On the other hand, many recent studies showed positive effects of PR on growth under many environmental conditions such as low-CO_2, high light, heat stress, or drought etc. (Hanawa et al., 2017; Busch et al., 2018; Shi et al., 2022). In higher plants, it has been shown that PR serves as an electron sink by transferring chloroplast NAD(P)H into the mitochondria, further attenuating photoinhibition under high-light conditions (Hanawa et al., 2017; Lim et al., 2020). In *Chlorella sorokiniana*, PR facilitates acetate assimilation by providing glyoxylate to drive up the glyoxylate cycle responsible for acetate uptake (Xie et al., 2016). PR interacts with nitrogen metabolism by transferring fixed-nitrogen from the chloroplast to the mitochondria for glycine synthesis which further fuels amino acid metabolism (Canvin, 1981; Busch et al., 2018). In Chlamydomonas, photorespiration is shown recently to be essential for acclimation to salt-stress (Shi et al., 2022). Further work is needed to elucidate the physiological functions of PR in green microalgae and to characterize the roles of the different actors. Whether photorespiration has a physiological role under natural environment is under investigation.

3.5. Starch and TAG as energy and carbon sinks

In addition to CO_2 photo-reduction, inorganic nitrogen assimilation and reduction, starch and de novo fatty acid biosynthesis are major reactions in the chloroplast that require NAD(P)H and ATP albeit at different ratios (Johnson and Alric, 2013; Burlacot et al., 2019; Launay et al., 2023). Synthesis of amino acids, fatty acids and starch are therefore considered electron sinks. Compared to the above-mentioned electron management mechanisms, synthesis of biomolecules (starch and TAG) takes time and occur at a much longer time scale, considered therefore as a means of carbon and energy storage. Starch and TAGs are observed to be made during the day and consumed at night to support cell

growth and respiration (Ral et al., 2006; Jüppner et al. , 2017). Mutants deficient in starch synthesis (i.e. *bafJ5* or *sta6*) are more susceptible to photoinhibition, had reduced photosynthetic performance, a higher level of ROS and impaired in growth, supporting that starch is a key electron sink to assimilate cellular energy and carbon (Krishnan et al., 2015). Consistent with the role of CEF in electron dissipation, one of the consequences of blocking starch synthesis is the upregulation of alternative electron pathways such as the CEF and the mitochondrial respiration in the light (Johnson and Alric, 2012; Krishnan et al., 2015).

However the interaction between lipid and starch as alternative or competing carbon or electron sinks are rather complex, and in some studies the starch less mutant (*sta6/bafj5*) was found to accumulate more TAG during N deprivation than a distantly related wild-type strain (rather than on a complemented strain) on a dry biomass basis (Li et al., 2010;), but in other reports it looks rather indifferent (Siaut et al., 2011). Later on, Blaby et al (2013) identified that in the *sta6/bafj5* mutant, the mutation is actually extended into a neighboring gene encoding a respiratory burst oxidase (Blaby et al., 2013). This finding, together with the reports of others, strongly suggest the use of proper reference strains in data comparison. Moreover, mutations in certain genes seem to drive up both starch and lipid synthesis as in the case of *mdh2*, *std1* or *tar1* mutants (Schulz-Raffelt et al., 2016; Kong et al., 2018; Shinkawa et al., 2019). These findings point to a common regulatory mechanism that controls the flux of carbon or energy to starch and lipid. Taken together, it does not seem to occur a simple competition between starch and lipid pools (at least not during N deprivation), rather these two types of carbon and electron sinks seem to play a complementary and collaborative role. Carbon storage and partitioning between starch and TAGs have not yet been evaluated during optimal growth, but in any case, starch seem to be a major reserve compared to TAGs regardless of N status.

Mutants deficient in TAG synthesis have not been isolated, which could indicate that such mutants are likely lethal. The physiological importance of TAG is further supported by the fact that multiple parallel TAG synthesis pathways occur in algae and plants i.e. the occurrence of 5 DGATs (diacylglycerol acyltransfereases) as well as the PDAT (phospholipid:diacylglycerol acyltransferase) pathway. In contrast, there is only one single pathway responsible for starch synthesis i.e. the AGPase (ADP-glucose pyrophosphorylase) pathway. Nevertheless, the *pgd1* mutants of Chlamydomonas impaired in fatty acid remodeling from the major galactolipid monogalactosyldiacylglycerol (MGDG) to TAG are chlorosis and showed higher level of ROS in the chloroplast during HL exposure (Li et al., 2012; Du et al., 2018). The *pgd1* mutants exhibited higher level of unsaturated fatty acids, reduced level of TAG consistent with a decrease in the flux of fatty acid from plastid lipids to TAG. The blockage of photosynthetic LEF by DCMU could reverse both ROS accumulation and chlorosis in the mutants further supporting that *de novo* fatty acid synthesis and further incorporation into TAG could serve as an alternative sink for photosynthetic electrons (Li et al., 2012; Du et al., 2018).

Starch and TAG massively accumulate under N deprivation, further supporting their role as carbon and energy sinks. Under N deprivation, the reductant usually used for N assimilation and reduction, and the carbon metabolites used for amino acid synthesis, are now available for synthesis of starch and fatty acid in the chloroplast. Molecular mechanisms underlying such a change has been interrogated using omics approaches. One finds significant increases in transcripts coding for enzymes of lipid and starch biosynthesis (Miller et al., 2010; Boyle et al., 2012; Li et al., 2014). In addition, one observes a decrease in many proteins of the photosynthetic electron transfer complexes

and the plastid ATPase, but an increase was found for proteins of mitochondria ATPase as well as proteins of the mitochondria respiratory complex, pointing to a reduced capacity in photosynthetic performance but with an increased or at least sustained respiratory activity under N starvation (Miller et al., 2010; Schmollinger et al., 2014; Juergens et al., 2015).

Furthermore, several studies have reported the remodeling of photosynthetic apparatus shifting from LEF-based energy (ATP and NADPH) production toward a more CEF-based ATP production when cells are exposed to N deprivation in Chlamydomonas (Schmollinger et al., 2014; Juergens et al., 2015; Saroussi et al., 2016). Moreover, the storage capacity of lipid and starch has been evaluated in strains of Chlamydomonas defected in CEF pathways during N starvation. The involvement of PGRL1 pathway was reported to be minor whereas the NDA2 pathway was shown to be the most important under photoautotrophic N deprivation (Saroussi et al., 2016). Under mixotrophic low-light condition, The PGRL1 mediated-CEF was reported to major source of ATP for TAG synthesis because the *pgrl1* mutant made 30% less oil than corresponding wild-type strain 48 h after N deprivation (Chen et al., 2015). Collectively these papers point to an increased requirement for ATP, produced by a combined action of photophosphorylation and oxidative phosphorylation. In *Chlorella sorokiniana*, the situation seems slightly different i.e. a reduction is observed for both the photosynthetic LEF and mitochondrial respiratory rates but with an increased rate of CEF during N starvation (Zhang et al., 2013; Chen et al., 2015). Taken together, despite some of the very precise characterization of the alternative electron pathways in current literature, their contribution to carbon storage (starch and fatty acid synthesis) has been explored only recently and need further investigation.

Additionally, under anaerobic condition when O_2 is not available as an electron acceptor, starch and TAG are found to be over-accumulated (Doebbe et al., 2010; Hemschemeier and Happe, 2011). The contribution of pseudo-CEF pathways (catalyzing the O_2-photoreduction) in the storage of lipid and starch has not yet been investigated under N deprivation. FLV, as a major mechanism of O_2 photoreduction (Chaux et al., 2017a), was found to be up regulated under S deprivation at the onset of anaerobic induction (Jokel et al., 2015). Although mutants deficient in FLV are available, the metabolic consequence on TAG and starch synthesis has not been evaluated. Here in this Thesis, we characterize the function of CEF and PCEF under N starvation, and we further evaluate its effect on carbon storage (**Chapter 1**).

Above findings suggest that cellular energetic balance play not only a role in cell growth (i.e. biomass accumulation) but also have an impact on biomass composition (starch, lipid or protein). Understanding this interaction could open new perspectives into engineering energy management pathways, paving the path towards diverting cell metabolism to produce energy-rich molecules for biotechnological applications.

4. Physiological functions of malate shuttles in plants and algae (TIPS doi: 10.1016/j.tplants.2021.11.007)

Trends in Plant Science

CellPress

Intro

Review

Physiological functions of malate shuttles in plants and algae

Ousmane Dao [1], Franziska Kuhnert [2], Andreas P.M. Weber [2], Gilles Peltier [1], and Yonghua Li-Beisson [1,*]

Subcellular compartmentalization confers evolutionary advantage to eukaryotic cells but entails the need for efficient interorganelle communication. Malate functions as redox carrier and metabolic intermediate. It can be shuttled across membranes through translocators. The interconversion of malate and oxaloacetate mediated by malate dehydrogenases requires oxidation/reduction of NAD(P)H/NAD(P)$^+$; therefore, malate trafficking serves to transport reducing equivalents and this is termed the 'malate shuttle'. Although the term 'malate shuttle' was coined more than 50 years ago, novel functions are still emerging. This review highlights recent findings on the functions of malate shuttles in photorespiration, fatty acid β-oxidation, interorganelle signaling and its putative role in CO_2-concentrating mechanisms. We compare and contrast knowledge in plants and algae, thereby providing an evolutionary perspective on redox trafficking in photosynthetic eukaryotes.

Highlights

The malate shuttle, as a valve for photosynthetic electron dissipation, has been proposed for >50 years, but only recently has this function been clearly demonstrated.

The plastidial NAD-MDH is essential for embryogenesis and chloroplast development. This role is not due to its enzymatic activity but rather to its ability to stabilize a large AAA-ATPase complex at the inner envelope. The plNAD-MDH is therefore a moonlighting protein.

The malate shuttle connects fatty acid biosynthesis in the chloroplast to mitochondrial reactive oxygen species (ROS) production and to programmed cell death in plants.

The malate shuttle connects fatty acid catabolism in the peroxisome to photosynthesis and chloroplast metabolism in algae.

Expression of malate shuttle components is responsive to CO_2 levels. The latest results indicate its critical role in plant photorespiration and points to a possible role in the algal CO_2-concentrating mechanism.

Malate as a major cellular redox carrier

Eukaryotic cells are compartmentalized, and distinct subcellular organelles house specific subsets of metabolic reactions that are physically separated from each other by biological membranes. Exchange of information and energy between compartments, mostly mediated by metabolites, is indispensable to achieve whole-cell homeostasis and ensure optimal growth [1,2]. While some of these exchanges occur through passive diffusion, most of them are mediated by transporters [3]. Understanding the complex interplay of energy and information between subcellular compartments is key towards the domestication of photosynthetic organisms for tailor-made production of valuable compounds.

Malate is a C4 dicarboxylic acid and is involved in a number of metabolic pathways, including the tricarboxylic acid (TCA), C4-dicarboxylic acid, and **glyoxylate cycles** (see Glossary) in plants and algae [4–6]. Malate can be produced by malate synthase (MAS) and metabolized malic enzyme (ME) or malate dehydrogenase (MDH) (Box 1). Amongst these, only MDH catalyzes a reversible reaction that is coupled to the reduction/oxidation of NAD(P)$^+$/NAD(P)H, while interconverting malate and oxaloacetate (OAA). In contrast to the main cellular redox couple, that is, the pyridine nucleotides NAD(P)(H), malate can be efficiently transported across membranes through di- or tricarboxylate translocators. Although specific transporters of NAD$^+$ are present in the membrane of the chloroplast, mitochondrion, or peroxisome [7,8], their activity is restricted in importing NAD$^+$ into organelles and is probably important in *de novo* loading of organelles with the NAD$^+$ pool. But these transporters show a very low affinity for NAD(P)H [9] and are therefore probably not sufficient for redox exchange between compartments. Malate trafficking thus serves as an indirect but efficient way of transporting reducing equivalents.

[1]Aix Marseille Univ, CEA, CNRS, BIAM, Institut de Biosciences et Biotechnologies Aix-Marseille, CEA Cadarache, Saint Paul-Lez-Durance 13108, France
[2]Institute of Plant Biochemistry, Cluster of Excellence on Plant Science (CEPLAS), Heinrich Heine University, 40225 Düsseldorf, Germany

*Correspondence: yonghua.li@cea.fr (Y. Li-Beisson).

© 2021 Elsevier Ltd. All rights reserved.

Box 1. Malate metabolism in photosynthetic cells

Malate is a versatile compound and its cellular metabolism involves malate synthase (MAS), malic enzyme (ME), or malate dehydrogenase (MDH) (Figure I). MAS catalyzes the formation of malate from acetyl-CoA and glyoxylate, which is a key step in the glyoxylate cycle [4,88]. The glyoxylate cycle allows cells to utilize two-carbon compounds (C2), such as acetate, and it is essential for the heterotrophic growth of some algae such as chlamydomonas [89]. The concerted action of MAS and isocitrate lyase (ICL) in the glyoxylate cycle forms succinate that enters the mitochondrial TCA cycle, bypassing the steps that result in carbon loss [4,64].

ME catalyzes the decarboxylation of malate to pyruvate, resulting in the production of NAD(P)H and CO_2. This reaction has been shown to be an important source of reducing equivalents for *de novo* fatty acid synthesis as well as desaturation in fungi [90], plants [91], and more lately in algae [92]. It is also a crucial reaction in C4 and CAM (Crassulacean acid metabolism) photosynthetic metabolism [93].

MDHs are the only enzymes catalyzing a reversible reaction, important for its function in modulating redox status. In arabidopsis, nine genes encoding MDHs are present in the genome, and the activities of MDH could be detected in most subcellular compartments, including the mitochondrion (mNAD-MDH1, 2), peroxisome (pNAD-MDH1, 2), cytosol (cyNAD-MDH1, 2, 3), and plastid (plNAD-MDH and plNADP-MDH) [10]. In contrast to land plants, five isoforms of MDH (MDH1-5) are encoded in the genome of chlamydomonas [94]. CrMDH5 (the only $NADP^+$ requiring MDH) is predicted to be chloroplastic, CrMDH2 peroxisomal [4,63], CrMDH3 is considered cytosolic, and CrMDH4 mitochondrial [95]. The situation is more complex with CrMDH1 which is predicted to be chloroplast-based on PredAlgo [95], but is found peroxisomal when the 25 aa of its N terminus is fused to yellow fluorescent protein (YFP) [4]. Therefore, subcellular localization(s) of CrMDH1 using full-length protein fusion or immunogold labeling would be needed to clarify its location.

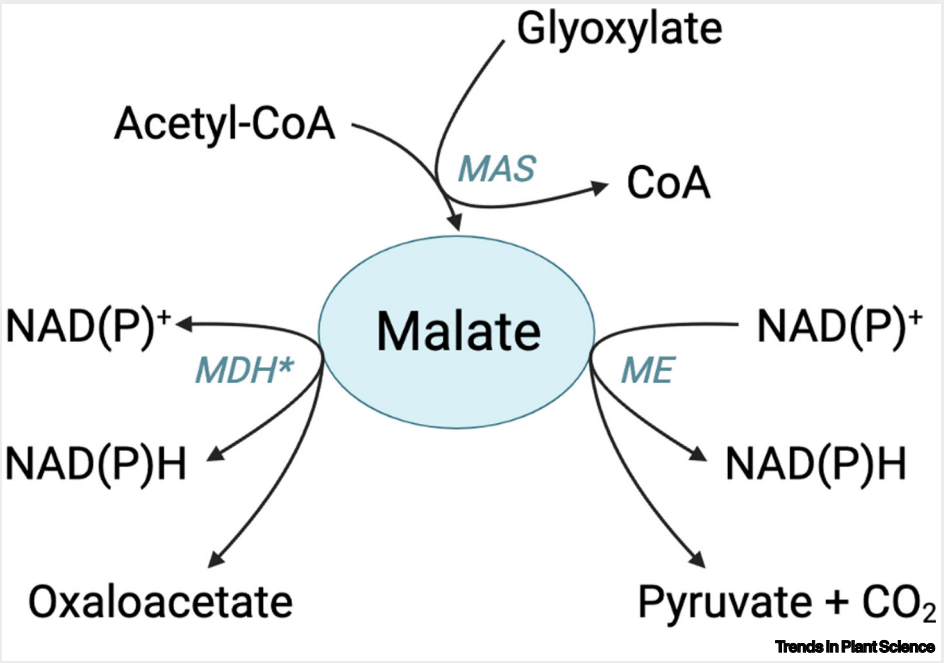

Figure I. Metabolic reactions that involve malate. Malate dehydrogenase (MDH), malic enzyme (ME), and malate synthase (MAS) are found in higher plants and algae. MAS catalyzes the biosynthesis of malate by condensing glyoxylate and acetyl-CoA. This reaction is part of the glyoxylate cycle. ME uses either $NADP^+$ or NAD^+ to decarboxylate malate into pyruvate, releasing CO_2; it is present in several subcellular compartments. MDH catalyzes the reversible interconversion between malate and oxaloacetate using either $NAD(P)^+$ or NAD(P)H as cofactor. This reaction occurs in the plastid, cytosol, peroxisome, and mitochondrion. CoA, Co-enzyme A; $NAD(P)^+$, nicotinamide adenine dinucleotide (phosphate). *Denotes that the MDH reaction is reversible.

Trafficking of malate between different subcellular compartments has been extensively studied in plants (Box 2) [10]. The inner membrane of the chloroplast and mitochondrion in plant and algal cells is equipped with several types of di- and tricarboxylate translocators catalyzing malate

Glossary

CO_2-concentrating mechanism (CCM): CCM, as the name implies, is a process of concentrating CO_2 to the active site of RuBisCo, the major protein of the carbon photoreduction cycle (i.e., often called Calvin–Benson–Bassham cycle). It is therefore considered a mechanism to reduce the rate of photorespiration. Depending on species, CCM could refer to the dicarboxylic acid cycle in C4 plants, CAM-based CCM in CAM plants, carboxysome based-CCM in cyanobacteria, and the biophysical CCM occurring in algae (the conversion of CO_2 to bicarbonate and its transport to the pyrenoid).

Cyclic electron flow (CEF): the recycling of electrons from the acceptor side of photosystem I through the cyt b_6/f complex, increasing the proton motive force (*pmf*). The *pmf* is then used to drive ATP synthesis. The CEF promotes ATP synthesis without additional NADPH production and is therefore considered a way to increase the ATP/NADPH ratio in response to metabolic or environmental situations. Several pathways of CEF have been characterized: (i) the plant type I NADPH dehydrogenase complex (NDH); (ii) the type II NDH (NDA2) unique to algae; and (iii) the proton gradient regulator 5 (PGR5)/PGR-like 1 (PGRL1)-mediated CEF pathway, which is common to plants, algae, and cyanobacteria.

Fatty acid β-oxidation: one of the major mechanisms of fatty acid degradation. Oxidation of fatty acids can occur either at the α-, β- or ω-carbon position of a given fatty acid; β-oxidation is found as a major pathway in plants and algae. This pathway ultimately breaks down fatty acids into acetyl-CoAs, which are further metabolized either for energy production, through the mitochondrial electron transport chain, or for the synthesis of sugars when coupled to glyoxylate and gluconeogenesis pathways.

Glyoxylate cycle: an anabolic pathway occurring widely in plants, bacteria, fungi, and algae. It allows the conversion of acetyl-CoA to succinate for the synthesis of carbohydrates, therefore allowing microorganisms to utilize two-carbon compounds as a carbon source. For example, it plays an essential role in the heterotrophic growth of green algae on acetate. It shares several steps

Box 2. Dicarboxylate and tricarboxylate translocators

In addition to MDHs, the malate shuttle requires translocators of malate/or other dicarboxylates or tricarboxylates from one compartment to another. Different translocators have been predicted and experimentally verified in arabidopsis chloroplasts and mitochondria [12,96]. The transfer of malate through the chloroplast envelope membrane can be mediated by at least three different translocators. The 2-oxoglutarate (OG)/malate-translocator 1 (OMT1 or DiT1) catalyzes the transport of malate in exchange for 2-OG [31]. AtOMT1 was also shown to have high affinity for OAA in reconstituted liposomes [22]. The dicarboxylate translocators 1 and 2 (DCT1 and 2, also sometimes called DiT2.1 and 2.2) are glutamate/malate-translocators importing malate in counterexchange with glutamate [31]. Very likely also, malate uniporters exist in the chloroplast envelope membrane. However, the corresponding genes have not been identified.

The transfer of malate across the mitochondrial inner membrane is mediated by at least three dicarboxylate carriers (DIC1, DIC2, DIC3) and one dicarboxylate-tricarboxylate carrier (DTC) belonging to the mitochondrial carrier family (MCF) [85,86]. The recombinant DICs, when introduced into liposomes, catalyze the transport of a wide range of dicarboxylates such as malate, OAA, succinate, but with low affinity for 2-OG. These DICs were proposed to be involved in the mitochondrial malate-OAA shuttle [86]. Very recently, the physiological function of DIC2 has been demonstrated in arabidopsis as being a high-affinity malate–citrate antiporter in the mitochondria, through evidence from the reverse genetic approach in combination with comprehensive *in vitro*, *in organello*, and *in vivo* analyses [87]. Conversely, in addition to dicarboxylates (malate, OAA, 2-OG, and succinate), DTC was shown to also transport tricarboxylates (such as citrate or isocitrate) [85]. Therefore, DTC can serve as a malate/2-OG translocator. A malate/aspartate shuttle has been proposed by [67] connecting mitochondria to the peroxisome, which requires coordinated functions of two types of translocators, that is, malate/2-OG carrier (likely DTC) and a glutamate/aspartate carrier.

Genes encoding putative proteins homologous to the plant di- or tricarboxylate translocators are present in the chlamydomonas genome (see Table 1 in main text). Three putative plastidial 2-OG/malate translocators (annotated as OMT1, OMT2, and low-carbon-inducible20 – LCI20), and one mitochondrial translocator known as MiTC14 and belonging to the MCF family, have been identified [94]. The protein sequence of LCI20 shares 55% and 60% similarity with DiT2.1 and DiT2.2, respectively, whereas AtDiT1 shares 63% of similarity with both CrOMT1 and CrOMT2, suggesting that they are evolutionarily related dicarboxylate translocators.

transport in counter-exchange with, for example, OAA, glutamate, or aspartate. It can function in either direction depending on the concentration gradient resulting from a metabolic demand [11,12]. Collectively, the trafficking of malate through specialized translocators from one compartment to another, combined with the malate processing enzymes (MDHs), is termed the **malate shuttle** [10].

Although the concept of the 'malate shuttle' has been around for over 50 years ago, components of this pathway remain hypothetical in microalgae, despite considerable progress has been made in land plants [10]. Depending on the type of carboxylates being transported, several variations of the 'malate shuttle' occur, which are, malate/OAA shuttle, malate/aspartate shuttle (Box 3), and malate/2-oxoglutarate shuttle. These various types of malate shuttle, their subcellular locations, and their involvement in different metabolic pathways are illustrated in Figure 1.

Box 3. Other players in the malate shuttle

Apart from MDH and the malate translocators listed in Table 1, other enzymes could also be involved in functioning of variants of the malate shuttle. One notable example is the malate–aspartate shuttle, which requires aspartate aminotransferases (AspATs), sometimes called glutamate-oxaloacetate transaminases (GOTs). AspATs are ubiquitous enzymes encoded by a multigenic family catalyzing the reversible interconversion between aspartate and 2-oxoglutarate with glutamate and OAA. In arabidopsis, five isoforms of eukaryotic type AspAT are present, that is, AspAT1 (mitochondrial), AspAT2 and AspAT4 (cytosolic), AspAT3 (peroxisomal), AspAT5 (chloroplastic), and one prokaryotic-type AspAT (PTA) localized in the chloroplast [97,98]. Activity of AspAT was also detected in chlamydomonas [99], and five genes *AST1–AST5* (phytozome v13) encode AspAT proteins [94], respectively: AST1, AST3 and AST4 (likely mitochondrial or peroxisomal), AST2 (chloroplastic), and AST5 (cytosolic). The plant peroxisomal and mitochondrial isoforms of AspAT have been proposed, in conjunction with MDHs, to play a role in shuttling reducing equivalents between both organelles through the malate–aspartate shuttle during photorespiration [100], but none of the algal proteins has been studied.

with the tricarboxylic acid (TCA) cycle but bypasses the steps that release CO_2.

Malate shuttle: this refers to the means of redox trafficking from one subcellular compartment to another through malate transport. It comprises two major protein components, that is, malate dehydrogenases and di- or tricarboxylate translocators.

Photorespiration: a metabolic pathway found in organisms that carry out oxygenic photosynthesis in which the major enzyme RuBisCo can fix either CO_2 or O_2 depending on their stoichiometric ratio. The oxygenation reaction produces 2-phosphoglycolate, a toxic metabolite, which is detoxified by conversion to the Calvin–Benson–Bassham Cycle intermediate 3-phosphoglycerate. This conversion involves a set of reactions occurring in four subcellular compartments, that is, chloroplast, cytosol, peroxisome, and mitochondria, and it entails the loss of CO_2, NH_4^+ and energy in the process.

Pseudo-cyclic electron flow (pseudo-CEF): a pathway in which electrons, generated from the splitting of water at PSII, are used to reduce O_2 to H_2O, thereby driving photosynthetic electron flow and generating a proton gradient, without NADPH production. In green algae, O_2-photoreduction is mostly mediated by the flavodiiron (FLV) proteins.

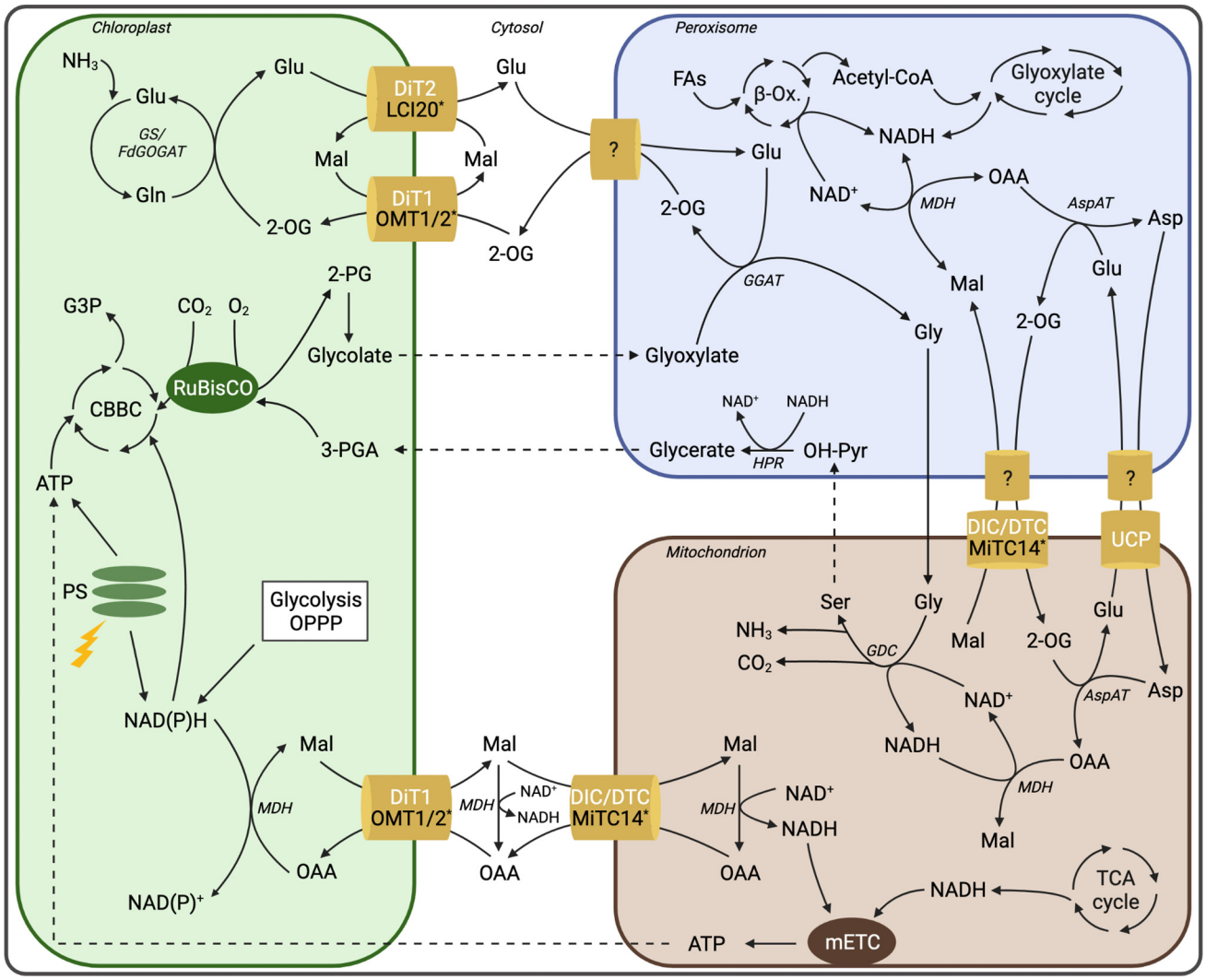

Trends in Cognitive Sciences

Figure 1. Known and putative steps of malate trafficking in a subcellular context. The known dicarboxylate/tricarboxylate translocators based on either *in vivo* or *in vitro* characterization are reported in Table 1. Transporter name in white refers to arabidopsis proteins and black refers to the chlamydomonas putative transporters (*) based on homology without any functional data. The question mark (?) represents the putative translocators involved in the malate shuttle. Dashed lines indicate reactions with several intermediate steps. Created with BioRender.com. ADP, adenosine diphosphate; ATP, adenosine triphosphate; Asp, aspartate; AspAT, aspartate aminotransferase (Box 3); β-Ox., β-oxidation; CBBC, Calvin–Benson–Bassham cycle; DIC/DTC, mitochondrial dicarboxylate/dicarboxylate-tricarboxylate carrier; DiT1/2, dicarboxylate translocator 1/2; FA, fatty acid; FdGOGAT, ferredoxin-dependent glutamine 2-oxoglutarate aminotransferase; G3P, glyceraldehyde-3-phosphate; GDC, glycine decarboxylase; GGAT, glutamate-glyoxylate aminotransferase; Gln, glutamine; Glu, glutamate; GS, glutamine synthase; HPR, hydroxypyruvate reductase; Mal, malate; MiTC14, mitochondrial substrate carrier protein 14; MDH, malate dehydrogenase; mETC, mitochondrial electron transport chain; NAD(P)H, nicotinamide adenine dinucleotide (phosphate); OAA, oxaloacetate; 2-OG, 2-oxoglutarate; OH-Pyr, hydroxypyruvate; OMT1/2, 2-oxoglutarate/malate translocator; OPPP, oxidative pentose phosphate pathway; 2-PG, 2-phosphoglycolate; 3-PGA, 3-phosphoglycerate; PS, photosystems; RuBisCO, ribulose-1,5-bisphosphate carboxylase/oxygenase; TCA cycle, tricarboxylic acid cycle; UCP, uncoupling protein.

Here, we review some of the most recent discoveries on the roles of malate shuttles in connecting carbon, nitrogen, and energy metabolism in plants and algae. While isoforms of MDHs and di-/tricarboxylate translocators have been well characterized in land plants, evidence is just emerging regarding their functions in algae. We provide a comparative analysis of the corresponding proteins between the model plant arabidopsis (*Arabidopsis thaliana*) and the model green alga chlamydomonas (*Chlamydomonas reinhardtii*) (Table 1). We discuss the malate shuttle's physiological

Table 1. Main components of the malate shuttle in arabidopsis and chlamydomonas[a,b]

Protein family	Chlamydomonas	Phytozome ID	Arabidopsis	TAIR ID	Localization	Refs
Malate dehydrogenases	CrMDH1	Cre03.g194850	plNAD-MDH	At3g47520	Chloroplast (arabidopsis) Peroxisome[c] (chlamydomonas)	[4,50,78–80]
	CrMDH2	Cre10.g423250	pMDH1	At2g22780	Peroxisome	[25,37,68]
			pMDH2	At5g09660		
	CrMDH3	Cre02.g145800	cyNAD-MDH1	At1g04410	Cytosol	[81,82]
			cyNAD-MDH2	At5g43330		
			cyNAD-MDH3	At5g56720		
	CrMDH4	Cre12.g483950	mMDH1	At1g53240	Mitochondria	[33,83,84]
			mMDH2	At3g15020		
	CrMDH5	Cre09.g410700	cpNADP-MDH	At5g58330	Chloroplast	[19,20,23]
Malate translocators	CrOMT1	Cre17.g713350	DiT1 (OMT1)	At5g12860	Chloroplast	[22,32,50]
	CrOMT2	Cre17.g713200				
	CrLCI20	Cre06.g260450	DiT2.1 (DCT1)	At5g64290		[30–32]
			DiT2.2 (DCT2)	At5g64280		
	CrMiTC14	Cre16.g672650	DIC1	At2g22500	Mitochondria	[11,85,86]
			DIC2	At4g24570		
			DIC3	At5g09470		
			DTC	At5g19760		

[a]Abbreviations: At, *Arabidopsis thaliana*; Cr, *Chlamydomonas reinhardtii*; 'pl', plastidial; 'p', peroxisome; 'cy', cytosol and 'm', mitochondria.
[b]Homology between chlamydomonas and arabidopsis proteins was identified through reversible BlastP search of TAIR (for arabidopsis) and Phytozome v13 (for chlamydomonas) proteins. Arabidopsis protein sequences were used first as baits. Note that the function assigned to mitochondrial malate translocators in arabidopsis is only based on *in vitro* experiments except for DIC2, which has recently been characterized *in vivo* [87]. Other players in the malate shuttle can be found in Boxes 2 and 3.
[c]Refers to a putative localization of CrMDH1 in the peroxisome based on fusion of N-terminus transit peptide with fluorescent tag.

importance in photosynthesis, **photorespiration**, and **fatty acid β-oxidation**, and we point to its possible implication in algal **CO_2-concentrating mechanisms** (**CCMs**). Finally, we highlight the role of malate shuttle in interorganelle communication through interaction with reactive oxygen species (ROS)-mediated signal transduction.

Malate shuttle as a valve for photosynthetic electron dissipation

During the linear electron flow (LEF) of photosynthesis, light energy is converted by two photosystems (PSII and PSI) into chemical energy in the form of NADPH and ATP, which are subsequently used to drive metabolic reactions, particularly CO_2 fixation by RuBisCo and its conversion into triose phosphates through the Calvin–Benson–Bassham (CBB) cycle [13]. However, the LEF is known to produce an insufficient amount of ATP (as compared to NADPH) than that required for optimal CO_2 photoreduction, leading to an imbalance [14]. The imbalance in ATP and NADPH could be further accentuated by changes in environmental conditions. For example, under CO_2 limiting conditions, photorespiration in plants, or a CCM in algae, requires additional ATP [14,15]. Excess reducing equivalents could potentially lead to ROS overproduction [16]. Coordination between production and usage of ATP and NAD(P)H is therefore essential for cell fitness and survival, particularly in a changing environment.

ATP and NADPH balance can be achieved by increasing ATP production in the chloroplast or through import, or by lowering the NADPH level through enhancing sink strength or export to other compartments (Figure 2). Several mechanisms are involved in the supply of extra-ATP, which include **cyclic electron flow** (**CEF**) around PSI, or the O_2-photoreduction by flavodiiron

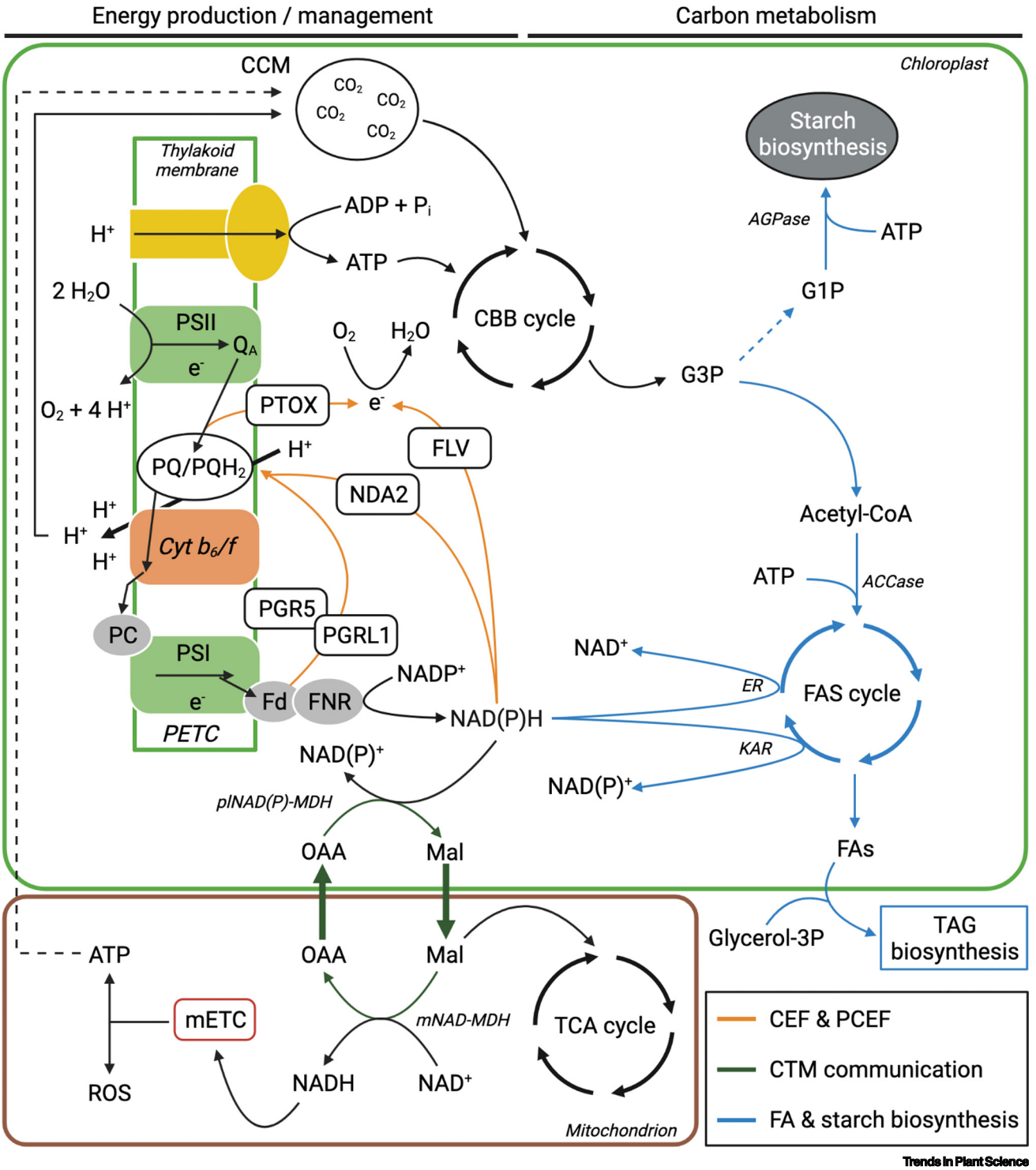

Figure 2. Photosynthetic redox production, management, and carbon metabolism in algae. The photosynthetic linear electron flow (LEF) occurring in the thylakoid membrane produces ATP and NADPH for the fixation of CO_2 in the Calvin–Benson–Bassham (CBB) cycle to yield carbohydrates. The G3P, ATP, and NAD(P)H are then used for starch and *de novo* fatty acid biosynthesis (blue arrows). Alternative electron pathways are represented by cyclic electron flow (CEF; orange

(Figure legend continued at the bottom of the next page.)

(FLV) proteins, also known as **pseudo-CEF**, or ATP import from mitochondria [17]. Conversely, NADPH dissipation can occur either through enhanced metabolic demand (e.g., boosting *de novo* fatty acid synthesis, which has a high need for reducing equivalents), or through its export to other subcellular compartments by the malate shuttle [18].

Despite having been hypothesized for several decades, the role of the malate shuttle in photosynthetic electron exportation (as a 'malate valve') has only recently been demonstrated. In arabidopsis, the knockout mutants in plastidial NADP-MDH (*nadp-mdh*) had a more reduced plastoquinone pool but with only slight impairment in growth under high light (HL) [19,20]. Strong growth defects, however, were observed under fluctuating light in a mutant in which one of its regulatory redox switches at its C terminus was deleted by genome editing [21]. The carboxylate translocator involved in the malate valve (AtOMT1) has also been characterized in arabidopsis. AtOMT1 is a high-affinity OAA translocator whose absence led to the hyperaccumulation of reducing power in the stroma, photoinhibition, and impaired growth under HL [22]. Taken together, the previously-mentioned studies demonstrate the essential role of the malate valve in chloroplast energy homeostasis, which is particularly important to balance the chloroplast redox status during fluctuating conditions.

In algae, none of the components of the chloroplast malate valve have been characterized at a physiological level. The chlamydomonas CrMDH5, the homolog of the arabidopsis NADP-MDH, has been studied *in vitro* [23]. The thioredoxin (TRX)-dependent redox regulation of the CrMDH5 activity is much faster (responding in an all-or-nothing way) than the plant homolog but the latter is fine-tuned due to the presence of an additional N-terminus disulfide regulatory domain. Even though its physiological function has not been shown directly, it was proposed that the malate valve may operate in the chlamydomonas mutant lacking the proton-gradient-like-1 (PGRL1)-mediated CEF in conditions of strong ATP/NADPH imbalance [24]. It was hypothesized that the malate valve helps to evacuate excess reducing equivalents towards cytoplasm and mitochondria. Nevertheless, there is no direct evidence of the operation of the malate valve in algae.

It is worth bearing in mind that the 'malate valve' in the chloroplast could also function in importing reducing power into the chloroplast. Responses of photosynthesis and chloroplast metabolism to changes in redox state in other subcellular compartments (mitochondria or the peroxisome) seem to support such a possibility [25,26]. Our understanding of redox homeostasis in the chloroplast is further complicated by the presence of both NAD^+- and $NADP^+$-dependent MDHs and the coexistence of two pyridine nucleotide pools (NADH versus NADPH) (discussed in Outstanding questions).

The role of the malate shuttle in plant photorespiration

Photorespiration, initiated by the oxygenation reaction of RuBisCo, is inevitable in an oxygen-containing atmosphere. The rate of photorespiration is reduced in land plants performing C4

arrows) and pseudo-CEF (PCEF; orange arrows). Chloroplast-to-mitochondrial (CTM) communication is represented in dark green arrows. Excess NAD(P)H is used by plNAD(P)-MDHs to reduce OAA to malate that is shuttled through chloroplastic malate translocators to fuel the mitochondrial electron transport chain (mETC) for the synthesis of ATP. The CO_2-concentrating mechanism (CCM) is represented in the chloroplast where atmospheric CO_2 is pumped then sequestrated into the pyrenoid. Part of energy needed for CCM comes from the proton motive force generated by photochemical reactions, and another part is likely to be derived from the mETC (dashed black arrow). Note that most of the reactions shown in this figure are also present in higher plants, except the algal CCM. Created with BioRender.com. ACCase, acetyl-CoA carboxylase; ADP, adenosine diphosphate; AGPase, ADP-glucose pyrophosphorylase; ATP, adenosine triphosphate; CBB, Calvin–Benson–Bassham cycle; CEF, cyclic electron flow; Cyt b_6f, cytochrome b_6f complex; ER, enoyl-acyl carrier protein (ACP) reductase; FA, fatty acid; FAS, fatty acid synthase; Fd, ferredoxin; FLV protein, flavodiiron protein; FNR, ferredoxin-$NADP^+$ reductase; G1P, glucose-1-phosphate; G3P, glucose-3-phosphate; KAR, ketoacyl-ACP reductase; Mal, malate; MDH, malate dehydrogenase; mETC, mitochondrial electron transport chain; NAD(P)H, reduced nicotinamide adenine dinucleotide (phosphate); NDA2, NAD(P)H dehydrogenase 2; OAA, oxaloacetate; PC, plastocyanin; PCEF, pseudo-CEF; PETC, photosynthetic electron transport chain; PGR5, proton gradient regulation 5; PGRL1, proton-gradient-like-1; PQ/PQH_2, plastoquinone/plastoquinol; PTOX, plastoquinone terminal oxidase; PS, photosystem; Q_A, quinone A; ROS, reactive oxygen species; TAG, triacylglycerol; TCA cycle, tricarboxylic acid cycle.

photosynthesis and in algae having a CCM [27]. Photorespiration consists of multiple metabolic reactions distributed over four subcellular compartments: chloroplast, cytosol, peroxisome, and mitochondrion, and it therefore requires intimate interorganelle communication. Photorespiratory reactions have a strong impact on cellular energetics, producing NADH in the mitochondria where two glycine molecules are converted to serine, but consuming it in the peroxisome where hydroxypyruvate is converted to glycerate (Figure 1). Therefore, NADH homeostasis in mitochondria and the peroxisome is critical for optimal functioning of photorespiration. Further, changes in the leaf internal CO_2 concentration, as a consequence of an altered stomatal aperture, can impact redox status in the respective organelles through photorespiration. Indeed, in land plants, malate shuttle components (i.e., plNADP-MDH, plNAD-MDH, DiT1, and DiT2.1) are upregulated upon acclimation to low CO_2 and downregulated under elevated CO_2 (where photorespiration is suppressed), suggesting their possible implication in the adaptation of cellular metabolism in response to fluctuating CO_2 availability [28,29].

The malate shuttle contributes to photorespiration at multiple levels (Figure 1). It is involved in the transamination of glyoxylate into glycine coupled with the conversion of glutamate to 2-oxoglutarate in the peroxisome catalyzed by the glutamate:glyoxylate aminotransferase (GGT). The plastidial malate/2-oxoglutarate shuttle provides glutamate from the chloroplast that serves as a donor of NH_3 for the transamination of glyoxylate [30]. Arabidopsis DiT2.1, but not DiT2.2, is a glutamate/malate translocator involved in photorespiration [31]. And moreover, DiT2.1 and DiT1 (AtpOMT1) work in concert for the optimal functioning of photorespiration, and the lack of either DiT2.1 or DiT1 led to growth impairment under photorespiratory conditions [22,31,32].

The malate shuttle is further involved in the export of NADH produced during glycine decarboxylation in mitochondria, thus recycling NAD^+ and ensuring proper functioning of photorespiration. The decrease of mNAD-MDH activity in the *mmdh1* knockout mutant had a strong effect on photorespiratory flux, leading to reduced growth under photorespiration-promoting conditions (i.e., very low CO_2) [33]. In fact, the *mmdh1* mutant displayed a high glycine/serine ratio indicative of impaired glycine decarboxylation due to the lack of the electron acceptor NAD^+ and an over-reduction in the mitochondria. The homeostasis of NAD^+/NADH can be achieved either by increasing the consumption of NADH by mitochondrial reactions or by exporting the excess NADH to other compartments. A likely route for exporting NADH from glycine decarboxylation is through a malate/aspartate shuttle towards peroxisomes where NADH could be consumed by the hydroxypyruvate reductase (HPR), another key reaction of photorespiration (Figure 1). The aspartate/glutamate translocators involved in this malate/aspartate shuttle have been recently characterized in arabidopsis as belonging to the uncoupling protein (UCP) family [11]. Both AtUCP1 and AtUCP2 are able to efficiently counterexchange aspartate and glutamate [11]. Similar to *mmdh1*, mutants of AtUCP1 are impaired in photorespiration with a reduced rate of glycine oxidation in the mitochondria [11]. Therefore, AtUCP1 and 2 and mNAD-MDH1 and 2 work together in photorespiration by forming the malate/aspartate shuttle that connects glycine decarboxylation in the mitochondria with hydroxypyruvate reduction in the peroxisome. We note that redox equivalents derived from photorespiratory glycine decarboxylation in mitochondria may not be necessarily shuttled to the peroxisome but could potentially fuel nitrate and/or hydroxypyruvate reduction in the cytoplasm [34,35]. Antisense repression of plastidial OMT1/DiT1 in tobacco, however, indicates a prominent role of the plastidial malate shuttle in supplying nitrate reduction with NADH [36]. Therefore, the contribution of mitochondria-derived NADH in nitrate reduction in the cytosol could only be minor.

Finally, at the step of hydroxypyruvate reduction into glycerate by the peroxisomal HPR, pNAD-MDH can oxidize malate imported from the cytosol to provide additional reducing equivalents

needed for HPR. Double mutants of pNAD-MDH1 and 2 were, however, viable under photorespiratory conditions (i.e., ambient CO_2), but, the stoichiometry of photorespiratory CO_2 generated per RuBisCo oxygenation was increased by 50% as compared to the wild type [37]. This was explained by an alternative pathway which was thought to be a non-enzymatic conversion of hydroxypyruvate to glycolate, thereby releasing extra CO_2. Timm *et al.* [35] showed that *HPR2* encodes a cytosolic hydroxypyruvate reductase activity (i.e., not peroxisomal) and that reduction of hydroxypyruvate can flexibly shift between peroxisomes and the cytoplasm.

A putative role of the malate shuttle in the algal CCM

To cope with the low CO_2-to-O_2 ratio, unlike plants where photorespiration plays a significant role, microalgae frequently use a CCM. The algal biophysical CCM is an energetic mechanism that pumps and sequestrates atmospheric CO_2 into the pyrenoid close to the active site of RuBisCo, key to the proliferation of algae in their natural habitat where the CO_2 level could be extremely low [27]. In the past 10 years, enzymes (carbonic anhydrases), transcription factors (CCM1), and also several inorganic carbon (Ci) transporters involved in the CCM have been identified and characterized in chlamydomonas [38,39]. Known transporters include the HL-activated 3 (HLA3) protein that is localized at the plasma membrane, a low-carbon inducible protein (LCIA) in the chloroplast envelope, and recently the thylakoid-localized bestrophin-like (BST) transporters [40–43]. However, not until recently has the energization mechanism of the CCM begun to be unveiled.

By studying double mutants of chlamydomonas lacking both PGRL1 and FLV-B mediating the CEF and pseudo-CEF respectively, Burlacot *et al.* [15] showed that double mutants are impaired in growth under air (i.e., a low CO_2 condition) as was the reduced affinity of photosynthesis of the double mutants for Ci. The authors concluded that the pmf produced through the combined action of CEF and pseudo-CEF mechanisms favors the conversion of bicarbonate anions transported by the thylakoid-localized BSTs into CO_2 at the active site of the carboxylating enzyme RuBisCo. By showing that inhibitors of mitochondrial respiration also decrease the affinity of photosynthesis for Ci, Burlacot *et al.* [15] further proposed that mitochondrial respiration serves as an alternative source of energy powering distant transporters involved in the CCM (located either at the plasma membrane or at the chloroplast envelope). Considering that the CCM is a light-driven process, it is thus highly plausible that the malate shuttle contributes to the CCM through mediating redox exchange between chloroplast and mitochondria (Figure 2).

Furthermore, implication of the malate shuttle in the CCM is supported by RNAseq-based transcriptome analyses, revealing the upregulation of putative chloroplastic 2-OG/malate translocators and MDHs in chlamydomonas and also in four phytoplankton species when transferred from a high to a low CO_2 condition [44–46]. Nevertheless, molecular actors and experimental evidence for such a function is yet to come, for example, by investigating the Ci affinity in mutants impaired in malate shuttle mediating the redox exchange between chloroplast and mitochondria.

The malate shuttle mediates interorganelle signaling through ROS

Intercompartmental exchange of signals is key for cellular homeostasis and the acclimation of photosynthetic organisms in fluctuating environments [47]. ROS signaling has been considered a powerful system for the regulation of gene expression, leading to a cascade of physiological adjustments, such as induction of programmed cell death (PCD) [48,49]. ROS can be generated in four major subcellular compartments, that is, chloroplast, peroxisome, mitochondria, and cytosol. ROS are produced when O_2 serves as an alternative electron acceptor during photosynthesis or during mitochondrial electron transport chain and is intimately linked to peroxisome-based fatty acid β-oxidation or photorespiration. ROS signaling has therefore been found to connect organelle

redox state between chloroplast and mitochondria, and between chloroplast and peroxisome [19,49,50]. In the following section, we discuss such examples.

ROS generation in the mitochondria was shown to trigger PCD in the arabidopsis mutant *mod1* (for *mosaic death 1*) affected in the chloroplast enoyl-ACP reductase (ENR) catalyzing the NADH-dependent enoyl-ACP reduction in the fatty acid synthase (FAS) complex [51]. A screen for *mod1* suppressors identified various components of the malate shuttle involved in chloroplast-to-mitochondrion communication, including plNAD-MDH, DiT1, and mNAD-MDH1 [50]. Fatty acid biosynthesis is a major sink for reductant in the chloroplast [52]. Therefore, impairment in ENR leads to overaccumulation of NADH in the chloroplast. The plNAD-MDH, in conjunction with DiT1, allows the export of reducing power in the form of malate. The translocator responsible for malate import into mitochondria is still unknown. Nevertheless, once inside the mitochondrion, malate oxidation by the mNAD-MDH1 generates NADH to fuel mitochondrial complex 1, ultimately resulting in the production of ROS [50]. These mitochondria-generated ROS have been considered as the signaling molecules in triggering PCD in the *mod1* mutant cells [50].

Interorganelle communication from chloroplast to peroxisome has also been proposed to play a role in retrograde signaling in arabidopsis [19]. Under conditions where the photosynthetic chain becomes over-reduced, due to the limitations of the electron acceptor $NADP^+$, molecular oxygen (O_2) can be used to accept electrons coming from PSI [53]. Photoreduction of O_2 can occur via two routes, that is, the non-enzymatic reaction (also known as Mehler reaction) [54,55] and the enzymatic reduction of O_2 [56,57]. In the Mehler reaction, the transfer of electrons from the PSI acceptor side to O_2 is associated with the generation of superoxide O_2^- that could be converted to H_2O_2 by superoxide dismutase (SOD) and then detoxified by the peroxidase located in the chloroplast, such as ascorbate peroxidase (APX). H_2O_2 can also diffuse out into other compartments where it can be detoxified, for instance, in the peroxisome by catalase (CAT) [58]. H_2O_2 is a cellular messenger and has been shown to play an important role as a signaling agent [59]. However, to take up such a role, the intracellular concentration of H_2O_2 must be sufficient to induce the expression of H_2O_2-responsive nuclear genes. The reversible inactivation of CAT in the peroxisome, allowing a burst in H_2O_2, requires the import of reducing equivalents originating from the chloroplast through the malate shuttle to the peroxisome [19,60]. This reversible inactivation of CAT was abolished in the arabidopsis *nadp-mdh* mutants [19], indicating the important role of the light malate valve (i.e., plNADP-MDH) in the regulation of CAT activity by transmitting the redox state of the chloroplast to the peroxisome.

An H_2O_2-based signaling pathway from peroxisome to chloroplast has also been proposed recently in chlamydomonas. The chlamydomonas mutants deficient in the peroxisomal MDH2 exhibited a higher rate of photosynthesis, starch, and *de novo* fatty acid biosynthesis in the chloroplast during photoautotrophic nitrogen deprivation [25]. Communication between the two organelles is proposed to be mediated by an H_2O_2/malate-dependent signaling pathway as supported by an elevated amount of H_2O_2 and malate in the *mdh2* knockout mutants. Exogenously supplied H_2O_2 has a strong positive effect on the expression of starch- and lipid- related genes in wild-type cells of chlamydomonas [61], corroborating that the increase in starch and lipid in the *mdh2* mutants resulted from the increase in the H_2O_2 intracellular concentration [25]. Collectively, the malate shuttle represents a redox-poise system communicating the redox state between compartments involving an H_2O_2-mediated signaling pathway.

The malate shuttle connects fatty acid catabolism to chloroplast metabolism

Fatty acid β-oxidation, photorespiration, and the glyoxylate cycle occur either totally or partially in the peroxisome, making it a third subcellular compartment involved in energy metabolism after

the chloroplast and the mitochondrion [62–64]. In addition, peroxisomes house reactions that produce H_2O_2. Fatty acid degradation and glyoxylate cycle generate the reducing equivalents NADH inside the peroxisome, whereas photorespiration consumes it. Therefore, CO_2 availability, by modulating the activity of photorespiration, can potentially impact these metabolic pathways. Plants and algae have therefore evolved several mechanisms that regulate NADH homeostasis in the peroxisome. This could be achieved either indirectly through the use of metabolite translocators involving the malate shuttle or directly through the import of NAD^+ via the NAD^+ carrier or through NAD^+ regeneration by a local antioxidant system [7,65,66]. In germinating castor bean, the transfer of NADH generated by fatty acid β-oxidation from the peroxisome to the mitochondria was postulated to occur through a malate/aspartate shuttle [67]. In arabidopsis, both direct and indirect routes occur, which include a peroxisomal NAD^+ carrier (PXN) belonging to the mitochondria carrier family (MCF) [7], the two peroxisomal MDHs (pMDH1, pMDH2) [68], the photorespiratory HPR [69], or the components of the ascorbate peroxidase/monodehydroascorbate reductase (APX/MDAR) electron transfer system [70]. The occurrence of these multiple mechanisms suggests the importance of the redox balance control in peroxisomes. Indeed, mutants deficient in either of these pathways have difficulty in seed germination, seedling rigor, or optimal growth.

The occurrence of plant-like peroxisomes has initially been debated in chlamydomonas, and this was mostly built on two observations (i) the lack of a crystalloid core under electron microscopy, typically observed in plant- or animal-type peroxisomes; and (ii) the likely location of catalase in mitochondria based on organelle purification studies [71]. But recent data have firmly established that chlamydomonas does have classical peroxisomes, and the evidence is: (i) peroxisomes have been observed in chlamydomonas under both confocal and electron microscopy [72,73]; (ii) the typical peroxisomal targeting signal 1 or 2 (PTS1/2) is functional in chlamydomonas [73]; (iii) the subcellular localization studies for enzymes of the glyoxylate cycle [4]; (iv) the identification of an H_2O_2-producing activity, that is acyl-CoA oxidase in the peroxisome and its role in fatty acid β-oxidation [63]; (v) catalase 1 is found to be peroxisomal in chlamydomonas [74]; and finally (vi) genes encoding homologs of the arabidopsis proteins involved in redox homeostasis (MDH, PXN, HPR, and MDAR) or in fatty acid β-oxidation are present [75].

That said, except for MDH2, experimental evidence for the function of the other proteins is still lacking. The chlamydomonas *mdh2* mutants, similar to its arabidopsis counterpart (the *pmdh1pmdh2* mutants), were compromised in oil remobilization during nitrogen recovery following a period of N deprivation [25], firmly establishing its contribution to fatty acid β-oxidation in green algae. Interestingly, in addition to peroxisome metabolism, metabolic responses have also been observed in the chloroplast, that is, enhanced photosynthetic activity and enhanced starch and *de novo* fatty acid biosynthesis under high CO_2 conditions (2% CO_2 supplementation of the air). It is worth mentioning here that the phenotypes of the chlamydomonas *mdh2* mutants were suppressed under atmospheric CO_2 levels (photorespiratory conditions), pointing to the complex contribution of diverse pathways to redox management and homeostasis. Nevertheless, the exact route and the molecular identity of the peroxisomal translocators involved remain to be identified (see Outstanding questions).

Concluding remarks and future perspectives

Because variations in environmental parameters may differentially affect the different cellular functions involved in the bioenergetics of photosynthetic cells, which are located in different subcellular compartments, plants and algae have evolved efficient trafficking of reducing equivalents between subcellular compartments to maintain redox homeostasis. Among these mechanisms, the 'malate shuttle' enables efficient transport of reducing equivalents between chloroplasts,

Outstanding questions

Does redox exchange occur between NADH and NADPH pools in the chloroplast? Both plant and algal chloroplasts contain two pools of pyridine nucleotides (NADH versus NADPH). Possible interaction between the two redox pools (NADH versus NADPH) in the chloroplast is not known but is likely mediated by the $NAD(P)^+$ transhydrogenase.

Do chlamydomonas chloroplasts contain an NAD-MDH? CrMDH1 is found peroxisomal based on fusion of the first 25 amino acids at the N terminus to the yellow fluorescent protein, but it is predicted to be chloroplastidial by PredAlgo. A key question is the subcellular location(s) of CrMDH1. The location of this enzyme could have implications for our understanding of metabolism and redox homeostasis not only for the chloroplast but also for the peroxisome.

Is there any connection between the enzymatic and non-enzymatic function of the plastidial NAD-dependent MDH? It was recently shown that the NAD-dependent MDH plays a moonlighting function in chloroplast metabolism and biogenesis. The moonlighting function is an interesting feature of some proteins to have more than one function in the cell. In addition to its enzymatic function as malate dehydrogenase, the plastidial NAD-dependent MDH plays a central role in chloroplast biogenesis through its physical interaction with the FtsH12–FtsHi protease complex. However, it is still not clear whether these two functions are connected or what is the biological significance of grouping these two functions (enzymatic and structural) in one widespread protein such as MDH.

What is the identity of the peroxisomal malate translocator? This is probably one of the most elusive components of peroxisome redox metabolism. Putative candidates are emerging with modern proteomics analysis of isolated peroxisomes.

What is the interaction between redox trafficking through the malate shuttle and carbon storage in microalgae? Starch and fatty acid biosynthesis are a major sink of cellular carbon and energy. Their synthesis requires a

cytosol, mitochondria, and peroxisomes. Research in recent decades has shed light on the role of the malate shuttle in key subcellular pathways, including photosynthesis, photorespiration, fatty acid β-oxidation, nitrogen assimilation, and interorganelle signaling, but has also raised new questions (detailed in Outstanding questions). Beyond physiology and energy homeostasis, emerging literature suggests a critical role for the malate shuttle in the CCM [15] and carbon storage [25].

Future investigations towards a detailed understanding of the malate shuttle mechanism in plants and algae should involve the combination of cutting-edge molecular genetics tools for creating combinatory mutations in different genes, overexpressing multiple isoforms combined with the use of ^{13}C labeling techniques to monitor changes in metabolic fluxes. We envision that emerging genetically encoded biosensors to monitor real-time changes in subcellular redox and ATP status will be valuable to monitor in real time redox status in subcellular compartments [76,77]. Taken together, by connecting energy homeostasis to carbon and nitrogen metabolism, the malate shuttle represents an exciting target for engineering the cellular energetic status for better climate resilience and for improved production of plant and algal biomass for food, fuel, and biomaterials, key to a sustainable and greener future.

carbon source, ATP, and NAD(P)H but at different ratios. Alterations of redox trafficking and cell energetic metabolism could have direct consequences for biomass productivity and composition.

What is the nature of the malate uniport mechanism in C4 plants? Using isolated chloroplasts from a range of C4 plants, two types of malate uniporters have been found, one coupled to sodium symport (in most C4 species tested), the other coupled to proton symport (in maize, sorghum, and sugar cane). In contrast to the metabolite translocators, this type of malate transporter would allow for net malate transport for, for example, the malic enzyme reaction.

Acknowledgments

O.D. thanks The French Atomic Energy and Alternative Energy Commission (CEA) for a PhD scholarship. G.P. and Y.L.-B. thank the continuous financial support of CEA (LD-power, CO2Storage). F.K. and A.P.M.W. acknowledge funding by the Deutsche Forschungsgemeinschaft (DFG, German Research Foundation) – Project-ID 267205415 – CRC 1208 and under Germany's Excellence Strategy EXC-2048/1, Project ID 390686111.

Declaration of interests

No interests were declared.

References

1. Raghavendra, A.S. and Padmasree, K. (2003) Beneficial interactions of mitochondrial metabolism with photosynthetic carbon assimilation. *Trends Plant Sci.* 8, 546–553
2. Weber, A.P.M. and Linka, N. (2011) Connecting the plastid: transporters of the plastid envelope and their role in linking plastidial with cytosolic metabolism. *Annu. Rev. Plant Biol.* 62, 53–77
3. Neuhaus, H.E. and Wagner, R. (2000) Solute pores, ion channels, and metabolite transporters in the outer and inner envelope membranes of higher plant plastids. *Biochim. Biophys. Acta (Biomembranes)* 1465, 307–323
4. Lauersen, K.J. *et al.* (2016) Peroxisomal microbodies are at the crossroads of acetate assimilation in the green microalga *Chlamydomonas reinhardtii*. *Algal Res.* 16, 266–274
5. Ludwig, M. (2016) The roles of organic acids in C4 photosynthesis. *Front. Plant Sci.* 7, 647
6. Eisenhut, M. *et al.* (2019) Mechanistic understanding of photorespiration paves the way to a new green revolution. *New Phytol.* 223, 1762–1769
7. van Roermund, C.W.T. *et al.* (2016) The peroxisomal NAD carrier from *Arabidopsis* imports NAD in exchange with AMP1 [OPEN]. *Plant Physiol.* 171, 2127–2139
8. Hashida, S. and Kawai-Yamada, M. (2019) Inter-organelle NAD metabolism underpinning light responsive NADP dynamics in plants. *Front. Plant Sci.* 10, 960
9. Palmieri, F. *et al.* (2009) Molecular identification and functional characterization of *Arabidopsis thaliana* mitochondrial and chloroplastic NAD^+ carrier proteins*. *J. Biol. Chem.* 284, 31249–31259
10. Selinski, J. and Scheibe, R. (2019) Malate valves: old shuttles with new perspectives. *Plant Biol. (Stuttg)* 21, 21–30
11. Monné, M. *et al.* (2018) Uncoupling proteins 1 and 2 (UCP1 and UCP2) from *Arabidopsis thaliana* are mitochondrial transporters of aspartate, glutamate, and dicarboxylates. *J. Biol. Chem.* 293, 4213–4227
12. Lee, C.P. and Millar, A.H. (2016) The plant mitochondrial transportome: balancing metabolic demands with energetic constraints. *Trends Plant Sci.* 21, 662–676
13. Allen, J.F. (2002) Photosynthesis of ATP – electrons, proton pumps, rotors, and poise. *Cell* 110, 273–276
14. Kramer, D.M. and Evans, J.R. (2011) The importance of energy balance in improving photosynthetic productivity. *Plant Physiol.* 155, 70–78
15. Burlacot, A. *et al.* (2021) Alternative electron pathways of photosynthesis drive the algal CO_2 concentrating mechanism. *bioRxiv* Published online February 27, 2021. https://doi.org/10.1101/2021.02.25.432959
16. Erickson, E. *et al.* (2015) Light stress and photoprotection in *Chlamydomonas reinhardtii*. *Plant J.* 82, 449–465
17. Alric, J. and Johnson, X. (2017) Alternative electron transport pathways in photosynthesis: a confluence of regulation. *Curr. Opin. Plant Biol.* 37, 78–86
18. Burlacot, A. *et al.* (2019) Subcellular energetics and carbon storage in *Chlamydomonas*. *Cells* 8, 1154
19. Heyno, E. *et al.* (2014) Putative role of the malate valve enzyme NADP–malate dehydrogenase in H_2O_2 signalling in *Arabidopsis*. *Philos. Trans. R. Soc. B Biol. Sci.* 369, 20130228
20. Hebbelmann, I. *et al.* (2012) Multiple strategies to prevent oxidative stress in *Arabidopsis* plants lacking the malate valve enzyme NADP-malate dehydrogenase. *J. Exp. Bot.* 63, 1445–1459
21. Yokochi, Y. *et al.* (2021) Redox regulation of NADP-malate dehydrogenase is vital for land plants under fluctuating light environment. *PNAS* 118, e2016903118
22. Kinoshita, H. *et al.* (2011) The chloroplastic 2-oxoglutarate/malate transporter has dual function as the malate valve and in carbon/nitrogen metabolism. *Plant J.* 65, 15–26
23. Lemaire, S.D. *et al.* (2005) NADP-malate dehydrogenase from unicellular green alga *Chlamydomonas reinhardtii*. A first step toward redox regulation? *Plant Physiol.* 137, 514–521

24. Dang, K.-V. *et al.* (2014) Combined increases in mitochondrial cooperation and oxygen photoreduction compensate for deficiency in cyclic electron flow in *Chlamydomonas reinhardtii*. *Plant Cell* 26, 3036–3050
25. Kong, F. *et al.* (2018) Interorganelle communication: peroxisomal malate dehydrogenase2 connects lipid catabolism to photosynthesis through redox coupling in *Chlamydomonas*. *Plant Cell* 30, 1824–1847
26. Massoz, S. *et al.* (2015) Isolation of *Chlamydomonas reinhardtii* mutants with altered mitochondrial respiration by chlorophyll fluorescence measurement. *J. Biotechnol.* 215, 27–34
27. Wang, Y. *et al.* (2015) The CO_2 concentrating mechanism and photosynthetic carbon assimilation in limiting CO_2: how *Chlamydomonas* works against the gradient. *Plant J.* 82, 429–448
28. Backhausen, J.E. and Scheibe, R. (1999) Adaptation of tobacco plants to elevated CO_2: influence of leaf age on changes in physiology, redox states and NADP-malate dehydrogenase activity. *J. Exp. Bot.* 50, 665–675
29. Li, Y. *et al.* (2014) Was low CO_2 a driving force of C4 evolution: *Arabidopsis responses* to long-term low CO_2 stress. *J. Exp. Bot.* 65, 3657–3667
30. Takahashi, S. *et al.* (2007) Impairment of the photorespiratory pathway accelerates photoinhibition of photosystem ii by suppression of repair but not acceleration of damage processes in *Arabidopsis*. *Plant Physiol.* 144, 487–494
31. Renné, P. *et al.* (2003) The *Arabidopsis* mutant dct is deficient in the plastidic glutamate/malate translocator DiT2. *Plant J.* 35, 316–331
32. Taniguchi, M. *et al.* (2002) Identifying and characterizing plastidic 2-oxoglutarate/malate and dicarboxylate transporters in *Arabidopsis thaliana*. *Plant Cell Physiol.* 43, 706–717
33. Lindén, P. *et al.* (2016) Reduced mitochondrial malate dehydrogenase activity has a strong effect on photorespiratory metabolism as revealed by 13C labelling. *J. Exp. Bot.* 67, 3123–3135
34. Bloom, A.J. *et al.* (2010) Carbon dioxide enrichment inhibits nitrate assimilation in wheat and arabidopsis. *Science* 328, 899–903
35. Timm, S. *et al.* (2008) A cytosolic pathway for the conversion of hydroxypyruvate to glycerate during photorespiration in arabidopsis. *Plant Cell* 20, 2848–2859
36. Schneidereit, J. *et al.* (2006) Antisense repression reveals a crucial role of the plastidic 2-oxoglutarate/malate translocator DiT1 at the interface between carbon and nitrogen metabolism. *Plant J.* 45, 206–224
37. Cousins, A.B. *et al.* (2008) Peroxisomal malate dehydrogenase is not essential for photorespiration in arabidopsis but its absence causes an increase in the stoichiometry of photorespiratory CO_2 release. *Plant Physiol.* 148, 786–795
38. Moroney, J.V. *et al.* (2011) The carbonic anhydrase isoforms of *Chlamydomonas reinhardtii*: intracellular location, expression, and physiological roles. *Photosynth. Res.* 109, 133–149
39. Mackinder, L.C.M. *et al.* (2017) A spatial interactome reveals the protein organization of the algal CO_2-concentrating mechanism. *Cell* 171, 133–147.e14
40. Duanmu, D. *et al.* (2009) Knockdown of limiting-CO_2-induced gene HLA3 decreases HCO_3^- transport and photosynthetic Ci affinity in *Chlamydomonas reinhardtii*. *PNAS* 106, 5990–5995
41. Wang, Y. and Spalding, M.H. (2014) Acclimation to very low CO_2: contribution of limiting CO_2 inducible proteins, LCIB and LCIA, to inorganic carbon uptake in *Chlamydomonas reinhardtii*. *Plant Physiol.* 166, 2040–2050
42. Mukherjee, A. *et al.* (2019) Thylakoid localized bestrophin-like proteins are essential for the CO_2 concentrating mechanism of *Chlamydomonas reinhardtii*. *Proc. Natl. Acad. Sci. U. S. A.* 116, 16915–16920
43. Kono, A. and Spalding, M.H. (2020) LCI1, a Chlamydomonas reinhardtii plasma membrane protein, functions in active CO_2 uptake under low CO_2. *Plant J.* 102, 1127–1141
44. Hennon, G.M.M. *et al.* (2017) Diverse CO_2-induced responses in physiology and gene expression among eukaryotic phytoplankton. *Front. Microbiol.* 8, 2547
45. Yamano, T. *et al.* (2008) Expression analysis of genes associated with the induction of the carbon-concentrating mechanism in *Chlamydomonas reinhardtii*. *Plant Physiol.* 147, 340–354
46. Miura, K. *et al.* (2004) Expression profiling-based identification of CO_2-responsive genes regulated by CCM1 controlling a carbon-concentrating mechanism in *Chlamydomonas reinhardtii*. *Plant Physiol.* 135, 1595–1607
47. Czarnocka, W. and Karpiński, S. (2018) Friend or foe? Reactive oxygen species production, scavenging and signaling in plant response to environmental stresses. *Free Radic. Biol. Med.* 122, 4–20
48. Dietz, K.-J. *et al.* (2016) Redox- and reactive oxygen species-dependent signaling into and out of the photosynthesizing chloroplast. *Plant Physiol.* 171, 1541–1550
49. Zhao, Y. *et al.* (2020) Malate circulation: linking chloroplast metabolism to mitochondrial ROS. *Trends Plant Sci.* 25, 446–454
50. Zhao, Y. *et al.* (2018) Malate transported from chloroplast to mitochondrion triggers production of ROS and PCD in *Arabidopsis thaliana*. *Cell Res.* 28, 448–461
51. Mou, Z. *et al.* (2000) Deficiency in fatty acid synthase leads to premature cell death and dramatic alterations in plant morphology. *Plant Cell* 12, 405–417
52. Li-Beisson, Y. *et al.* (2019) The lipid biochemistry of eukaryotic algae. *Prog. Lipid Res.* 74, 31–68
53. Allen, J.F. (1975) Oxygen reduction and optimum production of ATP in photosynthesis. *Nature* 256, 599–600
54. Mehler, A.H. (1951) Studies on reactions of illuminated chloroplasts: I. Mechanism of the reduction of oxygen and other hill reagents. *Arch. Biochem. Biophys.* 33, 65–77
55. Curien, G. *et al.* (2016) The water to water cycles in microalgae. *Plant Cell Physiol.* 57, 1354–1363
56. Chaux, F. *et al.* (2017) Flavodiiron proteins promote fast and transient O_2 photoreduction in *Chlamydomonas*. *Plant Physiol.* 174, 1825–1836
57. Gerotto, C. *et al.* (2016) Flavodiiron proteins act as safety valve for electrons in *Physcomitrella patens*. *PNAS* 113, 12322–12327
58. Mubarakshina, M.M. *et al.* (2010) Production and diffusion of chloroplastic H_2O_2 and its implication to signalling. *J. Exp. Bot.* 61, 3577–3587
59. Gadjev, I. *et al.* (2006) Transcriptomic footprints disclose specificity of reactive oxygen species signaling in *Arabidopsis*. *Plant Physiol.* 141, 436–445
60. Michelet, L. *et al.* (2013) Down-regulation of catalase activity allows transient accumulation of a hydrogen peroxide signal in *Chlamydomonas reinhardtii*. *Plant Cell Environ.* 36, 1204–1213
61. Blaby, I.K. *et al.* (2015) Genome-wide analysis on *Chlamydomonas reinhardtii* reveals the impact of hydrogen peroxide on protein stress responses and overlap with other stress transcriptomes. *Plant J.* 84, 974–988
62. Lazarow, P.B. (2016) Peroxisomes. In *Encyclopedia of Cell Biology* (Bradshaw, R.A. and Stahl, P.D., eds), pp. 248–272, Academic Press
63. Kong, F. *et al.* (2017) *Chlamydomonas* carries out fatty acid β-oxidation in ancestral peroxisomes using a bona fide acyl-CoA oxidase. *Plant J.* 90, 358–371
64. Plancke, C. *et al.* (2014) Lack of isocitrate lyase in *Chlamydomonas* leads to changes in carbon metabolism and in the response to oxidative stress under mixotrophic growth. *Plant J.* 77, 404–417
65. Gakière, B. *et al.* (2018) NAD^+ biosynthesis and signaling in plants. *Crit. Rev. Plant Sci.* 37, 259–307
66. Charton, L. *et al.* (2019) Plant peroxisomal solute transporter proteins. *J. Integr. Plant Biol.* 61, 817–835
67. Mettler, I.J. and Beevers, H. (1980) Oxidation of NADH in glyoxysomes by a malate-aspartate shuttle. *Plant Physiol.* 66, 555–560
68. Pracharoenwattana, I. *et al.* (2007) *Arabidopsis* peroxisomal malate dehydrogenase functions in β-oxidation but not in the glyoxylate cycle. *Plant J.* 50, 381–390
69. Pracharoenwattana, I. *et al.* (2009) Fatty acid beta-oxidation in germinating *Arabidopsis* seeds is supported by peroxisomal hydroxypyruvate reductase when malate dehydrogenase is absent. *Plant Mol. Biol.* 72, 101
70. Eastmond, P.J. (2007) Monodehyroascorbate reductase4 is required for seed storage oil hydrolysis and postgerminative growth in *Arabidopsis*. *Plant Cell* 19, 1376–1387

71. Kato, J. *et al.* (1997) Characterization of catalase from green algae *Chlamydomonas reinhardtii*. *J. Plant Physiol.* 151, 262–268
72. Hayashi, Y. *et al.* (2015) Increase in peroxisome number and the gene expression of putative glyoxysomal enzymes in *Chlamydomonas* cells supplemented with acetate. *J. Plant Res.* 128, 177–185
73. Hayashi, Y. and Shinozaki, A. (2012) Visualization of microbodies in *Chlamydomonas reinhardtii*. *J. Plant Res.* 125, 579–586
74. Kato, N. *et al.* (2021) Subcellular localizations of catalase and exogenously added fatty acid in *Chlamydomonas reinhardtii*. *Cells* 10, 1940
75. Kong, F. *et al.* (2018) Lipid catabolism in microalgae. *New Phytol.* 218, 1340–1348
76. Voon, C.P. *et al.* (2018) ATP compartmentation in plastids and cytosol of *Arabidopsis thaliana* revealed by fluorescent protein sensing. *PNAS* 115, E10778–E10787
77. Elsässer, M. *et al.* (2020) Photosynthetic activity triggers pH and NAD redox signatures across different plant cell compartments. *bioRxiv* Published online November 1, 2020. https://doi.org/10.1101/2020.10.31.363051
78. Beeler, S. *et al.* (2014) Plastidial NAD-dependent malate dehydrogenase is critical for embryo development and heterotrophic metabolism in *Arabidopsis*. *Plant Physiol.* 164, 1175–1190
79. An, Y. *et al.* (2016) Purification and characterization of the plastid-localized NAD-dependent malate dehydrogenase from *Arabidopsis thaliana*. *Biotechnol. Appl. Biochem.* 63, 490–496
80. Schreier, T.B. *et al.* (2018) Plastidial NAD-dependent malate dehydrogenase: a moonlighting protein involved in early chloroplast development through its interaction with an FtsH12-FtsHi protease complex. *Plant Cell* 30, 1745–1769
81. Huang, J. *et al.* (2018) Self-protection of cytosolic malate dehydrogenase against oxidative stress in *Arabidopsis*. *J. Exp. Bot.* 69, 3491–3505
82. Liszka, A. *et al.* (2020) Three cytosolic NAD-malate dehydrogenase isoforms of *Arabidopsis thaliana*: on the crossroad between energy fluxes and redox signaling. *Biochem. J.* 477, 3673–3693
83. Tomaz, T. *et al.* (2010) Mitochondrial malate dehydrogenase lowers leaf respiration and alters photorespiration and plant growth in *Arabidopsis*. *Plant Physiol.* 154, 1143–1157
84. Sew, Y.S. *et al.* (2016) Loss of mitochondrial malate dehydrogenase activity alters seed metabolism impairing seed maturation and post-germination growth in *Arabidopsis*. *Plant Physiol.* 171, 849–863
85. Picault, N. *et al.* (2002) Identification of a novel transporter for dicarboxylates and tricarboxylates in plant mitochondria. Bacterial expression, reconstitution, functional characterization, and tissue distributioN. *J. Biol. Chem.* 277, 24204–24211
86. Palmieri, L. *et al.* (2008) Molecular identification of three *Arabidopsis thaliana* mitochondrial dicarboxylate carrier isoforms: organ distribution, bacterial expression, reconstitution into liposomes and functional characterization. *Biochem. J.* 410, 621–629
87. Lee, C.P. *et al.* (2021) The versatility of plant organic acid metabolism in leaves is underpinned by mitochondrial malate–citrate exchange. *Plant Cell* Published online September 8, 2021. https://doi.org/10.1093/plcell/koab223
88. Nogales, J. *et al.* (2004) Functional analysis and regulation of the malate synthase from *Chlamydomonas reinhardtii*. *Planta* 219, 325–331
89. Bogaert, K.A. *et al.* (2019) Metabolic, physiological, and transcriptomics analysis of batch cultures of the green microalga *Chlamydomonas* grown on different acetate concentrations. *Cells* 8, 1367
90. Wynn, J.P. and Ratledge, C. (1997) Malic enzyme is a major source of NADPH for lipid accumulation by *Aspergillus nidulans*. *Microbiology* 143, 253–257
91. Zell, M.B. *et al.* (2010) Analysis of *Arabidopsis* with highly reduced levels of malate and fumarate sheds light on the role of these organic acids as storage carbon molecules. *Plant Physiol.* 152, 1251–1262
92. Zhu, B.-H. *et al.* (2018) he role of malic enzyme on promoting total lipid and fatty acid production in *Phaeodactylum tricornutum*. *Front. Plant Sci.* 9, 826
93. Schlüter, U. and Weber, A.P.M. (2020) Regulation and evolution of C4 photosynthesis. *Annu. Rev. Plant Biol.* 71, 183–215
94. Merchant, S.S. *et al.* (2007) The *Chlamydomonas* genome reveals the evolution of key animal and plant functions. *Science* 318, 245–250
95. Tardif, M. *et al.* (2012) PredAlgo: a new subcellular localization prediction tool dedicated to green algae. *Mol. Biol. Evol.* 29, 3625–3639
96. Weber, A.P.M. and Linka, N. (2011) Connecting the plastid: transporters of the plastid envelope and their role in linking plastidial with cytosolic metabolism. *Annu. Rev. Plant Biol.* 62, 53–77
97. Torre, F. de la *et al.* (2006) Identification and functional analysis of a prokaryotic-type aspartate aminotransferase: implications for plant amino acid metabolism. *Plant J.* 46, 414–425
98. Schultz, C.J. and Coruzzi, G.M. (1995) The aspartate aminotransferase gene family of *Arabidopsis* encodes isoenzymes localized to three distinct subcellular compartments. *Plant J.* 7, 61–75
99. Muñoz-Blanco, J. *et al.* (1988) Characterization of an l-aspartate aminotransferase activity in *Chlamydomonas reinhardtii*. *Physiol. Plant.* 74, 433–439
100. Journet, E.-P. *et al.* (1981) Role of glutamate-oxaloacetate transaminase and malate dehydrogenase in the regeneration of NAD^+ for glycine oxidation by spinach leaf mitochondria. *Plant Physiol.* 67, 467–469

II. Objectives of this PhD thesis

Objectives

Previous work in our lab has revealed that disruption of the peroxisomal malate dehydrogenase 2 (MDH2) led not only to a defect in TAG remobilization, but also affected photosynthesis and starch metabolism in the chloroplast (Kong et al., 2018). This finding points to the occurrence of active redox communication between subcellular organelles, and to the importance of subcellular energetic context on cell growth and carbon reserve formation. The aim of this PhD thesis is therefore to pursue effort in understanding the interplay between mechanisms that balance cellular energetic status with carbon storage in the model microalga *Chlamydomonas reinhardtii*. In another word, how the lack of those mechanisms affects the capacity of biomass production and the accumulation of carbon reserves such as lipids and starch. The relationship between energy trafficking and its impact on carbon reserve formation is conceptualized in **Figure II.1**.

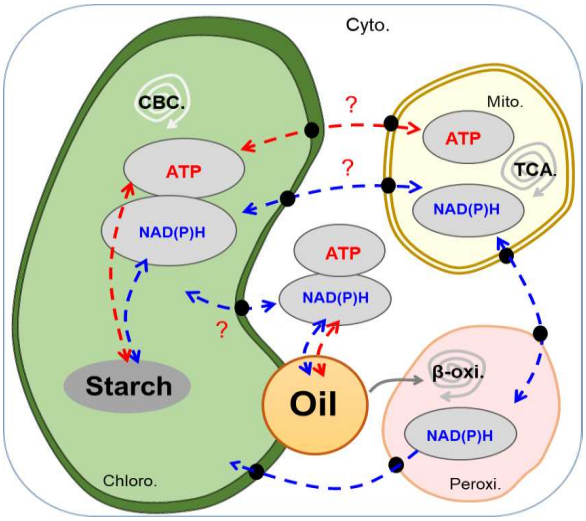

Figure II.1: The hypothetic inter-compartment exchange of cellular energy currencies, ATP and NAD(P)H, and their interactions with carbon storage in *Chlamydomonas reinhardtii*.
Question marks denote putative or unknown mechanisms/transporters that are likely to operate according to our hypothesis. NAD(P)H pool includes NAD^+, NADH and $NADP^+$ and NADPH. Blue arrows refer to reductant power exchange in the form of metabolite shuttles (such as malate, oxaloacetate etc.) whereas red arrows represent ATP/ADP exchange. Interactions with starch and oil are bidirectional and could be either synthesis (consumption) or degradation (release of energy).
Abbreviations: ATP, adenosine triphosphate; β-oxi., β-oxidation; CBC, Calvin Benson cycle; NAD(P)H, nicotinamide adenine dinucleotide (phosphate); TCA, tricarboxylic acid cycle.

To address this question, we took a reverse genetic approach by evaluating genotype-phenotype relations in mutants of Chlamydomonas defected in known or putative electron management pathways. Specifically,

- We examined photosynthetic performance and carbon storage capacity of some known CEF and PCEF mutants (*pgrl1*, *flvB*) already available in our group during N deficiency (**Chapter 1 and Annex 2**).
- We then focused on investigating putative actors of inter-compartment energy exchange including malate dehydrogenases (MDHs) and translocators involved in malate shuttle; ATP/ADP translocators involved in ATP import in the chloroplast and the nicotinamide nucleotide transhydrogenase (NNT) catalyzing the reversible exchange of reducing power between the NAD^+ and NADPH pools. These candidates and their hypothetic subcellular locations are shown in a metabolic context (**Fig. II.1**). For this, we took advantage of the CLiP collection, where large number of insertional mutants are available (Li et al., 2016). The corresponding mutants examined and preliminary characterizations of some of these mutants are collectively presented in **Chapter 2**.
- Finally, we characterized a low carbon inducible protein 20 (LCI20) annotated as a putative 2-oxoglutarate/malate translocator and we report here its physiological functions (**Chapter 3** and **Annex 3**).

In parallel, I participated in characterizing the role of alternative electron pathways (CEF and PCEF) in supplying energy to drive carbon-concentrating mechanism (CCM). This work is part of the PhD thesis work of Adrien Burlacot (in our team), and the key results have been published in Nature (Burlacot et al., 2022)(**Chapter 4** and **Annex 4).** I am a second author in this paper, where I have:

- characterized the growth performance of *pgrl1*, *flvB* and *pgrl1 flvB* under different CO_2 and light regime.
- performed immunoblot to assess the quantity of major CCM and photosynthetic proteins.
- characterized the photosynthetic performance of the *pgrl1 flvB* double mutants.
- determined the maximum PSII efficiency (Fv/Fm) of all the strains.
- performed PCR to validate genotype after genetic crosses.

I have been involved in dissecting the relative contribution of different photosynthesis alternative pathways in sustaining CO_2 fixation in Chlamydomonas (**Annex 1**). My contributions are: (1) Validate the effect of mitochondrial inhibitors on the growth rate by using spot testing to confirm the observed phenotype at the physiological level (MIMS). (2) Prepare and maintain the cultures for MIMS experiments.

Ongoing work and future directions are presented in the "General conclusion and Perspective" section. The combination of the above-mentioned approaches should allow us to make one step further in our understanding of the relationship between energy management pathways and carbon storage in microalgae.

III. Results

Chapter 1: Photosynthetic regulation during phototrophic nitrogen limitation

Foreword

Nitrogen (N) is an essential building block of all living organisms. Assimilation and reduction of inorganic nitrogen requires energy in the form of NAD(P)H. In C3 and C4 plants, 10-20% of total photosynthetic electron flow is dedicated for N reduction (Champigny, 1995). Limitation in N is one of the most important environmental phenomena that affects global primary biomass productivity on land and in the ocean (LeBauer and Treseder, 2008). Under such condition, cell division and photosynthesis are downregulated while the reductant usually used for N reduction together with the carbon backbone used for amino acid synthesis are channelled to synthesize starch and TAGs (Juergens et al., 2015). The regulatory mechanism for controlling photosynthetic electron production and management during N limitation is unknown and remains to be unveiled.

Several alternative pathways have been identified in the model green microalga *Chlamydomonas reinhardtii* (Chlamydomonas) including: The type II NADPH dehydrogenase (Nda)-mediated cyclic electron flow (CEF) (Desplats et al., 2009); the proton gradient regulator 5 (PGR5)/PGR like 1 (PGRL1)-mediated CEF (Tolleter et al., 2011) and the O_2 photoreduction mediated by the flavodiiron protein (FLV) (Gerotto et al., 2016; Chaux et al., 2017a). Those pathways have been extensively studied during the acclimation of photosynthesis to fluctuating light and CO_2 levels (Dang et al., 2014; Jokel et al., 2015; Chaux et al., 2017a; Burlacot et al., 2022). However, their function during nutrient shortage has been overlooked.

In this chapter, we dissected the role of PGRL1 and FLV in regulating photosynthetic electron flow and how they affect carbon storage capacity in Chlamydomonas during photoautotrophic N deficiency. Both PGRL1 and FLV are involved in extra ATP production by generating additional proton motive force used by the ATP synthase in the thylakoid membrane. In the absence of PGRL1, FLV mediated O_2-photoreduction was upregulated during high light (Dang et al., 2014). It has been shown that both are required for the functioning of algal CCM and can compensate each other during CCM energization (Burlacot et al., 2022). Compensation between the two pathways have therefore often been reported, but whether they play a role during N deficiency remains to be investigated. We investigated in this chapter therefore the role of PGRL1/FLV during adaptation to N starvation.

Chapter I

Cyclic and pseudo-cyclic electron pathways play antagonistic roles during nitrogen deficiency in *Chlamydomonas reinhardtii*

(BioRxiv DOI: 10.1101/2023.01.18.524499)

Ousmane Dao[1*], Adrien Burlacot[2,3], Felix Buchert[4], Marie Bertrand[1], Pascaline Auroy[1], Carolyne Stoffel[2], Jacob Irby[2], Michael Hippler[4,5], Gilles Peltier[1], Yonghua Li-Beisson[1*]

[1]Aix Marseille Univ, CEA, CNRS, Institute of Biosciences and Biotechnology of Aix Marseille, BIAM, CEA Cadarache, Saint Paul-Lez-Durance, France
[2]Department of Plant Biology, The Carnegie Institution for Science, Stanford, CA, 94305 USA
[3]Department of Biology, Stanford University, Stanford, CA, 94305, USA
[4]Institute of Plant Biology and Biotechnology, University of Münster, 48143 Münster, Germany
[5]Institute of Plant Science and Resources, Okayama University, Kurashiki 710-0046, Japan

***Correspondence to:** Yonghua Li-Beisson (yonghua.li@cea.fr) or Ousmane Dao (ousmanedao17@yahoo.fr)

ORCID IDs: 0000-0002-7040-5770 (O.D.), 0000-0001-7434-6416 (A.B.), 0000-0001-6704-6634 (F.B.), 0000-0001-5098-1554 (M.B), 0000-0002-3376-6550 (P.A.), 0000-0002-4078-6250 (C.S.), 0000-0001-9670-6101 (M.H.), 0000-0002-2226-3931 (G.P.), 0000-0003-1064-1816 (Y.L.-B.)

Competing Interest Statement: There are no conflicts of interest.

Classification: Biological Sciences: Plant Biology

Keywords: Nitrogen deficiency; Flavodiiron proteins; Cyclic electron flow; Triacylglycerol; Photosynthetic regulation

Abstract

Nitrogen (N) scarcity is a frequently encountered situation that constrains global biomass productivity. In response to N deficiency, cell division stops and photosynthetic electron transfer is downregulated, while carbon storage is enhanced. However, the molecular mechanism downregulating photosynthesis during N deficiency and its relationship with carbon storage are not fully understood. The Proton Gradient Regulator-like 1 (PGRL1) controlling cyclic electron flow (CEF) and Flavodiiron proteins involved in pseudo-(CEF) are major players in the acclimation of photosynthesis. To determine the role of PGRL1 or FLV in photosynthesis under N deficiency, we measured photosynthetic electron transfer, oxygen gas exchange and carbon storage in *Chlamydomonas pgrl1* and *flvB* knockout mutants. Under N deficiency, *pgrl1* maintains higher net photosynthesis and O_2 photoreduction rates, while *flvB* shows a similar response compared to control strains. Cytochrome b_6f and PSI are maintained at a higher abundance in *pgrl1*. The photosynthetic activity of *flvB* and *pgrl1 flvB* double mutants decreases in response to N deficiency similar to the control strains. Furthermore, the preservation of photosynthetic activity in *pgrl1* is accompanied by an increased accumulation of triacylglycerol depending on the genetic background. Taken together, our results suggest that in the absence of PGRL1-controlled CEF, FLV-mediated PCEF maintains net photosynthesis at a high level and that CEF and PCEF play antagonistic roles during N deficiency. It further illustrates how nutrient status and genetic makeup of a strain can affect the regulation of photosynthetic energy conversion in relation to carbon storage and provides new strategies for improving lipid productivity in algae.

Significance statement

Nitrogen (N) deficiency, an often-encountered phenomenon in nature, results in growth arrest, downregulation of photosynthesis and massive carbon storage in microalgae. However, more mechanistic insights involved in tuning photosynthetic electron transfer during N deficiency are required. Here, we provide evidence that a well-conserved protein in chlorophytes, the Proton Gradient Regulator-like 1 (PGRL1), is a key regulator of photosynthesis during N deficiency. In its absence, cells exhibited sustained photosynthesis thanks to the Flavodiiron (FLV) proteins. We propose that both PGRL1 and FLV, by having antagonistic roles in N deficiency, manage the redox landscape, carbon storage and biomass production. Our work revolves around the current paradigm of photosynthesis regulation during N deficiency and provides a new framework for improving biomass production and carbon storage in microalgae for biotechnological purposes.

Chapter I

Introduction

Nitrogen (N) deficiency is one of the most harsh environmental situation that constrains global primary biomass productivity in all ecosystems (Vitousek and Howarth, 1991; LeBauer and Treseder, 2008; Du et al., 2020). Under N deficiency, cell division stops and photosynthetic CO_2 assimilation is downregulated, the carbon and energy being used to synthesize starch and triacylglycerols (TAGs) (Siaut et al., 2011; Schmollinger et al., 2014; Juergens et al., 2015; Schulz-Raffelt et al., 2016). The downregulation of photosynthetic electron transfer (PET) reactions, together with a re-routing of the excess reducing power towards carbon storage, prevents the over-production of reactive oxygen species, thus ensuring cell fitness (Zhang et al., 2013; Park et al., 2015; Gargouri et al., 2017; Du et al., 2018; Tran et al., 2019).

Due to the variability in their natural habitat, microalgae must constantly adjust the photosynthetic conversion of energy to match the metabolic demand and have therefore developed a set of regulatory mechanisms to fine-tune electron transfer reactions. During photosynthesis, energy in the form of ATP and NADPH is mostly produced by the linear electron flow (LEF) (Allen, 2003). The balance of ATP and NADPH is essential for optimal CO_2 capture and metabolism to which cyclic electron flow (CEF) and pseudo-cyclic electron flow (PCEF) play a critical role (Dang et al., 2014; Bailleul et al., 2015; Burlacot et al., 2019; Saroussi et al., 2019; Peltier et al., 2023). Two pathways of CEF around PSI have been described in the green microalga *Chlamydomonas reinhardtii* (*Chlamydomonas* hereafter), one involving the type II NADPH dehydrogenase (NDA2) (Desplats et al., 2009), and the other being controlled by the proton gradient regulator 5 (PGR5)/PGR-like 1 (PGRL1) proteins (Tolleter et al., 2011).

Recent work in *Chlamydomonas* provided evidence that PGR5 and PGRL1 are involved in CEF (Petroutsos et al., 2009; Tolleter et al., 2011; Johnson et al., 2014). Hereby PGR5 is required for efficient stromal electron intake into the cytochrome b_6f complex (Cyt b_6f) (Buchert et al., 2020). Its deletion thereby strongly disturbs the Mitchellian Q cycle (Buchert et al., 2020). Also, deletion of PGRL1 impacts CEF in *Chlamydomonas* (Petroutsos et al., 2009; Tolleter et al., 2011). Despite the fact that PGRL1 has been implicated in plastoquinone reduction during CEF (Hertle et al., 2013), it appears that PGRL1 is rather important for PGR5 expression and protein stability, as in the absence of PGRL1, PGR5 is strongly diminished, mimicking PGR5 dependent phenotypes (DalCorso et al., 2008; Petroutsos et al., 2009; Rühle et al., 2021).

Both CEF pathways reduce the plastoquinone (PQ) pool by using either NADPH or ferredoxin (Fd) as electron donor respectively (Tagawa et al., 1963; Desplats et al., 2009; Hertle et al., 2013). CEF has been shown to contribute to the acidification of thylakoid lumen by generating an extra proton motive force (*pmf*) in addition to the one produced by LEF (Munekage et al., 2002; Desplats et al., 2009; Tolleter et al., 2011; Saroussi et al., 2016). PCEF mediated by Flavodiiron proteins (FLVs), by transferring electrons toward O_2 at the acceptor side of PSI, also contributes to the establishment of the *pmf* and therefore to the lumen acidification (Gerotto et al., 2016; Chaux et al., 2017a; Burlacot et al., 2022). The *pmf* is used to either (1) produce ATP (Allen, 2002), (2) trigger light energy quenching via a low lumenal pH (Peers et al., 2009; Bonente et al., 2011; Erickson et al., 2015), (3) convert HCO_3^- into CO_2 thanks to carbonic anhydrase in the lumen (Burlacot et al., 2022) or (4) repress electron transfer at the level the Cyt b_6f complex through the photosynthetic control triggered by the low lumenal pH (Stiehl and Witt, 1969; Foyer et al., 1990; Munekage et al., 2001; Munekage et al., 2002; Malone et al., 2021). Both CEF and PCEF have been shown to be critical under various conditions

of light, CO_2 availability or sulfur deficiency by playing a synergistic role (Dang et al., 2014; Jokel et al., 2015; Chaux et al., 2017a; Jokel et al., 2018; Burlacot et al., 2022).

Despite the importance of CEF and PCEF in response to dynamic environments, little is known about their role during N deficiency. The role of NDA2-involved CEF have been recently addressed during CO_2-limiting photoautotrophic N deficiency and the knockdown of NDA2 was shown to impair the establishment of non-photochemical quenching (Saroussi et al., 2016). The role of PGRL1/PGR5-controlled CEF has been investigated under mixotrophic N deficiency and the lack of PGRL1 was shown to decrease the rate of CEF and TAG production (Chen et al., 2015). However, the role of PGRL1 during photoautotrophic N deficiency and the possible bioenergetic interactions between carbon/energy sinks (TAG and starch) and CEF or PCEF pathways that generate ATP has not yet been explored so far. Considering that massive carbon reallocation occurs under N deficiency (Siaut et al., 2011), the bioenergetics governing this reallocation are likely critical. Fully understanding photosynthesis regulatory pathways and how they affect biomass production and reserve formation is needed towards engineering photosynthesis and carbon storage in conditions of nutrient deficiency.

Here, we evaluated the contribution of PGRL1/PGR5-controlled CEF in the regulation of photosynthesis during N deficiency and evaluate its metabolic consequences on carbon storage in *Chlamydomonas* cells grown in photoautotrophic conditions under non-limiting CO_2 concentrations (using 1% CO_2-enriched air), conditions which favor the accumulation of carbon reserves (Schulz-Raffelt et al., 2016; Kong et al., 2018; Wu et al., 2019). By monitoring photosynthetic activity based on chlorophyll fluorescence and O_2 exchange rate measurements, we observed high net photosynthetic activity in PGRL1-deficient strains under N deficiency compared to the control strains. Furthermore, the lack of PGRL1 in 137AH genetic background resulted in an over-accumulation of TAGs. Those effects being suppressed in double mutants deficient in both PGRL1 and FLVB. We conclude that FLVs, by maintaining a strong PCEF activity in the *pgrl1* mutants, catalyze high photosynthetic rates. Finally, we discuss how modulating photosynthetic electron flow could constitute an efficient strategy to improve photosynthesis and eventually boost further TAG production under N deficiency.

Results

Photosynthetic activity sustained longer in *pgrl1* under N deficiency.

To assess the role of the PGRL1/PGR5-controlled CEF in the regulation of photosynthesis during photoautotrophic N deficiency, we simultaneously monitored chlorophyll fluorescence and O_2 exchange following a dark-light-dark transition in N-replete and N-deprived cells. We compared the photosynthesis efficiency of a PGRL1-deficient strain (*pgrl1*$_{137AH}$) with its control wild-type strain (137AH) and a complemented line (Tolleter et al., 2011) (**Fig. 1 and Supplemental Fig. S1 and S2**). Under N replete conditions, both chlorophyll fluorescence and O_2 exchange patterns were mostly similar in *pgrl1*$_{137AH}$ and control cells (**Fig. 1*A, C, E and F* and Supplemental Fig. S1 *B-C***). After 2 days of N deficiency, the PSII operating yield measured in the light decreased by about 75% in the wild-type and only by 35% in *pgrl1* (**Fig. 1A, B, and *E*; Supplemental Fig. S1*C* and *E***). Conversely, *pgrl1*$_{137AH}$ showed twice higher net O_2 evolution and light-dependent O_2 uptake as compared to the wild-type (**Fig. 1*D*, *F***). As previously reported (Peltier and Schmidt, 1991; Schmollinger et al., 2014), the dark O_2 consumption rate was stimulated in the 137AH strain during N deficiency, this effect being reduced in *pgrl1*$_{137AH}$ **(Fig. 1*D*; Supplemental Fig. S2*B*)**. By using *pgrl1*$_{137AH}$

complemented line *pgrl1::PGRL1*-2 (Tolleter et al., 2011), we noticed a full recovery of all the observed phenotypes (**Fig. 1 *E-G;* Supplemental Fig. S1 and S2**).

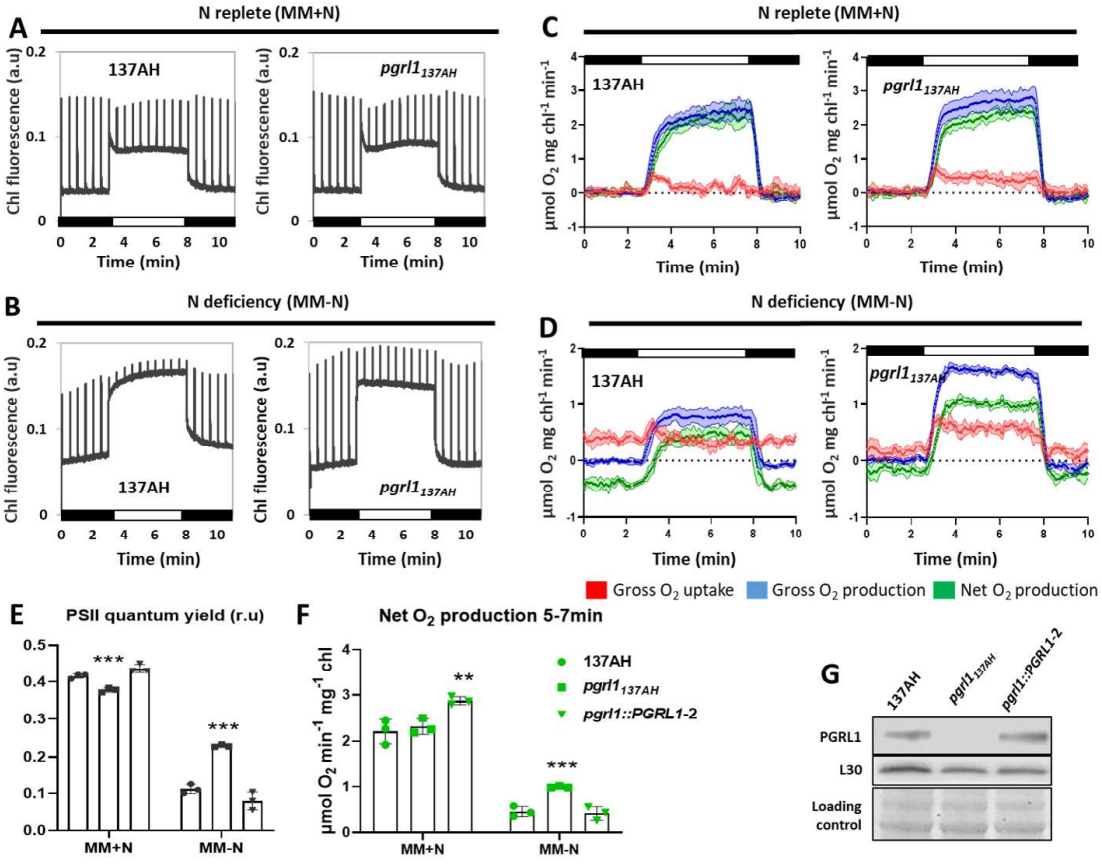

Figure 1. *pgrl1* showed sustained photosynthesis after 2 d of N deficiency. A-B, Chlorophyll fluorescence was measured using a Dual-PAM during the dark-light-dark transition from N-replete (**A**) and N-deficient (**B**) conditions. **C-D**, O_2 exchange rates were measured using a MIMS during the dark-light-dark transition from N-replete (**C**) and N-deficient (**D**) conditions. Net O_2 evolution (green) was calculated as gross O_2 evolution (blue) – gross O_2 uptake (red). **E**, PSII quantum yield before and after 2 d of N deficiency measured using green actinic light (1250 µmol photon m^{-2} s^{-1}, green LEDs) and calculated as ΦPSII= (F_M'-Fs)/ F_M' with F_M' the fluorescence value after saturating pulse, Fs the stationary fluorescence during actinic light exposure. **F**, The Net O_2 evolution before and after 2 d of N deficiency in the wild-type 137AH, *pgrl1 137AH* and the complemented line *pgrl1::PGRL1-2*. **G**, Immunoblot analysis of PGRL1 accumulation in the wild-type 137AH, *pgrl1* and the complemented line. L30 antibody was used as a positive control. Coomassie blue staining was used as the loading control. Protein samples were obtained from 2 d N-starved cells. N-replete wild-type 137AH, *pgrl1 137AH,* and *pgrl1::PGRL1-2* cells cultivated photoautotrophically with 1% CO_2 in air under continuous light (50 µmol photons m^{-2} s^{-1}) were transferred into N-free media for 2 d prior to measurements. Shown are an average of at least three biological replicates ± SD. Asterisks represent statistically significant differences compared to the control 137AH (* p<0.05, ** p<0.01 and *** p<0.001) using one-way ANOVA.

To further strengthen the phenotype-genotype relationship, we generated an additional *pgrl1*$_{CC125}$ mutant in the CC125 wild-type genetic background using CRISPR-Cas9. In line with our observation in the 137AH background **(Fig. 1*E-F*)**, we detected a sustained retention of photosynthetic PSII yield and higher net O_2 evolution in the *pgrl1*$_{CC125}$ during N deficiency compared to CC125 (**Supplemental Fig. S3**). The higher O_2 consumption under N deficiency in the dark-adapted 137AH strain from **Fig. 1*D*** was independent of PGRL1 in the CC125 background (**Supplemental Fig. S3 *D-E***). The preservation of photosynthetic activity in *pgrl1* suggests that PGRL1-controlled CEF contributes to repressing the PET reactions under photoautotrophic N deficiency.

The PGRL1 modulates the PSI donor and acceptor side during N deficiency.

The PGRL1/PGR5-controlled CEF is a determinant of the downstream PSI electron fate which prompted us to monitor P700, the primary PSI donor (**Fig. 2; Supplemental Fig. S4**). P700 forms three populations and only the first two are photo-oxidizable: 1. PSI donor shortage generates $P700^+$ in the environmental light, 2. PSI yield quantifies $P700^-$ during environmental acclimation that converts within the ms range to $P700^+$ upon a saturating light pulse, and 3. PSI acceptor side limitation represents a redox-inactive P700 pool (see Materials and Methods). In the absence of PGRL1/PGR5-controlled CEF the redox-inactive P700 pool is enhanced under CO_2-limiting conditions (Chaux et al., 2017b). This was also observed in the 137AH genetic background when *pgrl1* was grown photoautotrophically under 1% CO_2 (**Fig. 2*A, B***). The failure to produce $P700^+$ in the light gradually developed within 0.5 s and persisted throughout the illumination period (**Fig. 2*A, B***). However, *pgrl1* did not display lower PSI yields, typically detected in ambient CO_2 (DalCorso et al., 2008), since the diminished $P700^+$ was due to lower donor side limitation (**Fig. 2*B***). The P700 differences in *pgrl1* relied on PSII activity, pointing to a LEF/CEF entanglement. N depletion further increased the $P700^+$ pool in a strictly donor side-dependent fashion in both wild-type and mutant. Nevertheless, *pgrl1* displayed twice the PSI acceptor side limitation when PSII was active. Moreover, the mutant showed a delayed $P700^+$ formation within the first 200 ms of light when PSII was inhibited (**Fig. 2*A***). The latter feature was also displayed in N-deficient CC125 under DCMU conditions (**Supplemental Fig. S4*A***). This genetic background showed identical photo-oxidizable P700 pools between wild-type and mutant in the presence of N, with *pgrl1* producing slightly higher acceptor side limitation (**Supplemental Fig. S4*B***). N depletion came at the expense of PSI yields and *pgrl1* failed to alleviate the PSI acceptor side through sufficient donor side induction. These results suggest that PGRL1-controlled CEF facilitates the onset of photosynthetic control during photoautotrophic N deficiency by inducing a donor side limitation at PSI to alleviate its acceptor side redox pressure.

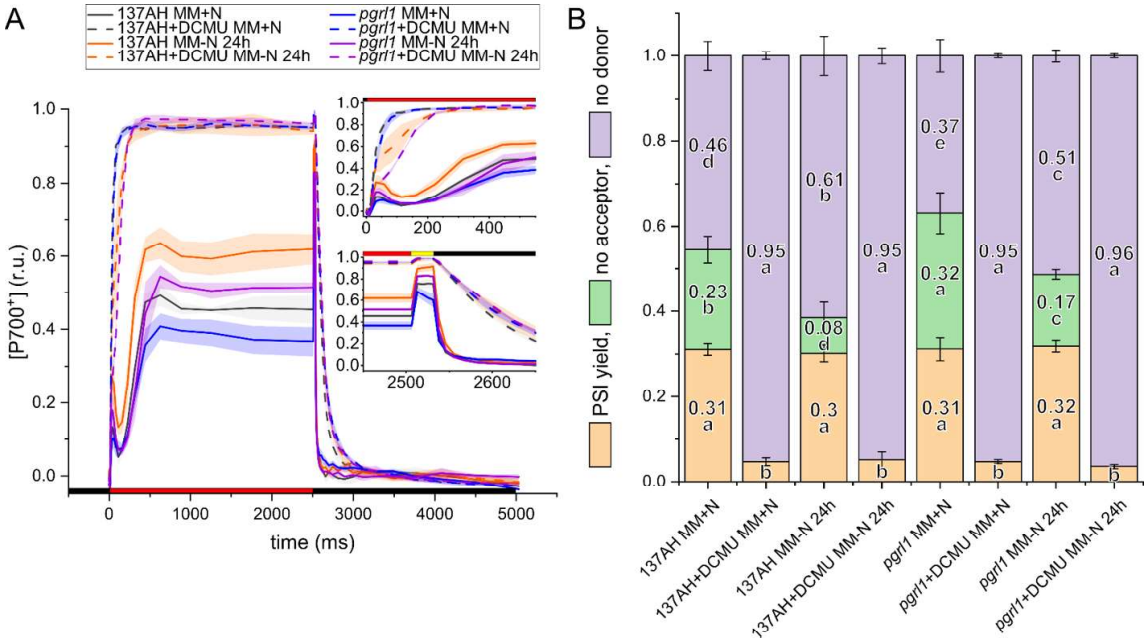

Figure 2. PSI oxidation is facilitated by PGRL1 under N deficiency. The influence of PGRL1 on the redox state of the primary PSI donor, P700, was monitored in the genetic background 137AH **(A-B)** and CC125 **(Supplemental Fig. S4)**. Panel A shows raw kinetics (red/yellow/black bars: 490/3000/0 µmol photons m^{-2} s^{-1}) in the presence and absence of PSII inhibitor DCMU (means ± SD of 4 biological replicates). Panel B quantifies the corresponding P700 pools at the end of the 2.5-s light period (letters indicate parameter-specific significances using one-way ANOVA/Fisher-LSD, $p<0.05$). At the time of quantification, P700 remained photo-oxidizable by a saturating pulse (PSI yield), was redox inactive (no acceptors) or was pre-oxidized (no donors). N-replete cells of wild-type 137AH and *pgrl1*$_{137AH}$ were cultivated photoautotrophically with 1% CO_2 in air under continuous light (50 µmol photons m^{-2} s^{-1}), and then transferred into N-free media for 24 h prior to measurements.

FLV-mediated O_2 photoreduction drives photosynthesis in *pgrl1* under N deficiency.

Because light-dependent O_2 uptake can lead to the generation of extra ATP and support CO_2 fixation but at various levels depending on the mechanism involved (Peltier et al., 2023), we sought to test the nature of the light-dependent O_2 uptake mechanism activated in *pgrl1* mutants during N deficiency (**Fig. 1*D***). FLVs have been reported to be a major O_2 uptake mechanism in the light (Chaux et al., 2017a; Burlacot et al., 2018; Burlacot et al., 2022). *pgrl1 flvB* double mutants impaired in both PGRL1 and FLVB have been recently generated by crossing the *pgrl1*$_{137AH}$ with a FLVB deficient strain (*flvB21*) as described in (Burlacot et al., 2022). Therefore, we used the parental lines as control strains (*flvB-21* and *pgrl1*$_{137AH}$) as well as sibling strains from the progeny of the crossing (WT1 and WT3) harboring both FLV and PGRL1 proteins (**Supplemental Fig. S1A)**. The two mutants (*pgrl1 flvB-3* and *pgrl1 flvB-5)* and control sibling (WT1 and WT3) strains used throughout the manuscript have been chosen for having similar maximal photosynthesis under N-replete conditions (V_{Max}) (Burlacot et al., 2022; Peltier et al., 2023). For all the experiments, we kept the *pgrl1*$_{137AH}$ alongside with its control 137AH and *pgrl1::PGRL1-2*; *flvB* mutants (*flvB21*, *flvB208* and *flvB308*) alongside with their control CC4533 and finally *pgrl1 flvB-3* and *pgrl1 flvB-5* alongside WT1 and WT3 as control. We evaluated

steady-state O_2 exchange rate in *pgrl1*$_{137AH}$, *flvB* mutants as well as in the *pgrl1 flvB* double mutants after 2 days of N deficiency (**Fig. 3**). The light-dependent O_2 uptake was highly increased in *pgrl1*$_{137AH}$ but strongly impaired in *flvB* and *pgrl1 flvB* mutants (**Fig. 3A; Supplemental Fig. S2**) which mirrors what has been reported for N-replete conditions in the presence of atmospheric CO_2 level (Chaux et al., 2017a; Burlacot et al., 2022). Interestingly, while the gross O_2 uptake, the gross O_2 and the net O_2 evolution measured during steady-state photosynthesis remained high in *pgrl1*$_{137AH}$, no difference was detected between *flvB*, *pgrl1 flvB* mutants and their respective control lines (**Figure 3*B-D* and Supplemental Fig. S2).** Taken together, these data show that the absence of FLV-mediated O_2 photoreduction (in *pgrl1 flvB* mutants) suppresses the effect of N deficiency observed in *pgrl1*$_{137AH}$ strain. We conclude that FLV-mediated O_2 photoreduction, by maintaining PET reactions in *pgrl1,* allows net photosynthesis to be maintained at a high-level during N deficiency.

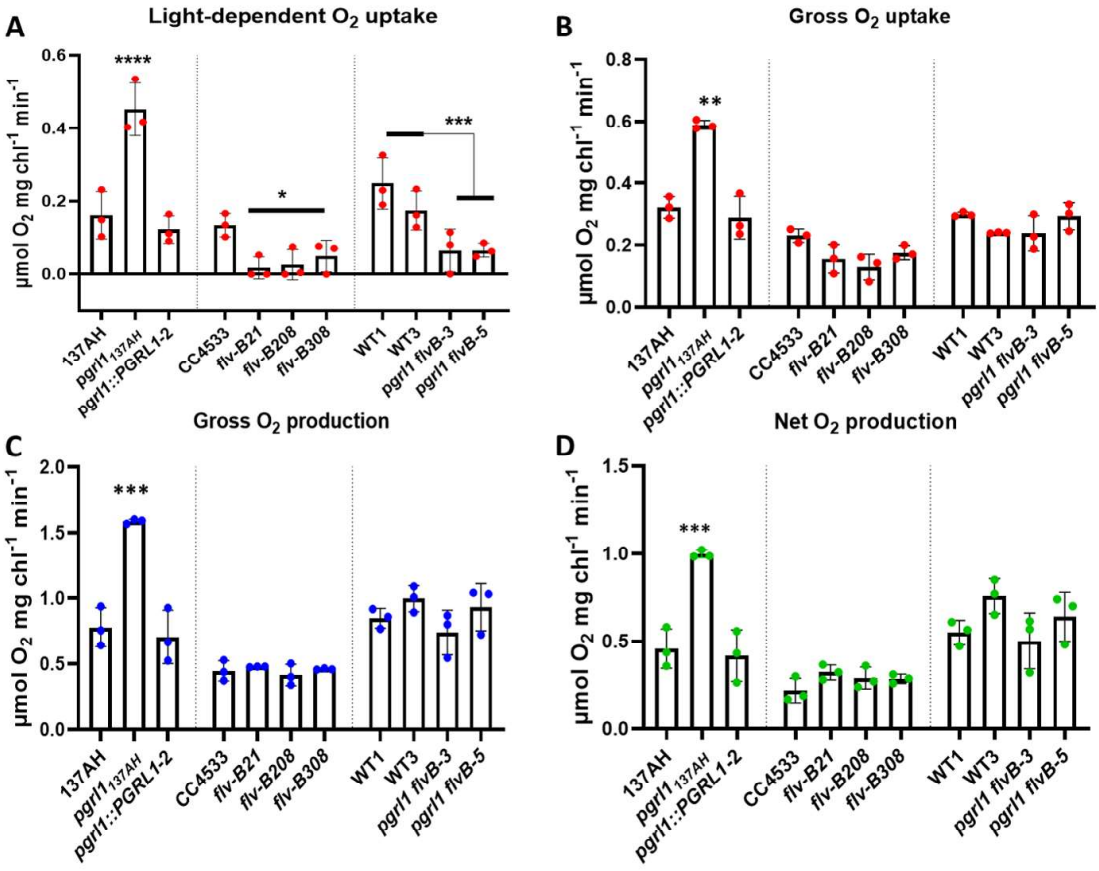

Figure 3. The photosynthesis in *pgrl1* is driven by FLV-mediated O_2 photoreduction under N deficiency. A, Light-dependent O_2 uptake attributed to FLV activity and calculated as the difference between the O_2 uptake during the 1st min of illumination and dark O_2 uptake as shown by the **Supplemental Figure 2**. **B**, Gross O_2 uptake measured between 5-7min as shown by the **Supplemental Figure 2**. **C,** Gross O_2 evolution measured between 5-7min as shown by the **Supplemental Figure 2**. **D**, Net O_2 evolution measured between 5-7min as shown by the **Supplemental Figure 2**. O_2 exchange rates were measured using a MIMS in the presence of [^{18}O]-enriched O_2. Net O_2 evolution (green) was calculated as gross O_2 evolution (blue) – gross O_2 uptake (red). Total proteins were extracted from N-replete and 2 days N-deprived cells and samples were loaded at

equal total proteins amounts as shown on Coomassie blue staining. Cells cultivated photoautotrophically with 1% CO_2 in air under continuous light of 50 µmol photons m^{-2} s^{-1} were transferred into N-free media for 2 days prior to measurements or sampling for immunoblot. Shown are an average of at least three biological replicates ± SD. Asterisks represent statistically significant difference compared to the wild-type strains (* p<0.05, ** p<0.01, *** p<0.001 and **** p<0.0001) using one-way ANOVA.

Cyt *b_6f and* PSI subunits accumulate to higher levels in *pgrl1* under N deficiency.

To gain insights into the mechanisms behind the high photosynthetic activity in *pgrl1* during N deficiency, we compared the relative abundance of representative catalytic core subunits from photosynthetic complexes in the *pgrl1*$_{137AH}$ and the 137AH wild-type during N deficiency (**Fig. 4*A and D***). Additionally, we also investigated potential changes in mitochondrial electron transport chain by probing Complex II (Cox IIB). We observed a sustained retention of the PSI subunit PsaD and Cyt *f* subunit of Cyt *b_6f* in *pgrl1*$_{137AH}$ compared to the 137AH (**Fig. 4*A and D***). Higher amounts of PsaD and Cyt *f* were observed in *pgrl1*$_{137AH}$ under N replete without any functional effect on PSII yield and Net O_2 evolution (**Fig. 1*E-F;* 4*A and D***). As for the stimulated dark O_2 consumption **(Fig. 1*D*)**, the amount of mitochondrial respiratory chains component Cox IIB was increased in the 137AH whereas it remains stable in the *pgrl1*$_{137AH}$ during N deficiency (**Fig. 4*A***). It is worth noting that the hallmark of autophagy, i.e., ATG8 was barely detectable in the *pgrl1*$_{137AH}$ whereas it was highly induced in the 137AH under N deficiency (**Fig. 4*A, D***). All the other proteins tested accumulated to a similar amount in *pgrl1*$_{137AH}$ and 137AH (**Fig. 4*A***). Note that higher amounts of Cyt *f* were also observed in CRISPR-generated *pgrl1*$_{CC125}$ mutant as compared to CC125 in response to N deficiency (**Supplemental Fig. S3*E***). We conclude from these experiments during N deficiency that the higher photosynthetic activity observed in mutants impaired in PGRL1 might result from a lower decrease in the amounts of PSI and Cyt *b_6f* complexes.

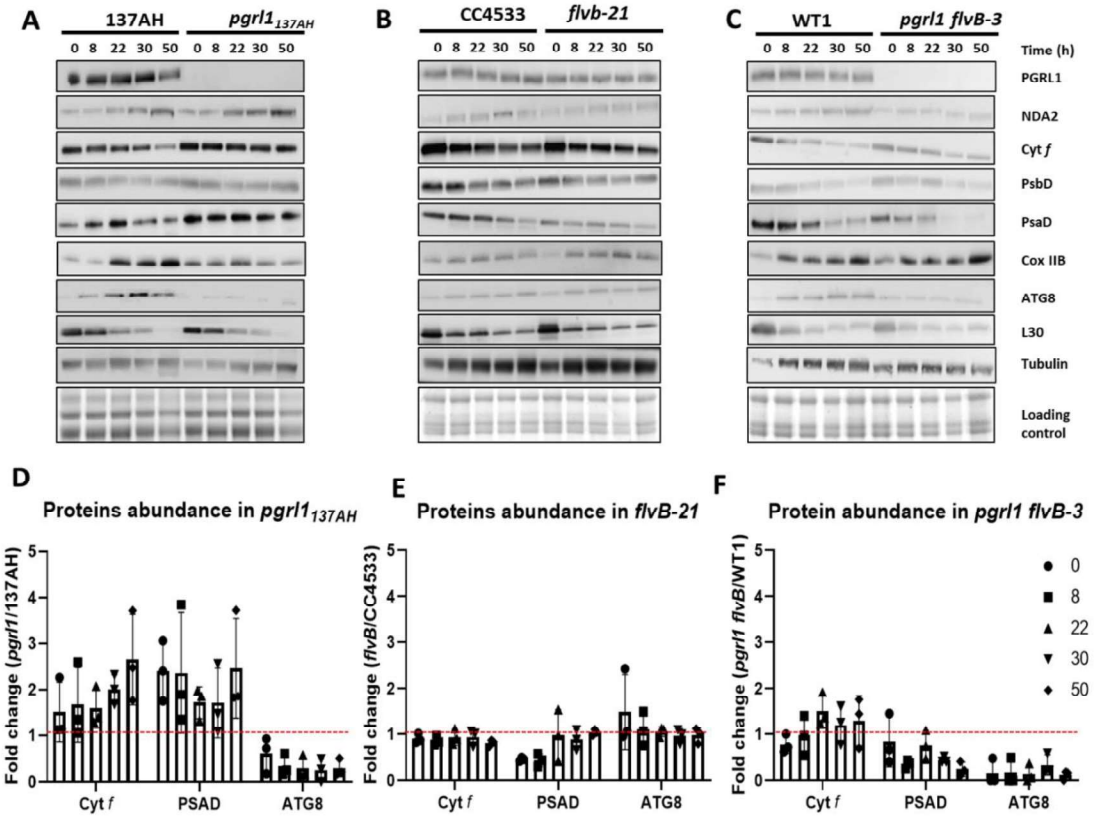

Figure 4. *pgrl1* accumulated more cytochrome Cyt b_6f and PsaD during N deficiency. **A-C**, Immunodetection of photosynthetic proteins in the *pgrl1*$_{137AH}$, *flvB-21* and *pgrl1 flvB-3* as compared to their controls during N deficiency. Cells were harvested at 0, 8, 22, 30 and 50 hours of N deficiency. Samples were loaded at equal total protein amounts as shown by Coomassie blue staining. Shown are representative images of three biological replicates. The α-tubulin was used as housekeeping protein whereas ATG8 and the chloroplast 50S ribosomal large subunit L30 are controls of N depletion (Upadhyaya et al., 2020; Crespo and Pérez-Pérez, 2023). **D-F**, Histogrammes showing the abundance Cyt *f*, PsaD and ATG8 proteins in the *pgrl1*$_{137AH}$, *flvB-21* and *pgrl1 flvB-3*during N deficiency in the wild-type cells. Shown represent the ratio of mutants over control strains. Data are average of at least three biological replicates.

To test whether the retention of the PSI and Cyt b_6f observed in the *pgrl1*$_{137AH}$ are consequences of the existence of a FLV activity, similar immunoblot analyses were performed in the *flvB-21* and *pgrl1 flvB-3* mutants. Consistent to the photosynthetic activity, immunoblot analyses showed a similar accumulation of tested proteins in the *flvB-21* and *prgl1 flvB-3* compared to controls with the exception of lower PsaD and ATG8 in *prgl1 flvB-3* (**Fig. 4 *B-C* and *E-F***).

Defects in CEF and PCEF altered carbon storage during N deficiency.

Emerging literature suggests that alterations in energy management pathways affect not only biomass production but also its composition (Saroussi et al., 2017; Kong et al., 2018; Burlacot et al., 2019; Saroussi et al., 2019). Starch and TAGs are major forms of carbon storage in *Chlamydomonas* during N deficiency. Since the *pgrl1*$_{137AH}$ mutant shows a

stronger net photosynthetic rate, we measured its ability to accumulate storage compounds. Starch accumulation was similar in *pgrl1*$_{137AH}$ and control lines under both N replete and deficiency (**Fig. 5*A*; Supplemental Fig. S5*A* and *S6A***). In contrast, twice more TAG accumulation was observed in *pgrl1*$_{137AH}$ compared to the control lines under N deficiency whereas no difference was observed under N-replete condition (**Fig. 5*D*; Supplemental Fig. S5*B* and S6*D***). Lipid droplet imaging confirmed the accumulation of higher TAG amounts (**Supplemental Fig. S5*D***). Intriguingly, the *PGRL1* knockout mutant did not induce TAGs or starch accumulation in response to N deficiency in the CC125 genetic background (**Supplemental Fig. S6 *G-J***), which may be related to the fact that photosynthesis preservation (PSII yield and net O_2 evolution) was lower in the *pgrl1*$_{CC125}$ background as in the *pgrl1*$_{137AH}$ background (**Supplemental Fig. S3**) thus limiting reserve accumulation, or indicating the existence of a metabolic limitation for storage compound accumulation in the CC125 background.

Under N replete, the *flvB* single mutants accumulated higher amounts of starch than the CC4533 wild-type (**Supplemental Fig. S6*B***) but accumulated lower amounts of TAG under N deficiency (**Fig. 5*E***). The double mutants *pgrl1*$_{137AH}$ *flvB* accumulated similar amounts of TAG and starch as compared to control strains either in N replete or N deprived conditions (**Fig. 5*C, F*; Supplemental Fig. S6*C, F***).

We then evaluated to which extent observed changes in photosynthesis affect biomass accumulation, by following changes in cellular volume as a proxy for biomass accumulation. After 6 days of N deficiency, the cell volume increased twice as fast in the *pgrl1*$_{137AH}$ compared to the control lines (**Supplemental Fig. S5*C***). We conclude from the above experiments that the higher photosynthetic activity in *pgrl1*$_{137AH}$ results in increased biomass and TAG productivity under N deficiency.

Altogether, our data suggested that during phototrophic N deficiency, photosynthetic electron flow mediated by FLVs could trigger higher TAG accumulation while PGRL1 tends to constrain it, likely via a photosynthetic control-related process or specific protease pathways that target Cyt b_6f. We propose that both PGRL1 (CEF) and FLVs (PCEF), by having an antagonistic role during N deficiency, manage the redox landscape, carbon storage and biomass production. It is worth pointing out that this modification of metabolism as a consequence of redox management depends not only on genetic background (137AH versus CC125) but also on the environmental state (+N versus –N).

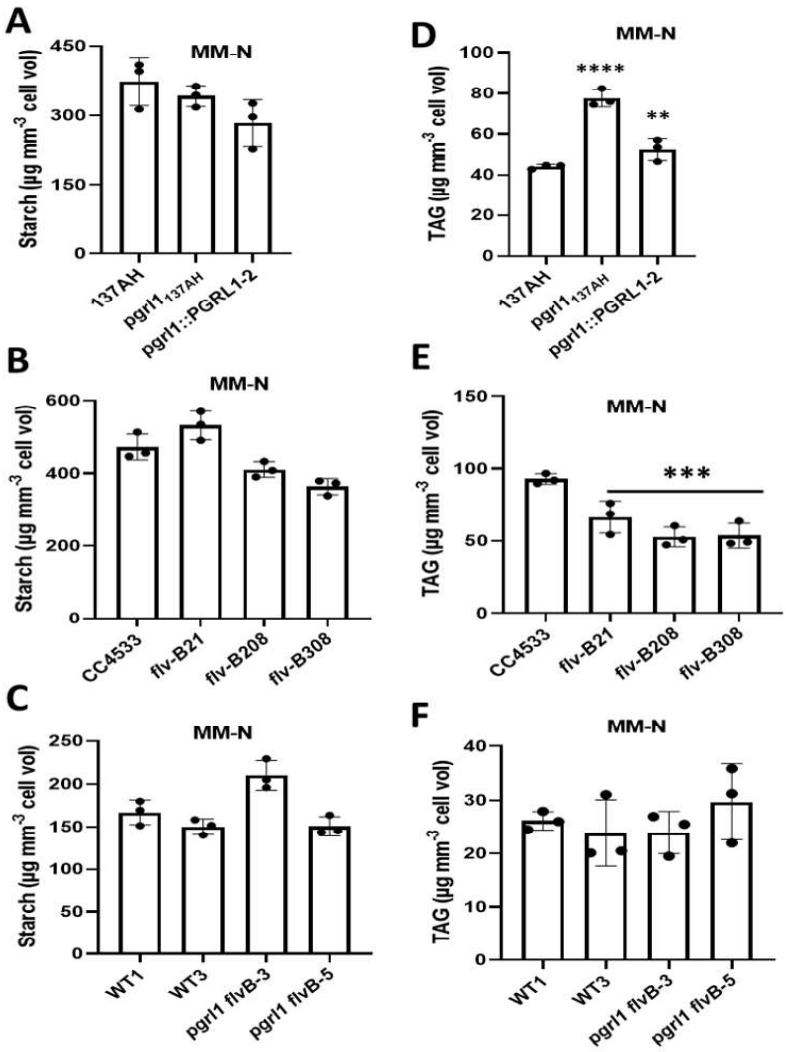

Figure 5. *pgrl1* over accumulated TAGs under N deficiency. Starch **(A-C)** and TAG (**D-F**) quantification in N-deprived cells of *pgrl1*$_{137AH}$, *flvB* and *pgrl1 flvB* mutants respectively. Cells were cultivated photoautotrophically with 1% CO_2 in air under continuous light of 50 µmol photons m^{-2} s^{-1}. For N deficiency, cells were transferred into N-free media for 2 d prior to sampling for starch and TAG. Shown are an average of at least three biological replicates ± SD. Asterisks represent statistically significant difference comparing mutants with their control strains (* p<0.05, ** p<0.01 and *** p<0.001) using one-way ANOVA.

Discussion

The ability of microalgae to coordinate their energy conversion (from light to chemical energy) to meet the metabolic demand is crucial for their survival in a constantly fluctuating environment. Mechanisms involved in photosynthesis regulations have been abundantly studied in response to light or CO_2 levels, but not much is known during nutrient deficiency when a massive re-orientation of metabolic pathways occurs. In the absence of N, the major cellular energy sinks (cell division, protein biosynthesis and photosynthetic CO_2 fixation) are restricted whereas the carbon and energy are stored as

TAGs or starch. Moreover, the PET reactions are downregulated under N deficiency. However, we do not know whether the downregulation of PET is a mean to match cells energy status with the limited metabolic demand. In other words, how the metabolism accommodates when photosynthesis remains high during N deficiency is not well understood. In this study, we demonstrated that PGRL1, which controls a CEF pathway, tunes PET during N deficiency. This tuning favors the photosynthetic control mechanism via Cyt b_6f to limit PSI donor availability (see below for details) and might affect energy-transducing enzyme ratios at least in chloroplasts. Lack of PGRL1 resulted in sustained photosynthetic activity up to 2 days of N deficiency. The misregulation of the PGRL1/PGR5-controlled CEF is notorious for decreasing the photosynthetic control efficiency and re-routing of electrons into alternative acceptors such as H_2 production by Hydrogenases or O_2 photoreduction by FLVs (14, 20, 50). Here, we have further shown that the higher FLVs-mediated PCEF in *pgrl1* mutants channels excess electrons toward O_2 under N deficiency. PCEF thus counteracts PSI over-reduction, likely facilitating ATP production and at the same time keeping PET active.

PGRL1/PGR5-controlled CEF contributes to photosynthetic control during N deficiency.

The photosynthetic control refers to mechanisms that restrict the PET reactions mostly occurring in response to environmental fluctuations and is typically achieved on the level of the Cyt b_6f upon acidification of the thylakoid lumen). The PGRL1-PGR5-controlled CEF increases lumen acidification efficiency and has been shown to contribute to the photosynthetic control in higher plants (Munekage et al., 2002; DalCorso et al., 2008; Yamamoto and Shikanai, 2019) as well as in microalgae (Petroutsos et al., 2009; Tolleter et al., 2011; Johnson et al., 2014; Steinbeck et al., 2015; Buchert et al., 2020). The induction of the photosynthetic control results in PSI donor side limitation in the light which is typically determined *in vivo* via $P700^+$ optical readouts (Yamamoto and Shikanai, 2019; Penzler et al., 2022; Zhou et al., 2023). Our results showed higher acceptor side limitation (at the expense of donor side limitation) in *pgrl1* mutants (**Fig. 2 and Supplemental Fig. S4**) indicating that they are affected in the induction of the photosynthetic control. The decrease in Cyt b_6f abundance could be an additional cellular strategy to further restrict the PET toward PSI (higher donor side limitation in wild-type, **Fig. 2 and Supplemental Fig. S4**). While the wild-type successfully relaxes the redox pressure on PSI and degrades Cyt b_6f under N deficiency, *pgrl1* mutants sustained PET and failed to degrade the Cyt b_6f. This dysfunctioning of the photosynthetic control in *pgrl1* (high acceptor side limitation and Cyt b_6f abundance**; Fig. 2 and 4*A***), promotes the recruitment of stromal electron carriers such as FLVs and TAG biosynthesis (in 137AH background). Similar observations were reported under sulphur deprivation where deletion of PGRL1 or PGR5 resulted in sustained linear electron flow toward H_2 production in *Chlamydomonas* (Tolleter et al., 2011; Steinbeck et al., 2015). Our work shows that impairing the accumulation of PGRL1 removes a bottleneck of photosynthetic electron flow during N deficiency under non-limiting CO_2 conditions (**Fig. 1-3; Supplemental Fig. S1-3**). This characteristic of photosynthetic control makes PGRL1/PGR5-controlled CEF a promising target for improving photosynthetic yield under nutrients deficiency. Indeed, the control of photosynthesis under N deficiency has been seen as safety mechanisms protecting cells from phototoxicity (Munekage et al., 2002; Yamamoto and Shikanai, 2019; Saroussi et al., 2023). Here, we show that thanks to the presence of FLVs, photosynthesis could be improved by removing PGRL1-controlled CEF during N deficiency under non-limiting CO_2 conditions.

FLVs become predominant in the absence of PGRL1/PGR5-controlled CEF.

So far, a compensation mechanism between PGRL1 and FLVs has been reported during algal adaptation to light or low-CO_2 conditions (Dang et al., 2014; Burlacot et al., 2022; Peltier et al., 2023). Under high light or low-CO_2 conditions, the increased activity of FLVs in the PGRL1-deficient strain does not improve the net photosynthesis despite its strong efficiency in generating ATP (Peltier et al., 2023). Similar compensation has also been observed in higher plants where orthologous expression of FLVs rescues the *pgr5* mutants phenotype without further improving photosynthesis (Wada et al., 2018; Yamamoto and Shikanai, 2019) although some levels of increased biomass were measured in wild-type Arabidopsis expressing FLVs under light fluctuations thanks to the protective role of FLVs in these conditions (Basso et al., 2022). In contrast, our results suggest that under N deficiency, FLVs and PGRL1 have an antagonistic role. Indeed, the increased activity of FLVs in the PGRL1-deficient strains resulted in higher net photosynthesis (**Fig. 3*D*; Supplemental Fig. S2**), which shows that rather than compensating each other, PGRL1 is indirectly controlling the activity of FLVs by limiting the maximal electron flow capacity. Our observation of the sustained accumulation of Cyt b_6f in the *pgrl1* but not in *pgrl1 flvB* double mutants under N deficiency **(Fig. 4 A and *D*)** could be attributed to the activity of FLVs-mediated PCEF draining electrons from the photosynthetic chain and indirectly preventing Cyt b_6f from degradation. The latter process is catalysed in *pgrl1 flvB* upon PCEF shortage. The presence of strong FLVs activity in *pgrl1* thereby allows maintaining high PET while generating ATP for CO_2 fixation and reserve formation.

Because CEF and PCEF are dominant pathways for supplying extra ATP in addition to LEF in the chloroplast, we were expecting that the removal of both PGRL1 and FLVs would have more severe consequences on cell physiology and metabolism as it was observed when CO_2 is limiting (Burlacot et al., 2022). Instead, we observed similar photosynthetic activity and TAG biosynthesis in the *pgrl1 flvB* double mutants as their control strains (**Fig. 3 and 5**), i.e. the additional removal of FLVs suppressed the phenotype of PGRL1 deficiency. A third pathway generating the energy required for photosynthetic CO_2 fixation and ensuring redox dissipation could be operating in the double mutant *pgrl1 flvB*. Both the NDA2-dependent CEF (Desplats et al., 2009; Saroussi et al., 2016) or a chloroplast-mitochondria electron flow (CMEF) (Peltier et al., 2023) could be good candidates. NDA2 protein level was shown to increase during air photoautotrophic N deficiency under atmospheric CO_2 level and the CEF rate in *Chlamydomonas* was decreased by 50% in *nda2* mutants (Saroussi et al., 2016). However, we observed a similar protein level of NDA2 in the *pgrl1 flvB* as their control lines (**Fig. 4*C***). Nevertheless, the protein level might not always correlate with the activity and other regulatory mechanisms (e.g., phosphorylation or redox regulation) can modulate enzyme activity. Additionally, the stimulated mitochondrial respiration rates as well as increased in Cox IIB protein level during N-deficiency in all the strains (except *pgrl1*$_{137AH}$) (**Fig. 4; Supplemental Fig. S3**) points to a strong activity of CMEF (Burlacot et al., 2022; Peltier et al., 2023), which might compensate for CEF and PCEF deficiency in *pgrl1 flvB* N-deprived cells. CMEF may have two distinct roles, either to supply additional ATP or favour redox dissipation. In the context of generating extra ATP, the Cox IIB pathways could take over the AOX1 alternative oxidase pathway because of its efficiency in generating ATP (Peltier et al., 2023). Further investigation would be required to identify the mechanisms generating ATP in the absence of PGRL1 and FLVs. Altogether, we conclude that FLVs maintain high photosynthetic activity under N deficiency in the

absence of PGRL1 by channeling excess electrons toward O_2 meanwhile generating ATP for CO_2 and downstream metabolic pathways (TAG production).

Relationship between cellular redox landscape and carbon storage.

A major biotechnological challenge in algal domestication for biofuel is the tradeoff between growth and lipid productivity. In *Chlamydomonas* as in many other microalgae, starch and TAG massively accumulate but mostly under stress conditions in particular N deficiency when cell division stops and productivity is impaired. Considerable efforts have focused on the study of the molecular mechanisms behind the onset of reserve accumulation by monitoring omics responses to a stress (Miller et al., 2010; Blaby et al., 2013; Schmollinger et al., 2014; Zienkiewicz et al., 2016; Takeuchi and Benning, 2019), or focused on specific steps of fatty acid and TAG biosynthesis, which have resulted in some limited improvement in productivity (Kong et al., 2019; Li-Beisson et al., 2019). Improving productivity requires a better understanding of the crosstalk between photosynthetic carbon fixation, environmental signals and the redox balance, which all govern reserve accumulation (Geigenberger et al., 2005; Michelet et al., 2013; Geigenberger and Fernie, 2014). Here by studying mutants affected in CEF and PCEF, we explored the relationships between the cellular redox status and carbon storage.

The increased accumulation of TAG but not starch observed in the PGRL1-deficient strain (137AH background) under N deficiency (**Fig. 5 *A* and *B***) is a consequence of continuous production of NADPH and ATP through PCEF-dependent PET. In line with our finding, the *Chlamydomonas pgd1* mutants (e.g. *Plastid galactoglycerolipid degradation 1)* with reduced LEF rate (less ATP and NADPH) are shown to produce less TAG under N starvation (Li et al., 2012; Du et al., 2018). The report that the *pgrl1* mutant made less TAG than wild-type under mixotrophic conditions (Chen et al., 2015) is not surprising. It is well known that the bioenergetics of *Chlamydomonas* under photoautotrophic conditions differ from mixotrophic conditions (Johnson and Alric, 2012; Johnson and Alric, 2013; Saint-Sorny et al., 2022). The presence of acetate can drastically affect cellular bioenergetics levels i.e. its uptake consumes ATP and its metabolism produces NADH, therefore further favoring oil synthesis (Goodson et al., 2011; Johnson and Alric, 2012; Johnson and Alric, 2013; Goodenough et al., 2014). TAGs accumulation was different in the CC125 background where the *pgrl1*$_{CC125}$ mutant made similar amounts of TAGs as its background strain (**Supplemental Fig. S6*J***). This seems not surprising when we consider that TAG accumulation is a metabolic consequence of changes in chloroplast redox state and in photosynthetic performance. The preservation of PSII yield and net O_2 evolution was less dramatic in the CC125 background than in the 137AH background, which could be one of the reasons behind strain-dependent phenotype. This further reflects the fact that oil content is a complex trait, and it is the consequence of the interaction between genetic makeup, its metabolic flexibility and the capacity of the extent of a given cell's response to environmental changes.

In contrast to *pgrl1*$_{137AH}$, the *flvB* mutants accumulated lower amounts of TAGs under N deficiency, and no difference in TAG was observed in the *pgrl1 flvB* double mutants, consisting again with the profile in photosynthetic performance and with their antagonistic roles. The *flvB* mutants accumulated higher amount of starch under N sufficient condition though. To conclude, this work further points to the importance of the role redox management on carbon allocation and storage, and that this effect is dependent on many factors including the genetic background, the trophic style, as well as the nutrient status.

Materials and methods

Growth conditions and strains

The *pgrl1*$_{137AH}$ (from the background 137AH) with its complementing strain (*pgrl1::PGRL1*-2), *flvB* mutants from the background CC-4533 and the *pgrl1 flvB* double mutants were previously described (Tolleter et al., 2011; Chaux et al., 2017a; Burlacot et al., 2022). *pgrl1*$_{CC125}$ mutants were generated in the CC125 background using CRISPR-Cas9 (see Supplemental Materials and Methods). All the information about the strains used are reported in **Supplemental Table 1**. Cells were routinely cultivated in an incubation shaker (INFORS Multitron pro) maintained at 25°C, with 120 rpm shaking and constant illumination at 50 µmol m^{-2} s^{-1}. Fluorescent tubes delivering white light enriched in red wavelength supplied lightings in the INFORS. All experiments were performed under photoautotrophic condition with minimum medium with or without nitrogen source (MM and MM-N) buffered with 20 mM MOPS at pH 7.2 in air enriched with 1% CO_2. Due to cell aggregation in the 137AH background (notably the *pgrl1* mutant) that prevent accurate cell counting, total cellular volume was measured using a Multisizer 4 Coulter counter (Beckman Coulter) and the different strains were diluted to reach a similar cellular concentration before N deficiency experiments.

Measurement of chlorophyll fluorescence using a Pulse Amplitude Modulation (PAM)

Chlorophyll fluorescence was measured using a PAM fluorimeter (Dual-PAM 100, Walz GmbH, Effeltrich, Germany) on the MIMS chamber as described in (Burlacot et al., 2018) using green actinic light (1250 µmol photon m^{-2} s^{-1}, green LEDs). Red saturating flashes (8,000 µmol photons m^{-2} s^{-1}, 600 ms) were delivered to measure the maximum fluorescence (FM) every 30 s (before and upon actinic light exposure). The maximum PSII quantum yield was calculated as $Fv/Fm = (Fm-Fo)/Fm$ where F_0 is the basal fluorescence obtained with the measuring light and Fm the fluorescence emitted after saturating pulse (Maxwell and Johnson, 2000). PSII operating yield (ΦPSII) was calculated as ΦPSII= (F_M'-Fs)/ F_M' with F_M' the fluorescence value after saturating pulse, Fs the stationary fluorescence during actinic light exposure.

O_2 exchange measurement using Membrane Inlet Mass Spectrometry (MIMS)

O_2 exchanges were measured in the presence of [^{18}O]-enriched O_2 using a water-jacketed, thermoregulated (25°C) reaction vessel coupled to a mass spectrometer (model Prima ΔB; Thermo Electronics) through a membrane inlet system (Burlacot et al., 2020). The cell suspension (1.5 mL) was placed in the reaction vessel and bicarbonate (10 mM final concentration) was added to reach a saturating CO_2 concentration. One hundred microliters of [^{18}O]-enriched O_2 (99% $^{18}O_2$ isotope content; Euriso-Top) was bubbled at the top of the suspension just before vessel closure and gas exchange measurements. O_2 exchanges were measured during a 3-min period in the dark, then the suspension was illuminated at 1250 µmol photons m^{-2} s^{-1} for 5 min using green LEDs followed by 3-min in the dark. Isotopic O_2 species [$^{18}O^{18}O$] (m/e = 36), [$^{18}O^{16}O$] (m/e = 34), and [$^{16}O^{16}O$] (m/e = 32) were monitored, and O_2 exchange rates were determined (Burlacot et al., 2020). Argon gas was used to correct O_2 exchange measured by the spectrometer as described in (Burlacot et al., 2020).

Redox state measurements of P700

The PSI primary electron donor, were obtained from optical signals (705 nm – 740 nm) using a Joliot-type spectrophotometer (JTS-150, Spectrologix USA), described in detail elsewhere (Klughammer and Schreiber, 1994; Buchert et al., 2020; Buchert et al., 2022). Harvested cells (2 min, 4000 rpm, 22°C) were resuspended in cuvettes to comparable densities in growth medium containing 20% Ficol (*w*/*v*). Samples were subjected to 2.5-s alterations of dark/light (490 µmol photon m^{-2} s^{-1}, 630-nm LEDs), leading to a partial P700 pre-oxidation during the light period (donor side limitation). Additional fractions of photo-oxidizable P700 (PSI yield) were obtained by a 25 ms saturating pulse before the dark period, revealing non-oxidizable P700 (acceptor side limitation) after comparison to fully oxidized P700 when measured in the presence of 20 µM 3-(3,4-dichlorophenyl)-1,1-dimethylurea (DCMU).

All other methods are described in ***SI Materials and Methods*** **(Annex 2).**

Acknowledgments
O.D. thanks The French Atomic Energy and Alternative Energy Commission (CEA) for a PhD scholarship. G.P. and Y.L.-B. acknowledge the continuous financial support of CEA (LD-power, CO2Storage). A.B. acknowledges the support from the Carnegie Institution for Science. We thank Bertrand Legeret for maintaining the HelioBiotec lipidomics platform and thank Mallaury Cabanel for assistance in performing immunoblot. We also acknowledge the ZoOM microscopy facility. M.H. (DFG Research Unit FOR 5573) and F.B. (BU 3426/3-1) acknowledge Deutsche Forschungsgemeinschaft for funding.

Author's Contributions:
Y.L-B., G.P., A.B., and O.D. conceived the study. Y.L-B., G.P. and A.B. provided supervision. O.D. performed most of the experiments. P.A., M.B. and O.D. carried out biochemical experiments. M.B. and O.D. performed starch and lipid analysis. G.P. supervised the MIMS experiments. C.S. and J.I. generated the CRISPR-mediated mutant lines under the supervision of A.B.. F.B. and M.H. performed and analyzed the P700 measurements. O.D. drafted the manuscript with contributions from A.B., G.P, F.B., M.H. and Y.L-B.

Conclusion

Overall, we reported a high photosynthetic activity, and hyper-accumulation of TAGs thanks to FLV activity in a PGRL1-deficient strain (137AH background) under N deficiency. We have further elucidated that PGRL1-controlled CEF facilitates the onset of photosynthetic control during photoautotrophic N deficiency by inducing a donor side limitation at PSI to alleviate its acceptor side redox pressure. In contrast, FLV-mediated PCEF by serving as alternative electron sink allow a continuous photosynthetic electron transfer. Therefore, this work is the first report showing that PGRL1-CEF and FLV-PCEF could play antagonistic role during N deficiency. Finally, we propose that modulating photosynthetic electron flow by enhancing FLV and repressing PGRL1 activities could constitute an efficient strategy to boost photosynthesis and TAG production under nutrient deficiency for biotechnological applications.

This work has also highlighted the importance of genetic background in the phenotypic characterization of a given mutation. Comparison between *pgrl1* mutant from 137AH and to that derived from CC125 showed that the $pgrl1_{137AH}$ has a stronger metabolic capacity of storing carbon reserve than the latter. Such a difference may result from the fact that photosynthesis was less reduced in the $pgrl1_{137AH}$ as compared to $pgrl1_{CC125}$ in response to N deficiency, so the measured net O_2 evolution and PSII yield are much higher in $pgrl1_{137AH}$ than in $pgrl1_{CC125}$. It may also result from different carbon storage abilities, which have been reported in Chlamydomonas to vary greatly depending on the genetic background (Siaut et al., 2011; Flowers et al., 2015; Zhang et al., 2022), or from phenotypical differences in the responses to N deficiency, for example, CC125 turning yellow after 2 days of starvation whereas 137AH remained green for more than 3 days. This also reflects the fact that carbon storage is a physiological manifestation of differences at several levels i.e. genetic/metablic/regulatory and its interaction with the changing environment. A full understanding of what is going on in a given scenario requires large scale works by integrating fluxomics, genomics and transcriptomics, which is at the moment beyond the scope of this current Thesis.

Chapter II

Chapter 2: Identification and mapping of mutants potentially involved in energy trafficking

2.1. Choice of candidate genes

Microalgae are eukaryotic photosynthetic organisms with distinct subcellular organelles housing specific subsets of metabolic reactions that are physically separated from each other by biological membranes. Exchange energy (ATP and NAD(P)H) between compartments is indispensable to achieve whole-cell homeostasis and ensure optimal growth (Raghavendra and Padmasree, 2003; Weber and Linka, 2011; Kong et al., 2018). Understanding the means of energy trafficking between distinct subcellular compartments is key towards the domestication of eukaryotic photosynthetic organisms.

Exchanges of reductant between subcellular organelles via malate shuttle was proposed a means to help balancing cellular energetic status (Scheibe, 2004). Although the concept of « malate shuttle » has been coined over 50 years ago, components of this pathway remain hypothetical in microalgae. Nevertheless, it is generally believed that the "malate shuttle" includes malate dehydrogenases (MDHs) and di- or tri-carboxylic acid transporters. It has been observed that these components are upregulated when plants and algae are subjected to HL, low CO_2, cold stress etc. suggesting their possible implication in the adaptation of cellular metabolism in response to a changing environment (Backhausen and Scheibe, 1999; Scheibe et al., 2005; Yamano et al., 2008).

In contrast to land plants, very little is known about the role of malate shuttle in green algae. Five orthologs of MDHs (MDH1-5) are encoded in the genome of *Chamydomonas reinhardtii* (Merchant et al., 2007). MDH1 and 5 (the only $NADP^+$ requiring MDH) are predicted to be chloroplastic whereas MDH3 is considered cytosolic and MDH4 mitochondrial (Tardif et al., 2012). Both MDH1 and MDH2 have been localized to the peroxisome based on fusion of N- or C-terminal transit peptide to fluorescent proteins (Lauersen et al., 2016; Kong et al., 2017). Therefore, a clear subcellular localization for MDH1 remain to be solved. The redox regulation of Chlamydomonas MDH5 activity has been characterized *in vitro* by site-directed mutagenesis (Lemaire et al., 2005), however, its physiological role in dissipating excess reductant is still missing. The peroxisomal MDH2 has recently been shown to participate in active fatty acid β-oxidation by re-oxidizing the NADH produced (Kong et al., 2018). The authors further showed that peroxisomal redox status could be communicated to chloroplast via malate- or H_2O_2-based signaling. This is supported by the observation that the absence of MDH2 (i.e. the *mdh2* mutants) resulted in a sustained photosynthetic activity and higher fatty acid and starch synthesis during photoautotrophic N deprivation.

In addition to MDHs, malate shuttle requires translocators of malate/or other di- or tri-carboxylic acids from one compartment to another. Different translocators have been predicted to occur in the chloroplast and mitochondria of Arabidopsis (Weber and Linka, 2011; Lee and Millar, 2016). While no translocator of malate or di-/tri-carboxylates has not been characterized in Chlamydomonas, orthologs could be found in its genome encoding for three putative plastidial 2-oxoglutarate/malate translocators (annotated as OMT1, OMT2 and LCI20) and one in mitochondria known as MiTC14 belonging to the mitochondrial substrate carrier protein family (Merchant et al., 2007; Johnson and Alric, 2013). For more details on the malate shuttle in plants and algae, refers to the review (Dao et al., 2022).

$NAD(P)^+$/NAD(P)H redox homeostasis is also critical for optimal growth specially in photosynthetic organisms that shift between different trophic lifestyle

(Hashida and Kawai-Yamada, 2019). Proton-translocating NAD(P)$^+$ transhydrogenases (NNTs) (EC.7.1.1.1) are membrane-bound enzymes found in a wide range of organisms from bacteria to photosynthetic eukaryotes but absent from most higher plants (Arkblad et al., 2001; Jackson, 2012). NNT catalyzes the reversible electron transfer between NAD(H) and NADP(H) pools coupled with proton translocation across the membrane (Jackson et al., 1999). A pyridine nucleotide transhydrogenase (PntAB) was reported to connect glycolytic metabolism with photosynthesis in *Synechocystis sp.* PCC 6803 by balancing the intracellular NADH/NADPH redox homeostasis in the direction of NADPH under low-light mixotrophic condition (Kämäräinen et al., 2017). A homolog of this transhydrogenase is encoded by a single *NNT* gene in Chlamydomonas and predicted to be mitochondrial (Tardif et al., 2012). However, proteomic studies reported the presence of NNT in the proteome of chloroplast (Terashima et al., 2011) and in another study, in the proteome of mitochondria (Atteia et al., 2009). Further studies are needed to figure out the exact localization or possible dual targeting of the Chlamydomonas NNT and its biochemical function.

ATP and ADP are involved in many biochemical reactions, and similar to NAD(P)H, ATP is large and requires help to move across membranes. The import of ATP from mitochondria to chloroplast has been postulated to poise ATP/NAD(P)H ratio in Chlamydomonas and diatoms (Lemaire et al., 1988; Bailleul et al., 2015). Orthologs of ATP/ADP translocators are present in Chlamydomonas genome but none of them has been characterized yet. Proteomic studies also revealed the presence of three putative ATP/ADP antiporter AAA1, 2 and 3 in the chloroplast and two adenine nucleotide translocator ANT1 and 2 in the mitochondria (Atteia et al., 2009; Terashima et al., 2011). In Arabidopsis, the expression of *NTT1* and *NTT2* (homologs of AAAs) is spatially and developmentally separated suggesting that they might have different function (Reiser et al., 2004). Null mutants of both NTTs exhibited impaired formation of thylakoid, over-accumulation of ROS and delayed growth as compared to the parental WT under low-light and short-day conditions (Reiser et al., 2004; Reinhold et al., 2007). Whether the different ATP/ADP translocases have redundant and/or separate function remain to be elucidated. Above-mentioned molecular components and their IDs are shown in **Table III.1**. Mapping of those candidates in the subcellular context and their putative biochemical reactions are shown in the **Figure III.1**.

Table III.1: Description of candidate genes and characterization of respective mutants.

- * Proof of RT-PCR showing the absence of gene product.
- The insertions into ADP/ATP translocases did not give conclusive results. Need to be retested with new primers.
- "Mixo" refers to mixotrophic growth with TAP.
- "Very-low-CO_2" (VLC) refers to photoautotrophic growth condition with air containing only 100 ppm of CO_2.

Target gene	Cre. accession	Mutant strains	Strain ID	Insertion site	Insertion validated	Growth phenotype
Malate dehydrogenase (MDH5)	Cre09.g410700	*mdh5_11*	LMJ.RY0402.081311	Intron 4	Yes	No
		mdh5_88	LMJ.RY0402.229688	3'UTR	Yes	No
2-Oxoglutarate/malate translocator (OMT2)	Cre17.g713200	*omt2_58*	LMJ.RY0402.144758	5'_Intron	Yes	No
		omt2_90	LMJ.RY0402.200790	3'UTR	Yes	No

		omt2_83	LMJ.RY0402.205883	Exon1-Intron2	Yes	Yes (Mixo)
2-Oxoglutarate/malate translocator (LCI20)	Cre06.g260450	*lci20_04*	LMJ.RY0402.091704	Exon 13	No	No
		lci20_46	LMJ.RY0402.199846	5'UTR	No	No
		lci20_96	LMJ.RY0402.211496	3'UTR	No	No
		lci20_44	LMJ.RY0402.205944	Intron 6	Yes*	Yes (Mixo)
ADP/ATP translocase (AAA1)	Cre08.g358526	*3a1_58*	LMJ.RY0402.160658	Exon 6	Yes	Yes (VLC)
ADP/ATP translocase (AAA2)	Cre13.g581400	*3a2_41*	LMJ.RY0402.160658	Exon 15	Not confirmed	No
ADP/ATP translocase (AAA3)	Cre17.g697950	*3a3_39*	LMJ.RY0402.109039	Exon 2	Not confirmed	Yes (VLC)
		3a3_58	LMJ.RY0402.072258	Intron 3	Not confirmed	Yes (VLC)
		3a3_75	LMJ.RY0402.138675	Intron 3	Not confirmed	No
NAD(P)+ transhydrogenase (NTH)	Cre01.g054500	*nth_51*	LMJ.RY0402.077451	Intron 3	Yes	Yes (Mixo)
		nth_05	LMJ.RY0402.143805	5'UTR	Yes	No
		nth_19	LMJ.RY0402.242519	3'UTR	No	No
		nth_95	LMJ.RY0402.174495	5'UTR	No	No

This chapter aimed to identify potential components of energy homeostasis and trafficking pathways, *i.e.* components of malate shuttle, or putative transporters, and then evaluate their role in cell growth, photosynthetic performance and reserve formation in Chlamydomonas. Based on the above literature survey, potential candidates and their corresponding mutants, if available, were ordered from the CLIP library (Li et al., 2016). The candidates examined in this study are the MDH5, two putative oxoglutarate/malate translocators (i.e. OMT2, and the low-carbon inducible 20 - LCI20), a NNT and three chloroplastic ATP/ADP translocators.

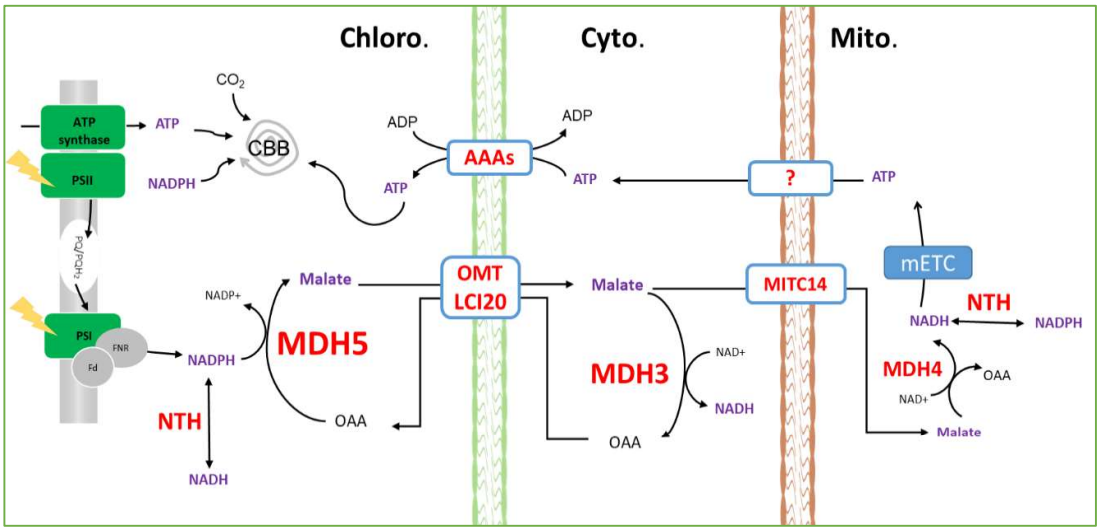

Figure III.1: **Mapping of candidate proteins pontentially involved in redox or ATP trafficking between subcellular compartmenets.** Candidate proteins are shown in red. Reducing equivalent and ATP are shown in purple. Sucellular localization is obtained from Predalgo (Tardif et al., 2012). The direction of trafficking is only speculation.

2.2. Validation of cassette insertion by PCR and expression level by RT-PCR

First, the position of the paromomycin insertion in the respective CLiP mutant lines was analyzed by PCR using gene-specific primers flanking the predicted site of insertion. Out of the 18 mutants ordered, nine was found to have insertion as predicted (**Table III.1** and **Fig. III.2A**). Mutant lines who have shown insertion in the predicted site were further analyzed by RT-PCR to verify whether such insertion could result in a defect in gene expression. These analyses showed that the insertion in the *lci20-44* mutant resulted in null expression of the *LCI20* gene whereas no conclusive results were obtained for the other mutants (**Fig. III.2B**).

2.3. Growth test In parallel to above genetic analysis, we also investigated growth and photosynthetic performance of these mutant strains under varying environmental conditions: i.e. HL, low CO_2. The goal of these experiments is to identify conditions when the candidate protein is required for growth. All mutants were subjected to growth test on solid agar plate (drop test) under a wide range of growth conditions (photoautotrophic or mixotrophic under different light intensities and CO_2 concentration). Interestingly, *omt2-83* and *lci20-44* mutants exhibited a strong growth delay under mixotrophic condition (i.e. TAP) but not during photoautotrophic air growth (**Fig. III.2 C, D**).

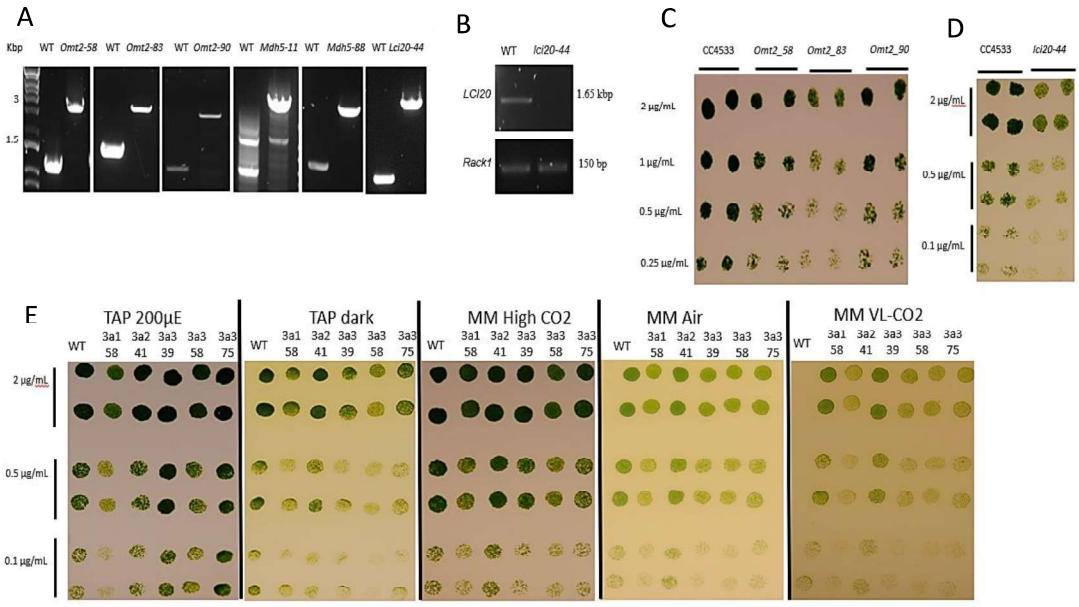

Figure IV.2: Mutant insertion validation and growth evaluation. (**A**) Representative images of PCR for the validation of insertion in the targeted genes. Mutants showing more or less 1.5 kb in addition to the WT PCR product size harbored the insertion of the paromomycin resistance cassette. WT corresponds to the reference strain and M refers to mutant. (**B**) RT-PCR for the confirmation of *LCI20* gene knockout. Rack1 was used as positive control. (**C** and **D**) Growth test of *omt2* and *lci20* mutants under mixotrophic condition in presence of acetate as external carbon source. (**E**) Growth test of putative

mutants of ATP/ADP translocators under wide range of growth condition. Cells were grown in liquid media in photoautotrophic condition to reach exponential phase prior to deposition on TAP agar plate at the same chlorophyll concentration as indicated. Images were taken 3 d after inoculation.

Mutants of putative chloroplastic ATP/ADP translocators (AAA1 and AAA3 but not AAA2) are impaired in growth under wide range of growth conditions including mixotrophic condition and photoautotrophic very-low-CO_2 condition (**Fig. III.2E**). Although we failed in validating the insertion in those mutants, their growth phenotype is in line with the function predicted for these ATP/ADP translocators.

2.4. Conclusion

Taken together, based on the genetic data together with the physiological observations, two proteins of the oxoglutarate/malate translocator (LCI20 or eventually also OMT2) and two translocators of ATP/ADP were considered strong candidates for further investigation. The *lci20-44* line was confirmed as a true knock-out, we reasoned that *omt2-83* is likely a knock-down. Genomic PCR on AAAs mutants did not help to map the insertion sites.

The *lci20-44* showed a severe growth defect during mixotrophic growth. This primary result therefore points to the important role of the putative 2-oxoglutarate/malate in cell physiology and energetic metabolism in Chlamydomonas. We have therefore chosen to focus on a detailed functional study of LCI20 and latest results are reported in **Chapter 3**.

Chapter 3. Role of malate shuttle in photosynthetic adaptation of Chlamydomonas to environmental fluctuations

Foreword

Plants and microalgae cells are made of subcellular organelles (chloroplast, mitochondria, peroxisome etc.) each performing a subset of metabolic reactions but physically separated from each other by biological membranes. Persistent exchange of signals (such as NO, H_2O_2, pH etc.), energies/co-factors (ATP, ADP, NAD(P)H etc.) and metabolites (ascorbate, malate, oxaloacetate etc.) between the various compartments are indispensable for achieving whole-cell homeostasis and optimal growth (Raghavendra and Padmasree, 2003; Elsässer et al., 2020). While some of those exchanges occur through passive diffusion, most of them are mediated by translocators located on the inner membrane of organelles (Neuhaus and Wagner, 2000; Taniguchi et al., 2002; Tyra et al., 2007). Understanding the complex interplay between cellular compartments is key towards rational engineering of metabolic pathways and the domestication of photosynthetic organisms for tailor-made production of valuable compounds.

Redox exchange between subcellular compartments through malate shuttle is a conserved mechanism in eukaryote cells. However, little is known about the function of this shuttle in microalgae. The model microalga *Chlamydomonas reinhardtii* can grow in three trophic styles with only light (phototrophy), reduced carbon source i.e. acetate (heterotrophy) or the combination of both (mixotrophy). Therefore, the location and mechanism of energy production may be different depending on the growth condition. While photosynthesis produces ATP and NADPH mostly in the chloroplast, acetate uptake consumes ATP at the expense of NADH therefore leading to elevated redox status. Redox exchange between the three organelles is mandatory to maintain an optimal ATP and NADPH ratio. Moreover, detailed characterization of the molecular players involved in redox trafficking is missing in microalgae.

In this chapter, we characterized the *low-carbon inducible 20* (*LCI20*) encoding a putative chloroplastic 2-oxoglutarate/malate translocator. We report here the role of LCI20 during the transition from photoautotrophy to mixotrophy as well as during fluctuations in the CO_2/O_2 ratio. We also investigated how a deficiency in LCI20 could affect carbon storage in Chlamydomonas under N replete conditions.

Chapter III

Role of malate shuttle in photosynthetic acclimation of Chlamydomonas to environmental fluctuations. (In prep)

Ousmane Dao[1], Saleh Alseekh[2], Adrien Burlacot[3,4], Marie Bertrand[1], Pascaline Auroy[1], Phuong-Chi Nguyen[1], Bertrand Légeret[1], Caroline Monteil[1], Anja Krieger-Liszkay[5], Andreas P.M. Weber[6], Alisdair R Fernie[2], Gilles Peltier[1*], Yonghua Li-Beisson[1*]

[1]Aix Marseille Univ, CEA, CNRS, BIAM, Institut de Biosciences et Biotechnologies Aix-Marseille, CEA Cadarache, Saint Paul-Lez-Durance 13108, France
[2]Department of Molecular Physiology, Max Planck Institute of Molecular Plant Physiology, Potsdam-Golm, Germany
[4]Department of Plant Biology, The Carnegie Institution for Science, Stanford, CA, 94305, USA
[4]Department of Biology, Stanford University, Stanford, CA, 94305, USA
[5]Institute for Integrative Biology of the Cell (I2BC), CEA, CNRS, Université Paris-Saclay, CEDEX, 91198 Gif-sur-Yvette, France
[6]Institute of Plant Biochemistry, Cluster of Excellence on Plant Science (CEPLAS), Heinrich Heine University, 40225 Düsseldorf, Germany

[*] Correspondence to: Yonghua Li-Beisson (yonghua.li@cea.fr), Gilles Peltier (gilles.peltier@cea.fr)

ORCID ID: 0000-0002-7040-5770 (O.D.), 0000-0003-2067-5235 (S.A.), 0000-0001-7434-6416 (A.B.), 0000-0001-5098-1554 (M.B.), 0000-0002-3376-6550 (P.A.), 0000-0002-0957-4700 (B.L.), 0000-0002-2834-6834 (C.M.), 0000-0001-9000-335X (A.R.F.), 0000-0001-7141-4129 (A.K.-L.), 0000-0002-2226-3931 (G.P.), 0000-0003-1064-1816 (Y.L.-B.)

Competing interests: there is no competing interests.

Author Contributions:
Y.L-B., G.P., O.D. conceived the study. Y.L-B. and G.P. supervised the work. O.D. performed most of the experiments. A.B. and G.P. supervised photosynthesis measurement performed by O.D.. P.A. M.B. and O.D. carried out immunoblots. A.K.-L and O.D. measured NAD(P)H production. C.M. performed phylogenetic analysis. S.A. and A.R.F. performed metabolomics. O.D., P.-C.N., and B.L. performed glycolate analysis. O.D. and Y.L-B. drafted the manuscript with contributions from A.P.M.W., A.K.L., A.B., G.P. and A.R.F..

Note: Main text of no more than 5,000 words and 10 display items (figures, tables). Articles allow up to 70 references.

Abstract

Redox exchange between subcellular compartments via the malate shuttle is a conserved mechanism and necessary for eukaryotic cells. Although well characterized in land plants, the function of the malate shuttle in microalgae is speculative and experimental evidence is scarce. Here, we report the role of a putative malate transporter, low-carbon inducible 20 (LCI20), during trophic transitions in Chlamydomonas. While *lci20* grew normally under steady-state photoautotrophic high (H) (2%) or low (L) -CO_2 (0.04%) and mixotrophic conditions, its growth is reduced during a transition from H-CO_2 to L or very low (VL)-CO_2 (0.01%), and from photoautotrophy to mixotrophy. *lci20* secreted a higher amount of glycolate when transferred from H to VL-CO_2, suggesting a defect in photorespiration. During the trophic transition, *lci20* exhibited reduced photosynthetic activity and an over-reduced chloroplast state. Furthermore, metabolomic analysis revealed an increase in malate and glutamate in *lci20*. Overall, our data suggest that LCI20 is a malate transporter that actively participates in redox balancing between chloroplast and extra-chloroplast compartments during environmental transitions, underscoring the success of microalgae in colonizing contrasting ecological niches.

Keywords: (3-10)
Chloroplast, redox balancing, malate shuttle, photorespiration, acetate metabolism

Introduction

Microalgae account for nearly half of the photosynthetic CO_2 fixation on Earth (Field et al., 1998; Smetacek, 1999), and are promising candidates for mitigating climate change by assimilating CO_2 and producing useful compounds, thereby contributing to the global bioeconomy (Fernández et al., 2021; Ullmann and Grimm, 2021; Reisoglu et al., 2023). During photosynthesis, light energy is converted to chemical energy (ATP and NAD(P)H) and CO_2 to reduced carbon in the chloroplasts of eukaryotic microalgae. At the subcellular level, ATP, NAD(P)H, and reduced carbon are ultimately required in different stoichiometric ratios for each metabolic process that occurs in different organelles that are physically separated from each other by biological membranes (Johnson and Alric, 2013; Burlacot et al., 2019). As light and CO_2 levels are constantly fluctuating, leading to an imbalance between energy conversion rate and utilization, microalgae have evolved a number of mechanisms to cope with those perturbations, such as the CO_2-concentrating mechanisms (CCM), non-photochemical quenching, and alternative photosynthetic pathways. In addition to their efficient photosynthesis, many microalgae have evolved a mixotrophic lifestyle (assimilation of both organic and inorganic carbon sources) to better adapt to environmental fluctuations and colonize different ecological niches (Selosse et al., 2017; Zuccaro et al., 2019; Mansour and Anestis, 2021; Villanova and Spetea, 2021; Lepori-Bui et al., 2022). At the biotechnological level, the mixotrophic mode favors high density cultures and improves biomass production (Fan et al., 2012; Goodenough et al., 2014; Marella et al., 2021; Villanova et al., 2021). How microalgae make the transition from photoautotrophy to mixotrophy or vice versa remains unknown. The bioenergetics of mixotrophy is rather complex and requires communication between subcellular compartments (Johnson and Alric, 2012; Plancke et al., 2014; Lauersen et al., 2016). Energy/carbon trafficking between subcellular organelles in eukaryotic microalgae is expected to be prevalent when adapting to fluctuating light and CO_2 levels or when switching between trophic modes for optimal growth (Burlacot et al., 2019; Kaye et al., 2019; Scheibe, 2019; Puzanskiy et al., 2023). However, little is known about the molecular mechanisms involved.

Redox exchange between subcellular organelles has been proposed in microalgae decades ago (Peltier and Thibault, 1985a; Lemaire et al., 1988; Cardol et al., 2003) and more recently (Dang et al., 2014; Bailleul et al., 2015; Kong et al., 2018; Burlacot et al., 2022; Peltier et al., 2023). Clear experimental evidence comes from the mitochondria-dependent photoautotrophic growth of *Chlamydomonas reinhardtii* (hereafter Chlamydomonas) FUD50su, which is deficient in the chloroplast ATP synthase (Lemaire et al., 1988). It has been proposed that the export of photosynthetic NADPH to the mitochondrial respiratory chain allows the generation of ATP to sustain CO_2 fixation in the chloroplast (Lemaire et al., 1988; Boschetti and Schmid, 1998). Similarly, the contribution of mitochondria in sustaining photosynthesis was suggested in *pgrl1*, a mutant defective in cyclic electron flow under high light and low CO_2 conditions (Dang et al., 2014). Conversely, mutations in the components of the mitochondrial electron transport chain (mETC) affected photosynthesis, stimulated the cyclic electron flow (CEF), and activated state transition in Chlamydomonas (Cardol et al., 2003). The function of the algal CCM was sensitive to mETC inhibitors, suggesting a role for chloroplast-to-mitochondrial electron flow (CMEF) in the CCM energization (Burlacot et al., 2022). The CMEF is also used during steady-state CO_2 fixation in Chlamydomonas even when CCM is inactive (Peltier et al., 2023). During the transition from photoautotrophy to mixotrophy, the expression levels of many chloroplast dicarboxylic

acid and triose phosphate transporters were upregulated, suggesting their role in inter-organelle communication during adaptation to the mixotrophic mode (Puzanskiy et al., 2020; Puzanskiy et al., 2023).

The exchange of reducing power (NAD(P)H, which is not membrane-permeable, between organelles has been proposed to operate via a "malate shuttle" composed of malate dehydrogenases (MDHs) and translocators (Fridlyand et al., 1998; Scheibe, 2004; Selinski and Scheibe, 2019; Dao et al., 2022). MDHs are ubiquitous enzymes that catalyze the reversible oxidoreduction of malate and oxaloacetate by using NAD(P)H or NAD(P)+, respectively. The role of MDHs in redox exchange between subcellular compartments has been demonstrated in land plants (Mettler and Beevers, 1980; Gietl, 1992; Fridlyand et al., 1998; Zhao et al., 2018; Selinski and Scheibe, 2019; Zhao et al., 2020; Yokochi et al., 2021). In Arabidopsis, malate generated in the chloroplast was shown to trigger the ROS production in mitochondria and activate programmed-cell death, suggesting a role of the malate shuttle in chloroplast-mitochondria communication (Zhao et al., 2018). Post-translational regulation of the chloroplastic NADP-MDH has also been demonstrated to be vital for land plants under fluctuating light environment highlighting the role of malate shuttle in photosynthesis (Yokochi et al., 2021). In microalgae, the function of MDHs is poorly understood. Of the five MDHs identified in Chlamydomonas (Dao et al., 2022), only MDH2 has been studied both in vivo and in vitro (Kong et al., 2018). In addition to MDHs, the malate shuttle requires translocators of malate and/or other di- or tri-carboxylic acids. In Arabidopsis, two related dicarboxylate transporters (DiT1 and DiT2) with overlapping substrate specificities mediate malate exchange across the chloroplast envelope (Weber and Flügge, 2002; Kinoshita et al., 2011; Weber and Linka, 2011; Dao et al., 2022). Both DiT1 and DiT2 are required for photorespiratory nitrogen assimilation (Renné et al., 2003; Schneidereit et al., 2006; Kinoshita et al., 2011). DiT1 has also been shown to function as a malate valve that exports excess reductant from the plastid during high light (Kinoshita et al., 2011). Despite the existence of a number of genes encoding putative chloroplastic malate translocators (Merchant et al., 2007; Johnson and Alric, 2013; Dao et al., 2022), none of them have been studied in Chlamydomonas.

Here, we report the physiological role of LCI20 in Chlamydomonas during trophic transitions. Mutants deficient in LCI20 (hereafter *lci20*) grow poorly during a transition from H-CO_2 to Very-Low (VL)-CO_2 and from photoautotrophic to mixotrophic conditions. By manipulating the CO_2/O_2 ratio and monitoring glycolate secretion, we show that the function of photorespiration, but not the CCM, is defective in *lci20*. Further investigations revealed a reduced photosynthetic electron transfer rate (ETR) and NADPH production capacity, and over-reduction of the chloroplast in *lci20*. Finally, by performing a metabolomics analysis, we observed hyper-accumulation of malate and glutamate in *lci20* under photoautotrophic L-CO_2, VL-CO_2, and mixotrophic conditions. Taken together, we have proposed that LCI20 is likely to be a malate/glutamate transporter involved in the export of reducing power from the chloroplast under excessive reducing conditions, i.e. during the activation of photorespiration in VL-CO_2 or during acetate supply. We discuss how the malate shuttle represents an efficient strategy for microalgae to colonize contrasting ecological niches.

Results

LCI20 encodes a putative malate transporter whose expression is dynamically modulated by light, CO_2 levels, and acetate supply.

To begin investigating the function of chloroplast-localized malate transporters in Chlamydomonas, we have identified three putative orthologues of previously characterized Arabidopsis DiT1 and DiT2 malate transporters i.e. the three putative chloroplast 2-oxoglutarate/malate translocators (annotated as OMT1, OMT2 and LCI20) (Merchant et al., 2007; Johnson and Alric, 2013). By re-analyzing previously published data reporting the dynamics of the Chlamydomonas transcriptome in response to day-night cycle, changing CO_2 levels, and during trophic transitions (Miura et al., 2004; Yamano et al., 2008; Fang et al., 2012; Zones et al., 2015), we found that *LCI20* (but not *OMT1* and *OMT2*) expression shows a strong transient induction at the beginning of the light period and after the transition from H-CO_2 (high-CO_2) into L-CO_2 (low CO_2) or VL-CO_2 (very-low CO_2) levels and from photoautotrophy to mixotrophy (**Fig. 1 *A*-*C***). These malate translocators likely exhibited subfunctionalization, as reflected by their expression levels and their temporally and environmentally distinct regulatory patterns. To determine whether LCI20, OMT1 and OMT2 share some similarities and conserved domains found in existing known malate transporters, we generated an unrooted maximum likelihood tree of the dicarboxylate transporter family (Citrate carrier CitT-related/ IPR030676) in plants and green microalgae. This phylogenetic analysis revealed that LCI20 is most closely related to the DiT2 transporters, is widespread in Chlorophyta, and is evolutionarily divergent from the OMT family (**Fig. 1*D* and Fig. S1**). Furthermore, LCI20 is the only putative malate transporter in Chlamydomonas that has been experimentally validated for chloroplast localization and belongs to the GreenCut2 (Karpowicz et al., 2011; Mackinder et al., 2017). The above-mentioned features of the LCI20 make it an interesting candidate as an essential malate transporter required for the adaptation of Chlamydomonas to environmental fluctuations.

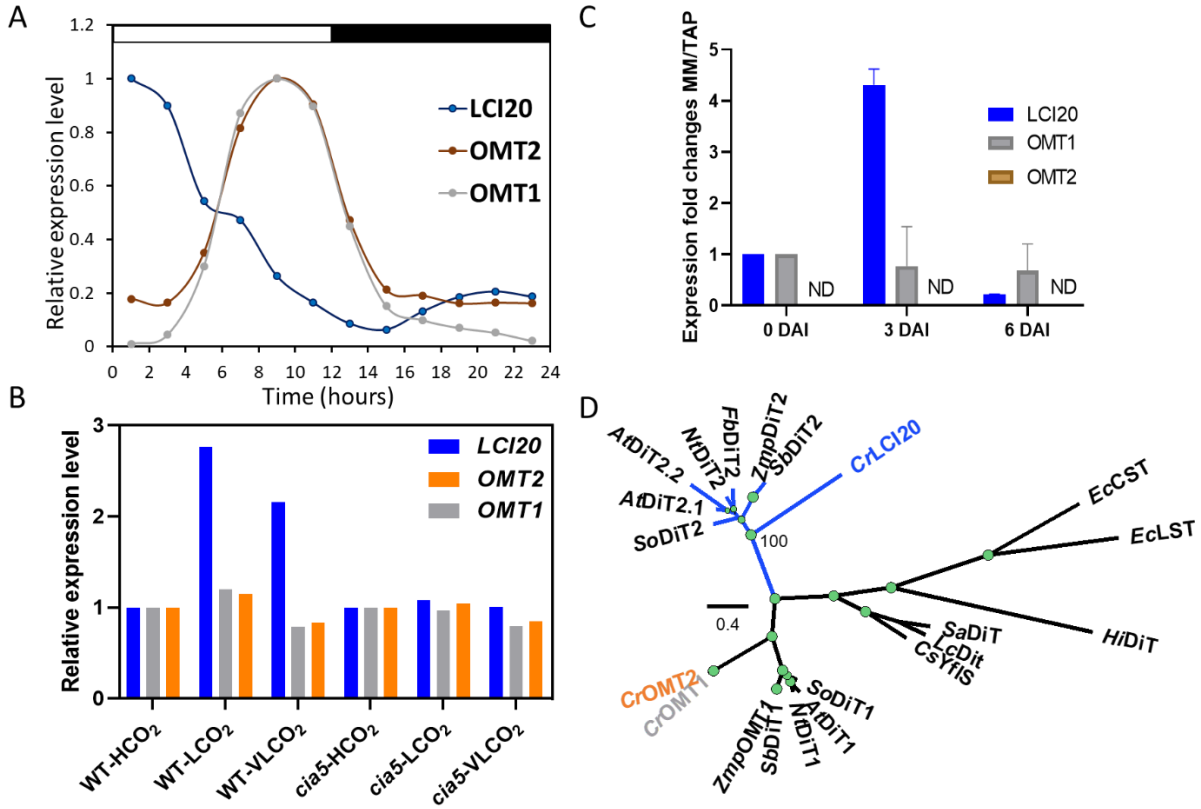

Fig. 1. *LCI20* putatively encodes a malate transporter, and its expression is highly dynamic in response to a day-night cycle, changing CO_2 levels and acetate supply. **(A)** Expression level of *LCI20*, *OMT1* and *OMT2* genes in Chlamydomonas WT during a

day/night cycle. **(B)** Expression level of *LCI20*, *OMT1* and *OMT2* genes in Chlamydomonas WT at different CO_2 levels. **(C)** Expression level of *LCI20*, *OMT1* and *OMT2* genes during a transition from photoautotrophy to mixotrophy. Data for ***A-D*** were derived from Fang et al., 2012; Zones et al., 2015; Puzanskiy et al., 2023. **(D)** Unrooted Maximum Likelihood tree of the dicarboxylate transporter family (InterPro entry IPR030676 / CitT-rel) in plants, Chlamydomonas reinhardtii and eubacteria showing the affiliation of the LCI20 gene to the Dit2 group. The first two letters of the acronyms indicate the species (At, Arabidopsis thaliana; Cr, Chlamydomonas reinhardtii; Cs, Clostridium saccharobutylicum; Ec, Escherichia coli; Fb, Flaveria bidentis; Hi, Haemophilus influenzae; Lc, Liquorilactobacillus cacaonum; Nt, Nicotiana tabacum; Sa, Staphylococcus aureus; So, Spinacia oleracea; Zm, Zea mays). The three following letters indicate the group of transporters (DiT, Dicarboxylate transporter; TST, L-tartrate/succinate transporter; CST, Citrate/succinate transporter; YlfS, 2-oxoglutarate/malate transporter). The tree was drawn to scale. The scale bar represents the number of substitutions per site. Tree topology was tested using an ultrafast bootstrap approximation approach with 1000 replicates. Gray circles represent bootstrap values and are drawn to scale. Dotted branches represent bacterial lineages. A full version of this tree with primary accession numbers is given in **Supplementary Fig. S1 (Annex 3)**.

The growth of the *lci20* is affected by a transition from high to low CO_2 or by the addition of acetate. To decipher the function of LCI20, we isolated a mutant harboring an antibiotic marker gene in the sixth intron of the LCI20 locus from the Chlamydomonas library project CLiP collection and named it *lci20* (Li et al., 2016) (**Fig. 2A**). We confirmed the insertion of the paromomycin resistance gene and the absence of the *LCI20* transcript in *lci20* (**Fig. 2*B-C***). We then performed genetic complementation of *lci20* by expressing the full-length genomic DNA encoding *LCI20* driven by the PSAD promoter (**Fig. 2*B-C*; Supplemental Fig. S2**). We examined the growth of *lci20* under photoautotrophic, mixotrophic, and heterotrophic conditions (**Fig. 2*D-I*; Fig. S2**). No growth defect was observed under steady-state photoautotrophic L-CO_2 (air CO_2 level) or at H-CO_2 (2%) (**Fig. 2*D-E*; Fig. S2*A-D***). Similar to the transcript abundance of *LCI20* after transition from H to L-CO_2, we found that the growth of *lci20* was slightly impaired after a transition from H-CO_2 (2%) to L-CO_2 (400 ppm in air) and severely impaired when transitioning from H- to VL-CO_2 (100 ppm in air) (**Fig. 2 *F-G*; Fig. S2 *E-F***). Remarkably, the growth of *lci20* was severely impaired under mixotrophic but not heterotrophic conditions (**Fig. 2 *H-I*; Fig. S2 *I-J***). Confocal microscopy revealed palmelloid formation in *lci20* under mixotrophic condition (**Fig. S3**). These results suggest that LCI20 is an important player in cell growth during photosynthetic adaptation to changing CO_2 levels and to acetate supply.

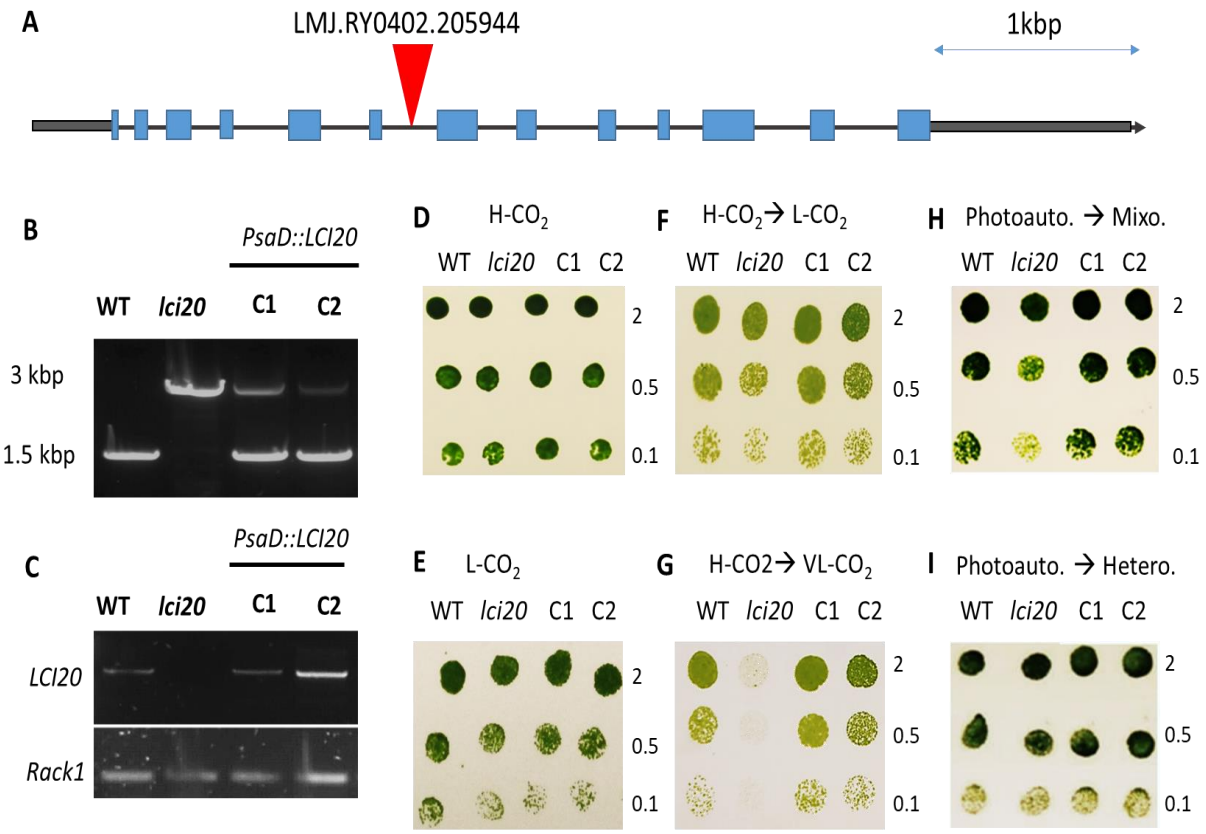

Fig. 2. The *lci20* growth is affected by the transition from high to low CO_2 and acetate supply. (**A**) Genomic structure of *LCI20* gene and the predicted insertion of the paromomycin resistance cassette. Gray boxes at both extremities represent the 5' and 3'UTR, respectively. Exons are colored blue. (**B**) Amplification of *LCI20* full-length genomic sequence by PCR in WT, the putative mutant, and the complemented lines. **(C)** Amplification of *LCI20* full-length CDS by RT-PCR. Rack1 was used as a control. **(D-I)** Growth performance of the *lci20* compared to the WT and complemented lines on agar plate exposed to various CO_2 concentrations or acetate as carbon source. Cells were grown in liquid culture in flasks under photoautotrophic air CO_2 level prior to spot testing. A drop containing 8 µL of culture was spotted for each strain at 2, 0.5 and 0.1 µg/mL of chlorophyll. Images were taken after 4 days at 80 µmol photons m^{-2} s^{-1} or 6 days for heterotrophic growth.

The *lci20* mutant is defective in photorespiratory glycolate metabolism. The growth defect of *lci20* during the transition from H-CO_2 to VL-CO_2 levels prompted us to investigate a possible involvement of LCI20 in the functioning of CCM and photorespiration, both mechanisms being induced during adaptation to limiting CO_2 conditions (Suzuki et al., 1990; Wang et al., 2015; Shi et al., 2021). In addition, LCI20 has been proposed to play a role in providing energy for the functioning of CCM via the malate shuttle in Chlamydomonas (Burlacot et al., 2022; Peltier et al., 2023). Two types of CCM could be activated in Chlamydomonas depending on the CO_2 levels i.e., the L-CO_2-based CCM (0.03-0.05% CO_2), which preferentially transports CO_2, and VL-CO_2-based (< 0.03%) CCM, which predominantly takes up HCO_3^- (Adler et al., 2022; Burlacot and Peltier, 2023). The normal growth of the *lci20* under steady-state air conditions (**Fig. 2*E***) ruled out any dysfunction of the former. To determine whether *lci20* could be affected in the very-low-CO_2-based CCM or photorespiration, we monitored the growth of *lci20* under photorespiratory (21% O_2) versus non-photorespiratory (2% O_2) conditions under VL-CO_2 (**Fig. 3**). As a positive control, we used the *cia5* mutant, which is known to be

defective in both CCM and photorespiration (Moroney et al., 1989; Marek and Spalding, 1991; Fukuzawa et al., 2001; Nakamura et al., 2005). The *lci20* grew poorly under photorespiratory conditions (100 ppm CO_2; 21% O_2), but the growth could be restored when photorespiration was suppressed (i.e. at 2% O_2) (**Fig. 3*A***), indicating a defect in photorespiration but not in VL-based CCM. Interestingly, the *cia5* mutant, which lacks most of the CCM proteins, could not grow under VL-CO_2 at 2% O_2, further confirming that LCI20 is not involved in CCM (**Fig. 3*A***). The amount of glycolate secreted into the culture medium is often used as a proxy to monitor photorespiratory activity in Chlamydomonas (Moroney et al., 1986; Nakamura et al., 2005; Taubert et al., 2019; Yun et al., 2021). Here, we observed higher glycolate secretion in *lci20* compared to WT when transferred to VL-CO_2 (**Fig. 3*B***). We conclude that *lci20* is defective in the photorespiratory glycolate metabolism during VL-CO_2 adaptation in Chlamydomonas.

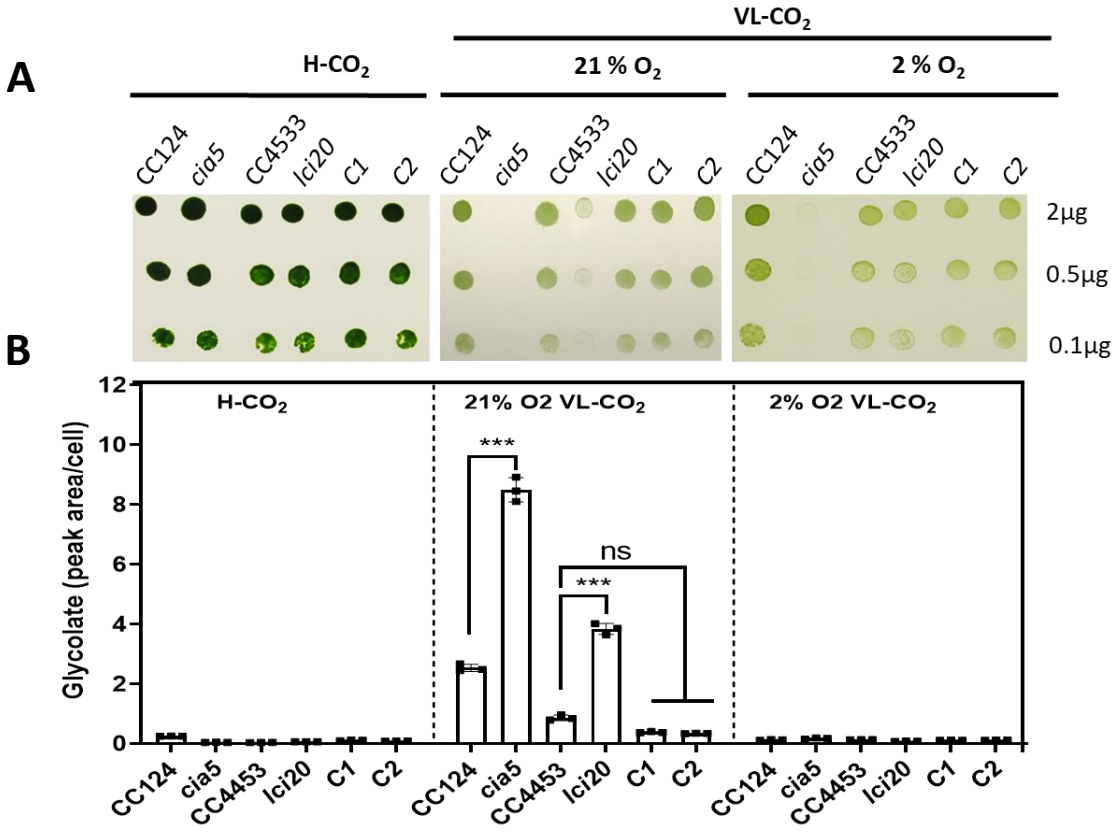

Fig. 3. The LCI20 plays a role in photorespiration. (A) A simplified schematic photorespiratory metabolic pathway in Chlamydomonas. **(B)** Growth performance under different CO_2/O_2 ratio on agar plate exposed to 80 µmol photons m^{-2} s^{-1}. **(C)** Quantification of glycolate secretion from liquid culture growth under indicated CO_2/O_2 ratio as in panel B. Cells cultivated photoautotrophically under air at 2% CO_2 and continuous light of 80 µmol photons m^{-2} s^{-1} were used for spot test (panel B) or acclimated for 20h into indicated CO_2 levels prior to secreted glycolate analysis (panel C). Shown are values from three biological replicates ± SD. Asterisks represent statistically significant difference compared to the wild-type strains (* p<0.05, ** p<0.01, *** p<0.001 and **** p<0.0001) using one-way ANOVA.

The *lci20* shows reduced photosynthetic activity and an over-reduced chloroplast. One of the long-standing hypothesized functions of the malate shuttle in photosynthetic organisms is to balance the cellular energy status by transporting photosynthetic electrons

as malate between energy organelles, such as mitochondria, peroxisomes, and chloroplasts (Kong et al., 2018; Selinski and Scheibe, 2019; Zhao et al., 2020). To investigate the role of LCI20 as a valve of photosynthetic electron during photoautotrophic growth in Chlamydomonas, we assessed chlorophyll a fluorescence at room temperature as a proxy to estimate PSII electron transfer rate (ETR) in photoautotrophic H-CO_2 and L-CO_2 grown cells (**Fig. 4 A-B**). Interestingly, *lci20* showed a reduced ETR compared to the controls under L-CO_2 but not under H-CO_2 (Fig. 4 A-B). To determine whether the reduced ETR in *lci20* is caused by an over-reduction of the chloroplast, we investigated the PQ redox state by analyzing the low temperature (77K) chlorophyll fluorescence emission (Virtanen and Tyystjärvi, 2022) (**Fig. 4 C-D**). Under H-CO_2, both WT and *lci20* showed an oxidized PQ pool as indicated by a higher fluorescence emission at 683 nm (from PSII antenna) compared to the emission at 710 nm (PSI antenna). When grown under L-CO_2, *lci20* exhibited an over-reduced PQ pool shown by an increase in the fluorescence emission at 710 nm. Both DCMU and far-red light treatment oxidize the PQ pool in *lci20*, as shown by a decrease in the fluorescence emission at 710 nm (**Fig. 4 E-F**) indicating that the over-reduced PQ pool in *lci20* is caused by PSII activity. Taken together, the absence of LCI20 results in an over-reduced photosynthetic electron transport chain, which slows down the photochemical reactions. LCI20 plays an important role in chloroplast redox balance by exporting excess electrons via the malate valve.

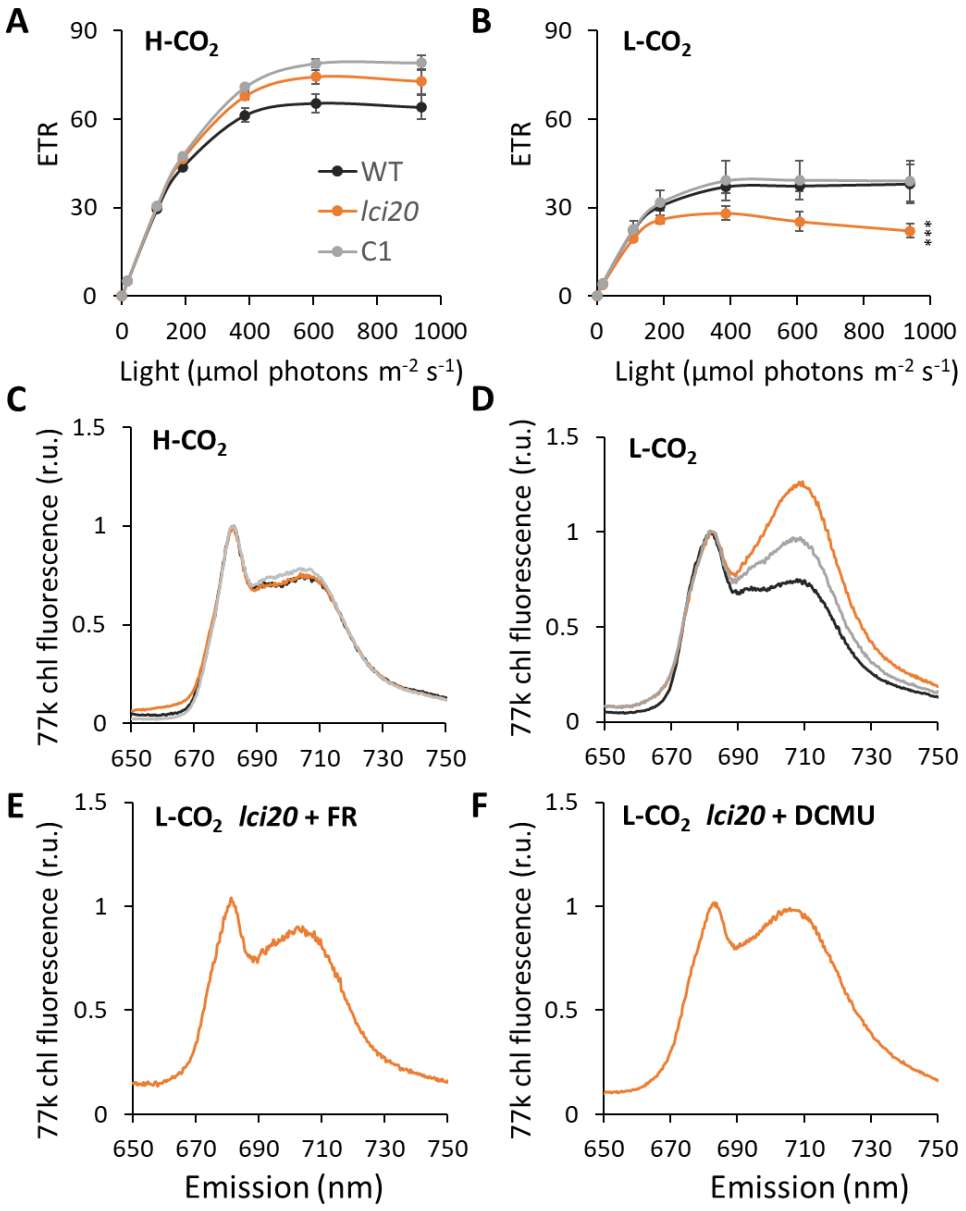

Fig. 4. Electron transfer rate and plastoquinone redox state in lci20 during photoautotrophic growth. (**A-B**) Photosynthetic electron transfer rate (ETR) measured from cells grown under photoautotrophic H-CO_2 and L-CO_2 conditions. Cells were exposed for 1 min at the following light intensity: 17, 110, 190, 380, 608 and 940 µmol photons m−2 s−1 respectively. Values are means of three biological replicates with standard deviation. Asterisks indicate statistical differences compared to the WT. (**C-D**) Low temperature (77K) chlorophyll fluorescence emissions obtained from cells grown under photoautotrophic H-CO_2 and L-CO2 conditions. (**E-F**) Low temperature (77K) chlorophyll fluorescence emissions obtained from L-CO_2 *lci20* grown cells (shown in D) exposed to far red light for 15 min or treated with 10µM DCMU for 1h. Fluorescence emissions were collected from 650 to 750 nm and data were normalized by the peak emission at 683 nm. Shown represents an average of three biological replicates.

Metabolomics analyses reveal an increased accumulation of malate and glutamate in *lci20* during mixotrophic and low CO_2 photoautotrophic growth. Metabolomic comparisons between one population and another can provide insights into underlying

metabolic adaptations (Kong et al., 2018; Saint-Sorny et al., 2022). We expected that any dysfunction in malate trafficking between organelles should potentially disrupt cellular metabolism and metabolite levels. Furthermore, this could provide an indirect indication of the metabolites transported by LCI20. To investigate the metabolic reorientation in *lci20*, we performed a metabolomics analysis of photoautotrophic H-CO_2, L-CO_2, VL-CO_2 as well as mixotrophic grown cells (**Fig. 5**). The metabolite profile of high-CO_2 grown *lci20* cells was identical to that of control cells (**Fig. 5*A, E***). Interestingly, we observed higher accumulation of malate and glutamic acid in *lci20* under mixotrophic, photoautotrophic L-CO_2 and, to a lesser extent, under VL-CO_2 conditions (**Fig. 5 *A, B-D***). The accumulation of the other detected metabolites was not consistently affected in *lci20* under the three conditions tested (photoautotrophic L-CO_2, VL-CO_2 and mixotrophic) (**Fig. 5 *A* and *B-D***). Based on these results, we suggest that LCI20 could transport malate and glutamate in vivo, and that the overaccumulation of malate leads to a higher reducing pressure in the chloroplast, thus underlying/explaining the observed phenotypes in the *lci20* cells.

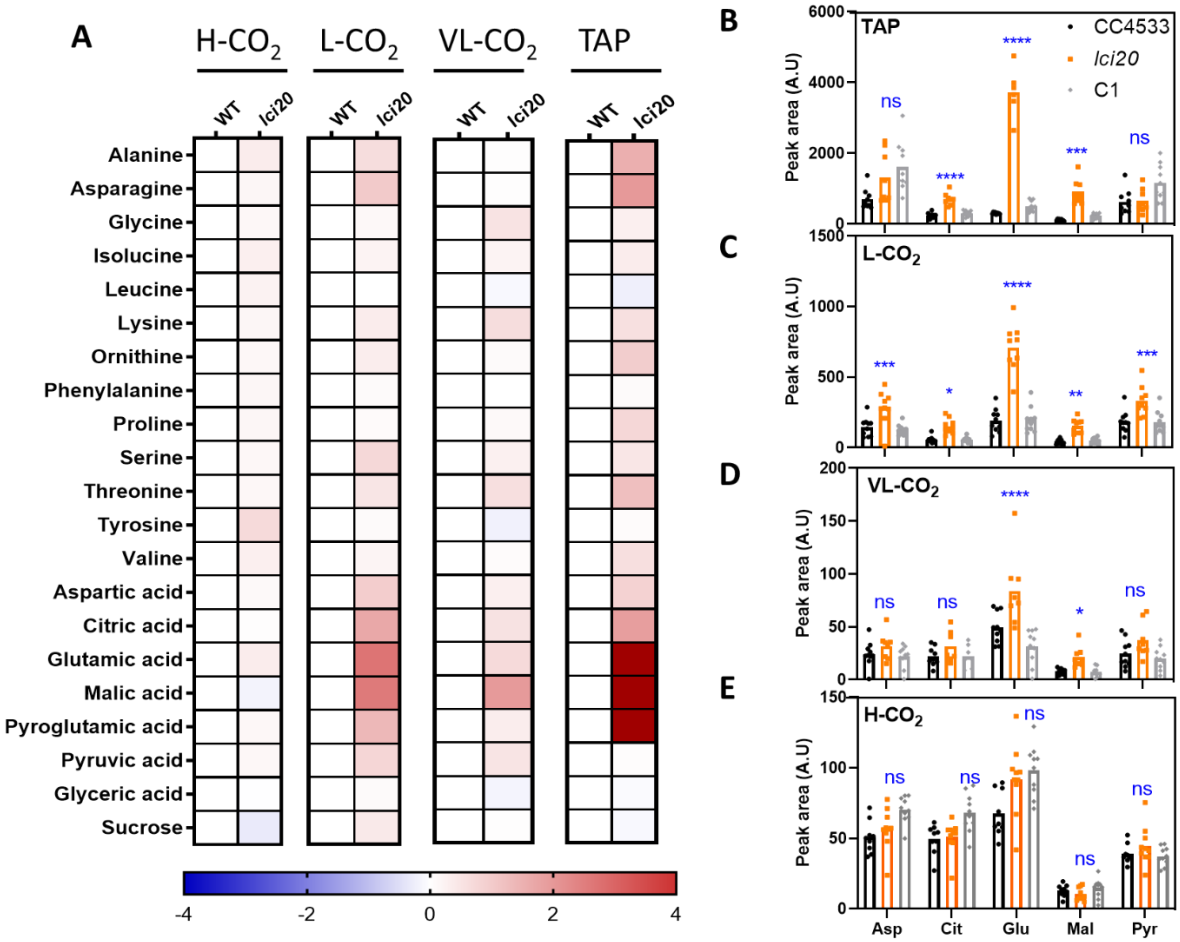

Fig. 6. The *lci20* over accumulates malate and glutamate during mixotrophic and L-CO_2 photoautotrophic growth. (**A**) Heat map showing fold-changes of metabolites in the *lci20* as compared to the WT under H-CO_2, L-CO_2, VL-CO_2 and TAP conditions. (**B-E**) Histograms showing the quantification of aspartic acid, citric acid, glutamic acid, malic acid and pyruvic acid under TAP (B), L-CO_2 (C), VL-CO_2 (D) and H-CO_2 (E) conditions in the WT, *lci20* and C1 strains. Values represent at least biological replicates for each strain. Asterisks represent statistically significant differences between strains (* p<0.05, ** p<0.01 and *** p<0.001) using one-way ANOVA.

Discussion

The success of eukaryotic photosynthetic organisms in colonizing diverse ecological niches is due to the flexibility and compartmentalization of their metabolism in subcellular organelles (Field et al., 1998; Smetacek, 1999; Alberts et al., 2002; Raghavendra and Padmasree, 2003; Falkowski et al., 2004; Gabaldón and Pittis, 2015). The malate shuttle, conserved in all eukaryotes, is one of the mechanisms of energetics exchange between organelles and has been well-studied in mammalian cells and land plants (Mettler and Beevers, 1980; Gietl, 1992; Fridlyand et al., 1998; Zhao et al., 2018; Selinski and Scheibe, 2019; Zhao et al., 2020). Unlike other known shuttles that are restricted to a specific organelle, such as the chloroplast-located triose phosphate shuttle (Huang et al., 2023), all subcellular compartments harbor malate dehydrogenases, making malate an ubiquitous reductant carrier (Gietl, 1992; Scheibe, 2004; Selinski and Scheibe, 2019; Dao et al., 2022). Despite its importance and ubiquity, only few studies have reported the role of the malate shuttle components in algal bioenergetics metabolism and none of the putative malate translocators have been characterized to date (Lemaire et al., 2005; Kong et al., 2018).

Here, we investigated the function of the chloroplast-localized putative malate transporter LCI20 in Chlamydomonas. We demonstrated the physiological role of LCI20 during the adaptation of Chlamydomonas to the transition between trophic styles and between changing CO_2/O_2 levels. The *lci20* mutant was unable to grow after a transition from H-CO_2 to VL-CO_2 at ambient O_2 levels and from photoautotrophic to mixotrophic lifestyle indicating a defect in photorespiration and in the export of reductant from the chloroplast respectively (**Fig. 2 *G, H* and Fig. 3*B***). Overall, we have observed a decrease in photosynthetic activity and an over-reduced chloroplast in *lci20* (**Fig. 4**). Based on the metabolomics analysis (**Fig. 5**) and the different phenotypes of *lci20*, we propose that LCI20 is a malate/glutamate transporter required to balance the redox status of chloroplasts. The metabolomics analysis performed here revealed hyper-accumulation of glutamate and malate, strongly suggesting a disruption of malate and glutamate metabolism in *lci20* (**Fig. 5**). From a physiological point of view, elevated levels of malate indicate over-reduction of the cells, whereas high levels of glutamate could indicate an imbalance between carbon and nitrogen metabolism (Wallsgrove et al., 1986; Renberg et al., 2010). Both cases are expected to occur when the photorespiratory pathway is impaired (Eisenhut et al., 2013).

Photorespiration, due to the oxygenation reaction of Rubisco, is inevitable in an oxygen-rich atmosphere and consists of multiple metabolic reactions that are distributed over several subcellular compartments, it therefore requires intimate inter-organelle communication. The occurrence of photorespiration in Chlamydomonas has so far been underestimated because the induction of CCM increases the internal inorganic carbon concentration and presumably suppresses the oxygenase activity of Rubisco (Marek and Spalding, 1991). Nevertheless, genes encoding for photorespiration proteins are present in the Chlamydomonas genome and are co-regulated with CCM genes by the CCM1 transcription factor (Fukuzawa et al., 2001; Miura et al., 2004; Yamano et al., 2008; Fang et al., 2012; Santhanagopalan et al., 2021). Transcriptomic analyses reported a transient upregulation of genes encoding for 11 key photorespiratory enzymes under low CO_2 conditions (air level, 400 ppm) concomitant with the induction of CCM (Miura et al., 2004; Yamano et al., 2008; Fang et al., 2012; Santhanagopalan et al., 2021). Therefore, photorespiration in Chlamydomonas is likely to function, at least transiently, in

combination with the CCM. Indeed, in Chlamydomonas WT, the glycolate produced during photorespiration is estimated to be half secreted and half metabolized in a photorespiratory pathway (Peltier and Thibault, 1985b; Moroney et al., 1986; Nakamura et al., 2005). We observed higher glycolate secretion and a strong growth retardation in *lci20* under VL-CO_2 at atmospheric levels (21%), but not under 2% O_2, indicating a defect in the photorespiratory pathway (**Fig. 3**). The defects in the growth of *lci20* during the transition from H- to L-CO_2 are similar to those reported for other photorespiratory mutants of Chlamydomonas, deficient in the phosphoglycolate phosphatase 1 (*pgp1*), the glycolate dehydrogenase 1 (*gdh1*), or the hydroxypyruvate reductase 1 (*hpr1*), respectively (Suzuki et al., 1990; Nakamura et al., 2005; Shi et al., 2021). The involvement of the malate shuttle in photorespiration, as in case of DiT2, is not new and has been documented for land plants under suboptimal CO_2 availability (Taniguchi et al., 2002; Renné et al., 2003; Schneidereit et al., 2006; Takahashi et al., 2007; Cousins et al., 2008; Lindén et al., 2016). In terms of molecular mechanisms, LCI20 could act as a malate/glutamate transporter like the Arabidopsis DiT2. Another alternative explanation is that the reductant exported from the chloroplast through LCI20 is used in subsequent steps of photorespiration in the peroxisomes or mitochondria. A similar proposal has been made for the DiT1 in plants (Kinoshita et al., 2011). Consistent with our report, malate and glutamate transporters in Arabidopsis plastids with strong homology to LCI20 (**Fig. 1 *D* and S1**), overaccumulate photorespiratory metabolites such as glutamate, 2-oxoglutarate, serine, malate, glyoxylate etc. when grown in the air (Somerville and Ogren, 1983; Weber et al., 1995; Taniguchi et al., 2002; Weber and Flügge, 2002; Renné et al., 2003; Kinoshita et al., 2011).

In addition to its autotrophic growth, Chlamydomonas has evolved a versatile lifestyle, i.e., the ability of mixotrophic and heterotrophic growth. The latter two require the metabolism of acetate through the glyoxylate cycle (Plancke et al., 2014; Lauersen et al., 2016). However, how cells balance the different carbon and energy sources in the light is not known. We show here that heterotrophic growth on acetate is normal in the *lci20* mutant, thus excluding a defect in the functioning of the glyoxylate cycle, but growth is impaired in the presence of light (**Fig. 2*H, 2I***). We conclude that LCI20 plays a critical role in the adaptation to mixotrophy by balancing photosynthesis and acetate utilization (Johnson and Alric, 2012; Johnson and Alric, 2013). Acetate uptake and conversion to acetyl-CoA require additional ATP, which can occur in three subcellular compartments, namely chloroplasts, mitochondria, and peroxisomes (Johnson and Alric, 2013; Plancke et al., 2014; Lauersen et al., 2016). It has been reported that acetate induces an over-reduction of the plastoquinone pool and consequently of the chloroplast stroma during mixotrophic growth (Polle et al., 2000; Johnson and Alric, 2012; Saint-Sorny et al., 2022). Saint-Sorny et al. have recently demonstrated the effect of acetate on the redox state of chloroplasts, supported by the high reduction state of the photosynthetic chain (Saint-Sorny et al., 2022). Overall, acetate assimilation increases the cellular NAD(P)H level at the expense of ATP, therefore leading to an imbalance in ATP/NAD(P)H ratio. In such a scenario, redistribution of reductant between compartments for use by anabolic pathways would be expected to be even more critical, thus explaining the stronger growth defect when *lci20* grew in the presence of acetate.

The absence of LCI20 resulted in decreased ETR, NADPH production rate, and O_2 evolution under L-CO_2 but not under high CO_2, consistent with its potential role in

modulating cellular redox as a malate valve (**Fig. 4**). The light-dependent formation of malate in the chloroplast is mediated by the NADP–MDH5, whose activation is thioredoxin-regulated and probably controlled by the stromal NADPH/$NADP^+$ ratio (Scheibe and Jacquot, 1983; Scheibe, 2004; Lemaire et al., 2005). However, the direction of malate transport is controlled by the gradient between the stroma and the cytosolic pool. Import of malate into the chloroplast could be expected when the malate concentration is higher in other organelles, as it was suggested during nitrogen starvation, which eventually serves as a feedback signal to repress photosynthesis (Kong et al., 2018). However, considering that photosynthesis per se generates an excess of reductant relative to ATP and the excess of reductant from acetate metabolism (in the case of mixotrophy), it is likely that LCI20 functions to export malate under the conditions used in the present work. The malfunction of malate transport through LCI20 will therefore lead to its over-accumulation and over-reduction of the chloroplast. Our metabolomics revealed higher levels of malate and glutamate in the *lci20* under photorespiratory and mixotrophic conditions (**Fig. 5**). Indeed, there is an active exchange of reducing power between subcellular compartments either in the presence of acetate or during photorespiration. Photorespiration is a highly energetic pathway that shuttles chloroplast-generated NAD(P)H to other subcellular organelles (Eisenhut et al., 2019; Lim et al., 2020; Dao et al., 2022; Segura Broncano et al., 2023). Photorespiratory mutants deficient in the glutamate/malate transporter in Arabidopsis showed photoinhibition of PSII caused by the accumulation of reductant in the chloroplast and negative feedback of photorespiratory metabolites on the activation of the Calvin cycle (Häusler et al., 1996; Takahashi et al., 2007).

In conclusion, this study firmly establishes the essential role of LCI20 in balancing the redox status of chloroplasts during the trophic transition from photoautotrophy to mixotrophy and from H-CO_2 to VL-CO_2. Furthermore, this work shows that the *lci20* mutant is defective in photorespiration, as evidenced by glycolate secretion. Restoration of *lci20* growth together with the suppression of glycolate secretion under VL-CO_2 at 2% O_2 strongly suggests that photorespiration could be inactivated even under suboptimal CO_2. This finding may help to distinguish between CCM and photorespiratory mutants. The presence of large amounts of glycolate in the ocean during algal blooms suggests an active photorespiration by phytoplankton (Leboulanger et al., 1994; Leboulanger et al., 1997; Leboulanger et al., 1998; Schnitzler Parker et al., 2004). Therefore, our progress in understanding of algal photorespiration (Schada von Borzyskowski et al., 2019; Shi et al., 2021; Yun et al., 2021) should therefore contribute to the understanding of carbon footprint in the ocean. Moreover, many recent studies point to the predominant role of mixotrophy in the adaptation of photosynthetic microorganisms to different terrestrial and aquatic ecosystems (Selosse et al., 2017; Mansour and Anestis, 2021; Villanova and Spetea, 2021) and in promoting high-density cultivation, which is important for an industrial exploitation of algae (Fan et al., 2012; Goodenough et al., 2014). Therefore, understanding of the energy exchange between subcellular organelles should therefore be crucial for climate research and algal biotechnology.

Methods

Growth conditions and strains. The *lci20* mutant (LMJ.RY0402.205944) and wild-type CC4533 were purchased from the CLiP collection (https://www.chlamylibrary.org) (Li et al., 2016). Cells were cultivated in an incubation shaker (INFORS Multitron pro)

maintained at 25°C, with 120 rpm shaking and constant illumination at 80 µmol m^{-2} s^{-1}. For the HL experiment (600 µmol m^{-2} s^{-1}), white light was provided by a cool LED, all other lightings used for cell cultivation in the INFORS were supplied by fluorescent tubes delivering white light enriched in red wavelength. For photoautotrophic conditions, cells were grown in minimum medium (MM) buffered with 20 mM MOPS at pH 7.2 in air or air enriched with 2% CO_2. Photorespiration was induced by transferring 2% CO_2-grown cells into 0.01% CO_2 under atmospheric O_2 level (21%) and suppressed with 2% O_2. Mixotrophic growth was achieved by growing cells in a Tris-Acetate-Phosphate (TAP) medium at pH 7.2 (Harris, 2009). Growth kinetics were monitored with a Multisizer 3 Coulter counter (Beckman Coulter) whereas cells appearance (palmelloid or multicellular structure) was observed using confocal microscopy. For spot test, cells were grown in liquid culture with MM media in air, harvested during exponential phase (around 10 µg mL^{-1} of chlorophyll) and resuspended in fresh MM medium to make series of dilution for example to 0.5, 1, or 2 µg mL^{-1} chlorophyll per spot. Eight-microliter drops were spotted on 1.5% of agar plates at pH7.2 (MM or TAP buffered with 20 µM MOPS or 20 µM Tris respectively) and exposed to various CO_2 and light regimes. Homogeneous light was supplied by a panel of fluorescent tubes whereas neutral filters were used to obtain the desired light intensity when needed.

Phylogenetic analysis. A phylogenetic tree of the dicarboxylate transporter family was built from reviewed sequences of the InterPro entry IPR030676 / CitT-rel (December 2023) and were completed with a selection of homologous sequences from the Viridiplantae, including Chlorophyta, and malate transporters from Eubacteria. The multiple sequence alignment was performed with MAFFT v7.49 (Katoh and Standley, 2013) using the L-INS-i strategy, and filtered for saturation with BMGE v1.12 (Criscuolo and Gribaldo, 2010) using the BLOSUM62 matrix and removing sites with >50% gaps without entropy-based trimming, to get a final alignment containing 462 sites and 66 sequences. The tree was built using the Maximum-Likelihood (ML) algorithm with IQ-TREE (Minh et al., 2020) and the Q.LG+F+I+G4 substitution model selected by ModelFinder (Kalyaanamoorthy et al., 2017) with the Bayesian Information Criterion (BIC), restricting model selection to the cpREV, WAG, Q.plant, Q.pfam and Q.LG matrices (**Supplementary Fig. S1**). The statistical support of the branches was estimated using a (UFBoot) approximation (Hoang et al., 2018) implemented in IQ-TREE with 1000 replicates. A second tree was built from a reduced dataset of 21 sequences inspired from Weber et al. (Weber and Flügge, 2002) and Renné et al. (Renné et al., 2003) (**Fig. 1*D***) using the same approach.

DNA and RNA extraction for PCR or RT-PCR, respectively. Total DNA was extracted by resuspending a colony (of approximately 0.5 to 1 million) of cells in 50 µL of NaEDTA 10 mM and heated for 5 min at 100°C in thermocycler. Insertions in the putative mutant strains were confirmed by PCR using *dreamTaq* DNA polymerase with green GC Buffer (Thermo Scientific) using primers listed in **Table S1**. PCR cycles were: 5 min at 95°C then 30 cycles: 30 s at 95°C, 30 s at 60°C, 2-3 min at 72°C and finally 4 min at 72°C for final extension. PCR products were separated on 1.5% (w/v) agarose gels. For RT-PCR, total RNA was extracted using the RNA reagent from Invitrogen (ref: 12322-012) following the same protocol as in (Nguyen et al., 2013). Briefly, 10 mL of culture in exponential phase was centrifuged for 1 min, 13,000 *g*, 4°C to collect the pellet in 0.5 mL of RNA reagent in precellys tubes previously cooled on dry ice prior to lysis by centrifugation at 5,500 rpm twice, 10 s each (Precellys 24; Bertin Technologies). The supernatant was collected by centrifugation for 2 min, 13000 *g* at RT then 100 µL of NaCl

5 M and 300 µL of chloroform was added prior to centrifugation for 10 min, 13000 *g*, 4°C to recover the supernatant. RNAs were precipitated with isopropanol (~ 500 µL) incubated at RT for 10 min and centrifuged for 10 min, 13,000 *g* at 4°C before washing with 500 µL ethanol at 75%. Ethanol was evaporated at RT and RNAs were recovered in ~ 30 µL H_2O. The RNA was treated with DNase I (Invitrogen) prior to reverse transcription to obtain cDNA. The RT-PCR protocol was the same as for normal PCR with small adjustments. *LCI20* gene-specific primers (LCI20_fwd and LCI20_rev, see **Supplemental Table S1**).

Cloning full-length genomic DNA coding for *LCI20* and Chlamydomonas transformation. For the construction of *pPSAD::LCI20:tPSAD*, full-length genomic sequence of *LCI20* was obtained by PCR using the high fidelity KOD Hot Start DNA Polymerase (Merck Millipore) from Chlamydomonas genomic DNA (extracted as previously described) using *LCI20* specific primers LCI20-fwd-ATG and LCI20-rev-TAA flanked by the restriction site of *Bbs*I enzyme. The PCR products were cloned through modular cloning into the level zero vector pAGM1287 using the Chlamydomonas MoClo kit (Crozet et al., 2018). The promoter and the terminator *PSAD* as well as the *LCI20* sequence, after digestion with *Bsa*I, were ligated into a pICH47732 plasmid to obtain a transcriptional unit. The resulting construct was then ligated with the hygromycin resistance cassette into a final plasmid pAGM8031 (Addgene). For transformation, the fragment harboring hygromycin resistance gene in addition to *pPSAD::LCI20:tPSAD* from the digested plasmid was incorporated into the genome of exponentially grown Chlamydomonas cells by electroporation and spread on TAP hygromycin (15 mg L^{-1}) agar plates. The growth of hygromycin-resistant colonies was assessed by spot test on TAP agar plate to screen for complemented lines.

Measurement of chlorophyll fluorescence and O_2 evolution. Chlorophyll fluorescence measurements were performed using a Dual Pulse Amplitude Modulated Fluorometer (DUAL-PAM-100; Walz) equipped with a red LED source of actinic light while O_2 evolution was measured using a Microx TX3 oxygen meter equipped with a needle-Type oxygen microsensor NTH-PSt1. Samples (3 mL of cells at 10 µg mL^{-1} chlorophyll) were placed into a cuvette under constant stirring at room temperature (25°C) and dark adapted for 15 min prior to measurement. The cuvette was closed with customized cup allowing the injection through a micro hole. The maximum PSII quantum yield was obtained by delivering a saturating pulse 10,000 µmol photons m^{-2} s^{-1}, 200 ms duration and calculated as *Fv*/*Fm= (Fm-Fo)/Fm* where Fo is the basal fluorescence obtained with the measuring light and Fm the fluorescence emitted after saturating pulse (Maxwell and Johnson, 2000). For ETR measurement, the actinic light was set at constant intensity of 245 µmol photons m^{-2} s^{-1} during 15 min or increased stepwise (every 1 min) starting from 17, 110, 190, 380, 608 and 940 µmol photons m^{-2} s^{-1} for the light curve, each actinic light intensity being separated by a saturating pulse 10,000 µmol photons m^{-2} s^{-1}, 200 ms duration. ETR was calculated as: ETR = Y(II) x PAR x 0.5 where Y(II) is the PSII yield parameter and PAR is the actinic light intensity. When indicated, a volume of 30 µL of 1 M $NaHCO_3$ (10 mM) was added to the 3 mL reaction mix.

77K cold-temperature fluorescence measurement. Low-temperature fluorescence spectra were measured on whole cells at 77K (-196°C) using the Ocean Insight FLAME-X optical fiber fluorescence spectrophotometer (Lamb et al., 2018). About 200 µL of cells (sampled directly from the culture at around 10 µg mL^{-1} of chlorophyll cultivated in the INFORS with light and a given CO_2 concentration were fast frozen in liquid nitrogen.

The excitation wavelength was 440 nm, and excitation and emission slits were 10 and 5 nm, respectively.

Immunoblot. For protein extraction, one mL of cells culture in exponential phase (around 10 µg mL^{-1} of chlorophyll) were harvested by centrifugation at 4000 *g* for 3 min at 4°C. Pellets were resuspended in 200 µL of 1% SDS, to which 800 µL of cold acetone were added to extract chlorophyll and the suspension was incubated for 30 min at -20°C. Samples were then centrifuged for 10 min, 13000 *g* at 4°C to precipitate proteins. Chlorophyll concentration was measured by spectrophotometry from supernatant. The pellet of proteins was resuspended with Novex™ Nupage™ LDS buffer 1x (Invitrogen™) containing reducing agent DTT, at a final volume corresponding to 1 µL per 0.1 µg chlorophyll measured (corresponding to 1 µg $µL^{-1}$ of protein), the resuspended proteins were then denatured for 20 min at 70°C. Ten µg of protein were loaded on Novex™ Nupage™ Bis tris 12% (Invitrogen™) gel, migrated 1 h at 190 V in Novex™ Nupage™ MOPS (Invitrogen™) buffer (or Novex™ Nupage™ MES (Invitrogen™) buffer according to protein molecular weight) and transferred to nitrocellulose membrane using semidry transfer technique. Immunodetection was performed using antibodies raised against PGRL1 (Tolleter et al., 2011), FLVB and FLVA (Chaux et al., 2017a), NDA2 (Desplats et al., 2009) and MDH2 (Kong et al., 2018). Other antibodies were ordered from Agrisera for PSBD (AS06 146), CAT1 (AS15 2991), FeSOD (AS06 125), F-type ATP synthase (AS05 085), COXIIB (AS06 151) and AOX1 (AS06 152).

Glycolate quantification. Secreted glycolic acid was analyzed from the supernatant after centrifugation of 1 mL culture at 4000 *g* for 2 min at 4°C. The supernatant was diluted 10x in acetonitrile and analyzed using a Vanquish UHPLC/Q Exactive Plus (ThermoScientific). Glycolic acid were separated using a HILIC stationary phase (SeQuant ZIC HILIC, 100 x 2.1 mm, 3.5 µm), heated to 35°C. A binary solvent system was used, in which mobile phase A consisted of acetonitrile: water (95:5, v/v) with 5 mM ammonium acetate and mobile phase B consisted of water:acetonitrile (95:5, v/v) with 5 mM ammonium acetate. Separations were done over a 32 min period following the gradient: 0-0.5 min: 5%B, 0.5-24.5 min: 5-95% B, 24.5-26.5 min: 95% B, 26.5-26.6 min: 95-5% B, 26.6-32 min: 5% B. The flow rate was set to 0.3 mL min^{-1} and the injection volume was 5 µL. After separation, glycolic acid was directed into the ESI source of the Q Exactive Plus (Orbitrap-mass spectrometer). The ESI source was set as following: negative mode ion spray voltage at -2.5 kV, capillary temperature at 300°C, S-lens RF level at 50. Data was acquired using a targeted t-SIM method with glycolic acid in inclusion list (formula C2H4O3, m/z 75.00877).

Metabolomics analysis. Cells were grown to exponential phase under photoautotrophic high-CO_2 conditions in the flask with 80 µmol photons m^{-2} s^{-1}. For low-CO_2 and very-low-CO_2 conditions, high-CO_2 adapted cells were transferred to either low or very-low CO_2 levels for 16 to 20 h prior to sampling. For mixotrophic conditions, photoautotrophic air-grown cells were inoculated into TAP media and incubated for 24 hours before sampling. About 60 million cell suspensions were injected into a -70°C cold quenching solution composed of 70% methanol in water using a thermoblock above dry ice to obtain a final concentration of 35% methanol. Centrifuge tubes containing the cell suspensions were cooled in a pre-chilled cooling box to keep the sample temperature below -20°C. Cell pellets were collected by centrifugation at 4000 *g* for 2 min at -10°C. The supernatant was decanted and residual liquid together with cells carefully transferred to a 2-mL Eppendorf tube and re-centrifuged 13000 *g* for 1 min at -10°C. The pellet was flash-

frozen in liquid nitrogen and lyophilized at -50°C. The extraction and derivation of the metabolites were performed as previously (Lisec et al., 2006). The analytic and quantification methods were exactly as reported in (Kong et al., 2018).

Statistics. All statistical tests used are noted in figure legends. One-way ANOVA using GraphPad Prism (GraphPad Software) was used to perform statistical analysis. The *p* values were computed by One-way ANOVA test (uncorrected *p* values) or using Turkey corrections for large datasets (adjusted *p* values). Shown are grouping of strains into statistical families according to *p* values indicated by asterisk (* for $p \leq 0.05$; ** for $p \leq 0.01$; *** for $p \leq 0.001$ and **** for $p \leq 0.0001$). The statistical significance (α) between strains was set as 0.05 (5%).

All supporting informations for **chapter 3** are in **annex 3**.

Acknowledgment. O.D. thanks the French Atomic Energy and Alternative Energy Commission (CEA) for a PhD scholarship. We thank Shiyan Zheng for assistance in performing the genetic complementation experiment; Stephanie Blangy for trials on generating antibodies against LCI20; Florian Veillet and Franziska Kuhnert for trials on the transport assays. This work is financially supported by the "L'économie Circular du Carbone" program of the CEA (CO2storage), and the Region Sud ("AlgalCO2" project). We acknowledge the European Union Regional Developing Fund (ERDF), the Région Provence Alpes Côte d'Azur, the French Ministry of Research and the CEA for funding the HelioBiotec platform. We thank the ZoOM Microscopy facility (CEA Cadarache). C.M. is grateful to the INRAE MIGALE bioinformatics facility (MIGALE, INRAE, 2020) for providing computing resources A.P.M.W. acknowledges funding by the European Union's H2020 research and innovation and the Horizon programs (grants GAIN4CROPS, GA No. 862087 and BEST-CROP, GA No. 101082091) and the Deutsche Forschungsgemeinschaft (Cluster of Excellence for Plant Sciences (CEPLAS) under Germany's Excellence Strategy EXC-2048/1 under project ID 390686111).

Conclusion

We report the essential role of LCI20 for the adaptation of Chlamydomonas to: (1) low CO_2 conditions by playing a role in photorespiration under high O_2/CO_2 ratio and (2) mixotrophic growth probably by serving as a malate valve. Indeed, either in the presence of acetate, or during photorespiration, active exchange of reducing power between subcellular compartments occurs (Johnson and Alric, 2012; Johnson and Alric, 2013; Eisenhut et al., 2019; Lim et al., 2020; Dao et al., 2022; Segura Broncano et al., 2023). Dysfunction of redox exchange of one compartment could have implication on the overall redox homeostasis. It is worth bearing in mind that the direction of malate transport across the chloroplast envelope is solely dependent on the concentration gradient between the cytosol and the stroma. Therefore, import of malate in the chloroplast could be expected when malate concentration is higher in other organelles as it was reported in Chlamydomonas (Kong et al., 2018).

In our effort to determine the panel of metabolites transported by LCI20, we have performed a metabolomics analysis and found hyper accumulation of glutamate and malate in *lci20*. From a physiological point of view, increased level of malate is indicative of over-reduction of the cells whereas high level of glutamate might indicate an imbalance between carbon and nitrogen metabolism (Wallsgrove et al., 1986; Renberg et al., 2010). Both cases are expected to occur during photorespiration or mixotrophic growth (Weber and Flügge, 2002; Xie et al., 2016; Eisenhut et al., 2019; Puzanskiy et al., 2023). Despite several attempts, we could not express LCI20 correctly in yeast cells. Targeted approaches using artificial liposomes or Oocyte systems should be further attempted in the future to fine tune the transport activity of LCI20 and other putative chloroplast malate translocators of Chlamydomonas.

Overall, our data suggest that LCI20 is a malate/glutamate transporter that actively participates in redox balancing between chloroplast and extra-chloroplast compartments during environmental transitions underscoring the success of Chlamydomonas in colonizing contrasting ecological niches (Sasso et al., 2018; Durán et al., 2021; Calatrava et al., 2023).

Chapter 4. The energization of the CO_2 concentrating mechanism in *Chlamydomonas reinhardtii*

Foreword

Photosynthesis is the main biological process driving CO_2 fixation on earth, capturing ten times more CO_2 than net anthropogenic emissions. Microalgae account for half of global photosynthesis, and most of microalgal species enhance their CO_2 fixation capacities by means of an energy-dependent CO_2-concentrating mechanism (CCM) that increases the CO_2 concentration at the catalytic site of rubisco. While main cellular components involved in the transport and concentration of inorganic carbon have been uncovered (Wang and Spalding, 2014a; Wang and Spalding, 2014b; Wang et al., 2015; Mackinder et al., 2017; Adler et al., 2022; Burlacot and Peltier, 2023), the energy supply network of the algal CCM remains elusive.

In this chapter, we explored the energetics of the CCM by characterizing *C. reinhardtii* mutants impaired in CEF and PCEF (see Intro section 2 and Chapter 1). We further show that mitochondrial respiration contributes to CCM energization, most likely by supplying ATP to non-thylakoid C_i transporters. We propose a global picture of the CCM energization network, describing how the different bioenergetics systems of algal cells cooperate to drive both CO_2 concentration and fixation. This work paves the way for biotechnological applications of CO_2 bioremediation, and for the transfer of a functional CCM into crop plants to improve productivity. My contribution in this work is detailed in the general objectives section.

Chapter IV

Article

Alternative photosynthesis pathways drive the algal CO_2-concentrating mechanism

https://doi.org/10.1038/s41586-022-04662-9

Received: 26 February 2021

Accepted: 18 March 2022

Published online: 27 April 2022

Check for updates

Adrien Burlacot[1,2], Ousmane Dao[1], Pascaline Auroy[1], Stephan Cuiné[1], Yonghua Li-Beisson[1] & Gilles Peltier[1]✉

Global photosynthesis consumes ten times more CO_2 than net anthropogenic emissions, and microalgae account for nearly half of this consumption[1]. The high efficiency of algal photosynthesis relies on a mechanism concentrating CO_2 (CCM) at the catalytic site of the carboxylating enzyme RuBisCO, which enhances CO_2 fixation[2]. Although many cellular components involved in the transport and sequestration of inorganic carbon have been identified[3,4], how microalgae supply energy to concentrate CO_2 against a thermodynamic gradient remains unknown[4–6]. Here we show that in the green alga *Chlamydomonas reinhardtii*, the combined action of cyclic electron flow and O_2 photoreduction—which depend on PGRL1 and flavodiiron proteins, respectively—generate a low luminal pH that is essential for CCM function. We suggest that luminal protons are used downstream of thylakoid bestrophin-like transporters, probably for the conversion of bicarbonate to CO_2. We further establish that an electron flow from chloroplast to mitochondria contributes to energizing non-thylakoid inorganic carbon transporters, probably by supplying ATP. We propose an integrated view of the network supplying energy to the CCM, and describe how algal cells distribute energy from photosynthesis to power different CCM processes. These results suggest a route for the transfer of a functional algal CCM to plants to improve crop productivity.

Microalgal photosynthesis in aquatic ecosystems has to overcome a low CO_2 availability resulting from the slow diffusion of CO_2 in water[7]. The CO_2-fixing enzyme RuBisCO has a low affinity[8] for CO_2, and thus the efficiency of algal photosynthesis is highly dependent on the CCM[9]. The algal CCM involves the sequential actions of inorganic carbon (C_i) transporters and carbonic anhydrases located in different cellular compartments[10], and results in active accumulation of CO_2 at the RuBisCO level[4,6]. Several CCM components have been identified in the green alga *C. reinhardtii*[3,4] (hereafter referred to as *Chlamydomonas*), particularly putative C_i transporters operating across the plasma membrane (high light activated 3[11] (HLA3)), the chloroplast envelope (low carbon inducible A[12,13] (LCIA)) and the thylakoid membrane (bestrophin-like transporters[14] (BSTs)). The C_i is eventually converted to CO_2 by a carbonic anhydrase[15] (CAH3), enabling its fixation by RuBisCO. The transport of C_i across membrane bilayers against a concentration gradient and its conversion to CO_2 are energy-dependent processes[6,14,16], and photosynthesis has a role in supplying the chemical energy required for the function of the CCM[17].

During photosynthesis, sunlight is converted to chemical energy by two photosystems (PSII and PSI) acting in series through the linear electron flow (LEF), reducing $NADP^+$ to NADPH and producing a pH gradient across the thylakoid membrane. The pH gradient is then leveraged for ATP synthesis, and both NADPH and ATP supply energy for CO_2 fixation. However, LEF produces less ATP than required for CO_2 fixation[18], and photosynthesis relies on additional mechanisms to rebalance this ratio[19]. These include (1) cyclic electron flow (CEF) around PSI, which involves both proton gradient regulation 5[20,21] (PGR5) and proton gradient regulation like 1[22,23] (PGRL1) proteins in plants and algae and (2) pseudo-cyclic electron flow (PCEF), which diverts electrons to O_2 at the PSI acceptor side[24], catalysed by flavodiiron proteins (FLVs) in cyanobacteria[25], bryophytes[26,27] and green microalgae[28]. Both CEF and PCEF generate a pH gradient without producing NADPH, thus re-equilibrating the high NADPH/ATP ratio of LEF. Another pathway involving several metabolic shuttles between chloroplast and mitochondria, which we designate chloroplast-to-mitochondria electron flow (CMEF), can also supply extra ATP for CO_2 fixation when CEF is deficient[29,30]. In this context, how photosynthesis energy is delivered to the different C_i transporters and how can this be done without compromising CO_2-fixation capacity are pivotal questions[4,6].

Here we have addressed these questions by studying *Chlamydomonas* mutants of the PGRL1-dependent CEF (*pgrl1*[23]), PCEF (*flvB*[28]) and BSTs[14]. We show that CCM activity is unaffected in single CEF or PCEF mutants but is severely impaired in double mutants and propose that the increased luminal proton concentration produced by the cooperative action of these mechanisms is used by CCM mechanisms operating downstream of BST thylakoid C_i transporters. We further establish that CMEF is involved in CCM functioning, most probably by supplying ATP to plasma membrane and/or chloroplast envelope C_i transporters, thus revealing how transport steps distant from the thylakoid can be powered.

[1]Aix Marseille Univ, CEA, CNRS, Institut de Biosciences et Biotechnologies Aix-Marseille, CEA Cadarache, Saint-Paul-lez-Durance, France. [2]Department of Plant Biology, Carnegie Institution for Science, Stanford, CA, USA. ✉e-mail: gilles.peltier@cea.fr

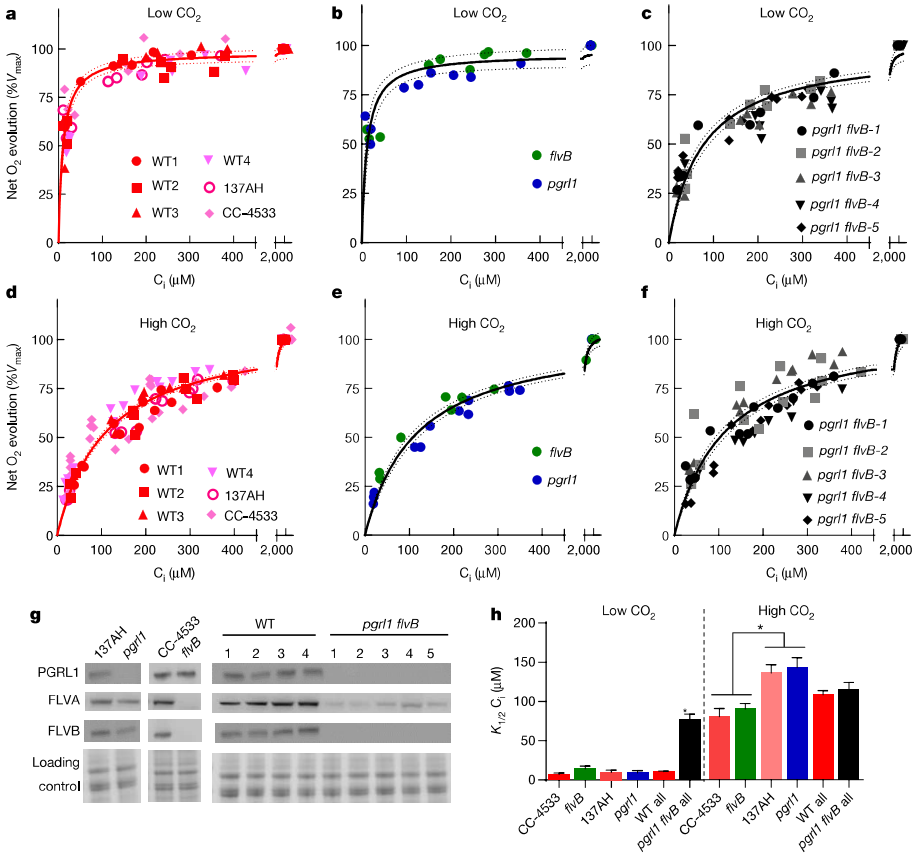

Fig. 1 | Deletion of PGRL1 and FLVB impairs photosynthetic affinity for C_i. **a–f**, Net O_2 production was measured at pH 7.2 in cells grown under air with 400 ppm (low CO_2) or 3% (high CO_2) CO_2. Shown are three replicates (dots) and hyperbolic fit (solid lines) with variability (dotted lines) for each strain. For each replicate, net O_2 production was measured following stepwise C_i addition, and normalized to the maximum photosynthetic net O_2 production. As these strains were generated in different genetic backgrounds (CC-4533 and 137AH) with contrasting photosynthetic activities (Extended Data Fig. 2a, c), the data are normalized to the V_{max}. **a**, **d**, 137AH and CC-4533 are the control strains for *pgrl1* and *flvB*, respectively. WT1–4 are four independent control strains obtained from the *pgrl1* × *flvB* crossing. **b**, **e**, *flvB* and *pgrl1* mutant strains. **c**, **f**, *pgrl1 flvB-1* to *pgrl1 flvB-5* are independent double-mutant strains. Data for each strain in **a–f** are from three biologically independent samples. **g**, Immunodetection of PGRL1, FLVA and FLVB in the different strains with Coomassie blue staining as loading control. **h**, $K_{1/2}$ values as determined from the hyperbolic fit for each strain. Data are mean ± s.d. of the fit of experimental data shown in **a–f** ($n = 3$ for single mutants and their controls), values for all double mutant strains (*pgrl1 flvB* all, $n = 15$) and their control strains (WT all, $n = 12$) have been pooled before fitting. *$P < 0.05$; one way ANOVA with Tukey correction.

Deletions of FLVs and PGRL1 impair C_i affinity

To investigate the involvement of FLV-dependent PCEF and PGRL1-dependent CEF in the energy supply to the CCM, we first measured net photosynthetic O_2 production at various C_i concentrations in *Chlamydomonas flvB*[28] or *pgrl1*[23] single mutants. When cells were grown under air (400 ppm CO_2 (low CO_2)), C_i affinities were similar for control wild-type (WT) strains and single mutants (half saturation constant ($K_{1/2}$) ≈ 10 µM), indicating a fully functional CCM (Fig. 1a, b, h). Under high CO_2 (air with 3% CO_2 supplementation), *flvB* and *pgrl1* mutants and their respective parental strains showed similar affinities for C_i, with a $K_{1/2}$ around 100 µM (Fig. 1d, e, h). To assess possible functional redundancy between FLVs and PGRL1, we obtained double mutants by genetic crossing of the single *pgrl1* and *flvB* mutants (Extended Data Fig. 1a). Among the progeny, we isolated five independent double mutants (*pgrl1 flvB-1*, *2*, *3*, *4* and *5*) as well as four independent control strains exhibiting normal accumulation of both FLVs and PGRL1 (WT1–4) (Fig. 1g, Extended Data Fig. 1). We observed no differences in C_i affinity between these strains when grown at high CO_2, but double mutants showed seven times lower affinity for C_i compared with control strains when grown at low CO_2 (Fig. 1c, f, h, Extended Data Fig. 2b, d).

Mutants defective in the CCM often cannot grow properly in low CO_2[31]. We compared growth at different CO_2 concentrations, pH and light intensities. Whereas all strains showed similar growth at high CO_2, the growth of *pgrl1 flvB* double mutants was impaired under low CO_2 and very low CO_2 (100 ppm CO_2 in air) (Fig. 2a), similar to the growth defect observed in the CCM-deficient mutant *cia5* (Fig. 2a, Extended Data Fig. 3). The growth defect observed in double mutants worsened with increasing light intensity but was barely affected by pH (Extended Data Fig. 3). The accumulation of the major CCM components, as evaluated by immunodetection, was similar in all strains, with the exception of LCI1, which was present at lower amounts in double mutants (Fig. 2b) and to a lesser extent in single mutants (Extended Data Fig. 4c). However, the fact that growth of the LCI1 knockout mutant is not affected[32]

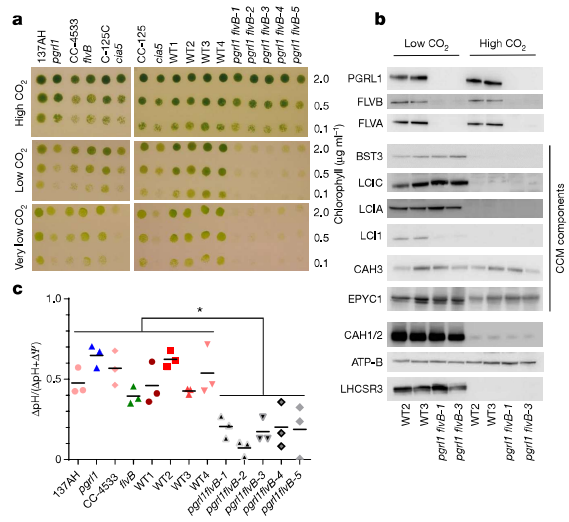

Fig. 2 | Growth of *pgrl1 flvB* double mutants is impaired at low CO_2 in the presence of CCM components. a, Growth tests for *pgrl1* and *flvB* mutants and the corresponding control strains (137AH and CC-4533, respectively) (left) and double mutants (*pgrl1 flvB-1* to *pgrl1 flvB-5*) and the corresponding control strains (WT1–4) (right). The *cia5* mutant was introduced as a CCM-deficient control together with its reference strain CC-125. Cells were spotted on plates containing minimal medium at pH 7.2 and grown under continuous illumination (60 µmol photon m^{-2} s^{-1}) under high CO_2, low CO_2 or very low CO_2 (100 ppm CO_2 in air). Spots shown are representative of ten independent experiments. **b**, Immunodetection of PGRL1, FLVA, FLVB and of the major CCM components in two independent *pgrl1 flvB* double mutants and controls grown under low or high CO_2. **c**, PMF partitioning between ΔpH and $\Delta\Psi$ determined from electrochromic shift measurements. Horizontal lines show the mean and dots show individual replicates ($n = 3$ biologically independent sample). *pgrl1 flvB* double mutants showed a significantly lower pH gradient contribution to PMF than the single-mutant and control strains ($P < 0.05$, one way ANOVA).

at low CO_2, suggests that the lower LCI1 level observed in double *pgrl1 flvB* mutants is not the cause, but rather the consequence, of CCM misfunctioning. Carbonic anhydrase activity measured in vivo was induced at low CO_2, reaching similar levels in all strains (Extended Data Fig. 4f). Double mutants and control strains showed similar maximal O_2 photosynthetic production (Extended Data Fig. 2a, c) and PSII quantum yields (Extended Data Fig. 4a), as well as similar levels of major photosynthetic complexes (Extended Data Fig. 4b). Thus PGRL1-dependent CEF and FLV-dependent PCEF contribute to the CCM operation, and can compensate for each other, as exemplified by the absence of a CCM phenotype in single mutants. The growth impairment of the *pgrl1* mutant observed under high light indicates that the compensation by PCEF induces a metabolic imbalance that may affect growth on the long term, as previously proposed[29].

CCM uses luminal H^+ generated by CEF and PCEF

We hypothesized that PGRL1 and FLVs may generate an extra trans-thylakoid pH gradient that could provide energy for CCM. Whereas control strains and single *pgrl1* or *flvB* mutants generated both a similar pH gradient and proton motive force (PMF) as their control in light conditions (Fig. 2c, Extended Data Fig. 5), *pgrl1 flvB* double mutants were strongly impaired in their capacity to generate both pH gradient and PMF (Fig. 2c, Extended Data Fig. 5). It has been proposed[16] that luminal protons could be used during the last step of CCM to convert HCO_3^- to CO_2. Thus, to gain further insight into the link between CEF, PCEF and CCM energization, we assessed changes in the luminal proton concentration during CCM function in the different mutant strains. We monitored the level of the rapidly reversible component (qE) of the non-photochemical quenching of chlorophyll fluoresence (NPQ), which has recently been identified as a sensitive and reliable probe of luminal pH[33,34] (Fig. 3a) and depends on light-harvesting complex stress-related 3 protein (LHCSR3) accumulation in cells grown under low CO_2 (Fig. 2b, Extended Data Fig. 4c). In control lines, the NPQ level was highest when C_i level was low, and rapidly and reversibly decreased either in the light upon C_i injection or at low C_i when light was turned off (Fig. 3b; Extended Data Fig. 6a, c, e). We confirmed that state transitions (another NPQ component) did not contribute to CO_2-dependent NPQ changes (Extended Data Fig. 7a–c) and that the NPQ measured at low C_i is fully relaxed by the ionophore nigericin that suppresses the trans-thylakoidal pH gradient and can therefore be attributed to qE (Extended Data Fig. 7d–f, h, i). The CO_2-dependency of qE was not affected in single mutants. However, qE was not induced in *pgrl1 flvB* double mutants at low C_i (Fig. 3c, Extended Data Fig. 6f, h), although these strains accumulated normal amounts of LHCSR3 (Fig. 2b) and maintained the capacity to induce substantial qE upon medium acidification (Extended Data Fig. 6i, j), which is consistent with the incapacity of the *pgrl1 flvB* double mutants to generate a pH gradient (Fig. 2c). We conclude from this experiment that CEF and PCEF contribute to energize the CCM through the generation of a low luminal pH, with both mechanisms being able to substitute for each other in single mutants.

Three BST-like proteins have been proposed to transport C_i at the thylakoid level[14]. To gain insight into the role of the luminal proton concentration in the CCM functioning, we assessed the kinetics of the NPQ in a BST-knockdown strain[14] (*bsti-1*) in response to repetitive C_i supply. *bsti-1* was found to accumulate variable levels of LHCSR3 depending on the growth conditions (Extended Data Fig. 4e)—we thus selected conditions under which accumulation of LHCSR3 was close to that in the control strain. Whereas the control strain showed a NPQ decrease for each C_i injection followed by an increase upon C_i depletion (Fig. 3d), the NPQ of *bsti-1* was barely affected (Fig. 3e). We validated that *bsti-1* displays a NPQ component attributable to qE and is able to generate a pH gradient similar to the control strain (Extended Data Figs. 5, 7g). In sum, *bsti-1* is able to generate a pH gradient and a low luminal pH but it is unable to use it to accumulate C_i.

CMEF energizes distant C_i transporters

To gain quantitative insight into the nature of compensation mechanisms in *pgrl1*, we investigated the C_i-dependence of the light-dependent O_2 consumption measured using ^{18}O-labelled O_2. As previously reported[35,36], O_2 consumption increased at low C_i in control strains (Extended Data Fig. 8a, e). In *pgrl1*, O_2 uptake rates were higher than in control strains (Extended Data Fig. 8a–d), which is consistent with a compensation of a defect in CEF by PCEF[29]. O_2 uptake rates were strongly diminished in *flvB*[28], but surprisingly, a C_i-dependent O_2 uptake process remained (Extended Data Fig. 8e, f). To determine whether mitochondrial respiration is responsible for the remaining light-dependent O_2 uptake, we used two mitochondrial respiration inhibitors, myxothiazol and salicyl hydroxamic acid (SHAM), which inhibit the cytochrome bc_1 complex and the mitochondrial alternative oxidase, respectively. We show that the remaining light-dependent O_2 uptake measured at low C_i in *flvB* is indeed owing to mitochondrial respiratory activity driven by photosynthesis and therefore attributed to CMEF (Extended Data Fig. 8k).

We then investigated the contribution of mitochondria to CCM energization in WT strains. Whereas addition of respiratory inhibitors had no effect on the maximal net O_2 production rate (V_{max}) and C_i affinity of high CO_2-grown strains ($K_{1/2} \approx 100$ µM) (Extended Data Fig. 9d–f, l, m), it reduced the C_i affinity of low CO_2-grown control strains by half ($K_{1/2} > 20$ µM) compared with untreated cells ($K_{1/2} \approx 10$ µM) (Fig. 3f). The

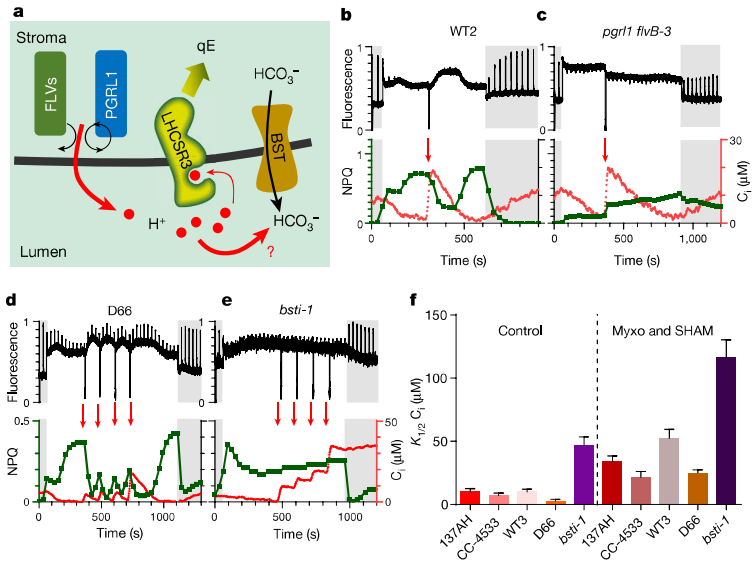

Fig. 3 | CEF, PCEF and CMEF contribute energy to the CCM. a, Schematic view describing the principle of using the qE component of NPQ to probe changes in luminal pH during CCM function. **b–e**, Combined measurements of chlorophyll fluorescence (top panels), C_i concentrations and NPQ (bottom panels) during dark–light–dark transitions in WT2 (**b**), *pgrl1 flvB-3* (**c**), the *bsti-1* control strain D66 (**d**) and *bsti-1* (**e**). All strains were grown at low CO_2. Results are from representative experiments ($n = 3$ biologically independent samples). Red arrows indicate stepwise addition of bicarbonate. **f**, Inhibitors of mitochondrial respiration decrease the phosynthetic affinity for C_i in cells grown under low CO_2. Net photosynthetic O_2 production was measured as in Fig. 1. $K_{1/2}$ values were determined from hyperbolic fits for the different strains in the presence or absence of the mitochondrial inhibitors myxothiazol (Myxo, 2.5 µM) and SHAM (400 µM), which act on the cytochrome bc_I complex and the alternative oxidase, respectively. Data are mean values ± s.d. of the fit of data shown in Extended Data Fig. 9a–c, g, h. When grown under low CO_2 and treated with myxothiazol and SHAM, all WT and mutant strains produced $K_{1/2}$ values that were significantly different compared with non-treated strains ($P < 0.05$; one way ANOVA with Tukey correction).

effect on C_i affinity was observed only when myxothiazol and SHAM were added together (Extended Data Fig. 10), indicating that both alternative oxidase and cytochrome bc_I electron pathways contribute to CCM energization. Notably, respiratory inhibitors also increased the $K_{1/2}$ of the air-grown *bsti-1* mutant (Fig. 3f, Extended Data Fig. 9h), thus showing that the contribution of mitochondria to CCM energization operates at the level of transporters distant from the thylakoids. The contribution of the different pathways (CEF, PCEF and CMEF) was deduced from O_2 consumption rates measured in the different mutants during C_i depletion (Extended Data Fig. 8). Whereas the contribution of the PGRL1-dependent CEF remained relatively constant, the contribution of FLV-dependent PCEF and CMEF increased markedly at low C_i (Fig. 4a).

Discussion

Although the requirement of the CCM for energy from photosynthesis has been long recognized[17], the associated molecular mechanisms have remained poorly understood[4]. The participation of PCEF[36] or CEF[37] has been proposed, but their actual and respective contributions have not been established. Here we demonstrate that both FLV-dependent PCEF and PGRL1-dependent CEF cooperate to supply energy to the CCM by the generation of a pH gradient. Moreover, we propose that the low luminal pH generated by both mechanisms is used by a thylakoid-localized CCM process linked to the functioning of BSTs. Because mammalian BSTs[38] are Cl^- channels that are highly permeable to HCO_3^-, protons that accumulates in the lumen from the combined actions of CEF and PCEF are probably used for the conversion of HCO_3^- to CO_2 mediated by CAH3, and the PMF generated by both mechanisms (Extended Data Fig. 5) is likely to favour HCO_3^- translocation through BSTs (Fig. 4b).

We further establish that mitochondrial respiration, whose role in CCM energization has been largely ignored, provides energy to CCM transporters that are distant from the thylakoids through efficient inter-organelle redox trafficking. From the analysis of the respective contribution of each mechanism as a function of C_i concentration, we conclude that whereas the contribution of CEF is relatively constant, the contribution of PCEF increases at low C_i concentrations, and that of CMEF also becomes important at the lowest C_i concentrations. As these are typical conditions in which putative ATP-dependent periplasmic and chloroplast envelope transporters (HLA3 and LCIA, respectively) are highly active[4,12,13], we propose that the ATP produced by CMEF at low C_i supplies energy to one or both transporters (Fig. 4). The lower growth decrease observed for *pgrl1 flvB* mutants at very low CO_2 (Extended Data Fig. 3d–f) indicates that external transporters (HLA3 and/or LCIA), which depend on the CMEF energy supply, may be the prime drivers of the CCM in these conditions. Of note, LCI1 accumulation, whose function is tightly linked to HLA3[3,32], decreased in *pgrl1*, *flvB*, *pgrl1 flvB* and *bsti-1*, indicating that an impairment of the CCM at the thylakoid level may regulate periplasmic transport processes mediated by LCI1. This could be owing to an increased cytosolic C_i concentration resulting from the absence of functional thylakoid C_i transport, which would in turn trigger down-regulation of LCI1 expression to avoid cytosolic C_i over-accumulation.

The presence of an active CCM is a key factor influencing phytoplankton biomass production in the oceans[2], especially for phytoplankton species producing large oceanic blooms[39]. However, the lack of knowledge about CCM activity in situ[9] makes it difficult to predict how global changes will affect phytoplankton communities[40]. We demonstrate here that the presence of a functional CCM can be probed by measuring C_i-dependent NPQ, which could be used as a simple parameter to determine CCM activity in aquatic ecosystems.

Chapter IV

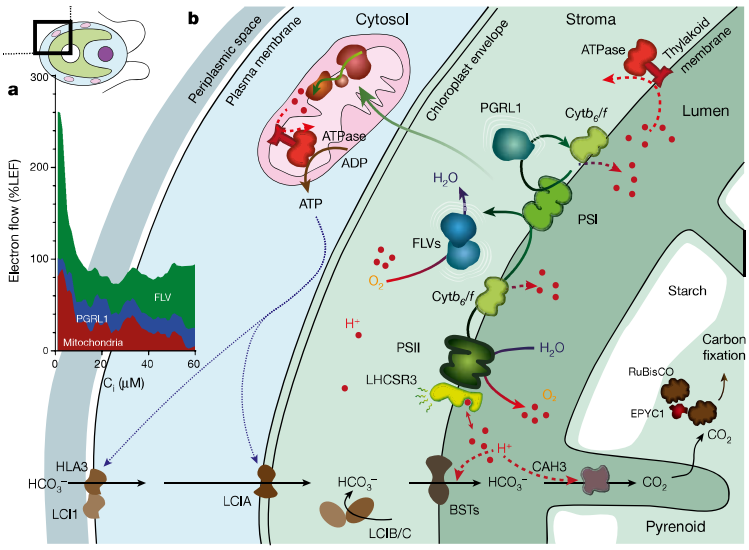

Fig. 4 | Proposed mechanism of the CCM-energization network in algal cells. a, Contributions of FLV-dependent PCEF, PGRL1-dependent CEF and CMEF to CCM energization at different C_i concentrations were quantified from O_2 exchange measurements performed in the different mutant strains and expressed as a percentage of LEF (Extended Data Fig. 8). **b**, Schematic view of the CCM-energization network. CCM components including LCI1, HLA3, LCIA and BST transporters, LCIB, LCIC, CAH3, EYPC1 and RuBisCO are shown in brown, and components of the photosynthetic electron transport chain (PSII, PSI, Cytb_6/f) are in green. We propose here that luminal protons generated by the combined action of FLV-dependent PCEF and PGRL1-dependent CEF are used to convert bicarbonate to CO_2 downstream of BST anionic channels. CMEF would generate the ATP needed to power C_i transporters distant from the thylakoid, such as LCIA and HLA3.

A potential limitation of a thylakoid CCM process consuming the luminal protons would be competition with the synthesis of ATP required for CO_2 fixation[14]. This is particularly critical as LEF is known to supply less ATP than is required for CO_2 fixation[19]. We suggest here that the combined action of the three alternative mechanisms, CEF, PCEF and CMEF, all of which result in an increase of the ATP/NADPH ratio, can fulfill the energy requirement of the CCM without compromising CO_2 fixation. A major biotechnological challenge in CCM research is the improvement of crop productivity by transferring microalgal components to higher plants[41–43]. Building a fully functional CCM in plants represents a tremendous scientific challenge, which has recently regained considerable interest[4,44]. Our study shows that an integrated understanding of the cellular energetics is key towards fulfilling the energy requirement of a synthetic CCM without compromising the efficiency of photosynthetic CO_2 fixation. For instance, the expression of FLVs in higher plants, which has been shown to supply extra PMF during photosynthesis[45–48], appears as a promising starting point to supply the extra energy needed to power thylakoid C_i transport. We foresee that future research coupling energy source and CCM expression should help to boost plant productivity.

Online content

Any methods, additional references, Nature Research reporting summaries, source data, extended data, supplementary information, acknowledgements, peer review information; details of author contributions and competing interests; and statements of data and code availability are available at https://doi.org/10.1038/s41586-022-04662-9.

1. Field, C. B., Behrenfeld, M. J., Randerson, J. T. & Falkowski, P. Primary production of the biosphere: integrating terrestrial and oceanic components. *Science* **281**, 237–240 (1998).
2. Mackey, K. R., Morris, J. J., Morel, F. M. & Kranz, S. A. Response of photosynthesis to ocean acidification. *Oceanography* **28**, 74–91 (2015).
3. Mackinder, L. C. M. et al. A spatial interactome reveals the protein organization of the algal CO_2-concentrating mechanism. *Cell* **171**, 133–147.e114 (2017).
4. Mackinder, L. C. M. The *Chlamydomonas* CO_2-concentrating mechanism and its potential for engineering photosynthesis in plants. *New Phytol.* **217**, 54–61 (2018).
5. Raven, J. A. Inorganic carbon acquisition by eukaryotic algae: four current questions. *Photosynth. Res.* **106**, 123–134 (2010).
6. Raven, J. A., Beardall, J. & Giordano, M. Energy costs of carbon dioxide concentrating mechanisms in aquatic organisms. *Photosynth. Res.* **121**, 111–124 (2014).
7. Maberly, S. C. & Gontero, B. Ecological imperatives for aquatic CO_2-concentrating mechanisms. *J. Exp. Bot.* **68**, 3797–3814 (2017).
8. Savir, Y., Noor, E., Milo, R. & Tlusty, T. Cross-species analysis traces adaptation of Rubisco toward optimality in a low-dimensional landscape. *Proc. Natl Acad. Sci. USA* **107**, 3475–3480 (2010).
9. Reinfelder, J. R. Carbon concentrating mechanisms in eukaryotic marine phytoplankton. *Annu. Rev. Mar. Sci.* **3**, 291–315 (2011).
10. Moroney, J. V. et al. The carbonic anhydrase isoforms of *Chlamydomonas reinhardtii*: intracellular location, expression, and physiological roles. *Photosynth. Res.* **109**, 133–149 (2011).
11. Duanmu, D., Miller, A. R., Horken, K. M., Weeks, D. P. & Spalding, M. H. Knockdown of limiting-CO_2-induced gene HLA3 decreases HCO_3^- transport and photosynthetic C_i affinity in *Chlamydomonas reinhardtii*. *Proc. Natl Acad. Sci. USA* **106**, 5990–5995 (2009).
12. Wang, Y. & Spalding, M. H. Acclimation to very low CO_2: contribution of limiting CO_2 inducible proteins, LCIB and LCIA, to inorganic carbon uptake in *Chlamydomonas reinhardtii*. *Plant Physiol.* **166**, 2040–2050 (2014).
13. Yamano, T., Sato, E., Iguchi, H., Fukuda, Y. & Fukuzawa, H. Characterization of cooperative bicarbonate uptake into chloroplast stroma in the green alga *Chlamydomonas reinhardtii*. *Proc. Natl Acad. Sci. USA* **112**, 7315–7320 (2015).
14. Mukherjee, A. et al. Thylakoid localized bestrophin-like proteins are essential for the CO_2 concentrating mechanism of *Chlamydomonas reinhardtii*. *Proc. Natl Acad. Sci. USA* **116**, 16915–16920 (2019).
15. Karlsson, J. et al. A novel α-type carbonic anhydrase associated with the thylakoid membrane in *Chlamydomonas reinhardtii* is required for growth at ambient CO_2. *EMBO J.* **17**, 1208–1216 (1998).
16. Raven, J. A. CO_2-concentrating mechanisms: a direct role for thylakoid lumen acidification? *Plant Cell Environ.* **20**, 147–154 (1997).
17. Badger, M. R., Kaplan, A. & Berry, J. A. Internal inorganic carbon pool of *Chlamydomonas reinhardtii*. *Plant Physiol.* **66**, 407–413 (1980).
18. Allen, J. F. Photosynthesis of ATP—electrons, proton pumps, rotors, and poise. *Cell* **110**, 273–276 (2002).
19. Allen, J. F. Cyclic, pseudocyclic and noncyclic photophosphorylation: new links in the chain. *Trends Plant Sci.* **8**, 15–19 (2003).
20. Munekage, Y. et al. PGR5 is involved in cyclic electron flow around photosystem I and is essential for photoprotection in *Arabidopsis*. *Cell* **110**, 361–371 (2002).

21. Johnson, X. et al. Proton gradient regulation 5-mediated cyclic electron flow under ATP- or redox-limited conditions: a study of ΔATPase pgr5 and ΔrbcL pgr5 mutants in the green alga *Chlamydomonas reinhardtii*. *Plant Physiol.* **165**, 438–452 (2014).
22. DalCorso, G. et al. A complex containing PGRL1 and PGR5 is involved in the switch between linear and cyclic electron flow in *Arabidopsis*. *Cell* **132**, 273–285 (2008).
23. Tolleter, D. et al. Control of hydrogen photoproduction by the proton gradient generated by cyclic electron flow in *Chlamydomonas reinhardtii*. *Plant Cell* **23**, 2619–2630 (2011).
24. Curien, G. et al. The water to water cycles in microalgae. *Plant Cell Physiol.* **57**, 1354–1363 (2016).
25. Helman, Y. et al. Genes encoding a-type flavoproteins are essential for photoreduction of O_2 in cyanobacteria. *Curr. Biol.* **13**, 230–235 (2003).
26. Gerotto, C. et al. Flavodiiron proteins act as safety valve for electrons in *Physcomitrella patens*. *Proc. Natl Acad. Sci. USA* **113**, 12322–12327 (2016).
27. Shimakawa, G. et al. The Liverwort, *Marchantia*, drives alternative electron flow using a flavodiiron protein to protect PSI. *Plant Physiol.* **173**, 1636–1647 (2017).
28. Chaux, F. et al. Flavodiiron proteins promote fast and transient O_2 photoreduction in *Chlamydomonas*. *Plant Physiol.* **174**, 1825–1836 (2017).
29. Dang, K. V. et al. Combined increases in mitochondrial cooperation and oxygen photoreduction compensate for deficiency in cyclic electron flow in *Chlamydomonas reinhardtii*. *Plant Cell* **26**, 3036–3050 (2014).
30. Bailleul, B. et al. Energetic coupling between plastids and mitochondria drives CO_2 assimilation in diatoms. *Nature* **524**, 366 (2015).
31. Wang, Y., Stessman, D. J. & Spalding, M. H. The CO_2 concentrating mechanism and photosynthetic carbon assimilation in limiting CO_2: how *Chlamydomonas* works against the gradient. *Plant J.* **82**, 429–448 (2015).
32. Kono, A. & Spalding, M. H. LCI1, a *Chlamydomonas reinhardtii* plasma membrane protein, functions in active CO_2 uptake under low CO_2. *Plant J.* **102**, 1127–1141 (2020).
33. Bonente, G. et al. Analysis of LhcSR3, a protein essential for feedback de-excitation in the green alga *Chlamydomonas reinhardtii*. *PLoS Biol.* **9**, e1000577 (2011).
34. Tian, L. et al. pH dependence, kinetics and light-harvesting regulation of nonphotochemical quenching in *Chlamydomonas*. *Proc. Natl Acad. Sci. USA* **116**, 8320–8325 (2019).
35. Sültemeyer, D. F., Klug, K. & Fock, H. P. Effect of dissolved inorganic carbon on oxygen evolution and uptake by *Chlamydomonas reinhardtii* suspensions adapted to ambient and CO_2-enriched air. *Photosynth. Res.* **12**, 25–33 (1987).
36. Sültemeyer, D., Biehler, K. & Fock, H. P. Evidence for the contribution of pseudocyclic photophosphorylation to the energy requirement of the mechanism for concentrating inorganic carbon in *Chlamydomonas*. *Planta* **189**, 235–242 (1993).
37. Lucker, B. & Kramer, D. M. Regulation of cyclic electron flow in *Chlamydomonas reinhardtii* under fluctuating carbon availability. *Photosynthesis Res.* **117**, 449–459 (2013).
38. Qu, Z. & Hartzell, H. C. Bestrophin Cl^- channels are highly permeable to HCO_3^-. *Am. J. Physiol. Cell Physiol.* **294**, C1371–C1377 (2008).
39. Rost, B., Riebesell, U., Burkhardt, S. & Sültemeyer, D. Carbon acquisition of bloom-forming marine phytoplankton. *Limnol. Oceanogr.* **48**, 55–67 (2003).
40. Basu, S. & Mackey, K. R. M. Phytoplankton as key mediators of the biological carbon pump: their responses to a changing climate. *Sustainability* **10**, 869 (2018).
41. Atkinson, N. et al. Introducing an algal carbon-concentrating mechanism into higher plants: location and incorporation of key components. *Plant Biotechnol. J.* **14**, 1302–1315 (2016).
42. Meyer, M. T., McCormick, A. J. & Griffiths, H. Will an algal CO_2-concentrating mechanism work in higher plants? *Curr. Opin. Plant Biol.* **31**, 181–188 (2016).
43. Nölke, G. et al. The integration of algal carbon concentration mechanism components into tobacco chloroplasts increases photosynthetic efficiency and biomass. *Biotechnol. J.* **14**, 1800170 (2019).
44. Hennacy, J. H. & Jonikas, M. C. Prospects for engineering biophysical CO_2 concentrating mechanisms into land plants to enhance yields. *Annu. Rev. Plant Biol.* **71**, 461–485 (2020).
45. Yamamoto, H., Takahashi, S., Badger, M. R. & Shikanai, T. Artificial remodelling of alternative electron flow by flavodiiron proteins in Arabidopsis. *Nat. Plants* **2**, 16012 (2016).
46. Wada, S. et al. Flavodiiron protein substitutes for cyclic electron flow without competing CO_2 assimilation. *Plant Physiol.* **176**, 1509–1518 (2017).
47. Gómez, R. et al. Faster photosynthetic induction in tobacco by expressing cyanobacterial flavodiiron proteins in chloroplasts. *Photosynth. Res.* **136**, 129–138 (2018).
48. Vicino, P. et al. Expression of flavodiiron proteins Flv2–Flv4 in chloroplasts of *Arabidopsis* and tobacco plants provides multiple stress tolerance. *Int. J. Mol. Sci.* **22**, 1178 (2021).

Publisher's note Springer Nature remains neutral with regard to jurisdictional claims in published maps and institutional affiliations.

© The Author(s), under exclusive licence to Springer Nature Limited 2022

Chapter IV

Methods

Chlamydomonas flvB, *pgrl1* and *bsti-1* mutants and their respective parental strains CC-4533, 137AH and D66 were previously described[14,23,28]. All strains were grown phototrophically under moderate light (80 µmol photons m^{-2} s^{-1}) in minimal medium either under low CO_2 or high CO_2. Gas exchange rates were measured using a membrane inlet mass spectrometer[49] and combined NPQ measurements were done as previously described[50]. All replicates shown are biological replicates from independent cultures. All data fitting, analysis, and plotting has been made using GraphPad Prism (v.6.07).

Chlamydomonas strains and cultivation

All *Chlamydomonas* strains were grown photo-autotrophically in 150-ml flasks at 25 °C in a buffered minimal medium (20 mM MOPS pH = 7.2) under constant illumination (80 µmol photons m^{-2} s^{-1}). Cells were collected during the exponential phase. The mt^+ *flvB-21* mutant generated in ref. [51] was crossed with the mt^- *pgrl1* mutant, and the progenies were screened based on chlorophyll fluorescence transients for *FLVB* insertion and PCR for *PGRL1* insertion (Extended Data Fig. 2b, c). Five independent strains exhibiting a *flvB* mutant-like chlorophyll fluorescence transient[50] and harbouring an insertion of the paromomycin cassette at the *PGRL1* locus were selected (Extended Data Fig. 2d). Four independent strains exhibiting WT chlorophyll fluorescence phenotype and no insertion at the *PGRL1* locus were selected as control strains (Extended Data Fig. 2d). The absence of FLVB and PGRL1 proteins in the five independent double mutants (named *pgrl1 flvB-1*, *-2*, *-3*, *-4*, and *-5*) and their presence in the four independent control strains (named WT1, 2, 3 and 4) was confirmed by immunodetection (Fig. 1g). The *bsti-1* mutant and its control strain D66 have been described[14].

DNA extractions and PCR amplification

Total DNA was extracted by mixing one cell colony in 50 µl of a 10 mM Na-EDTA (Sigma-Aldrich) solution. Putative insertion in the *PGRL1* locus was confirmed in progeny of the crossing by PCR using *dreamTaq* DNA polymerase with green GC Buffer (Thermo Scientific). The two primer sequences used to amplify the *PRGL1* locus were: 5′-TTACGCAGCGGCCTTAGCCTTCTTCTTGGC-3′ and 5′-GGCTAAGCGCTGTGTGCCGC-3′. PCR cycles were: 2 min at 95 °C for 40 cycles: 30 s at 95 °C, 30 s at 60 °C, 2 min at 72 °C, and 4 min at 72 °C for final extension. PCR products were separated on 1% (w/v) agarose gels.

Immunoblot analysis

For protein analysis, 10^6 exponentially growing cells (approximately 10 µg chlorophyll per ml) were collected by centrifugation at 4,000*g* for 3 min at 4 °C. Pellets were resuspended in 200 µl of 1% SDS and 800 µl of cold acetone was added to extract chlorophyll and incubated for 30 min at −20 °C. Samples were then centrifuged for 10 min, 16,000*g* at 4 °C and chlorophyll concentration measured on the supernatant. The protein pellet was resuspended with Novex Nupage LDS buffer 1× (Invitrogen), and proteins were then denaturated at 70 °C for 20 min. Protein extracts (10 µg protein) were loaded on Novex Nupage Bis tris 12% (Invitrogen) gel, run 1 h at 190 V in Novex Nupage (Invitrogen) MOPS buffer or MES (for PsaC) buffers and transferred to nitrocellulose membrane (or PVDF for LCIC) using semidry transfer technique. Immunodetection was performed using antibodies raised against PGRL1 (1:1,000)[23], FLVB (1:1,000) and FLVA (1:1,000)[28], NDA2 (1:5,000)[52]. Other antibodies against PsbD (AS06 146, 1:10,000), PsaC (AS10 939, 1:1,000), Cytb6 (AS03-034, 1:10,000), RbcL (AS03 037, 1:5,000), ATP-B (AS05-085, 1:5,000), COXIIB (AS06 151, 1:5,000), AOX1 (AS06 152, 1:2,000), FeSOD (AS06-125, 1:1,000), EPYC1 (AS09-602, 1:500), LHCSR3 (AS14-2766, 1:500), CAH1/2 (AS11-1737, 1:1,000) and CAH3 (AS05 073, 1:2,000) were obtained from Agrisera (https://www.agrisera.com/). The LCIC antibody (1:1,000) was generated against a synthetic peptide containing the sequence of 12 amino acids found in the C-terminus of LCIC as described[53]. Two rabbits were injected with the synthetic peptide for the production of LCIC antibody. BST3 (1:500, dilution) antibody was a gift from L. Mackinder, LCI1 (1:500, dilution) and LCIA (1:2,500, dilution) antibodies was a gift from H. Fukuzawa. Unless otherwise stated, PageRuler (ThermoFisher) was used as the molecular weight ladder. Uncropped and unprocessed scans of the blots shown in this study are visible in source data.

Growth tests

The different *Chlamydomonas* strains were cultivated at 400 ppm CO_2 (low CO_2), except *cia5* and CC125 which were grown under 3% CO_2 (high CO_2) and acclimatized to low CO_2 for 24 h before spotting as described[12], because the *cia5* mutant is unable to grow[54] autotrophically without high CO_2. Cells were collected during exponential growth and resuspended in fresh minimal medium to 0.1, 0.5 or 2 µg chlorophyll per ml. Eight-microlitre drops were spotted on plates at pH = 7.2 or 8.2 (buffered with 20 mM MOPS or Tris, respectively) and exposed to high CO_2, low CO_2 or very low CO_2. Homogeneous light was supplied by a panel of fluorescent tubes, and neutral filters were used to obtain the desired light intensity. Temperature was maintained at 25 °C at the level of plates by means of fans.

CO_2 affinity of net O_2 photosynthesis

CO_2 affinity was determined using membrane inlet mass spectrometry[49] (MIMS). Cells grown at air level or 3% CO_2 were collected, centrifuged at 450 *g* for 3 min and resuspended in fresh minimal medium (pH = 7.2) at 10 µg chlorophyll per ml. The cell suspension was then bubbled in the MIMS reaction vessel with a CO_2 depleted gas mixture (80 % N_2, 20 % O_2). Upon CO_2 depletion, the reaction vessel was closed, light was turned on (2,000 µmol photons m^{-2} s^{-1}; green LEDs) and gas exchange recorded. Increasing amounts of bicarbonate were then sequentially added to reach various C_i concentrations inside the reaction vessel during gas exchange measurements.

Carbonic anhydrase activity measurements

Carbonic anhydrase activity was determined in intact cells by monitoring $^{18}O/^{16}O$ isotope exchange between ^{18}O-enriched CO_2 and H_2O using MIMS as described[49]. Doubly labelled $^{13}C^{18}O_2$ was prepared by equilibrating 1 M $NaH^{13}CO_3$ (99% ^{13}C-atom, Euriso-top) with $H_2{}^{18}O$ (97 % ^{18}O-atom, Cambridge Isotope Lab.) for 24 h at room temperature. The reaction vessel (1.5 ml) contained minimal growth medium buffered with 20 mM MOPS (pH 7.2). At $t = 0$, 15 µl of a 1 M $NaH^{13}C^{18}O_3$ solution were added and the isotope exchange was measured by continuously recording the concentration of $^{13}C^{18}O^{18}O$ ($m/z = 49$), $^{13}C^{18}O^{16}O$ ($m/z = 47$) and $^{13}C^{16}O^{16}O$ ($m/z = 45$). CO_2 unlabelling was followed by determining the time constant of the isotope content decrease[49,55,56], first for 3 min in the absence of algae, and then for 3 min following addition of the algal sample (20 µl at 50 µg chlorophyll per ml). Total carbonic anhydrase activity of the algal sample was expressed on a chlorophyll content basis, as the time constant of the isotope content decrease, after subtracting the exchange activity measured in the absence of algae.

Electrochromic shift measurement

Electrochromic shift (ECS) was assessed by measuring the absorbance changes of cells at 520 and 545 nm using a JTS-100 spectrophotometer (BioLogic). Cells were collected in exponential phase, centrifuged, and resuspended at around 150 µg chlorophyll per ml in minimal growth medium buffered with 20 mM MOPS (pH 7.2) with a final concentration of 2 mM HCO_3^-. The cell suspension was injected into a thin-light path horizontal cuvette (BioLogic) and placed on the JST-100 in vertical mode. Cells were illuminated for 2 min with a 500 µmol photon m^{-2} s^{-1} red light (630 nm) to reach stable photosynthetic gas exchange reached before recording absorbance changes for ECS measurement and PMF size and partitioning determination. After 5 seconds of initiation of the recording, light was turned off and absorbance changes were recorded for 30 more seconds until full recovery of the signal. ECS signal was calculated as the difference between absorbance changes measured

at 520 and 545 nm. For each biological replicate, 3 technical replicates were taken and averaged. pH gradient and electric field ($\Delta\Psi$) composition of the ECS was calculated as described[57]. Total PMF size was calculated as $\Delta pH + \Delta\Psi$.

Chlorophyll fluorescence and NPQ measurements

Chlorophyll fluorescence was measured using a pulsed amplitude modulation (PAM) fluorimeter (Dual-PAM 100, Walz) on the MIMS chamber as described[50] using green actinic light (2,000 µmol photon m^{-2} s^{-1}; green LEDs). Red saturating flashes (8,000 µmol photons m^{-2} s^{-1}, 600 ms) were delivered to measure the initial maximal fluorescence yield (F_M) (in dark-acclimated samples) and then every 30 s to measure F'_M (upon actinic light exposure). NPQ was calculated as $(F_M - F'_M)/F_M$.

77K chlorophyll fluorescence spectra were measured on whole cells using an Ocean Insight FLAME-X optical fiber fluorescence spectrophotometer. About 200 µl of cell culture at around 10 µg chlorophyll per ml was fast frozen in liquid nitrogen. The excitation wavelength was 440 nm, and excitation and emission slits were 10 and 5 nm, respectively.

O_2 exchange measurement and calculations of electron fluxes though alternative pathways depending on C_i concentration

O_2 exchange was measured by MIMS using ^{18}O-enriched O_2 as described[49] on *pgrl1*, *flvB* and their respective control strains 137AH and CC-4533. Upon illumination, the C_i was depleted by photosynthesis, allowing to determine gas exchange rates at various C_i concentrations[58]. O_2 exchange rates were averaged from three biological replicates (Extended Data Fig. 8) and used to calculate the maximal capacity of each pathway. As the CCM functioning is not affected in *pgrl1* (Fig. 1), we considered that the increase in O_2 uptake rates between *pgrl1* and its control strain (O_2 difference$_{pgrl1}$) (Extended Data Fig. 8) reflects the additional electron flux to O_2 compensating the absence of PGRL1-mediated CEF. As CEF is 1.5 times less efficient than PCEF to generate a proton gradient[59], CEF was calculated as equal to 1.5 × O_2 difference$_{pgrl1}$. The FLV-mediated PCEF was calculated as the difference in O_2 uptake rates between CC-4533 and *flvB* (Extended Data Fig. 8). CMEF was calculated as the light-induced O_2 uptake remaining in the *flvB* mutant (Extended Data Fig. 8). To determine the contribution of alternative electron pathways to CCM energizing as compared to CO_2 fixation, CEF was normalized to net O_2 evolution measured in *pgrl1* and both PCEF and CMEF were normalized to net O_2 evolution in *flvB*.

Material availability

All biological material described in this study is available upon request.

Reporting summary

Further information on research design is available in the Nature Research Reporting Summary linked to this paper.

Data availability

Genes studied in this Article can be found on https://phytozome-next.jgi.doe.gov/ under the loci Cre12.g531900 (*FLVA*), Cre16.g691800 (*FLVB*), Cre07.g340200 (*PGRL1*), Cre16.g662600 (*BST1*), Cre16.g663400 (*BST2*) and Cre16.g663450 (*BST3*).

49. Burlacot, A., Burlacot, F., Li-Beisson, Y. & Peltier, G. Membrane inlet mass spectrometry: a powerful tool for algal research. *Front. Plant. Sci.* **11**, 1302 (2020).
50. Burlacot, A. et al. Flavodiiron-mediated O_2 photoreduction links H_2 production with CO_2 fixation during the anaerobic induction of photosynthesis. *Plant Physiol.* **177**, 1639–1649 (2018).
51. Burlacot, A., Richaud, P., Gosset, A., Li-Beisson, Y. & Peltier, G. Algal photosynthesis converts nitric oxide into nitrous oxide. *Proc. Natl Acad. Sci. USA* **117**, 2704–2709 (2020).
52. Desplats, C. et al. Characterization of Nda2, a plastoquinone-reducing type II NAD(P)H dehydrogenase in *Chlamydomonas* chloroplasts. *J. Biol. Chem.* **284**, 4148–4157 (2009).
53. Yamano, T. et al. Light and low-CO_2-dependent LCIB–LCIC complex localization in the chloroplast supports the carbon-concentrating mechanism in *Chlamydomonas reinhardtii*. *Plant Cell Physiol.* **51**, 1453–1468 (2010).
54. Moroney, J. V. et al. Isolation and characterization of a mutant of *Chlamydomonas reinhardtii* deficient in the CO_2 concentrating mechanism. *Plant Physiol.* **89**, 897–903 (1989).
55. Gerster, R. An attempt to interpret the kinetics of isotope exchange between $C^{18}O_2$ and the water of a leaf: experiments in the dark. *Planta* **97**, 155–172 (1971).
56. Silverman, D. N. In *Methods in Enzymology* Vol. 87 (ed. Purich, D. L.) 732–752 (Academic Press, 1982).
57. Cruz, J. A., Sacksteder, C. A., Kanazawa, A. & Kramer, D. M. Contribution of electric field (Δψ) to steady-state transthylakoid proton motive force (*pmf*) in vitro and in vivo. control of *pmf* parsing into Δψ and ΔpH by ionic strength. *Biochem.* **40**, 1226–1237 (2001).
58. Douchi, D. et al. Membrane-inlet mass spectrometry enables a quantitative understanding of inorganic carbon uptake flux and carbon concentrating mechanisms in metabolically engineered cyanobacteria. *Front. Microbiol.* **10**, 1356–1356 (2019).
59. Kramer, D. M. & Evans, J. R. The importance of energy balance in improving photosynthetic productivity. *Plant Physiol.* **155**, 70–78 (2011).

Acknowledgements This work was supported by the A*MIDEX (ANR-11-IDEX-0001-02) project and by the ANR OTOLHYD. A.B. acknowledges support from the Carnegie Institution for Science. O.D. is the recipient of a PhD grant awarded to Y.L.-B. We thank A. Grossman for use of the JTS-100; G. Peers for stimulating discussion; K. K. Niyogi and M. Iwai for critical reading of the manuscript; J. V. Moroney for the *bsti-1* mutant; L. Mackinder for the BST3 antibody; and H. Fukuzawa for the LCIA and LCI1 antibodies. We gratefully acknowledge the contributions of S. Moulin for artistic drawings in Fig. 4, S. Blangy for LCIC antibody preparation, E. Calikanzaros and V. Epting for technical assistance, and A. Gosset for performing genetic crosses of *flvB* and *pgrl1* mutants. The authors acknowledge the European Union Regional Developing Fund, the Region Provence Alpes Côte d'Azur, the French Ministry of Research, and the CEA for funding the HelioBiotec platform.

Author contributions A.B. and G.P. designed the research; A.B., O.D., P.A., S.C. and G.P. performed research; A.B. and G.P. contributed new reagents and analytic tools; A.B. and G.P. analysed data; A.B. and G.P. wrote the paper with input from Y.L.-B.

Competing interests The authors declare no competing interests.

Additional information

Supplementary information The online version contains supplementary material available at https://doi.org/10.1038/s41586-022-04662-9.

Correspondence and requests for materials should be addressed to Gilles Peltier.

Peer review information *Nature* thanks Cornelia Spetea Wiklund and the other, anonymous, reviewers for their contribution to the peer review of this work. Peer reviewer reports are available.

Reprints and permissions information is available at http://www.nature.com/reprints.

Conclusion

In this work, we demonstrated that both FLV-mediated PCEF and the PGRL1-mediated CEF contribute to the CCM energy supply and can widely compensate each other, thus explaining why their contribution has remained elusive. Moreover, we show that the trans-thylakoidal proton gradient generated by both mechanisms is the energy vector used by the last step of C_i transport mediated by the recently discovered trans-thylakoidal bestrophin-like transporters (Mukherjee et al., 2019). We further showed that mitochondrial respiration contributes in CCM by supplying energy to transporters other than bestrophins through the chloroplast-to-mitochondria electron flow (CMEF).

CMEF likely operate through metabolites shuttles. Malate is a perfect candidate since all subcellular compartments contains isoforms of malate dehydrogenases. Nevertheless, transporters of malate and MDHs involved in CMEF remain unknown in algae. Our work on LCI20 did not show its implication in CCM, indicating that LCI20 might not be the only malate transporter required for CMEF. A tandem of shuttle systems (that connect chloroplast to cytosol, and then cytosol to mitochondria) could be expected.

This work led us to question whether those different alternative photosynthesis pathways could have another energetic role beyond the CCM functioning. In our recent preprint (Peltier et al., 2023), we propose that CEF, PCEF and CMEF are required to supply energy for the CO_2 fixation even when CCM is inactive in Chlamydomonas. For more details see **Annex 1**.

IV. General conclusion and perspectives

In this thesis, we pursued effort in understanding the interplay between cellular energy status and carbon storage in the model green microalga Chlamydomonas. Nitrogen (N) and Carbon (C; organic or inorganic) sources are key nutrients that influence cell growth, their imbalance frequently encountered in natural conditions results in reduced photosynthetic efficiency therefore biomass formation (Vitousek and Howarth, 1991; Riebesell et al., 1993; Spalding et al., 2002; Du et al., 2020). In this study, by characterizing mutants deficient in cellular energy management pathways (cyclic, pseudo-cyclic, or energy trafficking between subcellular compartments), we shed light on some of the mechanisms used by Chlamydomonas during adaptation to N deficiency (**Chapter 1**), in transitioning between different levels or sources of C, i.e. from autotrophy (only CO_2) to mixotrophy (CO_2 + acetate) (**Chapter 2, 3**), and from high CO_2 to limiting CO_2 levels (**Chapter 3 and 4**).

N deficiency is widely encountered in nature and is also one of the most potent triggers to induce high accumulation of TAG and starch (Siaut et al., 2011; Schulz-Raffelt et al., 2016) and has therefore often been used in the laboratory to study underlying molecular mechanisms. Deeper understanding of N-induced carbon storage is required because in parallel to massive carbon accumulation, N deficiency results in growth arrest and decrease in photosynthetic efficiency therefore undermining productivity (Blaby et al., 2013; Zhang et al., 2013; Schmollinger et al., 2014; Juergens et al., 2015; Saroussi et al., 2016). Therefore, a major biotechnological challenge in algal domestication for biofuel is to produce strains so that they can maintain optimal photosynthesis and cell viability simultaneous to oil and starch accumulation. To achieve this goal, one needs to gain better knowledge on interaction between photosynthetic energy production, their management and downstream metabolic usage. We report here the role of PGRL1/PGR5-dependent CEF in the downregulation of PET during N deficiency. This down-regulation likely operates via the photosynthetic control mechanism at the level of Cyt b_6f. Lack of PGRL1 resulted in sustained efficient photosynthetic activity over several days of N deficiency. We have further shown that the release of photosynthetic control in *pgrl1* mutants resulted in higher FLV-mediated PCEF. We conclude that the PCEF channels excess electrons toward O_2, prevents PSI acceptor side-limitation and likely generates ATP, maintaining PET at a high level and potentially favoring high TAG accumulation.

This is a first report showing that PGRL1/PGR5-controlled CEF and FLV-mediated PCEF did not compensate each other at the physiological level. During N deficiency, whereas PGRL1-controlled CEF promotes photosynthetic control, FLVs favor elevated photosynthetic activity. Therefore, the activity of the two pathways lead to antagonistic phenotypic observation. In contrast to our report, compensation between PGRL1/PGR5-controlled CEF and FLVs were reported in Chlamydomonas during high light and low-CO_2 conditions (Dang et al., 2014; Burlacot et al., 2022). Orthologous expression of FLVs was also shown to rescue the *pgr5* phenotype in Arabidopsis and rice under fluctuating light conditions without a net increase of neither photosynthesis nor growth rate (Yamamoto et al., 2016; Wada et al., 2018).

Mechanistically, both CEF and PCEF generate extra *pmf* without a net NADPH production. By doing so, they contribute to either supplying additional ATP (when ATP is limiting) or dissipating excess energy (when H^+ is limiting for NQP). In both conditions, CEF and PCEF could compensate each other. However, recent studies reported a specific feature of PGRL1/PGR5 in tuning the activity and abundance of Cyt

b_6f (Buchert et al., 2020; Penzler et al., 2023). Under excessive reducing conditions, PGRL1/PGR5 promotes the degradation of Cyt *b_6f* to prevent acceptor side limitation and inhibition of PSI (Buchert et al., 2020; Penzler et al., 2023). We observed hyper-accumulation of Cyt *b_6f* and higher PSI donor side limitation in the *pgrl1* mutants during N deficiency. This indicates that conditions under which PSI acceptor side limitation prevails over ATP/H^+ supply, PGRL1/PGR5-controlled CEF and FLV-mediated PCEF may have antagonists rather than synergic role.

Considerable efforts for improving lipid productivity have focused on engineering specific steps of fatty acid and TAG biosynthesis/catabolism or genes over-expression which have resulted in some limited improvement (Schulz-Raffelt et al., 2016; Kong et al., 2019; Li-Beisson et al., 2019; Lee et al., 2020; Torres-Romero et al., 2023). Here, we have shown that manipulating the cellular energy status by modulating alternative photosynthesis pathways is a promising strategy for improving biomass and lipid productivity under low light and non-limiting CO_2 conditions. Such strategy could be applied for photobioreactors-based algal exploitation where conditions are fully customized. Whether it can be used in outdoor algal cultivation system remains to be tested. Nevertheless, improving the efficiency of photosynthesis did not always result in major increase in yield, especially for large scale-experimentation in outdoor conditions. It has been claimed in some study that crop yield cannot be substantially increased by alteration of crop photosynthesis (De Souza et al., 2022; Sinclair et al., 2023). It is important to note that photosynthesis is not always limiting crop/algal productivity. Other factors can also contribute to yield such as metabolic capacity, genetic traits etc. For example, in our work, improved biomass and higher lipid production was only observed in 137AH genetic background as the consequence of higher net photosynthesis, highlighting the importance of genetic background on phenotypic manifestations.

In the second part, we investigated the acclimation of Chlamydomonas to limiting CO_2 conditions. Different genes of Chlamydomonas are induced under low CO_2 and suppressed by high CO_2. Historically, those genes are considered to code for CCM components or photorespiration (Spalding et al., 1985; Marek and Spalding, 1991; Fukuzawa et al., 2001; Van et al., 2001). We identified a putative malate/glutamate translocator annotated as the Low-CO_2 Inducible 20 (LCI20). We demonstrated the physiological role of LCI20 in balancing chloroplast redox status during the adaptation of Chlamydomonas to changing CO_2/O_2 levels. Under ambient O_2 level, the *lci20* mutant secreted higher amount of glycolate and was unable to grow after a transition from H-CO_2 to VL-CO_2. Decreasing the O_2 level to 2% restored *lci20* growth and suppressed glycolate secretion. We conclude that LCI20 is involved in photorespiration and in the export of reductant out of the chloroplast.

We propose LCI20 as a malate/glutamate transporter based on a metabolomics analysis revealing hyper-accumulation of glutamate and malate in *lci20* mutant. Despite repeated efforts, we could not produce LCI20 in yeast neither in vitro to allow transport assays using artificial liposomes system. Therefore, it remains to be determined the exact transport activity of LCI20 and eventually the direction of the metabolites transported. Approaches such as yeast complementation assay based on auxotrophy or uptake assays in Xenopus laevis Oocytes could be also considered (Jørgensen et al., 2017; Fuhrmeister and Streubel, 2023). Another strategy is to perform metabolites (malate, glutamate etc.) feeding on intact isolated chloroplast (of WT and *lci20* mutant) and analyze the effect on photosynthesis (Mettler and Beevers, 1980). Nevertheless, the strong similarity between

LCI20 and plants DiT2 indicates that LCI20 is highly likely capable of mediating malate/glutamate transport in Chlamydomonas.

Although photorespiration has been under-estimated in microalgae performing an active biophysical CCM, genes coding for photorespiratory proteins are well present in cyanobacteria and in different microalgae species among primary and secondary endosymbionts (Paul et al., 1975; Paul and Volcani, 1976; Leboulanger et al., 1998; Eisenhut et al., 2008; Hagemann et al., 2016; Xie et al., 2016; Kern et al., 2020; Santhanagopalan et al., 2021). It was shown that CCM reduces but does not completely suppress the oxygenase activity of Rubisco. Our work reporting the growth defect of *lci20* after transition from H to VL-CO2 associated with higher glycolate secretion indicate that LCI20 transporter might be involved in photorespiratory glycolate metabolism and further support that CCM does not suppress photorespiratory activity.

Previous works have reported photorespiratory phenotype in mutants impaired in phosphoglycolate phosphatase (PGP1), glycolate dehydrogenase (GYD1; GDH), and hydroxypyruvate reductase 1 (HPR1) in Chlamydomonas (Suzuki et al., 1990; Nakamura et al., 2005; Shi et al., 2021). The *gdh1* and *pgp1* mutants were isolated as high-CO_2 requiring (HCR) with reduced growth rate under low-CO_2 based on the screening of Chlamydomonas mutant library (Van et al., 2001). The *pgp1* was shown to accumulate higher amount of 2-phosphoglycolate that inhibits several enzymes of the Calvin cycle causing the growth defect (Hernandez and Nägele, 2023). Similarly, *hpr1* is impaired in growth and secreted higher amount of glycolate after a transition from 3% CO_2 to air (Shi et al., 2021). Although the higher secretion of glycolate in *gdh1* seems to be supported, its growth phenotype could not be reproduced in different laboratories indicating that *gdh1* is not a true HCR mutant as reported (our lab and also personal communication of researchers at Carnegie Institution for Science to the Chlamy center). Taken together, mutants defective in photorespiration do not always manifest a growth defect, which could be a combination of several factors i.e. the metabolic step in the photorespiratory pathway that is blocked; the capacity to secrete glycolate; and the potential effect on the interaction with N metabolism etc.

Nevertheless, the physiological function of photorespiration is still controversial in microalgae and in land plants. On the one hand, photorespiration is considered a wasteful metabolic process because it releases carbon (in the form of CO_2 or glycolate) and consumes photosynthetic energy (Fernie and Bauwe, 2020; Shi and Bloom, 2021). Therefore, alternative photorespiratory pathways aiming to reduce the energy demand or CO_2 release have recently been proposed for improving crop productivity (Shen et al., 2019; Cavanagh et al., 2022; Segura Broncano et al., 2023). In diatoms, suppression of photorespiration by decreasing O_2 availability enhances growth and biomass productivity (Sun et al., 2022). On the other hand, recent studies reported the essential role of photorespiration in photoprotection, N assimilation and metabolism, abiotic stress tolerance in land plants and microalgae (Champigny, 1995; Weber and Flügge, 2002; Xie et al., 2016; Hanawa et al., 2017; Busch et al., 2018; Shi et al., 2022). It was reported that photorespiratory ATP consumption plays a role in regulating chloroplastic ATP synthase activity in *Nicotiana tabacum* (Smith et al., 2023). The above controversies likely indicate that photorespiration could have both good and bad consequences on plants/microalgal growth depending on the environmental conditions (steady-state vs fluctuations) and nitrogen source, temperature, light intensity etc.

A specificity of microalgae (at least in Chlamydomonas) is that photorespiration and CCM are co-regulated by the same environmental cues and the CCM1 transcription

factor which implies a possible cross-talk between the two pathways (Fang et al., 2012; Santhanagopalan et al., 2021; Adler et al., 2022). Previous studies have reported that a photorespiratory metabolite is required for the induction of the CCM during acclimation to low CO_2 (Spalding and Ogren, 1982; Marcus et al., 1983; Spalding et al., 1985). Under non-photorespiratory conditions (2.6% O_2), the lag period of CCM induction was doubled during adaptation of *Anabaena variabilis* to low CO_2 (Marcus et al., 1983). In Chlamydomonas, mutants deficient in PGP1 exhibited similar affinity for Ci comparable to the WT which indicate that the signal metabolites should be upstream of glycolate metabolism (Suzuki et al., 1999). Whether photorespiration really serves in the induction of CCM require further investigations. To dissect this process, one can perform growth test and measure CCM activation/functioning in WT and different photorespiratory mutant after transition from high to low CO_2 level at 2% and 21% O_2. The crosstalk between photorespiration and CCM is currently under investigation in our team.

In a broader context, microalgal photorespiration could be of crucial importance in natural ecosystems. High concentrations of glycolate was detected in the oceans during phytoplanckton blooming (Leboulanger et al., 1994; Leboulanger et al., 1997; Leboulanger et al., 1998; Schada von Borzyskowski et al., 2019). Photorespiration is the major natural biosynthetic pathway producing glycolate (Taubert et al., 2019). The glycolate secreted during bloom formation was shown to serve as a carbon source for marine proteobacteria suggesting the role of photorespiration in trophic interaction between autotrophic phytoplankton and heterotrophic bacterioplankton (Schada von Borzyskowski et al., 2019). It was also proposed that photorespiratory glycolate production and metabolism might have been one of the prime selective forces in the establishment of the primary endosymbiosis between the cyanobacterial endosymbiont and the chlamydial host (Tyra et al., 2007; Facchinelli et al., 2013; Karkar et al., 2015; Hagemann et al., 2016). Whether photorespiration plays a role in microalgal-bacterial interactions is worth further investigation (Sasso et al., 2018; Durán et al., 2021; Calatrava et al., 2023).

Many microalgae including Chlamydomonas are not strict photoautotrophs, and they can use reduced carbon such as acetate as sole carbon source (heterotrophy) or associated with photosynthesis (mixotrophy). The latter is particularly biotechnologically important because it favors higher biomass production (Fan et al., 2012; Villanova et al., 2021). However, our understanding on how microalgae make the transition from photoautotrophy to mixotrophy is elusive. We report here the essential role of two chloroplast malate transporters, LCI20 and OMT2, during the transition from photoautotrophy to mixotrophy. It was shown that mixotrophic growth in Chlamydomonas results in over-reduction of the chloroplast (Johnson and Alric, 2012; Roach et al., 2013; Saint-Sorny et al., 2022). We propose that those two transporters could serve in exporting reductants through the malate valve (Scheibe, 2004; Selinski and Scheibe, 2014; Selinski and Scheibe, 2019). To address this question, we have generated double mutants *lci20 omt2* by genetic crossing. Our first investigation showed no deleterious effect of lacking both LCI20 and OMT2 during steady-state photoautotrophic growth. An important question for future research will be to determine whether LCI20 and OMT1/2 could compensate each other under dynamic environmental fluctuations.

Malate shuttle function is not limited to photorespiration. Redox communications through the malate shuttle was shown to be essential for FA beta-oxidation in Chlamydomonas and Arabidopsis (Pracharoenwattana et al., 2007; Kong et al., 2018), balancing chloroplast redox state and preventing against oxidative stresses in plants

(Kinoshita et al., 2011; Hebbelmann et al., 2012; Zhao et al., 2018; Yokochi et al., 2021; Dao et al., 2022) etc. In microalgae, there is no direct evidence of the operation of the malate valve despite being postulated to function in chloroplast-to-mitochondrial electron flow (CMEF) (Cardol et al., 2003; Dang et al., 2014; Bailleul et al., 2015; Kaye et al., 2019; Burlacot et al., 2022; Peltier et al., 2023). Functional redundancy between isoforms of MDHs (e.g. Chloroplastic MDH5 and MDH1) or malate translocators (e.g. LCI20, OMT1/2 etc) could be expected, making difficult to reveal phenotype. Therefore, creating double or multiple mutations could help revealing any functional redundancy. Future investigations towards a detailed understanding of the malate shuttle mechanism and its components in microalgae should involve the use of cutting-edge molecular genetics tools for creating combinatory mutations in different genes.

V. Annex:

Annex 1: Alternative electron pathways of photosynthesis power green algal CO2 capture. (The plant Cell 10.1093/plcell/koae143)

Authors: Gilles Peltier[1], Carolyne Stoffel[2], Justin Findinier[2], Sai Kiran Madireddi[2], Ousmane Dao[1], Virginie Epting[1], Amélie Morin[1], Arthur Grossman[2,3], Yonghua Li-Beisson[1], Adrien Burlacot[2,3*]

Affiliations:

[1] Aix Marseille Univ, CEA, CNRS, Institut de Biosciences et Biotechnologies Aix-Marseille, CEA Cadarache, 13108 Saint Paul-lez-Durance, France

[2] Department of Plant Biology, The Carnegie Institution for Science, Stanford, CA, 94305 USA

[3] Department of Biology, Stanford University, Stanford, CA, 94305, USA

[*]corresponding author: A.B., aburlacot@carnegiescience.edu

ORCID IDs: 0000-0001-7434-6416 (A.B.), 0000-0002-4078-6250 (C.S.), 0000-0001-9019-8900 (J.F.), 0000-0002-1820-1033 (S.M.), 0000-0002-7040-5770 (O.D), 0000-0003-1064-1816 (Y.L.-B.), 0000-0002-3747-5881(A.G.), 0000-0002-2226-3931 (G.P.)

Author contributions: A.B. led and coordinated the research, A.B. and G.P. designed research; A.B., C.S., J.F., O.D., S.M., V.E., A.M. and G.P. performed research; A.B. and G.P. contributed new reagents/analytic tools; A.B. analyzed data and made all figures; A.B. and G.P. wrote the paper with inputs from Y. L.-B. and A.G.

One sentence summary: Quantifying the contribution of the main electron flow pathways to algal CO_2 fixation.

Annex I

Abstract

On Earth, microalgae contribute to about half of global net photosynthesis. During photosynthesis, sunlight is converted into chemical energy (ATP and NADPH) used by metabolism to convert CO_2 into biomass. Alternative electron pathways of photosynthesis have been proposed to generate additional ATP that is required for sustaining CO_2 fixation, but the relative importance of each pathway remains elusive. Here, we dissect and quantify the contribution of cyclic, pseudo-cyclic and chloroplast to mitochondria electron flows for their ability to sustain net photosynthesis in the microalga *Chlamydomonas reinhardtii*. We show that each pathway has the potential to energize substantial CO_2 fixation, can compensate each other, and that the additional energy requirement to fix CO_2 is more than 3 times higher than previous estimations. We further show that all pathways have very different efficiencies at energizing CO_2 fixation, with the chloroplast- mitochondria interaction being the most efficient, thus laying bioenergetic foundations for biotechnological improvement of CO_2 capture.

Introduction

Oxygenic photosynthesis is the main process responsible for the carbon input into ecosystems on Earth, with net CO_2 fixation by photosynthesis representing more than ten times anthropic CO_2 emissions (IPCC, 2021). During photosynthesis, carbon fixation is powered by the combined action of photosystems (PS) I and II, establishing a linear electron flow (LEF) that produces reducing power (NADPH) and a trans-thylakoidal proton motive force (*pmf*) used to generate ATP. Both ATP and NADPH fuel the CO_2 fixation reactions of the Calvin-Benson-Bassham (CBB) cycle and the further processing of the glyceraldehyde-3-phosphate (G3P) to regenerated ribulose-1-5 bisphosphate and produce building blocks used for the elaboration of biomass (Johnson and Alric, 2013). However, given the insufficiency of the LEF to generate an adequate *pmf* and the conversion efficiency of the chloroplastic ATP-synthase (ATPase), it has been long recognized that the LEF only generates 85% of the theoretical ATP requirements of the CBB cycle (Allen, 2003).

Cyclic electron flow, which recycles reducing equivalents around PSI (CEF) and pseudo-cyclic electron flow (PCEF), which reduces molecular O_2 at the acceptor side of PSI (**Fig. 1**), were proposed to contribute to the production of extra ATP during photosynthesis (Arnon, 1959, 1984). In most angiosperms and mosses, CEF entails two main pathways, one involving the proton gradient generation (PGR) 5 (Munekage *et al.*, 2002) and PGR-Like 1 proteins (DalCorso *et al.*, 2008) and another involving the plastidial NDH-1 complex (Joët *et al.*, 2001; Munekage *et al.*, 2004). In green microalgae, the plastidial NDH-1 complex is absent (Peltier *et al.*, 2016) and it was reported that two CEF pathways operate, one controlled by PGRL1 and PGR5 (Tolleter *et al.*, 2011; Johnson *et al.*, 2014) and the other involving the plastidial NAD(P)H dehydrogenase Nda2 (Jans *et al.*, 2008; Desplats *et al.*, 2009; Saroussi *et al.*, 2016). Since the Nda2 pathway is mostly active during nitrogen deprivation (Peltier and Schmidt, 1991; Saroussi *et al.*, 2016), hereafter CEF refers to the PGRL1/PGR5-controled CEF. PCEF involves Flavodiiron proteins (FLVs) that catalyse O_2 photoreduction at the PSI acceptor side (**Fig. 1**) in cyanobacteria(Helman *et al.*, 2003; Allahverdiyeva *et al.*, 2013), green microalgae (Chaux *et al.*, 2017), mosses (Gerotto *et al.*, 2016), liverwort (Shimakawa *et al.*, 2017) and gymnosperms (Ilík *et al.*, 2017).

Another mechanism that can supply ATP to photosynthesis involves metabolic cooperation between chloroplasts and mitochondria (Raghavendra and Padmasree, 2003). Reducing power generated within the chloroplast is transferred to the mitochondria by metabolic shuttles where it is converted into ATP by the mitochondrial respiratory chain and might be shuttled back to the cytosol and the chloroplast (**Fig. 1**). Such a cooperation, called here Chloroplast to Mitochondria Electron Flow (CMEF) was first evidenced from the restoration of photoautotrophic growth in a mutant of the green microalgae *Chlamydomonas reinhardtii* (hereafter *Chlamydomonas*) deficient in the plastidial ATPase (Lemaire *et al.*, 1988). Similar cooperation was later suggested from the study of *Chlamydomonas* mutants affected in mitochondrial respiration (Cardol *et al.*, 2003) or in CEF (Dang *et al.*, 2014) as well as in the moss *Physcomytrum patens* (Mellon *et al.*, 2021), and in diatoms (Bailleul *et al.*, 2015).

It is generally considered that both PCEF and CMEF act essentially as electron valves, operating either transiently in the case of PCEF to alleviate excess electrons generated by photosynthesis under light fluctuating regimes (Alric and Johnson, 2017; Chaux *et al.*, 2017; Alboresi *et al.*, 2019) or more continuously for CMEF under high light stress (Kaye *et al.*, 2019). Although in *Chlamydomonas*, CMEF, PCEF and CEF

have been recently shown to all contribute to supply energy to the CO_2 concentrating mechanism (CCM) (Burlacot *et al.*, 2022), evidence of their role in powering the CBB cycle and downstream carbon metabolism processes are scarce.

In this work, we show that each pathway (CEF, PCEF and CMEF) has the capacity to sustain net CO_2 fixation to varying degrees and can compensate for the absence of the other pathways, whereas CO_2 fixation is completely abolished in the absence of all three pathways. Moreover, we introduce a new metric: the electron quantum yield of net photosynthesis for each pathway and use it to show that CMEF is by far the most efficient at energizing CO_2 fixation. We further discuss our data in relation to the relative contribution and efficiency of the different alternative pathways to the net primary productivity of terrestrial and oceanic ecosystems.

Results

Net photosynthesis fully relies on mitochondrial respiration when PCEF and CEF are impaired. To test whether PCEF and CEF are required for maximal net photosynthesis (V_{Max}), we first measured photosynthetic O_2 exchange rates using Membrane Inlet Mass Spectrometry (Burlacot *et al.*, 2020) in air-grown *Chlamydomonas* mutants impaired in both CEF and PCEF (*pgrl1 flvB-1 and 3*) and in control strains (WT2 and 3)(Burlacot *et al.*, 2022). Since the *pgrl1* and *flvB* mutants are affected in the functioning of the CO_2 concentration mechanism (CCM) (Burlacot *et al.*, 2022), photosynthesis measurements were performed in the presence of a saturating concentration of inorganic carbon (C_i) when the CCM is inactive. As previously reported (Burlacot *et al.*, 2022), *pgrl1 flvB* double mutants can perform photosynthesis at maximum rates comparable to the single *pgrl1* or *flvB* mutants and to the parental and sibling control strains (**Fig. 2; Sup Figs. S1 A, S2, S3**), therefore showing that neither CEF nor PCEF are essential to reach V_{Max}. To test a possible contribution of mitochondrial respiration to photosynthesis, *pgrl1 flvB* double mutants were treated with myxothiazol (Myxo) and salicylhydroxamic acid (SHAM), inhibitors of mitochondrial electron transport, respectively acting on complex III and the alternative oxidases (AOX) (**Fig. 1**)(Cournac *et al.*, 2002). While the addition of both inhibitors had minimal impact (about 10-20% decrease) on the V_{Max} of control strains (**Fig. 2 A, C, Sup Figs. S1 A, S2, S3**), they completely abolished photosynthesis of *pgrl1 flvB* double mutants (**Fig. 2 B, C, Sup Figs. S1, S2)**.

In *Chlamydomonas*, the cellular location of mitochondria depends on the CO_2 supply, with the mitochondria located at the cell periphery in low CO_2-grown cells and mostly inside the chloroplast cup in high CO_2 (Geraghty and Spalding, 1996) (**Fig. 2E, F**). Since this location might affect CMEF (Burlacot and Peltier, 2023), we sought to examine the involvement of the mitochondrial sub-cellular localization on the role of CMEF. Similar to air-grown cells, mitochondrial inhibitors fully stopped net photosynthesis on 2% CO_2-grown *pgrl1 flvB* mutants while having a marginal effect (about 10-20% decrease) on the control strains (**Fig. 2D, Sup Fig. S4**). To control the location of the mitochondria in the different strains, we visualized the spatial distribution of an expressed, mitochondria-targeted fluorophore (Clover). There was similar re-localization of mitochondria depending on the CO_2 supply during growth (at periphery under very low CO_2) of both the single and double mutants and a control strain (**Fig. 2E, F, Sup Fig. S5**). We conclude from this experiment that in the absence of both CEF and PCEF, near wild type levels of photosynthesis can be achieved that fully rely on CMEF, the role of CMEF being independent of the spatial distribution of the mitochondria.

CEF, PCEF and CMEF each have the potential to sustain most net photosynthesis. We quantified the potential of CEF, PCEF and CMEF to energize net photosynthesis, by measuring the effect of mitochondrial inhibitors on photosynthesis rates in single and double *pgrl1* and *flvB* mutants (**Fig. 3 A, B, C, D**). Inhibition of respiration decreased net photosynthesis by 40-50% in both the *flvB* and *pgrl1* single mutants (**Fig. 3 A, B, Sup Figs. S1 A, S2**), showing that both CEF and PCEF have the potential to energize 50-60% of V_{Max} on their own (**Fig. 3 E, Sup Fig. S1A, B**). Inhibition of respiration decreased the V_{Max} of all control strains by 10-20% (**Fig. S1 A, S2, S3**) showing that combined activities of CEF and PCEF can power approximately 85% of photosynthesis (**Fig. 3 E**). Based on the effects of SHAM or myxothiazol individually, on V_{Max} in *pgrl1 flvB* mutants (**Fig. 3C, D, E, Sup Figs. S1 A, S2**), we conclude that while the complex III-IV pathway of CMEF (**Fig. 1**) can power most net photosynthesis on its own (**Fig. 3D**), the AOX pathway (**Fig. 1**) can only sustain approximately 45% of V_{Max} (**Fig. 3E**). Because the amount of the terminal oxidases involved in CMEF does not differ in the *pgrl1 flvB* mutants and their control strains (**Sup Fig. S6**), these values likely reflect wild type capacities. We also quantified net photosynthesis based on inorganic carbon (C_i) uptake (**Sup Figs. S7, S8**). On all strains tested, the inhibitory effects on V_{max} measured as net C_i uptake was similar to that observed on net O_2 production (**Sup Figs. S7**). We conclude from these experiments that CEF, PCEF and CMEF can sustain photosynthetic C_i uptake on their own but that only the complex III-IV pathway of CMEF is efficient enough to reach near maximal photosynthesis levels.

CEF, PCEF and CMEF show different efficiencies in sustaining net photosynthesis. Mechanistically, for each electron flowing once through the different pathways (CEF, PCEF, the AOX, or the complex III-IV pathway of CMEF), the total number of protons translocated across the thylakoid and/or the inner mitochondrial membranes, highly differ (Burlacot, 2023). To quantify the potential of the different pathways in energizing net photosynthesis, we introduce a new metric, the electron (e^-) quantum yield of a pathway defined by the following equation:

$$e^- quantum\ yield = \frac{e^-(net\ photosynthesis)}{e^-(net\ photosynthesis) + e^-(alternative\ pathway)}$$

Where e^- (net photosynthesis) is the flux of photosynthetic electrons directly used for net photosynthesis and e^- (alternative pathway) is the flux of photosynthetic electrons through a given alternative pathway under conditions where only this alternative pathway is active. Therefore, the e- quantum yield of an alternative pathway, which is determined when only this alternative pathway is operating, characterizes the efficiency of electrons passing through it in powering net photosynthesis. Note that the e^- quantum yield, thus does not reflect the rate or the importance of the pathway considered but rather its capacity to produce ATP for each electron. We used this equation and experiments from **Fig. 3 A-E** to quantify the e^- quantum yield of each pathway (**Fig. 3 F, Sup Fig. S9**). The e^-quantum yield of PCEF was estimated at 0.65, whereas that of CMEF at 0.85 (**Fig. 3F**), indicating a better efficiency of CMEF in driving CO_2 fixation as compared to PCEF. In the absence of an established method to quantifying CEF in physiologically relevant conditions (Burlacot *et al.*, 2022), CEF quantum efficiency was estimated to be around 0.55 by hypothesizing that an electron passing once through CEF is 1.5 time less efficient at generating a *pmf* than if it would pass through PCEF (Kramer and Evans, 2011; Burlacot, 2023) (**see Materials and Methods**). In the case of CMEF, the e^- quantum yield of the AOX pathway was lower than that of the complex III-IV pathway (**Fig. 3F**), likely reflecting the proton translocating capacity of each pathway (**Fig. 1)(Burlacot, 2023)**.

Using the e^- quantum yields of each pathway, we then compared the flux of electrons required to power the same amount of net photosynthesis relative to PCEF (**Fig. 3G**). Strikingly, theoretical values were in accord with values experimentally determined by the e^- quantum yields (**Fig. 3 G**). We conclude from these experiments that CMEF pathways are more efficient than PCEF and CEF at energizing CO_2 fixation and that this difference arises from a higher H^+/e^- transfer capacity likely leading to a higher capacity to generate ATP.

Estimating the respective contributions of CEF, PCEF and CMEF during steady state photosynthesis and growth. We then sought to estimate (*i*) the electron flux via each pathway expressed as an additional electron flow relative to net photosynthesis (*%-LEF*) and (*ii*) their contribution to energize net photosynthesis. We used two different approaches, one based on the effect of mutations, the other based on the effect of respiratory inhibitors. As both approaches are based on pathway inhibition, they are potentially biased by the high level of redundancy existing between the different AEFs and the existence of compensatory mechanisms (Cardol *et al.*, 2009; Dang *et al.*, 2014; Burlacot *et al.*, 2022). The two approaches differ, however, in the way compensatory mechanisms likely contribute, mutants being more subject to compensation than short-terms effects of inhibitors. In the mutant-based approach, PCEF was quantified by subtracting O_2 uptake rates in the *flvB* mutant from its control parental strain (allowing the calculation of $PCEF_{mut}$ and $CMEF_{mut}$) (**Sup Fig. S10**). In the inhibitor-based approach, CMEF was quantified by subtracting O_2 uptake rates between SHAM plus Myxo treated and untreated control strains (allowing the calculation of $PCEF_{inhib}$ and $CMEF_{inhib}$) (**Sup Fig. S10**). The two methods differ somewhat in their estimates of PCEF and CMEF (**Fig. 4 A, B, Sup Fig. S11**), with a higher CMEF contribution being estimated using the mutant method. On average, PCEF and CMEF represent a flux of between 10-20*%-LEF* and 5-10*%-LEF*, respectively (**Fig. 4 A**). Thanks to the respective e^- quantum yield of each pathway, we can estimate that 10-30% and 30-60% of CO_2 fixation is sustained by PCEF and CMEF respectively (**Fig. 4 B**). Since CEF sustains the remaining net photosynthesis, we estimated that 25-30% of CO_2 fixation is powered by CEF (**Fig. 4 B**), which corresponds to a CEF of about 25*%-LEF* assuming an e^- quantum yield of CEF of 0.55 (**Fig. 4 A**).

To further assess the contribution of CEF, PCEF and CMEF over the long term, growth tests were performed on the different strains in the absence or presence of the respiration inhibitor Myxo. While Myxo has no effect on the growth of control strains and single *flvB* or *pgrl1* mutants in moderate light intensities (**Fig. 4 C**), growth of *pgrl1 flvB* was impaired in the presence of the inhibitor (**Fig. 4 C**). Interestingly, at low light intensity (30 µmol photons m^{-2} s^{-1}), the effect of Myxo on the double mutant was absent (**Sup Fig. 12 A**), suggesting that the AOX pathway of CMEF has the potential to fully power net photosynthesis in low light conditions. Therefore, whereas CEF, PCEF, and CMEF all contribute to energizing photosynthesis, CMEF, although representing a relatively small flux, has the potential to fuel CO_2 fixation and biomass accumulation thanks to its high e^- quantum yield.

Discussion

Since the first description of CEF by Arnon in 1959 (Arnon, 1959), the question was raised as to whether LEF could sustain the ATP requirement of photosynthetic CO_2 fixation (Arnon, 1959), and it was proposed that photosynthetic electron flows, other than LEF, are involved in balancing the ATP/NADPH ratio to sustain CCB cycle function

(Arnon, 1959; Allen, 2003). Since then, several mechanisms of CEF, PCEF and CMEF have been uncovered (Munekage *et al.*, 2002; Helman *et al.*, 2003; Munekage *et al.*, 2004; Tomaz *et al.*, 2010) as well as some compensations between those different mechanisms (Cardol *et al.*, 2009; Petroutsos *et al.*, 2009; Dang *et al.*, 2014; Storti *et al.*, 2019; Storti *et al.*, 2020; Burlacot *et al.*, 2022), but the importance and relative efficiency of each mechanism remain mostly unknown. Here we have shown that in *Chlamydomonas* PGRL1-controlled CEF, FLV-mediated PCEF, and both the AOX and complex III/IV/cytochrome oxidase pathways of CMEF can all supply additional energy to complement LEF for CO_2 fixation. The e^- quantum yields of CEF, PCEF and CMEF greatly differ; CMEF is the most electron efficient and contributes importantly to the extra ATP requirements of CO_2 fixation in continuous, saturating light. Note, that in spite of the ongoing controversy on how PGRL1 is involved in CEF (Nawrocki *et al.*, 2019), a clear integration is observed between PGRL1-controled CEF, PCEF and CMEF in which these different pathways can compensate each other in powering photosynthesis. Importantly, we observed similar effects on net O_2 and CO_2 exchange (**Sup Fig. S7**), thus showing that all effects measured on net photosynthesis correspond to changes in CO_2 fixation and eventually biomass production and growth (**Fig. 4 C**).

Some compensation between CEF, PCEF, and CMEF has been previously reported; a *Chlamydomonas* PGRL1-deficient strain exhibits increased CMEF and PCEF (Dang *et al.*, 2014) and mutants of complexes I and III show enhanced rates of CEF (Cardol *et al.*, 2009). We observed an elevated CMEF in the absence of FLV (**Fig. 4 A, B**) with a higher level of terminal oxidases associated with CMEF (**Sup Fig. 6**), corroborating cross-compensation among all three mechanisms of electron flow. In diatoms, while CMEF is considered to be a major driver of CO_2 fixation, inhibition of CMEF only leads to a ~20% decrease of the PSII yield (Bailleul *et al.*, 2015), which might also reflect compensation by CEF. We also conclude, based on the fact that no CO_2 fixation could be detected in the double *pgrl1 flv* mutants treated with inhibitors of mitochondrial respiration, that neither the NDA2-mediated CEF, nor O_2 reduction mediated by the plastid terminal oxidase or Mehler reactions have the potential by themselves to sustain a measurable amount of net photosynthesis, which is in agreement with previous studies concluding that these pathway represent a small fraction of alternative electron flow (Alric *et al.*, 2010; Nawrocki *et al.*, 2019) (Houille-Vernes *et al.*, 2011)(**Fig. 2 B**).

The quantitative contribution of each pathway in the wild-type strain in the absence of perturbation of any AEFs is a challenging task to which the approaches we have developed here provides an imperfect answer. Indeed, the quantification of each pathway we have proposed relies on the assumption that inhibiting one pathway (CMEF or PCEF) does not affect the flow through the others, assumption which is most likely not verified since compensation between different AEFs mechanisms have been previously documented (Cardol *et al.*, 2009; Dang *et al.*, 2014; Burlacot *et al.*, 2022). It should therefore be considered as a first attempt to evaluate the respective contributions of each pathway until an integrative quantification method is available. Here, the mutant method likely overestimates CMEF and the inhibitor method likely overestimates PCEF, both approaches likely overestimating CEF. It is clear however, that no single pathway sustains net photosynthesis by itself (**Sup Fig. S11 B**) which might reflect a rather balanced contribution of the different pathways to CO_2 fixation in the WT. In any case, it seems highly likely that, considering the high redundancy of AEFs and the ability of each of them to sustain CO_2 fixation at a high rate, a dynamic mix of the different pathways may

be involved in different environmental conditions, each pathway being more or less advantageous in specific conditions (Burlacot, 2023).

The e^- quantum yield, a new tool to evaluate the efficiency of electron transport pathways.

In support to LEF, a combination of PGRL1-controled CEF and PCEF cannot sustain more than 80% of maximal CO_2 fixation (**Fig. 3 E**) whereas each individual flux can help sustain 60% of it (**Fig. 3 F**). This suggests the existence of an intrinsic limitation of the flow of electrons through the photosynthetic electron transport chain, which is likely due to a *pmf*-induced photosynthetic control occurring at the cytochrome b_6f level (Johnson and Berry, 2021; Malone *et al.*, 2021); an elevated *pmf* eliciting a block in electron flow across the b_6f complex. Engaging an electron pathway with a high e^- quantum yield, such as CMEF, might be a way to avoid this limitation since less electrons would be needed to power the same level of CO_2 fixation. Such a strategy seems to be used by diatoms (Bailleul *et al.*, 2015) which lack FLVs and mosses, whose photosynthetic activity is impaired by inactivation of the mitochondrial respiratory complex I (Mellon *et al.*, 2021).

Throughout the green lineage, the nature and activity of alternative electron flows are quite different. For example, angiosperms lack FLV-dependent PCEF (Peltier *et al.*, 2010), harbour a NDH-1-dependent CEF pathway (Peltier *et al.*, 2016) and have a weakly active CMEF (Raghavendra and Padmasree, 2003). Since the NDH-1 dependent CEF translocates $4H^+/e^-$ (Strand *et al.*, 2017), its e^- quantum yield is close to that of CMEF, strongly suggesting that in angiosperms the NDH-1 complex can compensate when the CMEF capacity is diminished. The latter is illustrated by the poor growth of *Arabidopsis thaliana* mutants impaired in both CEF pathways (PGR and NDH-1) (Munekage *et al.*, 2004). Because of the number of key proteins and biochemical reactions involved in CMEF, its high e^- quantum yield may not be as rapidly accessible as CEF or PCEF during environmental fluctuations. While under light limiting conditions a high e^- quantum yield pathway might be advantageous, a less efficient pathway would contribute to the safe dissipation of excess absorbed light energy and diminished reactive oxygen production at saturating light intensities. Overall, it remains to be determined to what extent harbouring a palette of alternative electron flows with varying quantum yields and likely different time responses, is critical for sustaining photosynthetic performance under dynamic conditions in nature.

Note here that while modulation of the capacity of membranes to transform *pmf* into ATP may modulate the absolute e^- quantum yield of each pathway, the relative e^- quantum yield of CEF and PCEF would not change if they are embedded in the same thylakoid system. Similarly, even in conditions where the mitochondrial respiration would be partially or fully uncoupled, the e^- quantum yield of CMEF would be at least as good as PCEF due to the generation of a *pmf* across the thylakoid membranes (Burlacot, 2023). Hence, if CEF, PCEF and CMEF are all competing for the same photosynthetic electrons, electrons passing through CMEF and PCEF should always be more efficient than CEF in powering net photosynthesis. Measuring a relative positioning of the e^- quantum yield of each pathway that is different than the one described here would be an indication of spatially separated electron transport chains dedicated to specific pathways *in vivo*.

Additional energy cost of photosynthesis.

Allen previously estimated that a PCEF representing only 16%-*LEF* would be sufficient, in addition to LEF, to satisfy the ATP and NADPH requirement of the CBB cycle (Allen, 2002). Our conclusions are strikingly different since we estimate that if only PCEF was active, it would have to represent 54%-*LEF* to sustain CO_2 fixation. This discrepancy may reflect the fact that the actual metabolic cost of CO_2 fixation exceeds the ATP requirement of the CBB cycle. This may result from the involvement of additional ATP-consuming metabolic pathways or transporters, or to the presence of proton leakages from energized membranes. In addition, in natural environments, either terrestrial or aquatic, CO_2 fixation is further limited by the concentration of atmospheric CO_2, which can trigger photorespiration in C_3 plants or induction of the carbon concentration mechanisms in C_4 plants and algae. All these mechanisms would require additional energy for their activities (Osmond, 1981; Takabayashi *et al.*, 2005; Walker *et al.*, 2014; Burlacot *et al.*, 2022), making alternative electron pathways of photosynthesis even more critical for sustaining plant and algal CO_2 capture.

Acknowledgements

The authors acknowledge the constructive comments on the manuscript from Dr. Joe Berry, Dr. Jennifer Johnson, Evan Saldivar, Leron Perez and technical support from Michel Philibert and Emmanuel Capra. This work was supported by the Carnegie Institution for Science (AB, AG), and the ANR grants OTOLHYD n°ANR-18-CE05-0029 (GP) and AlgalCCM n°ANR-22-CE44-0023-01 (GP, AM). This work was also in part supported by DOE award DE-SC0019417 to AG.

Figure legend:

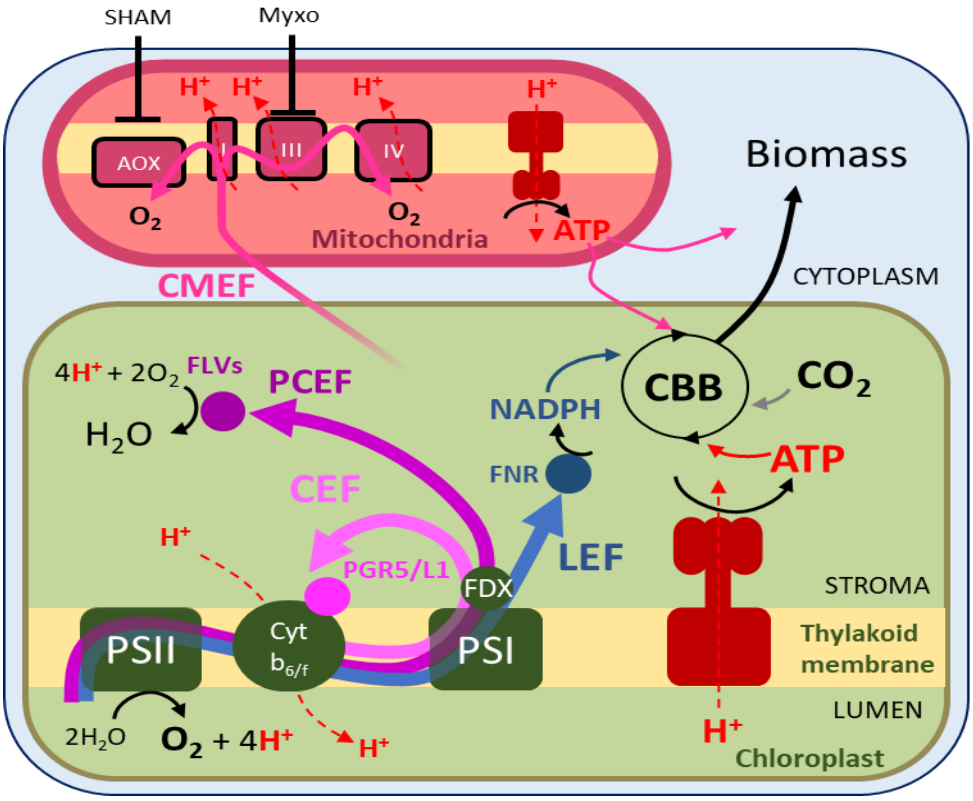

Figure 1. Electron transport pathways operating during oxygenic photosynthesis and their role in ATP generation. Linear electron flow (LEF) operates from PSII to PSI

and reduces $NADP^+$ to NADPH using electrons from water. It also generates a *pmf* across the thylakoid membrane composed of a proton gradient (ΔpH) and electrical gradient (ΔΨ); the *pmf* is used by the ATPase to generate ATP. Cyclic electron flow (CEF) and pseudo cyclic electron flow (PCEF) both contribute to the generation of the *pmf* but do not produce reducing equivalents since the e^- used for PCEF reduce O_2 to water. Chloroplast to mitochondria electron flow (CMEF) encompasses multiple metabolic pathways by which reductants generated in the chloroplast is shuttled to the mitochondria and converted into ATP by the mitochondrial electron transport chain. NADPH and ATP generated by these different pathways are eventually used for transforming CO_2 into biomass, which reflects net photosynthesis. Other abbreviations: AOX, alternative oxidase; ATP, adenosine triphosphate; CBB, Calvin Benson Bassham; FDX, ferredoxin; FLVs, flavodiiron proteins; FNR, ferredoxin-$NADP^+$ reductase; Myxo, myxothiazol; NADPH, reduced form of nicotinamide adenine dinucleotide phosphate; PS, photosystem; PGR5/L1, proton gradient generation 5/like-1; SHAM, salicyl hydroxamic acid.

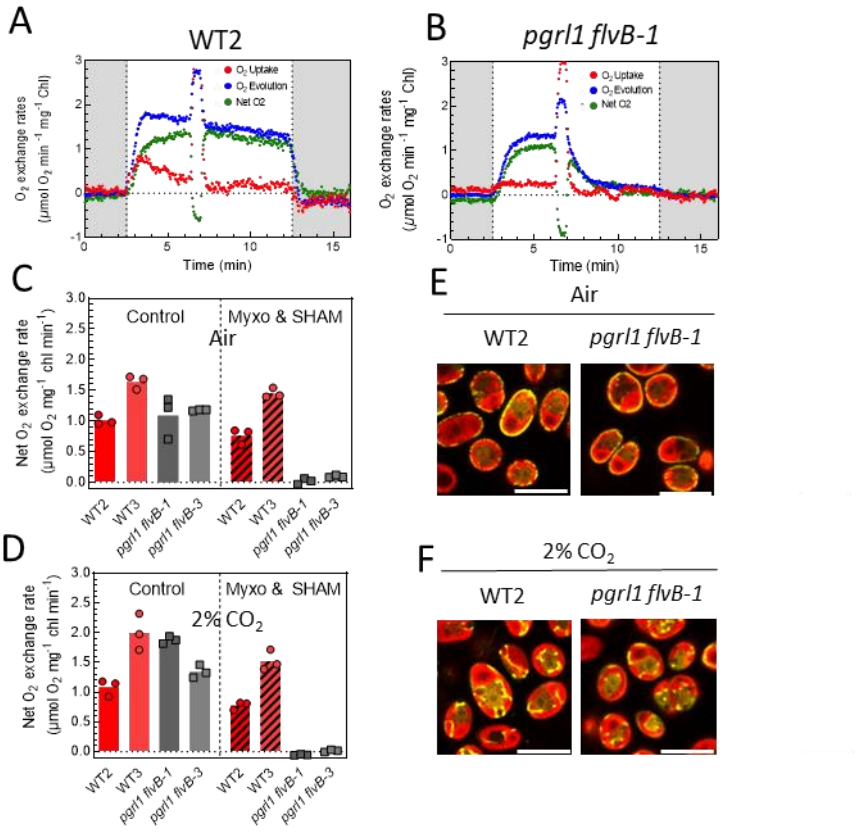

Figure 2. Dependence of net photosynthesis on CEF, PCEF and CMEF. A, B, O_2 exchange rates upon a dark to light transition in WT2 (**A**) and *pgrl1 flvB-1* (**B**). At t=6min, mitochondrial respiration inhibitors myxothiazol (2.5 μM) and salicylhydroxamic acid (SHAM, 400 μM) were added to the reaction. Shown are representative traces of $n = 3$ biologically independent samples. **C and D**, Net O_2 evolution in *pgrl1 flvB-1* and *pgrl1 flvB*-3 and their control strains (WT2 and WT3) in the absence (control) or presence (Myxo & SHAM) of myxothiazol (2.5 μM) and salicylhydroxamic acid (SHAM, 400 μM) in cells grown in air (**C**) or in 2% CO_2-enriched air (**D**). Values are taken after 9 min of illumination upon a dark to light transitions. Bars show the average and dots show individual replicates ($n = 3$ biologically independent samples). Typical experiments used to extract these data are shown in **Sup. Fig. S2**. **E** and **F**, Cross section images

showing subcellular localization of mitochondria-localized Clover (yellow fluorescence) in *pgrl1 flvB-1* and a control strain (WT2), grown in air (**E**) or 2% CO_2-enriched air (**F**). Images are representative of 2 independent experiments. Scale bar: 10 µm. Brightfield, Clover fluorescence, Chlorophyll autofluorescence and Clover/Chlorophyll merge signals are shown. Images are representative of 2 experiments. Scale bar: 10 µm.

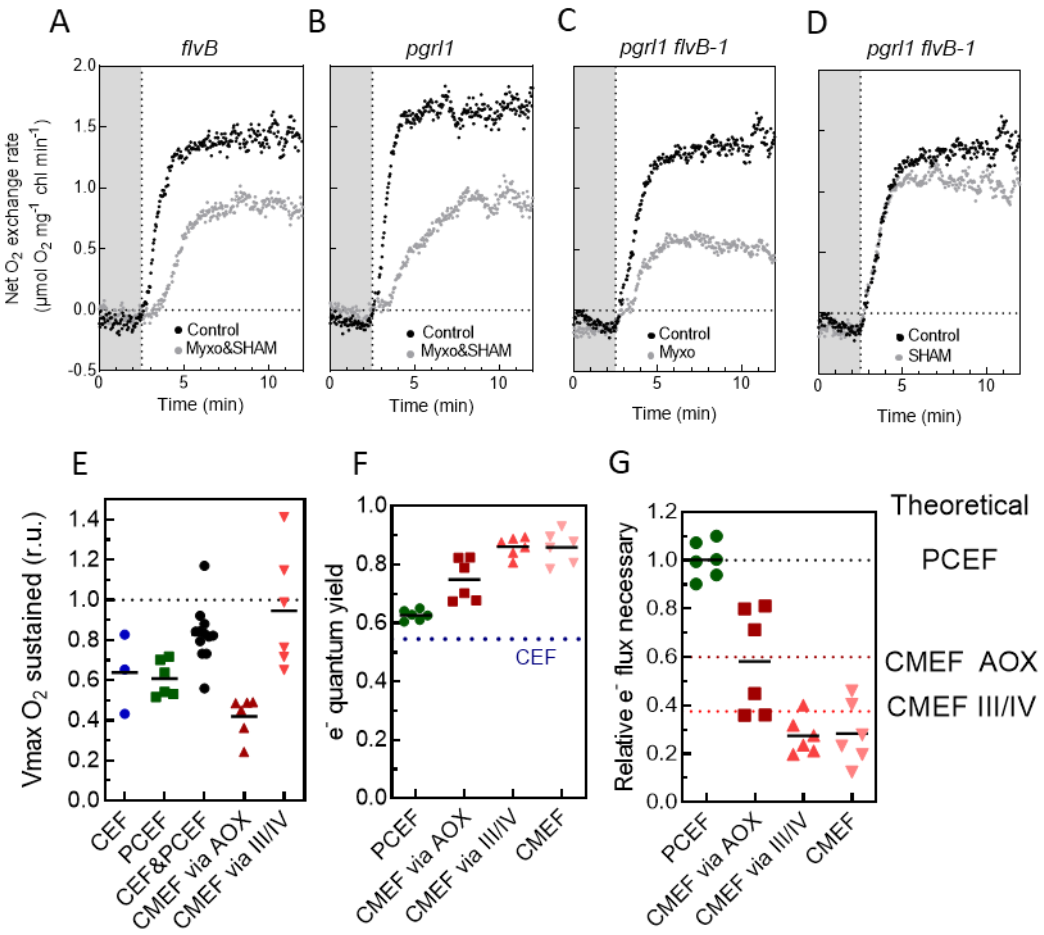

Figure 3. Relative efficiencies of CEF, PCEF and CMEF in energizing net photosynthesis. A-D, Net O_2 evolution measured during a dark to light transition in *flvB* (**A**), *pgrl1* (B), *pgrl1 flvB*-2 (**C**, **D**), treated (gray dots) or not treated (black dots) with both myxothiazol (Myxo, 2.5 μM) and salicylhydroxamic acid (SHAM, 400 μM) (**A, B**), or with only one inhibitor (**C,D**). Shown are representative traces of 3 biological replicates. **E**, Relative V_{max} measured when a given set of alternative electron pathways are active after treatment with myxothiazol (Myxo, 2.5 μM), salicylhydroxamic acid (SHAM, 400 μM) or both inhibitors; CEF (blue, *flvB* treated with Myxo and SHAM), PCEF (green, *pgrl1* treated with Myxo and SHAM), CEF&PCEF (dark, control strains treated with Myxo and SHAM), CMEF via AOX (purple, *pgrl1 flvB* treated with Myxo), CMEF via III/IV (red, *pgrl1 flvB* treated with SHAM). **F,** Electron quantum yield of PCEF (green), CMEF via AOX (purple), CMEF via III/IV (red), CMEF (pink) and CEF (dotted line). Similar electron quantum yields were also determined for PCEF in 2% CO_2-grown cells and a slightly lower quantum yield for CMEF (**Sup Fig. S9 D**). **G**, Electron flux relative to PCEF required to power similar levels of net photosynthesis when relying on a single pathway. Data shown are individual extrapolations based on measured

electron quantum yields. In **E, F** and **G,** bars show the average and dots show individual replicates ($n \geq 3$ biologically independent sample).

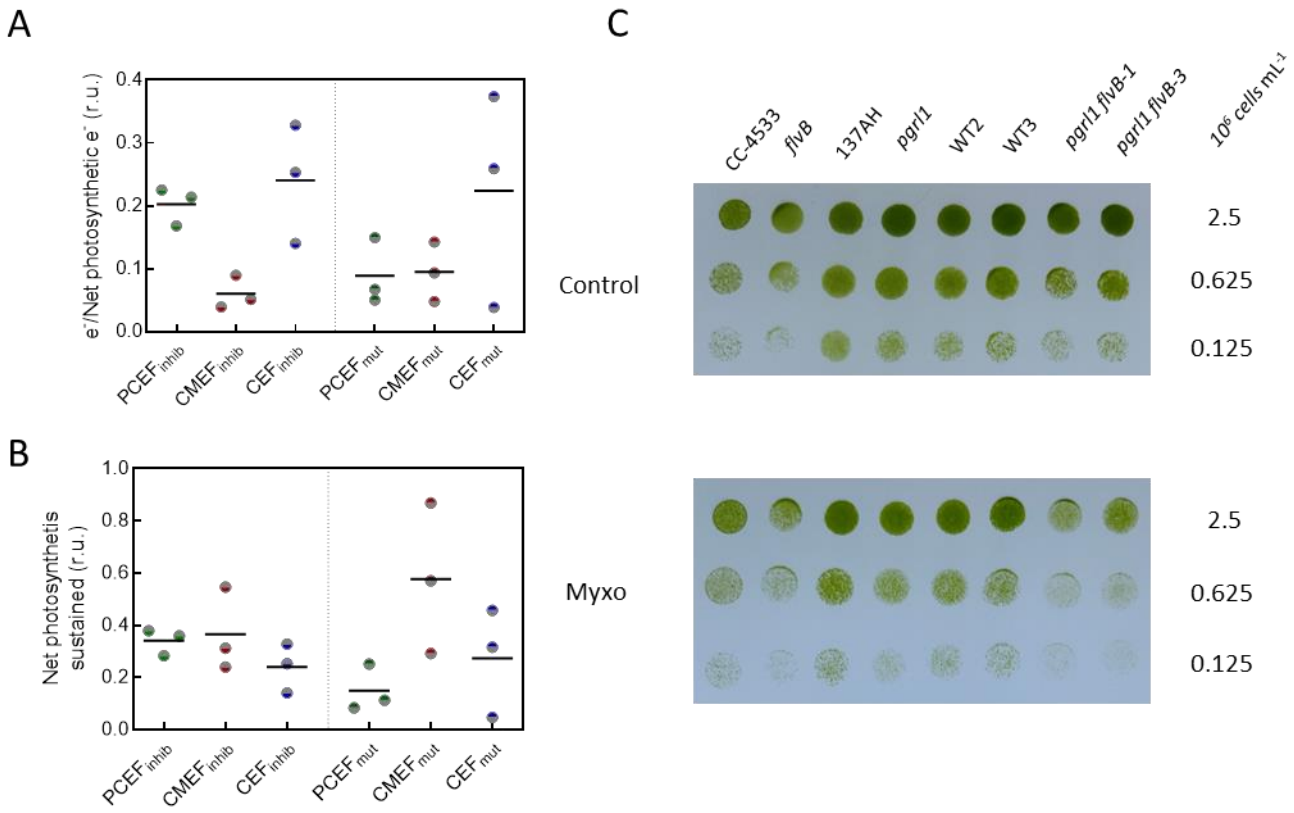

Figure 4. Contribution of CEF, PCEF and CMEF to the electron flow, net photosynthesis and growth. A Electron flow through PCEF, CEF and CMEF relative to LEF were determined in the wildtype strain CC-4533 by two different methods, one based on the use of inhibitors (inhib) the other on mutants (mut). Data used for these calculations are the same as for **Fig. 2 C** and **Sup Fig. 2**. **B** Proportion of net photosynthesis powered by each electron flow (PCEF, CEF and CMEF) in the control strain CC-4533 as measured by the inhibition (inhib) or mutant (mut) method. CC-4533 was chosen because it is the control strain for *flvB* and is therefore the only strain where both methods could be used. Data used for these calculations are the same as for **A**. In **A** and **B,** bars show the average and dots show individual replicates (n=3 biologically independent sample). **C**, Growth tests for *flvB* and *pgrl1* mutants, their corresponding control strains (CC-4533 and 137AH, respectively) and double mutants (*pgrl1 flvB-1 and pgrl1 flv-3*) and their corresponding control strains (WT2 and 3). Cells were spotted on plates containing minimal medium at pH 7.2 and grown under continuous illumination (60 µmol photon m^{-2} s^{-1}) in the absence (upper panel) or presence (lower panel) of 2.5µM Myxothiazol (Myxo) in air enriched at 2% CO_2. Spots shown are representative of 10 independent experiments.

Material and Methods

Strains and growing conditions. *Chlamydomonas flvB* and *pgrl1* single mutants and their respective parental strains CC-4533 (for *flvB*), 137AH (for *pgrl1*) where previously described (Tolleter *et al.*, 2011; Chaux *et al.*, 2017). *flvB pgrl1*-1, -2 and -3 double mutant and their respective sibling strains WT2 and WT3 (used here as control strains) have been described previously (Burlacot *et al.*, 2022) and are all from the progeny of a crossing of *flvB* and *pgrl1* performed in (Burlacot *et al.*, 2022). Because *pgrl1 flvB* double mutants were obtained by crossing the two single mutants which have different genetic backgrounds (as described in (Burlacot *et al.*, 2022)), the control strains used are siblings that resulted from the cross and that contained wild-type copies and levels of the FLVB and PGRL1 proteins. *pgrl1-2* is a mutant impaired in accumulation of the PGRL1 protein originating from crossing *flvB* and *pgrl1* performed in (Burlacot *et al.*, 2022). All strains were grown photo-autotrophically in 125-mL flasks with cotton stoppers at 25 °C in a buffered minimal medium (20 mM MOPS pH 7.2) under constant illumination (80 µmol photons m^{-2} s^{-1}) either under ambient CO_2 or 2% CO_2 in air. Amongst *pgrl1 flvB* double mutants and their control strains already described (Burlacot *et al.*, 2022), *pgrl1 flvB*-1 and *pgrl1 flvB*-3 and WT2 and 3, respectively, were used for physiological measurements since their maximal photosynthesis was representative of other double mutants and control strains (Burlacot *et al.*, 2022). All strains used in this study are available under the same names used here (except for *flvB* which is available as *flvB-21*) at the Chlamydomonas Resource Center (www.chlamycollection.org). Spectrum of the growing light used are shown in **Sup Fig. 13**.

Gas exchange measurements. Gas exchange rates were measured using membrane inlet mass spectrometry (MIMS). Cells grown in air enriched or not at 2% CO_2 were collected during the exponential phase by centrifugation at 450 g for 3 min and resuspended in 1.5 mL of fresh buffered minimal medium (pH 7.2) at 30 µg chlorophyll mL^{-1}. HCO_3^- was subsequently added to the cell suspension (10 mM final concentration). The cell suspension was then placed in the MIMS reaction vessel, 2 mL of ^{18}O-enriched O_2 (97% ^{18}O Eurisop, France) were bubbled in the suspension. After closing the vessel, gas exchange was recorded during a dark to light transition (2,000 µmol photons m^{-2} s^{-1}; green LEDs picked at 525nm; Luminus reference PT-121-G-L11-MPK). Light intensity was set to be saturating (**Sup Fig. 14**) using weakly absorbed green light for better homogeneity. Calculations of gross and net photosynthesis were done using the MIMS analysis software as previously described (Burlacot *et al.*, 2020). In some experiments salicyl hydroxamic acid (SHAM, 400 µM final concentration) and/or myxothizol (Myxo, 2.5 µM final concentration) were added 1 min before the beginning of the measurements, except for the data presented in **Fig. 2A**, **B** where inhibitors were added during the measurement. Note here that SHAM has been reported to not inhibit the plastid terminal oxidase (Cournac *et al.*, 2000). All Net O_2, Net CO_2, e^- quantum yield, e^- flow and Net photosynthesis sustained shown as histograms in **Figs. 2, 3, 4** and **Sup. Figs. 1, 7, 9, 11** are based on measurements after 9 minutes of illumination.

Clover expressing cells. 137AH, WT2, *pgrl1*, *flvB*, *pgrl1flvB*-1 and -2 expressing the mitochondria targeted fluorophore Clover (mito-Clover) were generated as described in (Harmon *et al.*, 2022). Briefly, cells were transformed with a linearized plasmid encoding mito-Clover and a hygromycin-resistance cassette using the Max Efficiency Reagent (Invitrogen). Resistant clones to hygromycin were screened for Clover fluorescence using a M1000 Tecan plate reader (Excitation: 488/7 nm; Emission: 515/10 nm) and mitochondrial signal was checked by confocal microscopy. Selected clones were grown

at 80 µmol photons m^{-2} s^{-1} in 25 mL minimal medium in 125 mL flasks, in the presence of either normal or 2% CO_2-enriched air until they reached a density of ~10 µg chlorophyll mL^{-1}. An aliquot of each culture was then briefly concentrated by centrifugation at 1,500g and cells layered on a 18-well microscope slide. Images were acquired using a TCS SP8 confocal laser-scanning microscope (Leica) and a ×63 objective. Acquisition settings were as follows: Clover excitation 488 nm, emission 500-547 nm; Chlorophyll excitation 488 nm, emission 694-733 nm. For homogeneity and clarity, signal intensities of each channel were adjusted using the Fiji software.

Growth tests. The different *Chlamydomonas* strains were cultivated at air level of CO_2 under moderate light (80 µmol photons m^{-2} s^{-1}) at 25 °C. Cells were collected during exponential growth and diluted in fresh minimal medium to 0.125, 0.625 or 2.5 10^6 cells mL^{-1}. Seven-microlitre drops were spotted on 2% Agar plates of minimal medium (buffered with 20mM MOPS pH 7.2) with or without myxothiazol (2.5µM final concentration) and exposed to air enriched with 2% CO_2. Homogeneous light was supplied by LED panels (see its spectrum in **Sup Fig. 13 B**), the different light intensities were obtained with various neutral filters. Temperature was maintained at 25 °C at the level of plates by means of fans.

Electron quantum yield calculation. The e^- quantum yield of a given alternative electron pathway is defined as the proportion of electrons generated downstream PSI that are used for net photosynthesis when only this alternative electron pathway is active, following this equation:

$$(1)\ e^- quantum\ yield = \frac{e^-(net\ photosynthesis)}{e^-(net\ photosynthesis)+e^-(alternative\ pathway)}$$

Where e^-(net photosynthesis) is the flux of photosynthetic electrons directly used as reductants for net photosynthesis and e^-(alternative pathway) is the flux of photosynthetic electrons through an alternative pathway. Because for PCEF and CMEF the sum of e^- (alternative pathway) and e^-(net photosynthesis) equals gross photosynthesis, electron quantum yields of PCEF and CMEF were quantified using gross and net O_2 evolution in mutants harbouring: only PCEF (*pgrl1* and *pgrl1-2* mutants treated with Myxo and SHAM), or only the AOX or the complex III/IV pathway of CMEF (*pgrl1 flvB*-1 and 3 mutants treated with Myxo or SHAM, respectively). The electron quantum yield was then calculated for each pathway using the following equation:

$$(2)\ e^- quantum\ yield = \frac{net\ O_2 evolution}{gross\ O_2 evolution}$$

The theoretical electron quantum yield of CEF was calculated based on the assumption that CEF translocates 1.5 less protons per electron across the thylakoid membranes than PCEF (Kramer and Evans, 2011; Burlacot, 2023) and that this is the driving force leading to net photosynthesis energization. Note that this later assumption is well supported by the independent results from **Fig. 3 G** showing that the relative electron quantum yield of CMEF pathways and PCEF corresponds to their relative capacity at translocating protons across membranes. Hence, for the same net photosynthesis powered, CEF should be 1.5 times higher than PCEF, and the electron quantum yields of CEF could be written as:

$$(3)\qquad e^- quantum\ yield\ (CEF) = \frac{e^-(net\ in\ pgrl1\ Myxo\ SHAM)}{e^-(net\ in\ pgrl1\ Myxo\ SHAM)+e^-(PCEF)\times 1.5}$$

Where e^-(net in *pgrl1* Myxo SHAM) is the net photosynthesis measured in the *pgrl1* mutant treated with Myxo and SHAM (hence having only PCEF active) and e^- (PCEF) being the O_2 uptake rate in the same strain and condition.

Based on equation (1), we can rewrite e^-(PCEF) as:

$$(4) \qquad e^-(PCEF) = \frac{(1-e^-quantum\ yield(PCEF))}{e^-quantum\ yield(PCEF)} \times\ e^-(net\ in\ pgrl1\ Myxo\ SHAM)$$

Hence, combining (3) and (4):

$$(5) \qquad e^-quantum\ yield\ (CEF) = \frac{e^-quantum\ yield\ (PCEF)}{1.5-\frac{e^-quantum\ yield\ (PCEF)}{2}}$$

The electron quantum yield of CEF shown in **Fig. 3** is using equation (5) with the average electron quantum yield of PCEF. Note that the quantifications of the e^- quantum yield in *Chlamydomonas* assumes that removing two pathways (elimination of CEF and CMEF in the *pgrl1* mutant treated with inhibitors of respiration, and CEF and PCEF in the *pgrl1 flvB* double mutants) makes CO_2 fixation dependent only on the third pathway. This dependency is supported by the finding that the *pgrl1 flvB* double mutant treated with inhibitors of respiration are unable to support any CO_2 fixation, which also support the hypothesis that the contribution of other pathways, such as the NDA2-dependent CEF, is marginal.

Calculation of electron flows via each pathway and their contribution to net photosynthesis in wildtype strains. The electron flow through PCEF and CMEF were deduced on wildtype strain using two independent methods based on measurements of gross O_2 uptake made in **Sup. Fig. 2 and 3**. In the so called "mutant" method, CMEF was quantified as being the gross O_2 uptake measured in the *flvB* mutant. Then, PCEF was quantified by subtracting the CMEF to the O_2 uptake of CC-4533 (**Sup. Fig. S10**). This method was only used for CC-4533 since it is the only control strain for the *flvB* mutant. In the so called "inhibitor" method, PCEF was quantified as being the gross O_2 uptake remaining in control strains treated with SHAM and Myxo. Then, CMEF was quantified by subtracting the PCEF to the O_2 uptake in the same untreated control strain (**Sup. Fig. S10**). The calculated electron flows of PCEF and CMEF were then used for each strain to quantify the net photosynthesis powered by each of them following the equations derived from (1):

$$net\ photoynthesis\ (AEF) = e^-(AEF) \times \frac{e^-quantum\ yield\ (AEF)}{1 - e^-quantum\ yield\ (AEF)}$$

Where net photosynthesis (AEF) is the net photosynthesis sustained by a specific alternative electron flow, e^-(AEF) being the electron flow through this AEF and e^- quantum yield (AEF) being the electron quantum yield of this alternative electron flow.

The total of net photosynthesis powered in a strain by PCEF and CMEF was then compared to the measured net photosynthesis in this same strain to quantify the "missing"

net photosynthesis that had to be powered by CEF. Then the electron flow through CEF (e^-(CEF)) was calculated by the following equation derived from (1):

$$e^-(CEF) = missing\ net\ \times \frac{1 - e^- quantum\ yield\ (CEF)}{e^- quantum\ yield\ (CEF)}$$

Where "missing net" is the calculated net photosynthesis that is not powered by PCEF and CMEF and e^- quantum yield (CEF) being the electron quantum yield of CEF.

Protein extraction and Immunodetection. Cells were harvested by centrifugation at 1,000g for 5 minutes. Total cellular protein was extracted by heating the cell pellet at 100°C for one minute using an extraction aqueous solution composed of 1% SDS, 100 mM DTT, 1mM Aminocaproic acid, and 1mM benzamidine hydrochloride buffered with 60mM Tris (pH 6.8). The resulting cell lysate was then centrifuged at 10,000 g for 5 minutes to obtain the supernatant. The supernatant was subsequently incubated with acetone (80% final concentration) at -20°C for 1 hour. The protein pellet was collected by centrifugation at 5,000 g for 5 minutes and stored in aqueous solution containing 1% SDS, 5 mM DTT and buffered with 60mM Tris (pH 6.8). Protein content was estimated (Microplate BCA protein assay Kit-reducing agent compatible, Thermo Scientific) with bovine serum albumin as the standard. Protein extracts (10 µg protein) were loaded on a 12% SDS-PAGE gel and run for 1h at 150V in Tris-glycine SDS buffer and transferred onto a nitrocellulose membrane using semi-dry transfer (Transblot turbo, Biorad). Immunoblot detection was performed using antibodies raised against FlvB (1:1,000)(Chaux *et al.*, 2017), and Pgrl1 (1:5,000)(Tolleter *et al.*, 2011). Other antibodies against AOX1 (1:10,000) (AS06 152), COXIIB (1:10,000) (AS06 151) were obtained from Agrisera (https://www.agrisera.com/). An anti-rabbit HRP-conjugated antibody (1:50,000) (AS09 602) was used as a secondary antibody for immunodetection. Precision Plus Protein Dual Color Standards (Biorad) was used as the molecular weight marker. Uncropped and unprocessed scans of the blots shown in this study are visible in source data.

Data Availability. Genes studied in this article can be found on https://phytozome-next.jgi.doe.gov/ under the loci Cre12.g531900 (FLVA), Cre16.g691800 (FLVB), Cre07.g340200 (PGRL1), Cre09.g395950 (AOX1), Cre03.g169550 (AOX2) and Cre01.g049500 (COXIIB).

References:

Alboresi A, Storti M, Morosinotto T (2019) Balancing protection and efficiency in the regulation of photosynthetic electron transport across plant evolution. New Phytol. **221:** 105-109 10.1111/nph.15372

Allahverdiyeva Y, Mustila H, Ermakova M, Bersanini L, Richaud P, Ajlani G, Battchikova N, Cournac L, Aro EM (2013) Flavodiiron proteins Flv1 and Flv3 enable cyanobacterial growth and photosynthesis under fluctuating light. Proc. Natl. Acad. Sci. U.S.A. **110:** 4111-4116 10.1073/pnas.1221194110

Allen JF (2002) Photosynthesis of ATP—Electrons, Proton Pumps, Rotors, and Poise. Cell **110:** 273-276 https://doi.org/10.1016/S0092-8674(02)00870-X

Allen JF (2003) Cyclic, pseudocyclic and noncyclic photophosphorylation: new links in the chain. Trends Plant Sci. **8:** 15-19 10.1016/s1360-1385(02)00006-7

Alric J, Johnson X (2017) Alternative electron transport pathways in photosynthesis: a confluence of regulation. Curr. Op. Plant. Biol. **37:** 78-86 https://doi.org/10.1016/j.pbi.2017.03.014

Alric J, Lavergne J, Rappaport F (2010) Redox and ATP control of photosynthetic cyclic electron flow in *Chlamydomonas reinhardtii* (I) aerobic conditions. Biochim. Biophys. Acta **1797:** 44-51

Arnon DI (1959) Conversion of light into chemical energy in photosynthesis. Nature **184:** 10-21 10.1038/184010a0

Arnon DI (1984) The discovery of photosynthetic phosphorylation. Trends Plant Sci **9:** 258-262 https://doi.org/10.1016/0968-0004(84)90159-2

Bailleul B, Berne N, Murik O, Petroutsos D, Prihoda J, Tanaka A, Villanova V, Bligny R, Flori S, Falconet D, Krieger-Liszkay A, Santabarbara S, Rappaport F, Joliot P, Tirichine L, Falkowski PG, Cardol P, Bowler C, Finazzi G (2015) Energetic coupling between plastids and mitochondria drives CO_2 assimilation in diatoms. Nature **524:** 366 10.1038/nature14599

Burlacot A (2023) Quantifying the roles of algal photosynthetic electron pathways: a milestone towards photosynthetic robustness. New Phytol. **n/a**https://doi.org/10.1111/nph.19328

Burlacot A, Burlacot F, Li-Beisson Y, Peltier G (2020) Membrane Inlet Mass Spectrometry: A Powerful Tool for Algal Research. Front. Plant. Sci. **11**10.3389/fpls.2020.01302

Burlacot A, Dao O, Auroy P, Cuiné S, Li-Beisson Y, Peltier G (2022) Alternative photosynthesis pathways drive the algal CO_2 concentrating mechanism. Nature https://doi.org/10.1038/s41586-022-04662-9

Burlacot A, Peltier G (2023) Energy crosstalk between photosynthesis and the algal CCM. Trends Plant Sci. https://doi.org/10.1016/j.tplants.2023.03.018

Cardol P, Alric J, Girard-Bascou J, Franck F, Wollman FA, Finazzi G (2009) Impaired respiration discloses the physiological significance of state transitions in *Chlamydomonas*. **106:** 15979-15984 10.1073/pnas.0908111106

Cardol P, Gloire G, Havaux M, Remacle C, Matagne R, Franck F (2003) Photosynthesis and state transitions in mitochondrial mutants of *Chlamydomonas reinhardtii* affected in respiration. Plant Physiol. **133:** 2010-2020 10.1104/pp.103.028076

Chaux F, Burlacot A, Mekhalfi M, Auroy P, Blangy S, Richaud P, Peltier G (2017) Flavodiiron proteins promote fast and transient O_2 photoreduction in Chlamydomonas. Plant Physiol. **174:** 1825-1836 10.1104/pp.17.00421

Cournac L, Latouche G, Cerovic Z, Redding K, Ravenel J, Peltier G (2002) *In vivo* interactions between photosynthesis, mitorespiration, and chlororespiration in *Chlamydomonas reinhardtii*. Plant Physiol. **129:** 1921-1928 10.1104/pp.001636

Cournac L, Redding K, Ravenel J, Rumeau D, Josse E-M, Kuntz M, Peltier G (2000) Electron flow between photosystem II and oxygen in chloroplasts of photosystem I-deficient algae is mediated by a quinol oxidase involved in chlororespiration. **275:** 17256-17262

DalCorso G, Pesaresi P, Masiero S, Aseeva E, Nemann DS, Finazzi G, Joliot P, Barbato R, Leister D (2008) A complex containing PGRL1 and PGR5 is involved in the switch between linear and cyclic electron flow in *Arabidopsis*. Cell **132:** 273-285 10.1016/j.cell.2007.12.028

Dang KV, Plet J, Tolleter D, Jokel M, Cuine S, Carrier P, Auroy P, Richaud P, Johnson X, Alric J, Allahverdiyeva Y, Peltier G (2014) Combined increases in mitochondrial cooperation and oxygen photoreduction compensate for deficiency

in cyclic electron flow in *Chlamydomonas reinhardtii*. Plant Cell **26:** 3036-3050 10.1105/tpc.114.126375

Desplats C, Mus F, Cuine S, Billon E, Cournac L, Peltier G (2009) Characterization of Nda2, a plastoquinone-reducing type II NAD(P)H dehydrogenase in *Chlamydomonas* chloroplasts. J. Biol. Chem. **284:** 4148-4157 10.1074/jbc.M804546200

Geraghty AM, Spalding MH (1996) Molecular and structural changes in *Chlamydomonas* under limiting CO_2 (a possible mitochondrial role in adaptation). **111:** 1339-1347 10.1104/pp.111.4.1339

Gerotto C, Alboresi A, Meneghesso A, Jokel M, Suorsa M, Aro E-M, Morosinotto T (2016) Flavodiiron proteins act as safety valve for electrons in Physcomitrella patens. Proc. Nat. Acad. Sci. U.S.A. **113:** 12322-12327 10.1073/pnas.1606685113

Harmon J, Findinier J, Ishii NT, Herbig M, Isozaki A, Grossman A, Goda K (2022) Intelligent image-activated sorting of *Chlamydomonas reinhardtii* by mitochondrial localization. Cytometry Part A **101:** 1027-1034 https://doi.org/10.1002/cyto.a.24661

Helman Y, Tchernov D, Reinhold L, Shibata M, Ogawa T, Schwarz R, Ohad I, Kaplan A (2003) Genes encoding a-type flavoproteins are essential for photoreduction of O_2 in cyanobacteria. Curr. Biol. **13:** 230-235

Houille-Vernes L, Rappaport F, Wollman F-A, Alric J, Johnson X (2011) Plastid terminal oxidase 2 (PTOX2) is the major oxidase involved in chlororespiration in *Chlamydomonas*. Proc. Nat. Acad. Sci. U. S. A. **108:** 20820-20825 10.1073/pnas.1110518109

Ilík P, Pavlovič A, Kouřil R, Alboresi A, Morosinotto T, Allahverdiyeva Y, Aro E-M, Yamamoto H, Shikanai T (2017) Alternative electron transport mediated by flavodiiron proteins is operational in organisms from cyanobacteria up to gymnosperms. New Phytol. **214:** 967-972 10.1111/nph.14536

IPCC (2021) Climate Change 2021: The Physical Science Basis. Contribution of Working Group I to the Sixth Assessment Report of the Intergovernmental Panel on Climate Change Cambridge University Press, Cambridge, United Kingdom and New York, NY, USA

Jans F, Mignolet E, Houyoux PA, Cardol P, Ghysels B, Cuine S, Cournac L, Peltier G, Remacle C, Franck F (2008) A type II NAD(P) H dehydrogenase mediates light-independent plastoquinone reduction in the chloroplast of *Chlamydomonas*. Proc. Natl. Acad. Sci. U.S.A. **105:** 20546-20551 10.1073/pnas.0806896105

Joët T, Cournac L, Horvath EM, Medgyesy P, Peltier G (2001) Increased sensitivity of photosynthesis to antimycin A induced by inactivation of the chloroplast ndhB gene. evidence for a participation of the NADH-dehydrogenase complex to cyclic electron flow around photosystem I. Plant Physiol. **125:** 1919-1929 10.1104/pp.125.4.1919

Johnson JE, Berry JA (2021) The role of Cytochrome b6f in the control of steady-state photosynthesis: a conceptual and quantitative model. Phot. Res. **148:** 101-136 10.1007/s11120-021-00840-4

Johnson X, Alric J (2013) Central carbon metabolism and electron transport in *Chlamydomonas reinhardtii*: metabolic constraints for carbon partitioning between oil and starch. Eukaryotic Cell **12:** 776-793 10.1128/ec.00318-12

Johnson X, Steinbeck J, Dent RM, Takahashi H, Richaud P, Ozawa SI, Houille-Vernes L, Petroutsos D, Rappaport F, Grossman AR, Niyogi KK, Hippler M, Alric J (2014) Proton Gradient Regulation 5-mediated cyclic electron flow under

ATP- or redox-limited conditions: A study of Δ*ATPase pgr5* and *ΔrbcL pgr5* mutants in the green alga *Chlamydomonas reinhardtii*. Plant Physiol. **165:** 438-452 10.1104/pp.113.233593

Kaye Y, Huang W, Clowez S, Saroussi S, Idoine A, Sanz-Luque E, Grossman AR (2019) The mitochondrial alternative oxidase from *Chlamydomonas reinhardtii* enables survival in high light. J. Biol. Chem. **294:** 1380-1395 10.1074/jbc.RA118.004667

Kramer DM, Evans JR (2011) The importance of energy balance in improving photosynthetic productivity. Plant Physiol. **155:** 70-78 10.1104/pp.110.166652

Lemaire C, Wollman FA, Bennoun P (1988) Restoration of phototrophic growth in a mutant of *Chlamydomonas reinhardtii* in which the chloroplast *atpB* gene of the ATP synthase has a deletion: an example of mitochondria-dependent photosynthesis. Proc. Natl. Acad. Sci. USA **85:** 1344-1348

Malone LA, Proctor MS, Hitchcock A, Hunter CN, Johnson MP (2021) Cytochrome b6f – Orchestrator of photosynthetic electron transfer. Biochim. Biophys. Acta **1862:** 148380 https://doi.org/10.1016/j.bbabio.2021.148380

Mellon M, Storti M, Vera-Vives AM, Kramer DM, Alboresi A, Morosinotto T (2021) Inactivation of mitochondrial complex I stimulates chloroplast ATPase in Physcomitrium patens. Plant Physiol. **187:** 931-946 10.1093/plphys/kiab276

Munekage Y, Hashimoto M, Miyake C, Tomizawa K-I, Endo T, Tasaka M, Shikanai T (2004) Cyclic electron flow around photosystem I is essential for photosynthesis. Nature **429:** 579-582 10.1038/nature02598

Munekage Y, Hojo M, Meurer J, Endo T, Tasaka M, Shikanai T (2002) PGR5 is involved in cyclic electron flow around photosystem I and is essential for photoprotection in *Arabidopsis*. Cell **110:** 361-371 https://doi.org/10.1016/S0092-8674(02)00867-X

Nawrocki WJ, Bailleul B, Picot D, Cardol P, Rappaport F, Wollman FA, Joliot P (2019) The mechanism of cyclic electron flow. Biochim. Biophys. Acta Bioenerg. **1860:** 433-438 https://doi.org/10.1016/j.bbabio.2018.12.005

Osmond CB (1981) Photorespiration and photoinhibition: Some implications for the energetics of photosynthesis. Biochim. Biophys. Acta **639:** 77-98 https://doi.org/10.1016/0304-4173(81)90006-9

Peltier G, Aro EM, Shikanai T (2016) NDH-1 and NDH-2 plastoquinone reductases in oxygenic photosynthesis. Ann. Rev. Plant Biol. **67:** 55-80 10.1146/annurev-arplant-043014-114752

Peltier G, Schmidt GW (1991) Chlororespiration - an adaptation to nitrogen deficiency in *Chlamydomonas reinhardtii*. Proc. Natl. Acad. Sci. USA **88:** 4791-4795 10.1073/pnas.88.11.4791

Peltier G, Tolleter D, Billon E, Cournac L (2010) Auxiliary electron transport pathways in chloroplasts of microalgae. Photosynth. Res. **106:** 19-31

Petroutsos D, Terauchi AM, Busch A, Hirschmann I, Merchant SS, Finazzi G, Hippler M (2009) PGRL1 participates in iron-induced remodeling of the photosynthetic apparatus and in energy metabolism in *Chlamydomonas reinhardtii*. J. Biol. Chem. **284:** 32770-32781 10.1074/jbc.M109.050468

Raghavendra AS, Padmasree K (2003) Beneficial interactions of mitochondrial metabolism with photosynthetic carbon assimilation. Trends Plant Sci. **8:** 546-553 https://doi.org/10.1016/j.tplants.2003.09.015

Saroussi SI, Wittkopp TM, Grossman AR (2016) The Type II NADPH dehydrogenase facilitates cyclic electron flow, energy-dependent quenching, and

chlororespiratory metabolism during acclimation of *Chlamydomonas reinhardtii* to nitrogen deprivation Plant Physiol. **170:** 1975-1988 10.1104/pp.15.02014

Shimakawa G, Ishizaki K, Tsukamoto S, Tanaka M, Sejima T, Miyake C (2017) The Liverwort, Marchantia, drives alternative electron flow using a flavodiiron protein to protect PSI. Plant Physiol. **173:** 1636-1647 10.1104/pp.16.01038

Storti M, Alboresi A, Gerotto C, Aro E-M, Finazzi G, Morosinotto T (2019) Role of cyclic and pseudo-cyclic electron transport in response to dynamic light changes in *Physcomitrella patens*. Plant Cell Environ. **42:** 1590-1602 10.1111/pce.13493

Storti M, Segalla A, Mellon M, Alboresi A, Morosinotto T (2020) Regulation of electron transport is essential for photosystem I stability and plant growth. New Phytol. **228:** 1316-1326 https://doi.org/10.1111/nph.16643

Strand DD, Fisher N, Kramer DM (2017) The higher plant plastid NAD(P)H dehydrogenase-like complex (NDH) is a high efficiency proton pump that increases ATP production by cyclic electron flow. J. Biol. Chem. **292:** 11850-11860 10.1074/jbc.M116.770792

Takabayashi A, Kishine M, Asada K, Endo T, Sato F (2005) Differential use of two cyclic electron flows around photosystem I for driving CO_2-concentration mechanism in C4 photosynthesis. Proc. Natl. Acad. Sci. USA **102:** 16898-16903 10.1073/pnas.0507095102

Tolleter D, Ghysels B, Alric J, Petroutsos D, Tolstygina I, Krawietz D, Happe T, Auroy P, Adriano JM, Beyly A, Cuine S, Plet J, Reiter IM, Genty B, Cournac L, Hippler M, Peltier G (2011) Control of hydrogen photoproduction by the proton gradient generated by cyclic electron flow in *Chlamydomonas reinhardtii*. Plant Cell **23:** 2619-2630 10.1105/tpc.111.086876

Tomaz T, Bagard M, Pracharoenwattana I, Lindén P, Lee CP, Carroll AJ, Ströher E, Smith SM, Gardeström P, Millar AH (2010) Mitochondrial malate dehydrogenase lowers leaf respiration and alters photorespiration and plant growth in *Arabidopsis*. Plant Physiol. **154:** 1143-1157 10.1104/pp.110.161612

Walker BJ, Strand DD, Kramer DM, Cousins AB (2014) The response of cyclic electron flow around photosystem I to changes in photorespiration and nitrate assimilation Plant Physiol. **165:** 453-462 10.1104/pp.114.238238

Supplemental figures

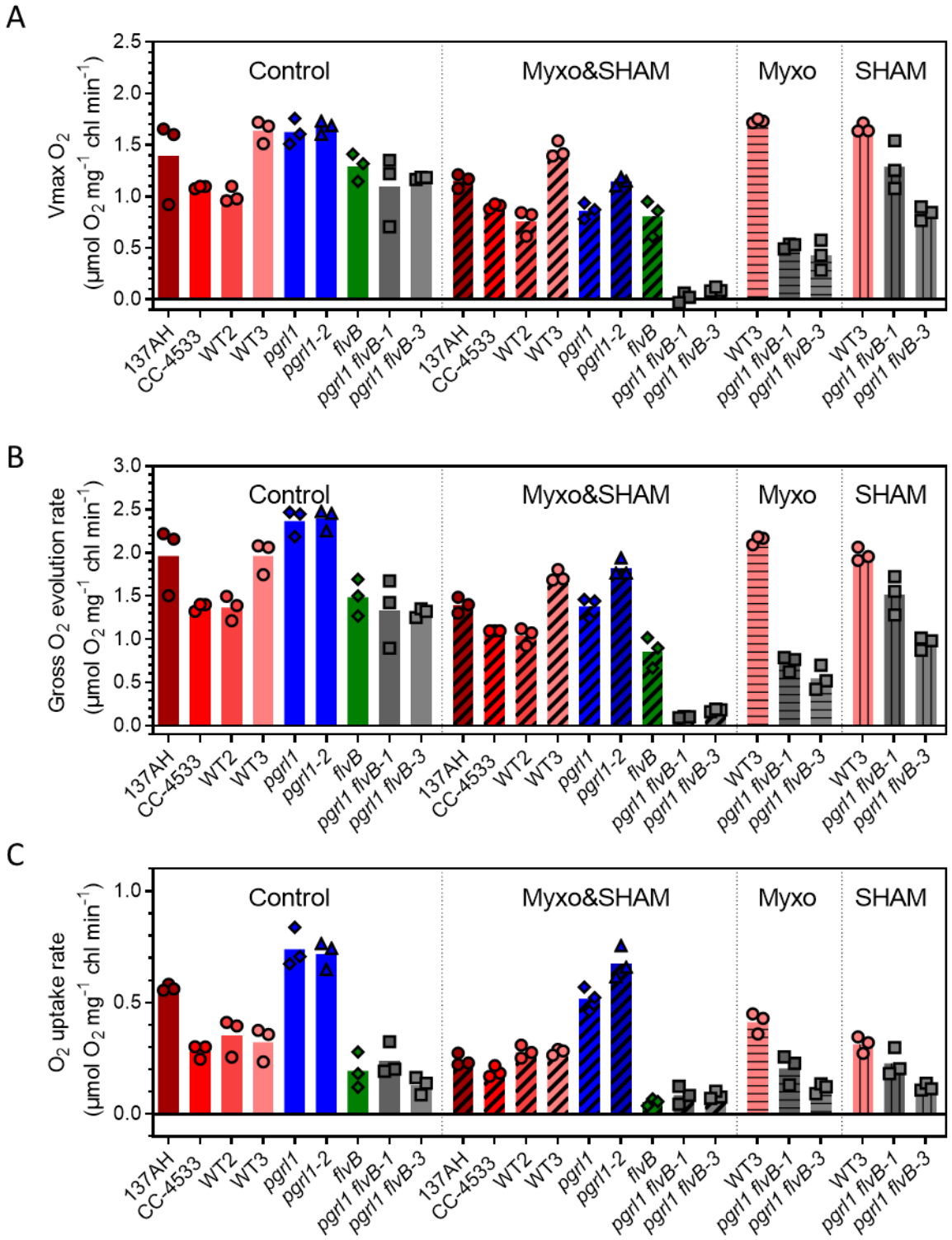

Supplemental Figure S1. Effect of mitochondrial inhibitors on O2 exchange rates on mutants and control strains grown at air level of CO2. O2 exchange rates are measured from same experiments used in Fig. 2 A-C, Sup Figs. S2, S3, S9, S11 and S12. Maximal net O2 production (Vmax O2) (A), gross O2 evolution (B) and gross O2 uptake (C) was measured on cells treated with myxothiazol (Myxo, 2.5 µM), salicylhydroxamic acid

(SHAM, 400 µM), both Myxo and SHAM (Myxo&SHAM) or untreated (Control). Shown are the values measured after 9 minutes of illumination to reach steady state photosynthesis. Bars show the mean and dots show individual replicates (n = 3 biologically independent samples).

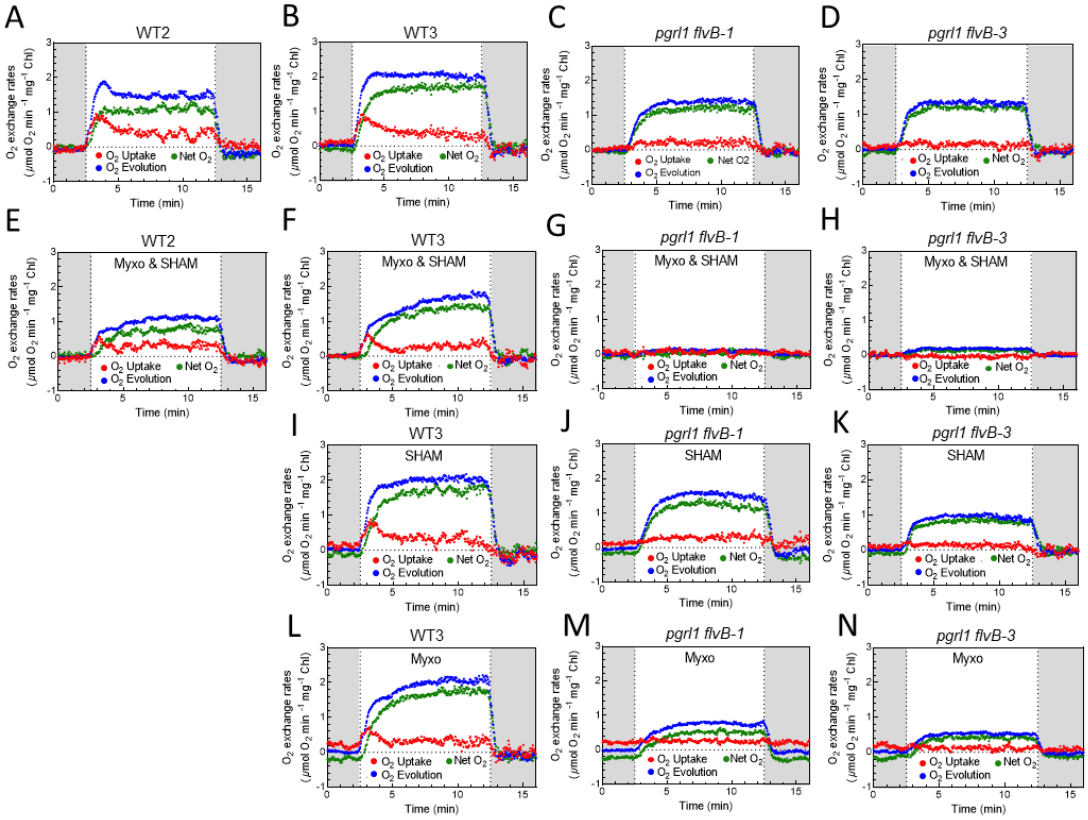

Supplemental Figure S2. O_2 exchange rated in *pgrl1 flvB* double mutants and their control strains grown at air level of CO_2. A-N Gross and net O_2 exchange rates upon a dark (grayed areas)-light-dark transition on cells treated with myxothiazol (Myxo, 2.5 μM) (**L**, **M**, **N**) , salicylhydroxamic acid (SHAM, 400 μM) (**I**, **J**, **K**) , both Myxo and SHAM (**E**, **F**, **G**, **H**) or untreated (**A**, **B**, **C**, **D**) . Cells were grown at air level of CO_2, shown are representative traces of n=3 biologically independent experiments for *pgrl1 flvB*-1 (**C**, **F**, **I**, **M**), *pgrl1 flvB-3* (**D**, **G**, **J**, **O**), *flvB* (**H**, **J**) and their control strains WT2 (**A**, **K**) and WT3 (**B**, **E**, **H**, **L**).

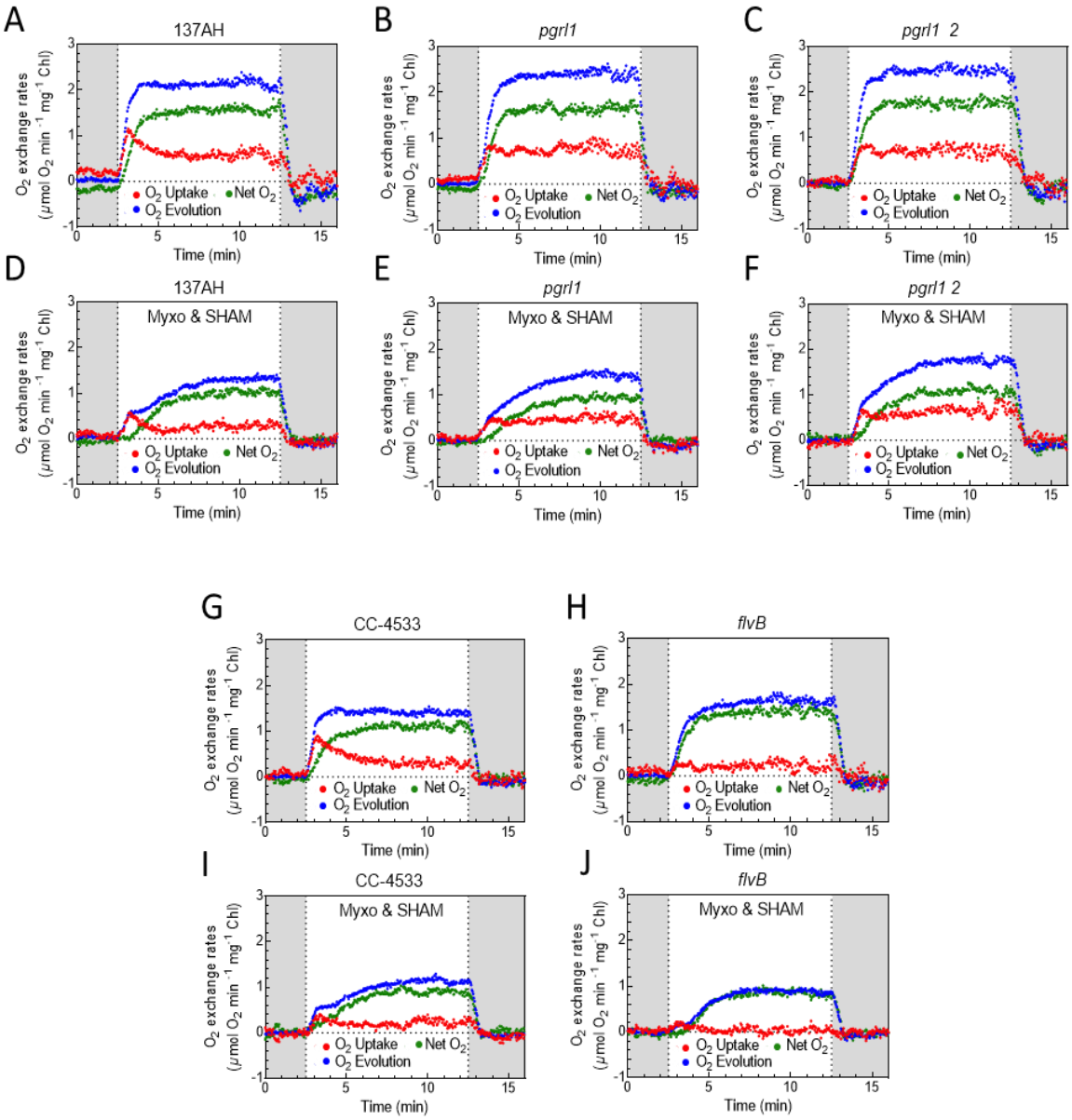

Supplemental Figure S3. O_2 exchange rates in *pgrl1* and *flvB* single mutants and their control strains grown at air level of CO_2. Gross and net O_2 exchange rates upon a dark (grayed areas) -light-dark transition on cells treated (**D**, **E**, **F**, **I**, **J**) or not (**A**, **B**, **C**, **G**, **H**) with myxothiazol (Myxo, 2.5 μM) and salicylhydroxamic acid (SHAM, 400 μM). Cells were grown at air level of CO_2, shown are representative traces of n=3 biologically independent experiments for *pgrl1* (**B**, **E**), *pgrl1* 2 (**C**, **F**), *flvB* (**H**, **J**) and their respective control strains 137AH (**A**, **D**) and CC-4533 (**G**, **I**).

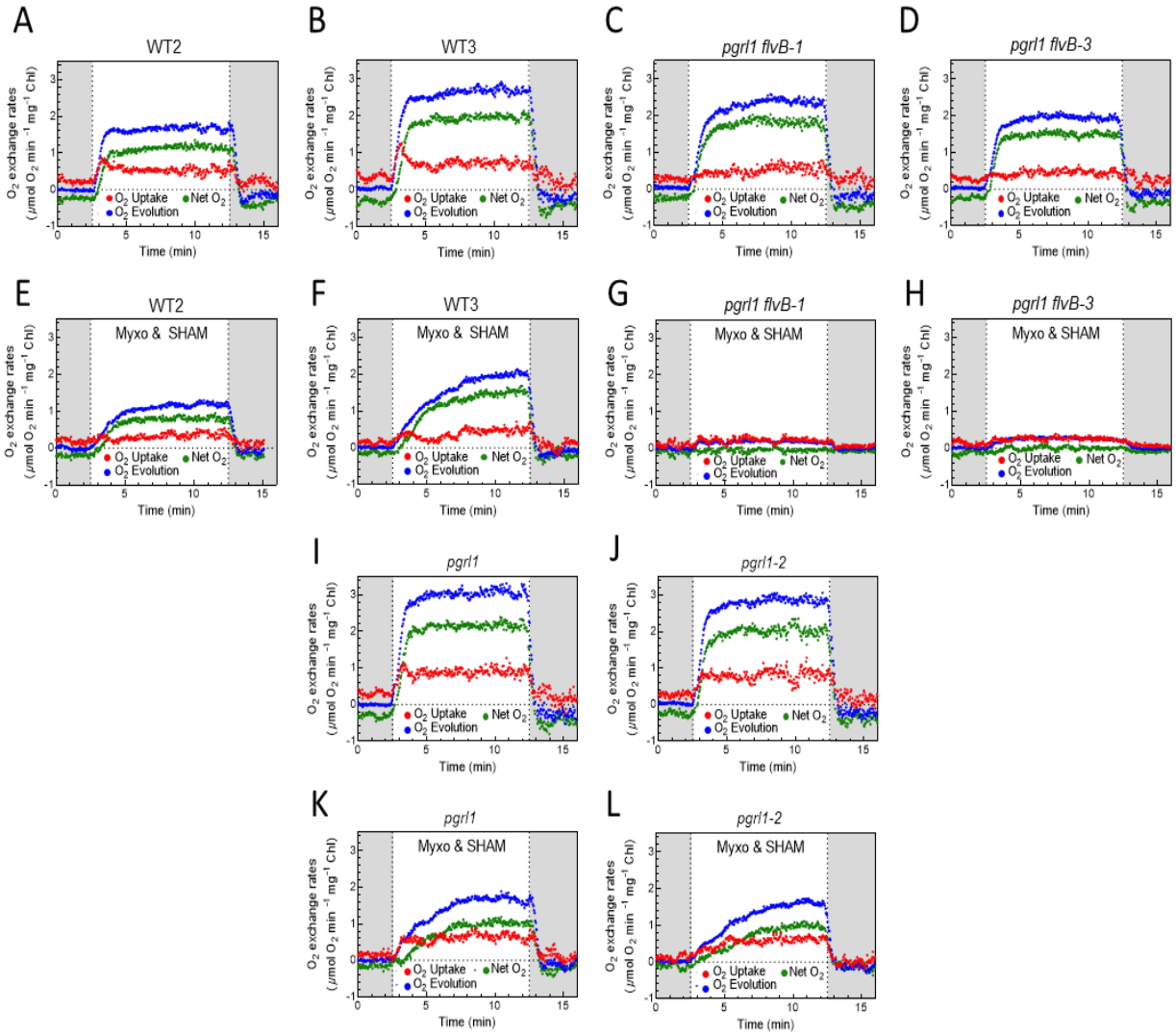

Supplemental Figure S4. O_2 exchange rated in *pgrl1*, *pgrl1 flvB* and their control strains grown in air enriched with 2% CO_2. Gross and net O_2 exchange rates upon a dark (grayed areas) -light-dark transition on cells treated (**E**, **F**, **G**, **H, K, L**) or not (**A**, **B**, **C**, **D**, **K**, **L**) with myxothiazol (Myxo, 2.5 μM) and salicylhydroxamic acid (SHAM, 400 μM). Cells were grown with air enriched with 2% CO_2, shown are representative traces of n=3 biologically independent experiments for *pgrl1 flvB*-1 (**C**, **G**), *pgrl1 flvB-3* (**D**, **H**), their respective control strains WT2 (**A**, **E**) and (**B**, **F**), *pgrl1* (**I**, **K**) and *pgrl1* 2 (**J**, **L**).

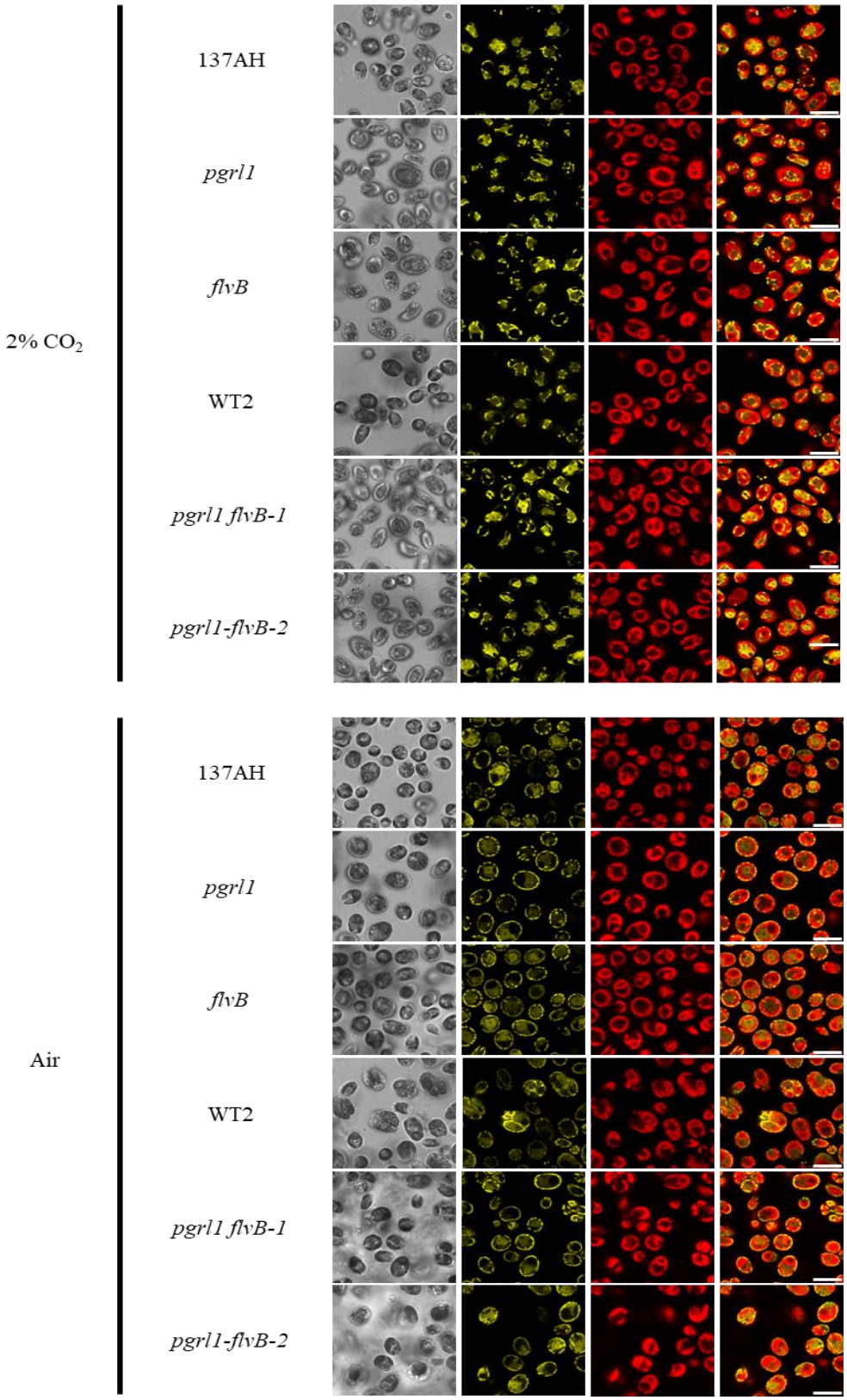

Supplemental Figure S5. Localization of mitochondria in *pgrl1*, *flvB*, *pgrl1 flvB-1* and -2 and their control strain in air enriched or not with 2% CO_2. Cross section images showing subcellular localization of the mitochondria-localized mito-Clover and chlorophyll fluorescence in *pgrl1*, *flvB*, *pgrl1 flvB-1*, *pgrl1 flvB-2* and the control strains 137AH and WT2, grown in air or 2% CO_2-enriched air. Shown are representative of two independent experiments.

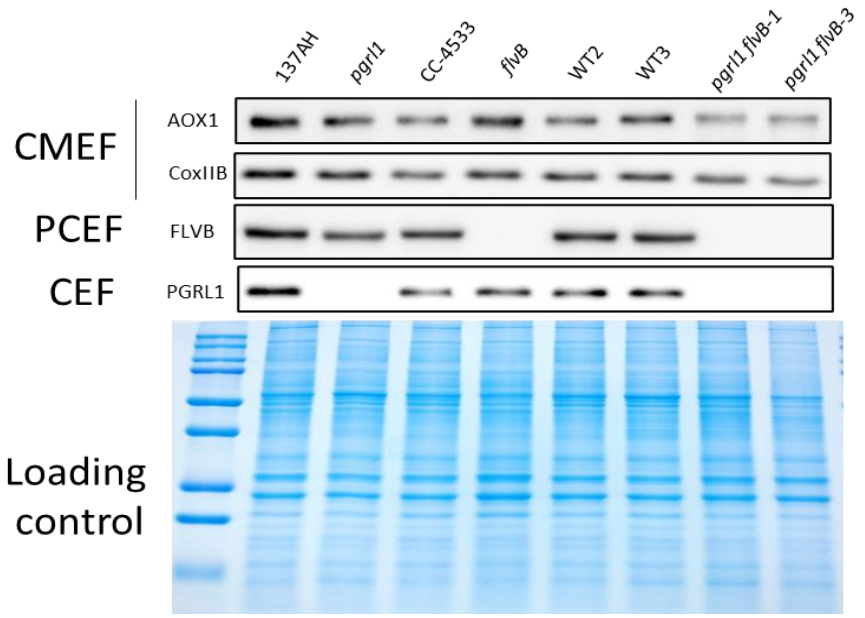

Supplemental Figure S6. Immunodetection of proteins involved in CMEF, PCEF and CEF in the strains used in this study. Immunodetection of PGRL1, FLVB, AOX1, CoxIIB in pgrl1, flvB mutants and *pgrl1 flvB* double mutants and their respective controls grown at air level of CO_2.

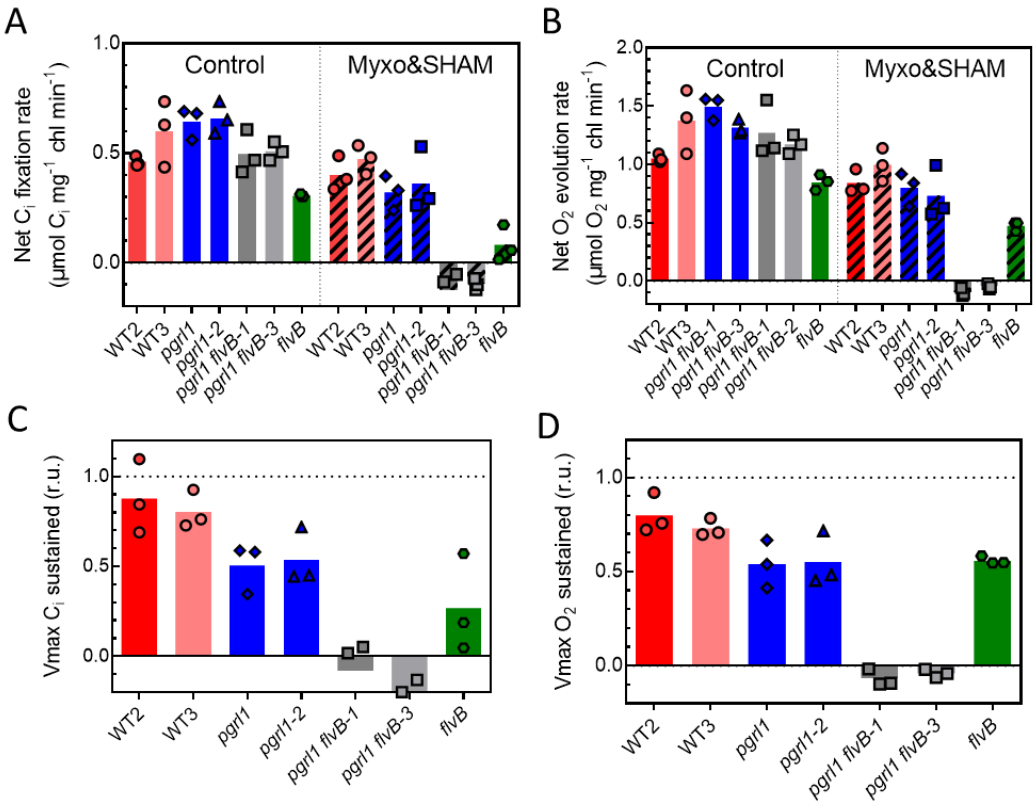

Supplemental Figure S7. Comparison of net inorganic carbon fixation and net O_2 production. Inorganic carbon (C_i) and O_2 exchange rates are measured concomitantly during a dark to light transition. Data shown are from same experiments used in **Sup Figs. S8**. **A**, **B** Net O_2 evolution (**B**) and C_i fixation (**A**) on cells treated (right panels) or not (left panels) with myxothiazol (Myxo, 2.5 μM) and salicylhydroxamic acid (SHAM, 400 μM). **C, D** Maximal net C_i fixation (**C**) and net O_2 evolution (**D**) sustained after treatment with myxothiazol and salicylhydroxamic acid. Cells were grown at air level of CO_2, shown are representative traces of n=3 biologically independent experiments for *pgrl1*, *pgrl1* 2, *flvB*, *pgrl1 flvB-1*, *pgrl1 flvB-3* and the control strains WT2 and WT3.

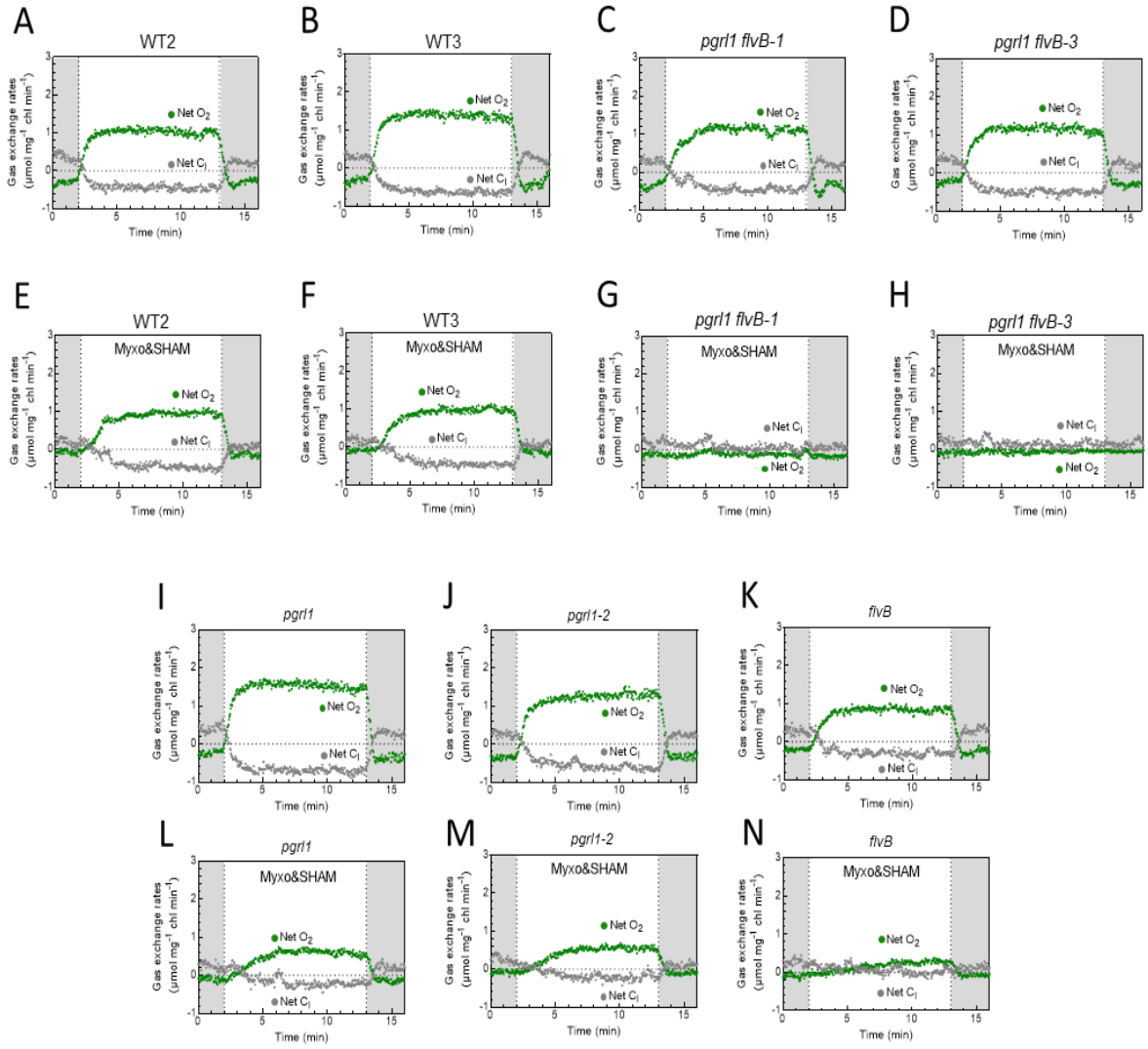

Supplemental Figure S8. Net C_i and O_2 exchange rated in *pgrl1* and *flvB* single and double mutants and the control strains WT2 and WT3. Inorganic carbon (C_i) and O_2 exchange rates are measured concomitantly upon a dark (grayed areas) -light-dark transition on cells treated (**E**, **F**, **G**, **H, L, M, N**) or not (**A**, **B**, **C**, **D**, **I**, **J**, **K**) with myxothiazol (Myxo, 2.5 μM) and salicylhydroxamic acid (SHAM, 400 μM). Cells were grown at air level of CO_2, shown are representative traces of n=3 biologically independent experiments for *pgrl1* (**I**, **L**), *pgrl1* 2 (**J**, **M**), *flvB* (**K**, **N**), *pgrl1 flvB-1* (**C**, **G**), *pgrl1 flvB-3* (**D**, **H**) and the control strains WT2 (**A**, **E**) and WT3 (**B**, **F**).

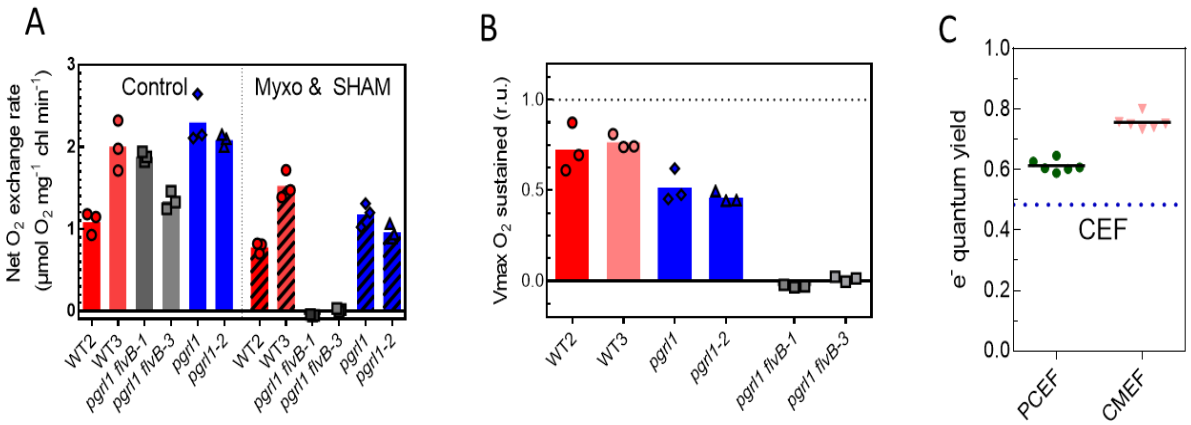

Supplemental Figure S9. Net O_2 exchange rates characteristic and e^- quantum yield measured in strains grown in air enriched with 2% CO_2. Data shown are obtained from the same experiments used in **Fig. 2 D**, **Sup Fig. S4**. **A**, Net O_2 evolution on cells treated (right panels) or not (left panels) with myxothiazol (Myxo, 2.5 μM) and salicylhydroxamic acid (SHAM, 400 μM). **B** Maximal net O_2 evolution sustained after treatment with myxothiazol and salicylhydroxamic acid. **C** Electron quantum yield of PCEF (green), CMEF (pink) and CEF (dotted line). Cells were grown in air enriched with 2% CO_2, Bars show the mean and dots show individual replicates ($n = 3$ biologically independent samples).

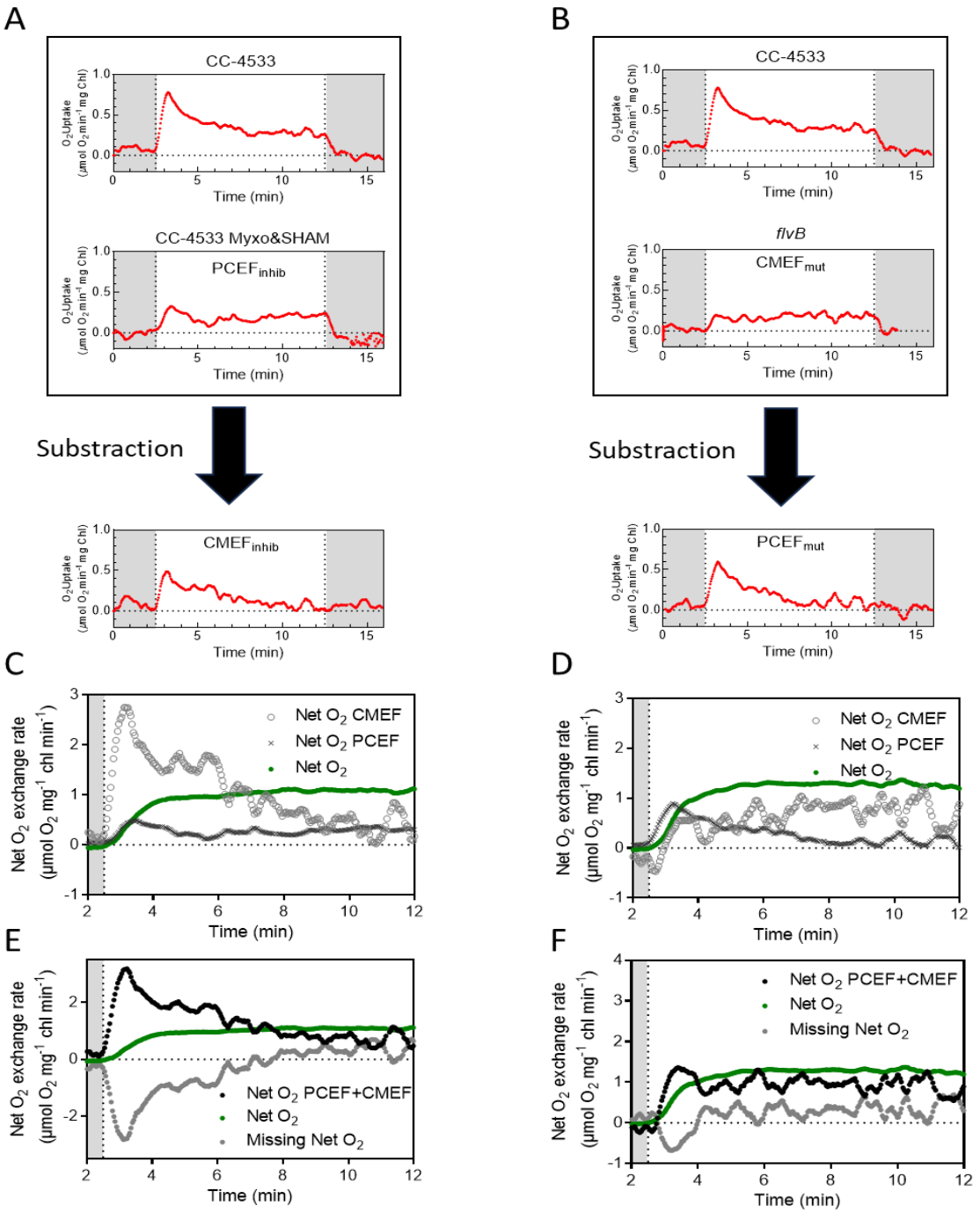

Supplemental Figure S10. Illustration of the method used to quantify of the contribution of each photosynthetic electron flow to CO_2 fixation. Illustrated here are the two different methods used, one based on the use of inhibitors (inhib) (**A**, **C**, **E**) the other on mutants (mut) (**B**, **D**, **F**). The first step for both methods is to calculate the gross O_2 uptake mediated by CMEF and PCEF either by first quantifying $PCEF_{inhib}$ and deducting $CMEF_{inhib}$ (**A**), or by first quantifying $CMEF_{mut}$ and deducting $CPEF_{mut}$ (**B**). Then, those fluxes are combined with the e^- quantum yield of each flux to predict the net O_2 evolution powered by CMEF (gray cirlces) and PCEF (gray crosses) (**C**, **D**). The net O_2 hence powered by CMEF and PCEF (gray dots) is then compared to the actual net O_2 evolution measured (green dots) to compute the net O_2 evolution that should be powered by CEF (missing Net O_2) (**E**, **F**). Shown here are average signals of $n = 3$ biologically independent samples.

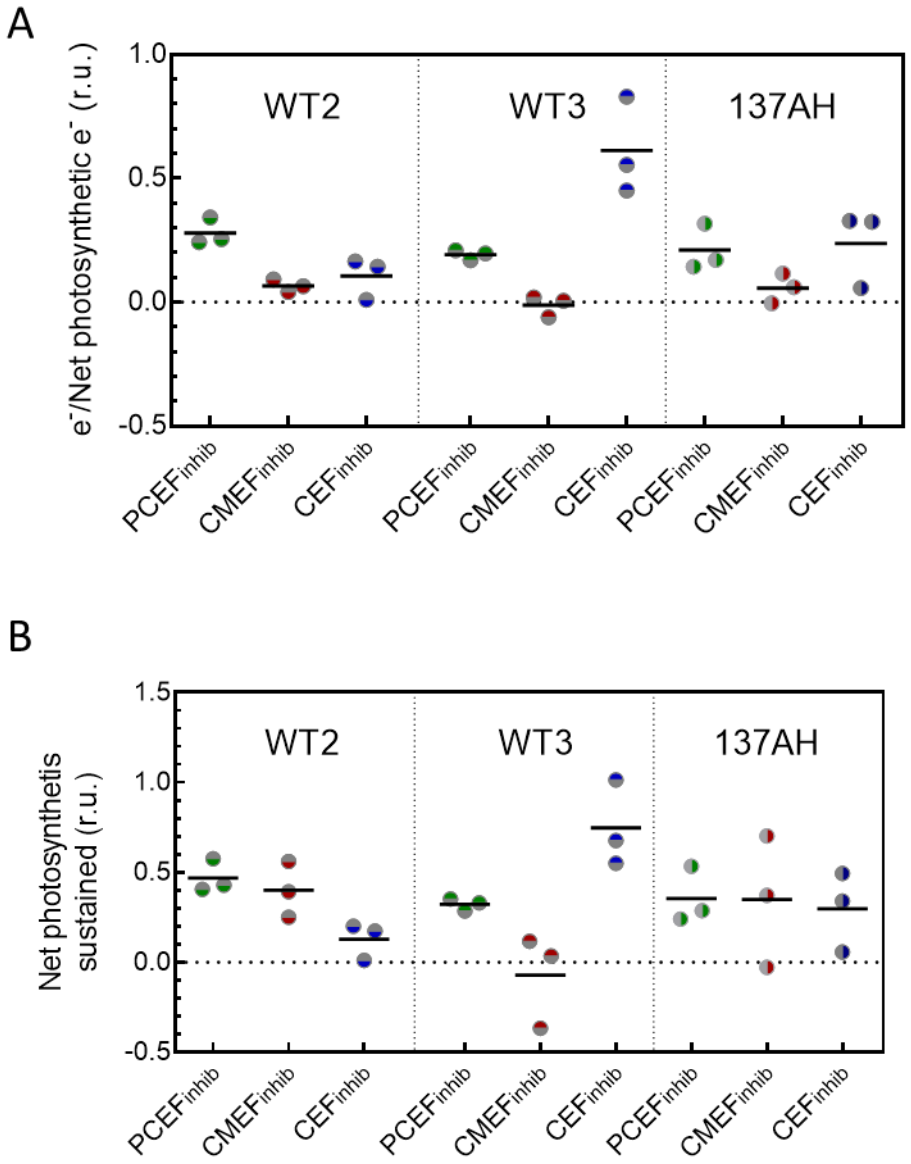

Supplementatl Figure S11. Quantification of the contribution of each photosynthetic electron flow to net photosynthesis. Data used for this calculation are the same as the one in **Supplemental Figs. S1, S2, S3.** Evaluation of the electron flow through PCEF, CMEF and CEF relative to LEF (**A**), and net photosynthesis sustained by PCEF, CMEF and CEF (**B**) based on the inhibitor method (**Sup. Fig. 12**) on WT2, WT3 and 137AH. Because of an twice greater dark O_2 uptake in 137AH, CMEF of 137AH was lowered by the dark O_2 uptake. Cells were grown at air levels of CO_2, Bars show the mean and dots show individual replicates ($n = 3$ biologically independent samples).

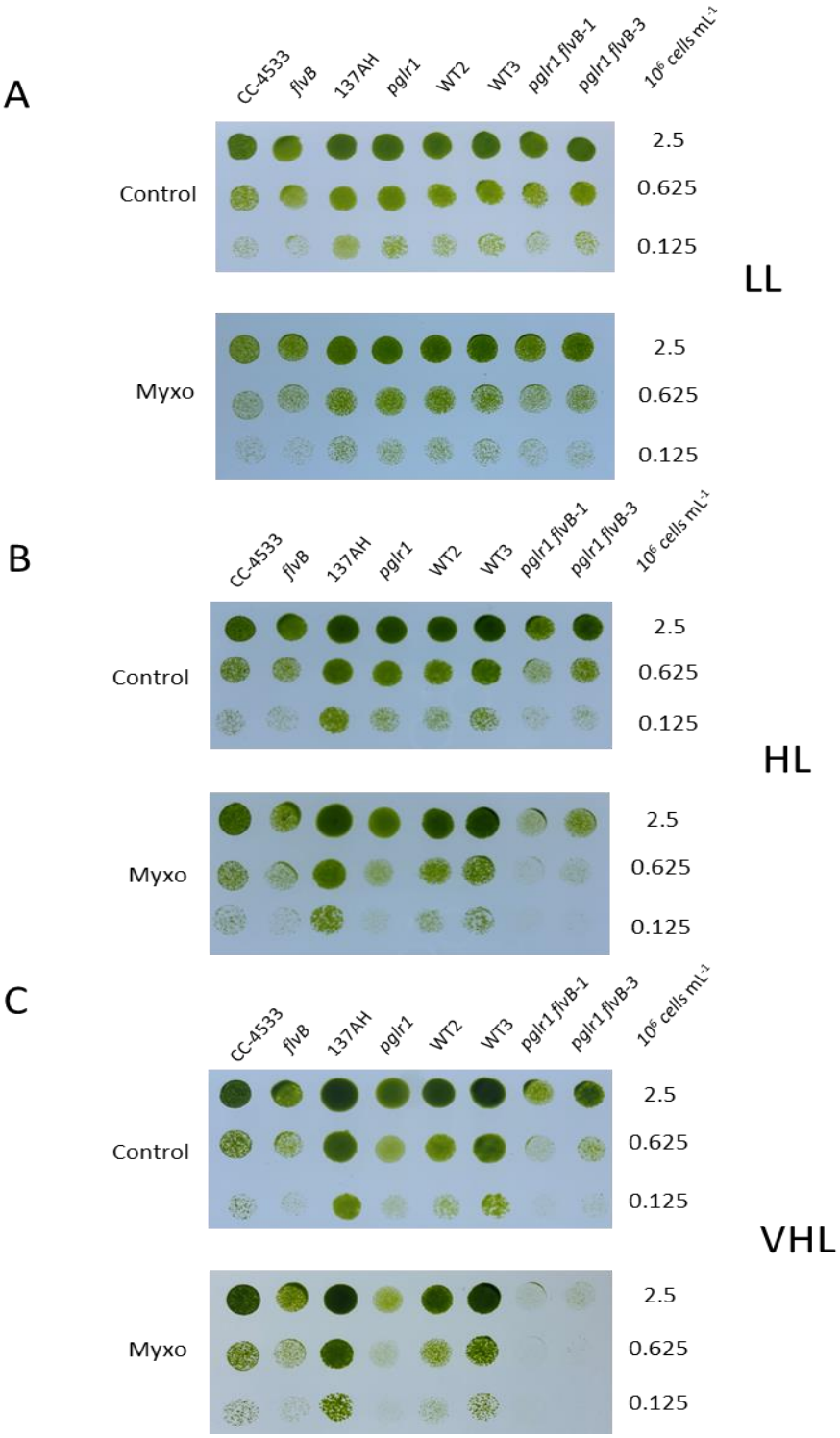

Supplemental Figure S12. Growth of mutant and control strains at various light intensities. Cells were spotted on plates containing minimal medium in the absence (control) or presence (Myxo) of myxothiazol (2.5µM) and grown under low light (LL, 30 µmol photons m^{-2} s^{-1}), high light (HL, 100 µmol photons m^{-2} s^{-1}) or very high light (VHL, 200 µmol photons m^{-2} s^{-1}). Cells were grown in air enriched with 2% of CO_2 at 25°C. Growth was assessed after three days in *pgrl1*, *flvB*, and their respective control strains (137AH and CC-4533) and on double mutants (*pgrl1 flvB*-1 -3) and their control strains (WT2, WT3). Shown are representative spot tests of n = 10 independent experiments.

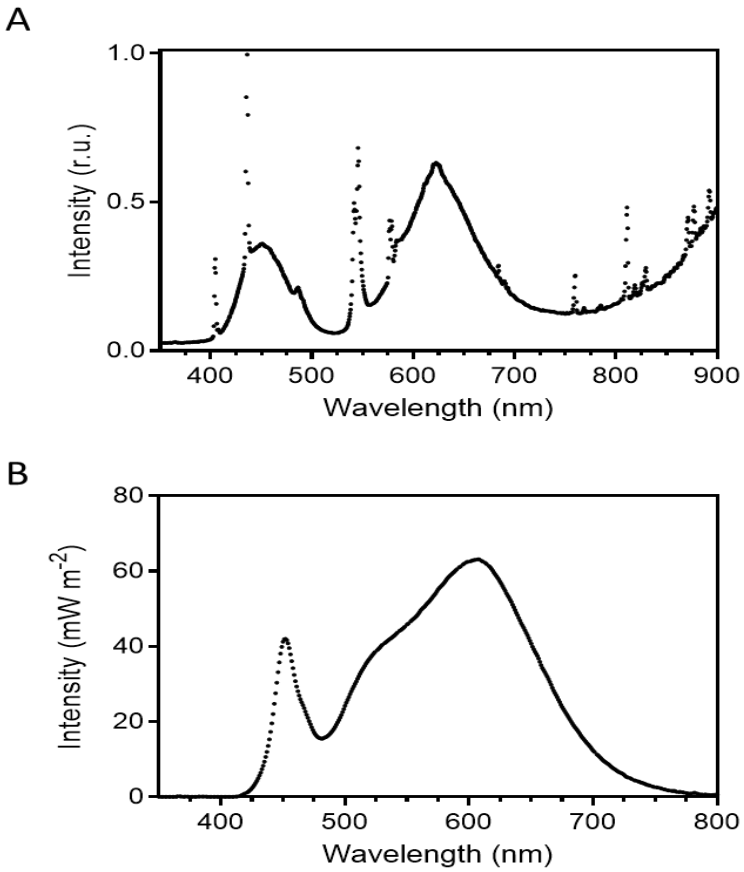

Supplemental Figure S14. Growing light spectra. Light spectra of light sources used for liquid cultures throughout the manuscript (**A**) or for cultures on solid media (**B**) in **Fig. 3 C** and **Sup Fig. 12**.

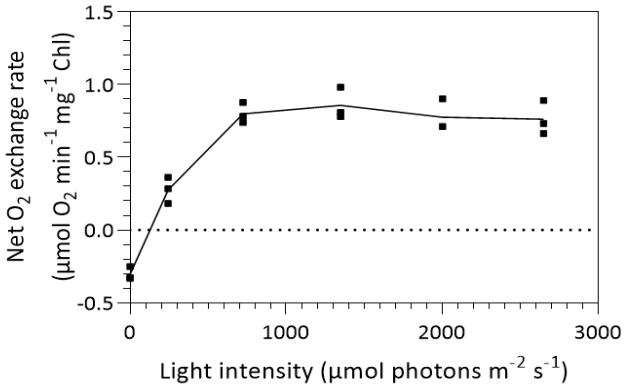

Supplemental Figure S15. Light saturation curve of net O_2 exchange rate measured with green actinic light. Cells were grown at air CO_2 level, collected during the exponential phase by centrifugation and resuspended in 1.5 mL of fresh buffered minimal medium (pH 7.2) at 30 µg chlorophyll mL^{-1}. $NaHCO_3^-$ (10 mM final concentration) was added to the cell suspension. After 2 minutes dark acclimation in the MIMS cuvette, green light was switched on and gradually increased every 3 minutes. Connecting line shows the mean and dots show individual replicates ($n = 3$ biologically independent samples).

Annex 2: Supporting information of Chapter 1

Annex II

Supplemental Materials and methods for:

Cyclic and pseudo-cyclic electron pathways play antagonistic roles during nitrogen deficiency in *Chlamydomonas reinhardtii*

Generation of *pgrl1* mutant in the CC125 background

Chlamydomonas mutant showing targeted insertion in the *PGRL1* locus was generated in the CC-125 background (mt+, nit-) using CRISPR/Cas-9 mutagenesis. Single guide RNAs (sgRNAs) (**Supplemental Table 2**) were designed by CHOPCHOP (Labun et al., 2019) using version 5.6 of the *Chlamydomonas reinhardtii* genome. Ribonucleic proteins (RNPs) were prepared by duplexing the sgRNA (20% volume per volume - v/v-) and Cas-9 (IDT, Ref# 427093062.) (20% v/v) with duplex buffer (IDT, Ref# 325470395) (60% v/v). Prior to electroporation, cells in the CC-125 background were grown in Tris-acetate-phosphate (TAP) at 22 °C under continuous illumination of 50 µmol photons $m^{-2}s^{-1}$. After treatment with autolysin for 3 hours, cells were electroporated in the presence of hygromycin resistance cassette (2 µg mL^{-1}), and the RNP mixture. The cells were resuspended in 10 mL TAP with 40 mM sucrose and left shaking overnight in dim light (10-20 µmol photons $m^{-2}s^{-1}$). Hygromycin resistant transformants were selected on TAP-agar plates containing hygromycin (20 µg mL^{-1}). sgRNA targeted regions were amplified via PCR to check for full or partial insertion of the hygromycin resistance cassette at the target site (**Supplemental Table 3 and Fig. 2*D***).

Starch quantification

Starch was quantified from 1 mL of culture containing ~5 million cells. Briefly, cells were harvested by centrifugation at 13000 *g* for 4 min at 4°C. Pellet was resuspended into 1 mL of methanol, mixed vigorously, and stored at −20°C before analysis. The supernatants were removed and the residual methanol was evaporated from the pellets incubated at room temperature in a fume hood. Pellets were resuspended in 400 µL of distilled water and autoclaved for 20 min at 120°C to solubilize the starch polymer. Total starch was quantified using an enzymatic starch assay kit (Sigma-Aldrich; ref. SA-20) following the manufacturer's instructions. Glucose converted from the starch was quantified using an automated YSI 2700 glucose analyzer (YSI Life Sciences) previously calibrated using a commercial glucose standard.

TAG quantification

Exponentially grown cells (~20 millions) were harvested by centrifugation at 4000 *g* for 3 min at 4°C. Pellets were resuspended in 1 mL of hot isopropanol containing 0.01% butylated hydroxytoluene (BHT) (w/v) for 10 min at 85°C to quench lipases (Légeret et al., 2016). A mixture of methyl tert-butyl ether (MTBE):H_2O (3/1, v/v) was added to extract lipids, vortexed and allow for phase separation. Finally, lipids were recovered from the upper organic phase after centrifugation at 4000 *g* for 3 min at 4°C. Solvent was evaporated under a stream of N_2 and total lipid extract was dissolved in 200 µL of chloroform:methanol (2:1 v/v) prior to analysis. TAG was separated from other lipid classes by Thin Layer Chromatography (TLC) and quantified based on densitometry method via comparing a standard curve generated from loading known amount of the standard TAG51:0 (17:0/17:0/17:0) (Sigma-Aldrich) to the same plate as described previously in (Siaut et al., 2011). Total fatty acids were quantified as described in (Siaut et al., 2011). Briefly, part of the extracted lipids was converted to FAMEs by acid-catalysed transmethylation, extracted into hexane and analyzed by gas

chromatography coupled to flame ionization detector and mass spectrometry (GC-FID-MS) (Agilent 7890A GC and Agilent 5975C MS, Agilent Technologies, Palo Alto, CA, USA).

Immunoblot

For protein extraction, exponentially grown cells (3 mL at around 10 µg mL^{-1} of chlorophyll) were harvested by centrifugation at 4000 *g* for 3 min at 4°C. Pellets were resuspended in 200 µL of 1% SDS, to which 800 µL of cold acetone were added to extract chlorophyll and the suspension was incubated for 30 min at -20°C. Samples were then centrifuged for 10 min, 13000 *g* at 4°C to precipitate proteins. Chlorophyll concentration was measured by spectrophotometry from supernatant. The protein pellet was resuspended with Novex™ Nupage™ LDS buffer 1x (Invitrogen™) containing reducing agent DTT, at a final volume corresponding to 1 µL per 0.1 µg chlorophyll measured (corresponding to 1 µg $µL^{-1}$ of protein), the resuspended proteins were then denatured for 20 min at 70°C. Ten µg of protein were loaded on Novex™ Nupage™ Bis tris 12% (Invitrogen™) gel, migrated 1 h at 190 V in Novex™ Nupage™ MOPS (Invitrogen™) buffer (or Novex™ Nupage™ MES (Invitrogen™) according to protein molecular weight and transferred to nitrocellulose membrane using semidry transfer technique. Immuno-detection was performed using antibodies raised against PGRL1 (Tolleter et al., 2011), NDA2 (Desplats et al., 2009). Other antibodies were ordered from Agriserea for PSBD (AS06 146) 1/10000, PSAD (AS09 461), Cyt *f* (AS06 119) 1/500, Cox IIB (AS06 151) 1/5000, ATG8 (AS14 2769) 1/2000 (Upadhyaya et al., 2020; Crespo and Pérez-Pérez, 2023), 50S ribosomal protein L30 (AS08 331) 1/1000 and α-Tubulin (AS10 680) 1/1000. Secondary anti-rabbit peroxidase-conjugated antibodies (Sigma-Aldrich; no. AQ132P) (1/10,000) were used for the detection with the G:BOX Chemi XRQ system (Syngene) using ECL detection reagents (GE Healthcare). Images were captured with a CCD camera equipped with a GeneSys Image Acquisition Software (Syngene).

Statistical analysis

One-way ANOVA using GraphPad Prism (GraphPad Software) was used to perform statistical analysis. The *p* values were computed by One-way ANOVA test (uncorrected *p* values) or using Turkey corrections for large datasets (adjusted *p* values). Shown are grouping of strains into statistical families according to *p* values indicated by asterisk (* for $p \leq 0.05$; ** for $p \leq 0.01$; *** for $p \leq 0.001$ and **** for $p \leq 0.0001$) or letters indicating parameter-specific significances. The statistical significance (α) was set as 0.05 (5%).

Supplemental Tables

Table S1: List and origins of mutants used in this study.

Gene ID	Strains	Genetic background	Mutant generation	Reference article
Cre07.g340200 (PGRL1)	*pgrl1*$_{137AH}$	137AH	Random insertion	(Tolleter et al., 2011)
	pgrl1$_{CC125}$	CC125	CRISPR-Cas9	This article
Cre16.g691800 (FLVB)	*flvB-21*	CC4533	Random insertion (CLiP)	(Chaux et al., 2017a)
	flvB-208	CC4533	Random insertion (CLiP)	(Chaux et al., 2017a)

	flvB-308	CC4533	Random insertion (CLiP)	(Chaux et al., 2017a)
Cre07.g340200/Cre16.g691800 (PGRL1 and FLVB)	WT1	137AH x CC4533	Mating between *pgrl1*$_{137AH}$ and *flvB-21*	(Burlacot et al., 2022)
	WT3	137AH x CC4533	Mating between *pgrl1*$_{137AH}$ and *flvB-21*	(Burlacot et al., 2022)
	pgrl1 flvB-3	137AH x CC4533	Mating between *pgrl1*$_{137AH}$ and *flvB-21*	(Burlacot et al., 2022)
	pgrl1 flvB-5	137AH x CC4533	Mating between *pgrl1*$_{137AH}$ and *flvB-21*	(Burlacot et al., 2022)

Table S2: sgRNAs to knockout target genes

Mutant	Gene ID	sgRNA Sequence	Target Exon
pgrl1$_{CC125}$	Cre07.g340200	CTTGCCCTCGTAGTACCACGAGG	1

Table S3: Primer pair sequences for genotyping mutants

Target Gene	Target Exon	Primer Name	Oligo Sequences	Predicted Band Size in CC-125 (bp)
PGRL1	1	oAB0013	GCAATGTTGCTGCTGACTACTG	225
	1	oAB0014	AGTCCTCGTCAGTCATAATGGG	
STT7	1	oAB0033	GCACGAACCAAGACACACATAG	237
	1	oAB0034	GTAGACGATGTCACCGCACTT	

Supplemental Figures

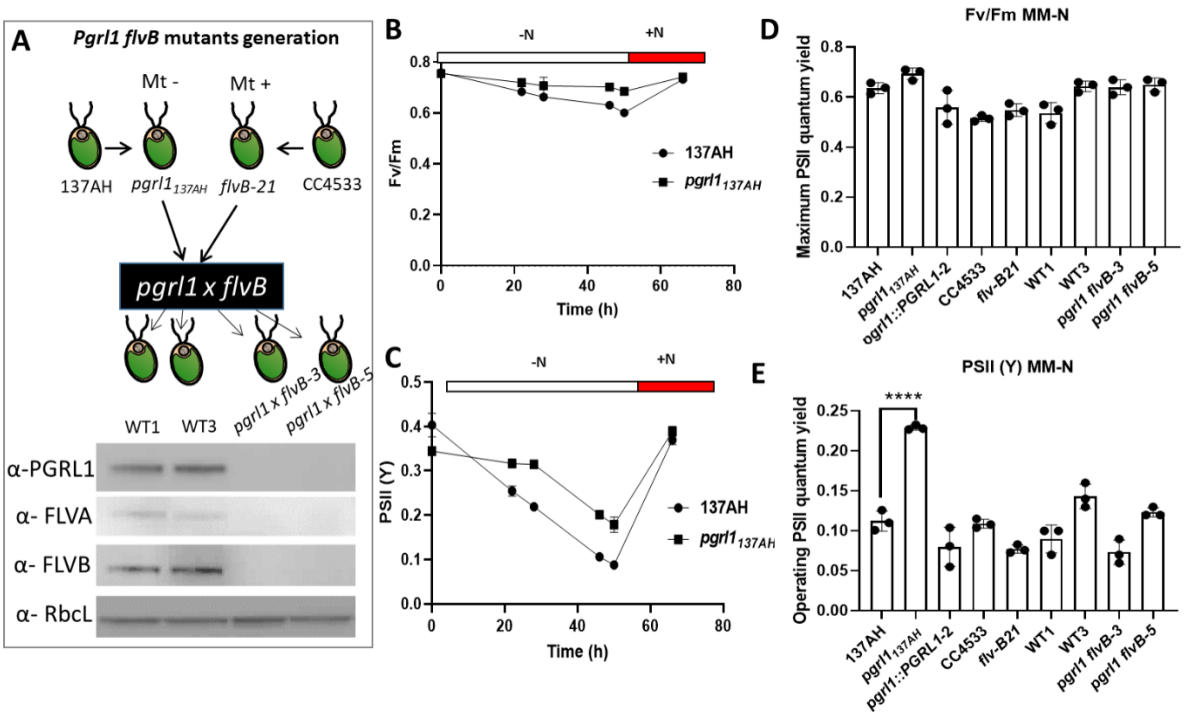

Supplemental Figure 1. PSII activity measurement using PAM in *pgrl1*$_{137AH}$, *flvB* and *pgrl1 flvB* mutants upon N deficiency. A, Generation of *pgrl1 flvB* double mutants by crossing and their genealogy. Antibodies against PGRL1, FLVA and FLVB were used to confirm the genotype. RbcL is used as a positive control.

B-C, Maximum quantum efficiency and the operating yield of PSII were measured from 15min dark-adapted cells of *pgrl1*$_{137AH}$ and 137AH after 0, 22, 28, 46 and 50 h of N deficiency and 12 h after N resupply. Shown are an average of at least three biological replicates ± SD.

D-E, Maximum quantum efficiency and the operating yield of PSII were measured from 15min dark-adapted cells after 48 h of N deficiency. PSII yield were calculated after 4min of illumination using green actinic light (1250 µmol photon m^{-2} s^{-1}, green LEDs). Shown are an average of at least three biological replicates ± SD. Asterisks represent statistically significant difference comparing mutants with their control strains (* p<0.05, ** p<0.01 and *** p<0.001) using one-way ANOVA.

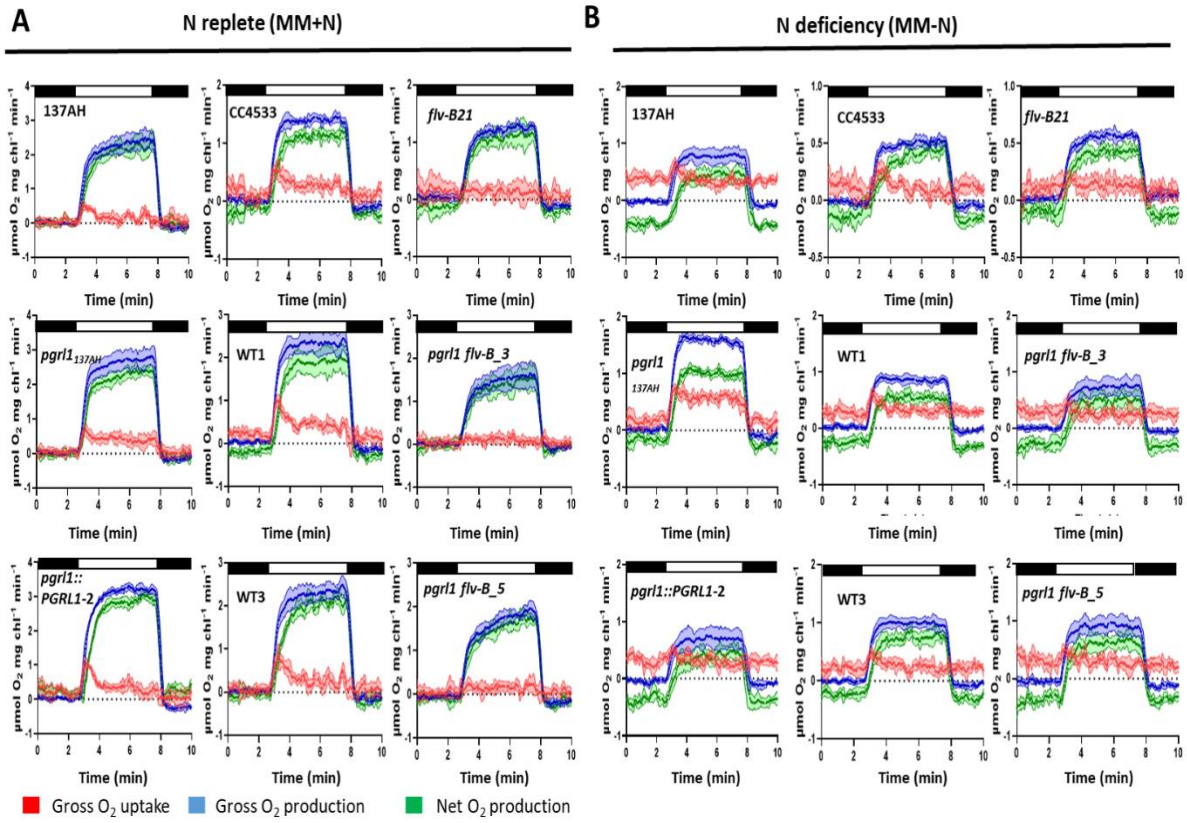

Supplemental Figure 2. O_2 exchange measurement under N replete and deficiency in *pgrl1*$_{137AH}$, *flvB* and *pgrl1 flvB* mutants.

A, O_2 exchange under N replete.

B, O_2 exchange under N deficiency.

O_2 exchange rates were measured during the dark-light-dark transition from N replete and deficient cells of *flvB*, *pgrl1 flvB* and respective control lines using a MIMS in the presence of [^{18}O]-enriched O_2. Net O_2 evolution (green) was calculated as gross O_2 evolution (blue) – gross O_2 uptake (red). Shown are an average of at least three biological replicates ± SD.

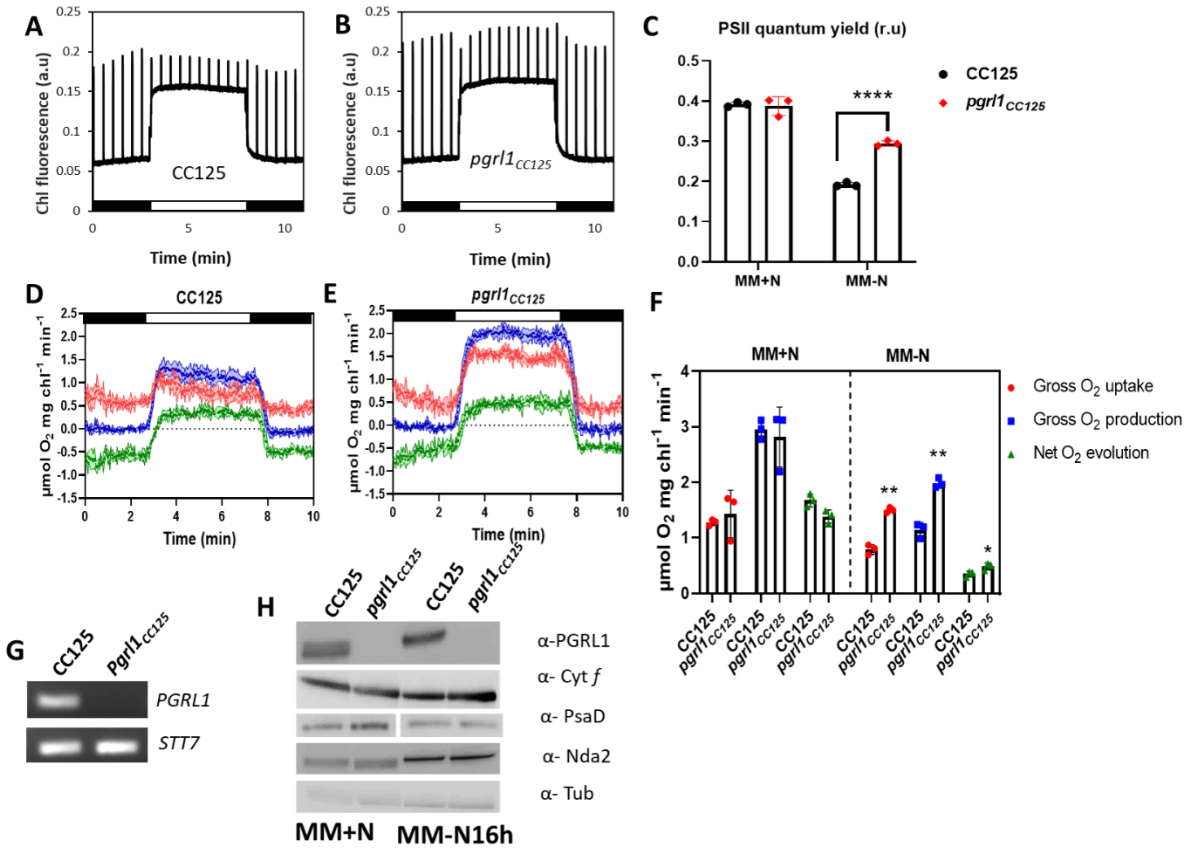

Supplemental Figure 3. Photosynthetic activity in CRISPR-Cas9 generated *pgrl1*$_{CC125}$ mutant.

A-B Chlorophyll fluorescence during the dark-light-dark transition under N replete and after 16h of N deficiency.

C, PSII operating yield N replete and after 16h of N deficiency.

D-F, O_2 exchange rates were measured using a MIMS during the dark-light-dark transition from N-replete (**D**) and N-deficient (**E**) conditions. Net O_2 evolution (green) was calculated as gross O_2 evolution (blue) – gross O_2 uptake (red).

G, Genetic characterization of mutants using PCR on genomic DNA. Primers and expected size are listed in **Supplemental Table 1 and 2**. STT7 was used as a control.

H, Immunoblot showing the accumulation of PGRL1, Cyt *f*, PsaD, Nda2 and Tub in *pgrl1*$_{CC125}$ under N replete and after 16h of N deficiency.

Wild type CC125, *pgrl1*$_{CC125}$ N-replete cells cultivated photoautotrophically with 1% CO_2 in air under continuous light (50 µmol photons m^{-2} s^{-1}) were transferred into N-free media for 16h prior to measurements. PSII yield were calculated from (**A** and **B)** after 4min of illumination using green actinic light (1250 µmol photon m^{-2} s^{-1}, green LEDs). Shown are an average of at least three biological replicates ± SD. Asterisks represent statistically significant difference comparing mutants with their control strains (* p<0.05, ** p<0.01 and *** p<0.001) using one-way ANOVA.

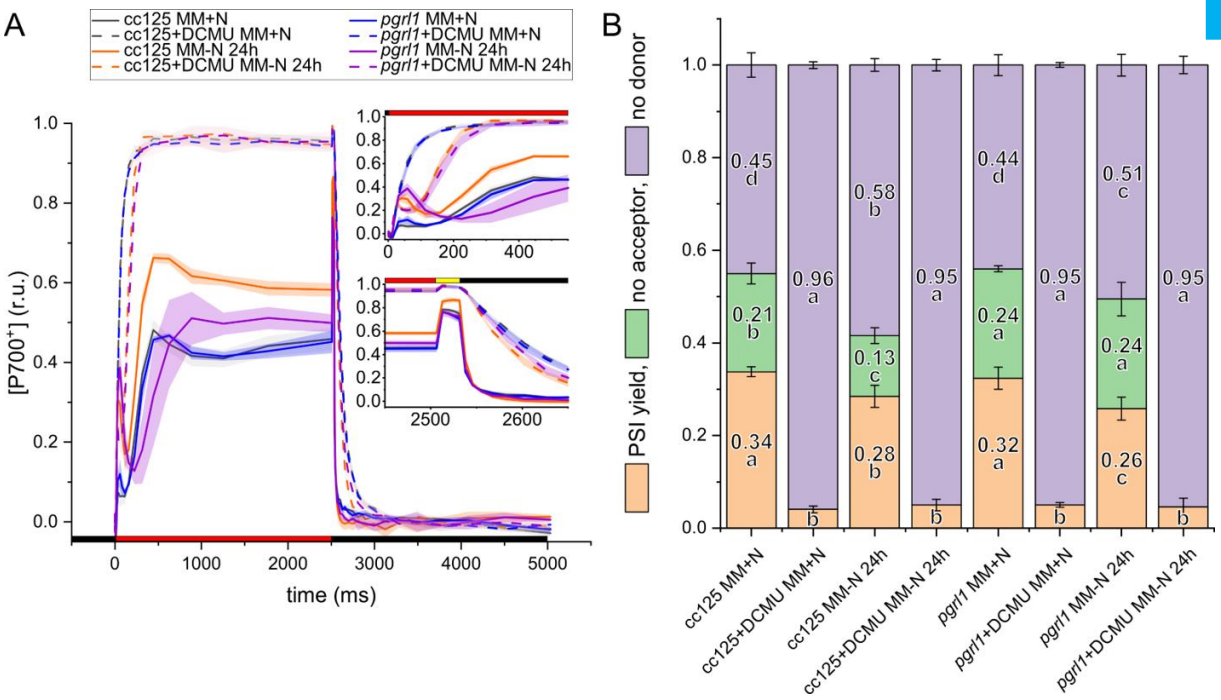

Supplemental Figure 4. Redox state measurements of P700 in *pgrl1*$_{CC125}$ mutant. The influence of PGRL1 on the redox state of the primary PSI donor, P700, was monitored in the genetic background CC125 **(A-B)**. Panel A shows raw kinetics (red/yellow/black bars: 490/3000/0 µmol photons m^{-2} s^{-1}) in the presence and absence of PSII inhibitor DCMU (means ± SD of 4 biological replicates). Panel B quantifies the corresponding P700 pools at the end of the 2.5-s light period (letters indicate parameter-specific significances using one-way ANOVA/Fisher-LSD, p<0.05). At the time of quantification, P700 remained photo-oxidizable by a saturating pulse (PSI yield), was redox inactive (no acceptors) or was pre-oxidized (no donors). Wild-type CC125, *pgrl1*$_{CC125}$ N-replete cells cultivated photoautotrophically with 1% CO_2 in air under continuous light (50 µmol photons m^{-2} s^{-1}) were transferred into N-free media for 24 h prior to measurements.

Annex II

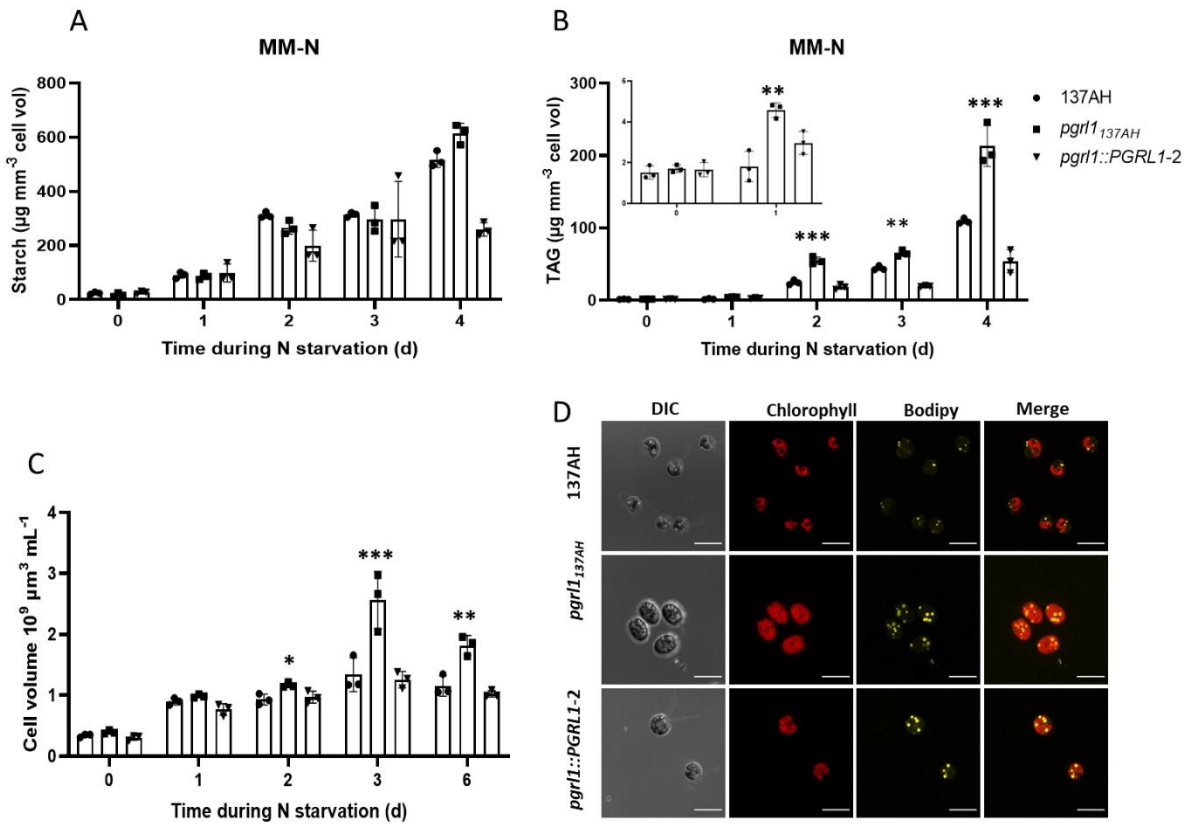

Supplemental Figure 5. Evaluation of biomass and carbon storage during N deficiency in *pgrl1*$_{137AH}$.

A, Kinetics of starch accumulation during N deficiency.

B, Kinetics of TAG accumulation during N deficiency.

C, Cell growth as a function of cellular volume during N deficiency.

D, representative images of confocal microscopy observation of lipid droplet stained with Bodipy dye. Pseudo-colors were used: BODIPY-stained LDs in yellow, chlorophyll autofluorescence in red. DIC: differential interference contrast. Scale bar = 5 µm.

Cells, cultivated photoautotrophically with 1% CO_2 in air under continuous light of 50 µmol photons m^{-2} s^{-1}, were transferred into N-free media and samples were harvested at different times as indicated on the graphs. Shown are an average of at least three biological replicates ± SD. Asterisks represent statistically significant difference compared to the control 137AH (* p<0.05, ** p<0.01 and *** p<0.001) using one-way ANOVA.

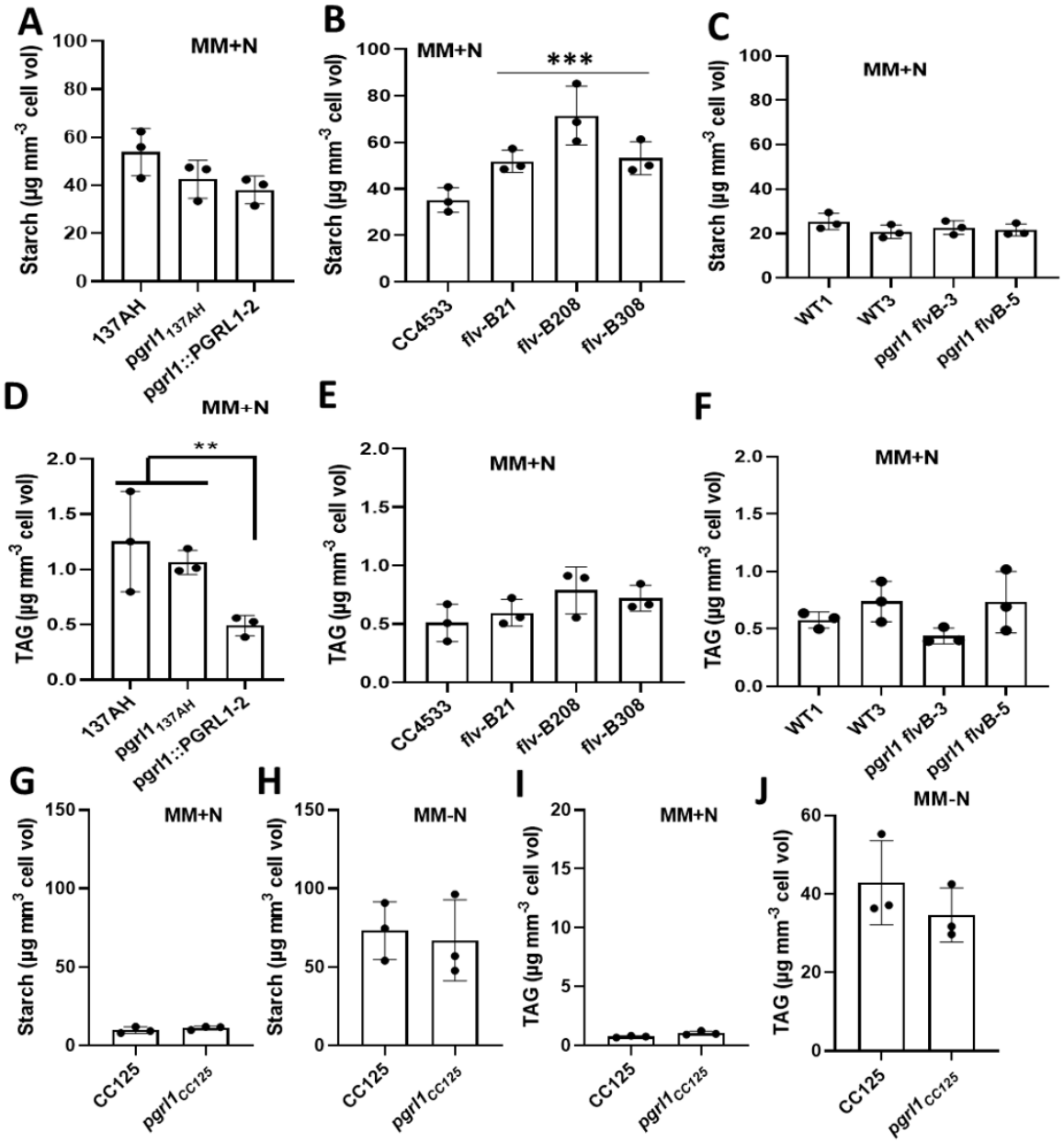

Supplemental Figure 6. Starch and TAG production in *pgrl1*$_{137AH}$, *flvB*, *pgrl1 flvB* and *pgrl1*$_{CC125}$.

A-C Starch quantification in N replete cells of *pgrl1*$_{137AH}$, *flvB* and *pgrl1 flvB* mutants.
D-F TAG quantification in N replete cells of *pgrl1*$_{137AH}$, *flvB* and *pgrl1 flvB* mutants.
G-J Starch and TAG quantification in N replete and after 24 hours of N deficiency in *pgrl1*$_{CC125}$.
Cells were cultivated photoautotrophically with 1% CO_2 in air under continuous light of 50 µmol photons m^{-2} s^{-1}. Shown are an average of at least three biological replicates ± SD. Asterisks represent statistically significant difference comparing mutants with their control strains (* p<0.05, ** p<0.01 and *** p<0.001) using one-way ANOVA.

Annex III

Annex 3: Supporting information of Chapter 3

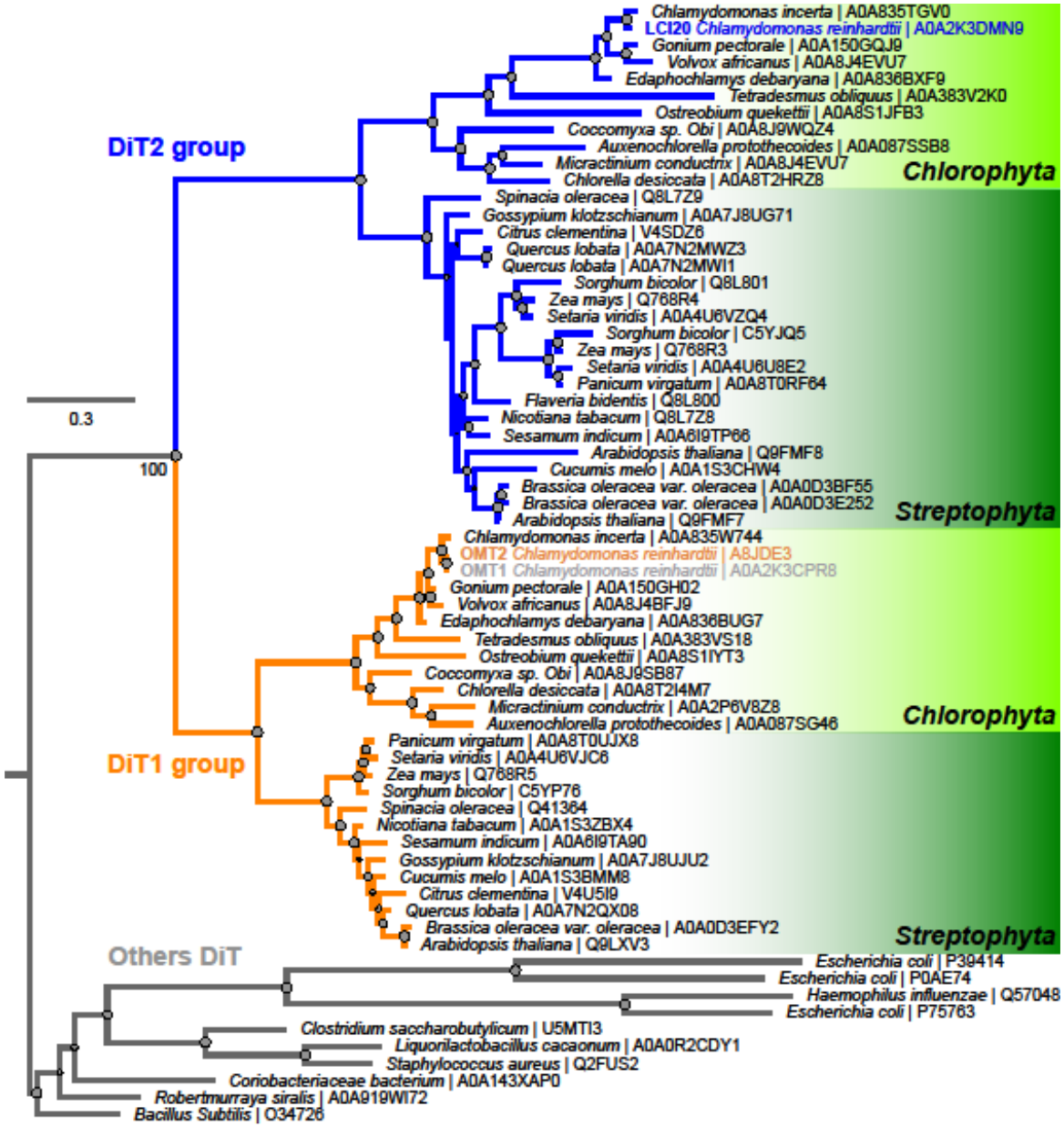

Fig. S1. Maximum Likelihood tree of the dicarboxylate transporter family (Citrate carrier CitT-related / IPR030676). The tree was rooted with Eubacteria sequences. Each sequence is associated to its primary accession number in the public database UniProtKB (https://www.uniprot.org). The tree was drawn to scale. The scale bar represents the number of substitutions per site. Tree topology was tested using an ultrafast bootstrap approximation approach with 1000 replicates. Gray circles represent bootstrap values and are drawn to scale.

Annex III

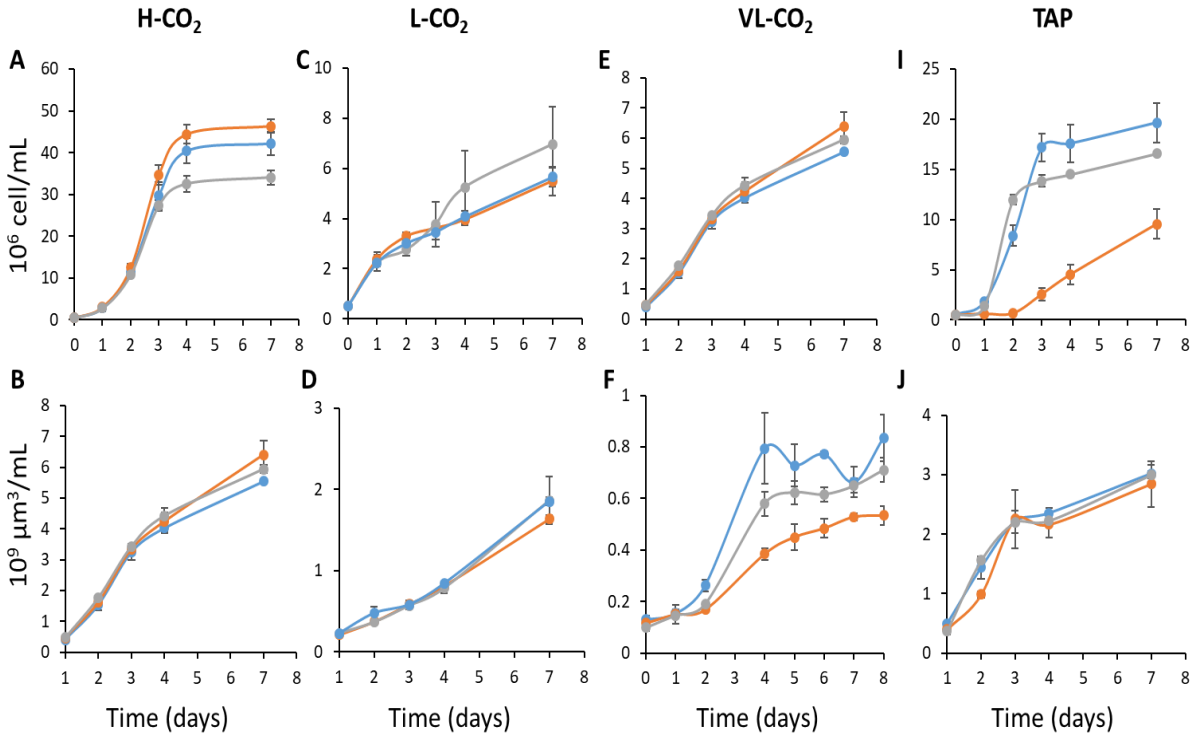

Fig. S2. The growth of the *lci20* in liquid culture is impaired under photoautotrophic VL-CO_2 and mixotrophic conditions. (**A, C, E and I**) Growth kinetics of the *lci20* from liquid cultures normalized by cell number. (**B, D, F and J**) Growth kinetics of the *lci20* from liquid cultures normalized by cell volume. Photoautotrophic air grown cells were used to inoculate fresh growth media at 0.5 million cells/mL cell density at the day zero. Continuous light 80 µmol photons m^{-2} s^{-1} was used throughout the kinetics. Data are means of three biological replicates for each strain with standard deviation. Blue (WT), orange (*lci20*) and gray (C1, a complemented line of *lci20*).

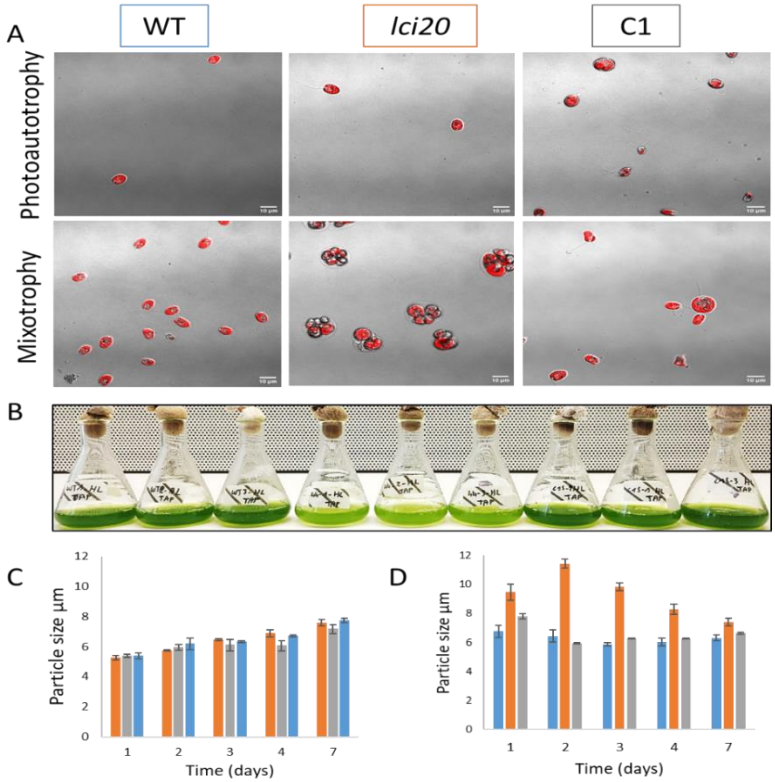

Fig. S3. The *lci20* forms multicellular structure in response to acetate supply. (A) Confocal observation of WT, *lci20* and C1 cells during photoautotrophic and mixotrophic growth. (B) Representative image of mixotrophic growth 48 h after inoculation (as shown in Fig. S1. *I* and *J*). Three biological replicates are shown for each strain. The scale bar is 10 µm.

Annex III

Annex 4: Supporting information of Chapter 4

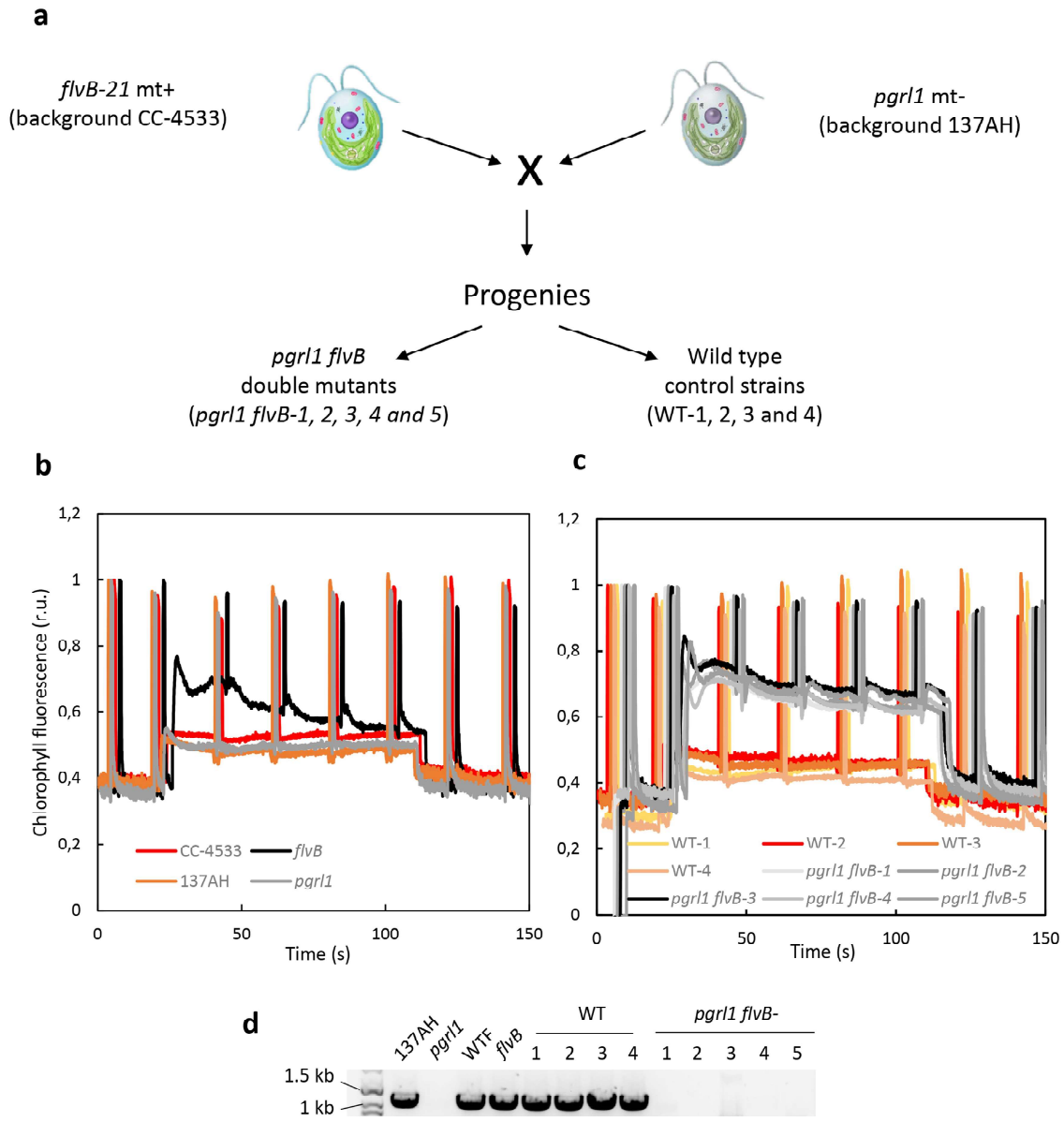

Extended Data Fig. 1 | Obtaining and characterizing of *pgrl1flvB* double mutants. a, Upon crossing of *pgrl1* and *flvB*-21 opposite mating types, progenies were screened for FLVB deficiency based on the chlorophyll fluorescence pattern, and for insertion in the *PGRL1* locus by PCR. Five independent double mutants and control strains were randomly selected among the pool of double mutants and wild-types for further analysis. **b**, **c**, Chlorophyll fluorescence patterns of parental strains (*pgrl1* and *flvB*-21) and of their respective control strains (137AH and CC-4533 respectively) in **b**, and of progenies of the crossing (*pgrl1flvB*-1, 2, 3, 4 and 5; WT-1, 2, 3, 4) in **C**. Chlorophyll fluorescence measurements were performed using a PAM fluorimeter in the dark and under red actinic light (100 µmol photon m^{-2} s^{-1}, from t = 22 s to t = 110 s) at a C_i concentration of 1 mM. Data are normalized to initial F_M and slightly shifted on the time axis for clarity. **d**, PCR amplification targeting the *PGRL1* locus in the different strains. Shown is representative of n = 3 independent experiments.

Annex IV

Article

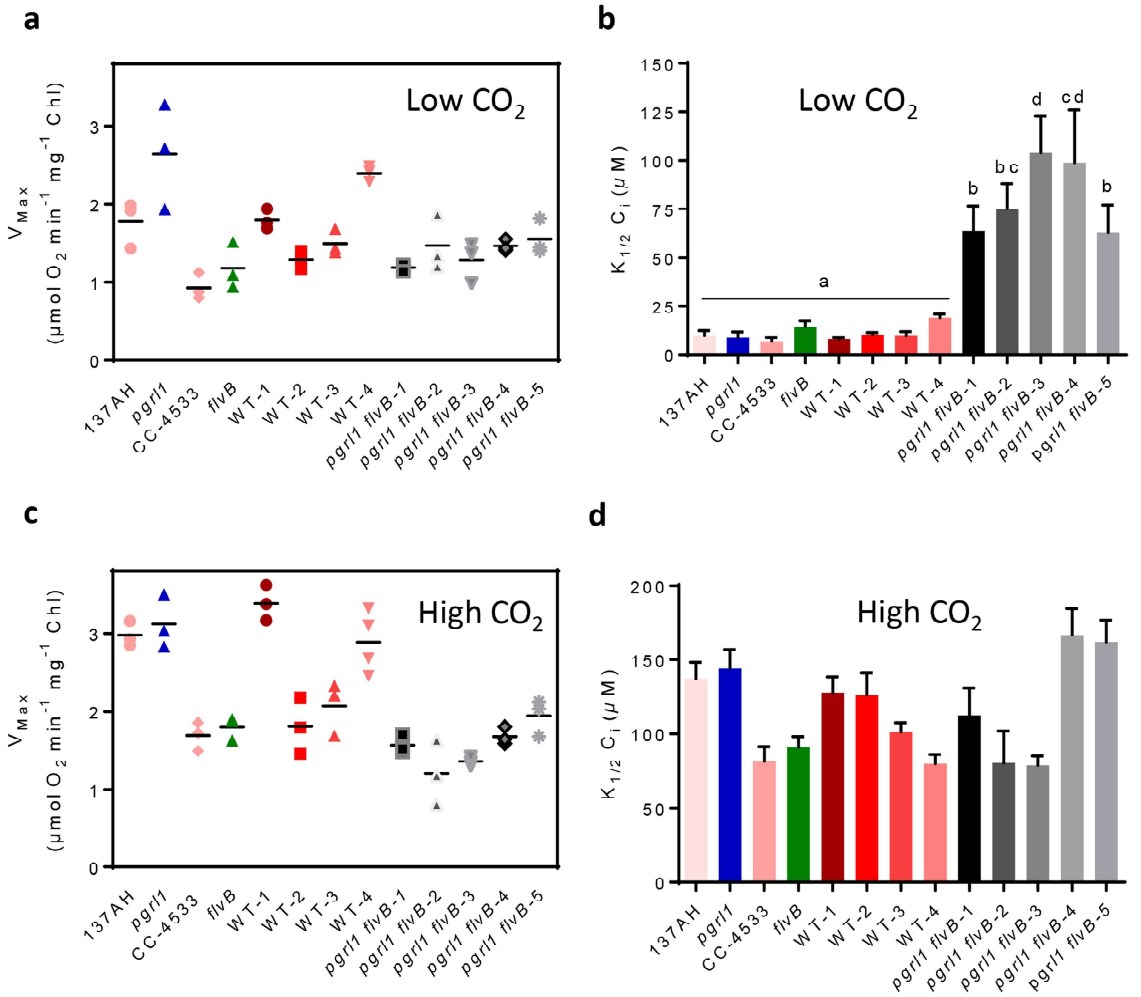

Extended Data Fig. 2 | Maximum net O_2 evolution and $K_{1/2}$ values measured in *pgrl1*, *flvB*, *pgrl1flvB* and their respective controls when grown under Low CO_2 or High CO_2. Net O_2 production rates were measured as described in Fig. 1 in low CO_2 (**a**, **b**) or high CO_2 (**c**, **d**) grown cells. **a**, **c**, Maximal net O_2 production rates. Shown are mean values and replicates (n = 3 biologically independent sample). **b**, **d**, $K_{1/2}$ values determined for each strain from hyperbolic fits. Shown are mean values ±SD of the fit of data shown in Fig. 1 **a**–**f**. Letters (a–d) above bars in (**b**) represent significant differences ($p < 0.05$) between strains based on one-way ANOVA analysis.

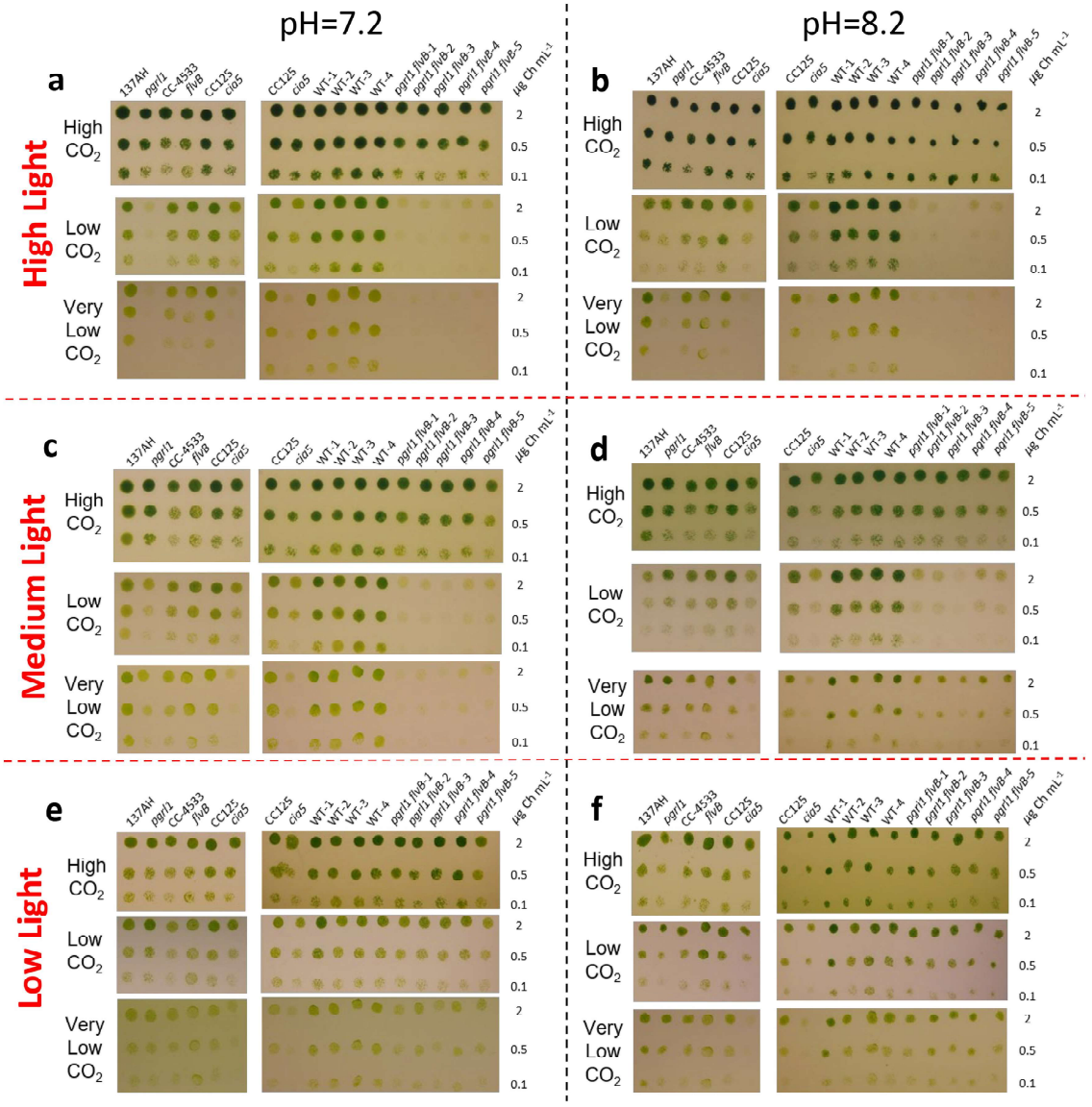

Extended Data Fig. 3 | Growth of *pgrl1*, *flvB*, *pgrl1flvB* mutants and their control strains. Cells were spotted on plates containing minimal medium at pH 7.2 (**a**, **c**, **e**) or pH 8.2 (**b**, **d**, **f**) and grown under continuous high light (100 µmol photon m^{-2} s^{-1}, **a**, **b**), medium light (60 µmol photon m^{-2} s^{-1}, **c**, **d**) or low light (30 µmol photon m^{-2} s^{-1}, **e**, **f**). For each pH and light conditions, cells were grown either at 100 ppm CO_2 (Very low CO_2), 400 ppm CO_2 (Low CO_2) or 3% of CO_2 (High CO_2). Growth was assessed in *pgrl1*, *flvB*, and their respective control strains (137AH and CC-4533) (left panels) and on double mutants (*pgrl1flvB*-1 to -5) and their control strains (WT-1 to -4) (right panels); the CCM1 mutant *cia5* was introduced as a CCM-deficient control together with its reference strain CC-125. Shown are representative spot tests of n = 10 independent experiments.

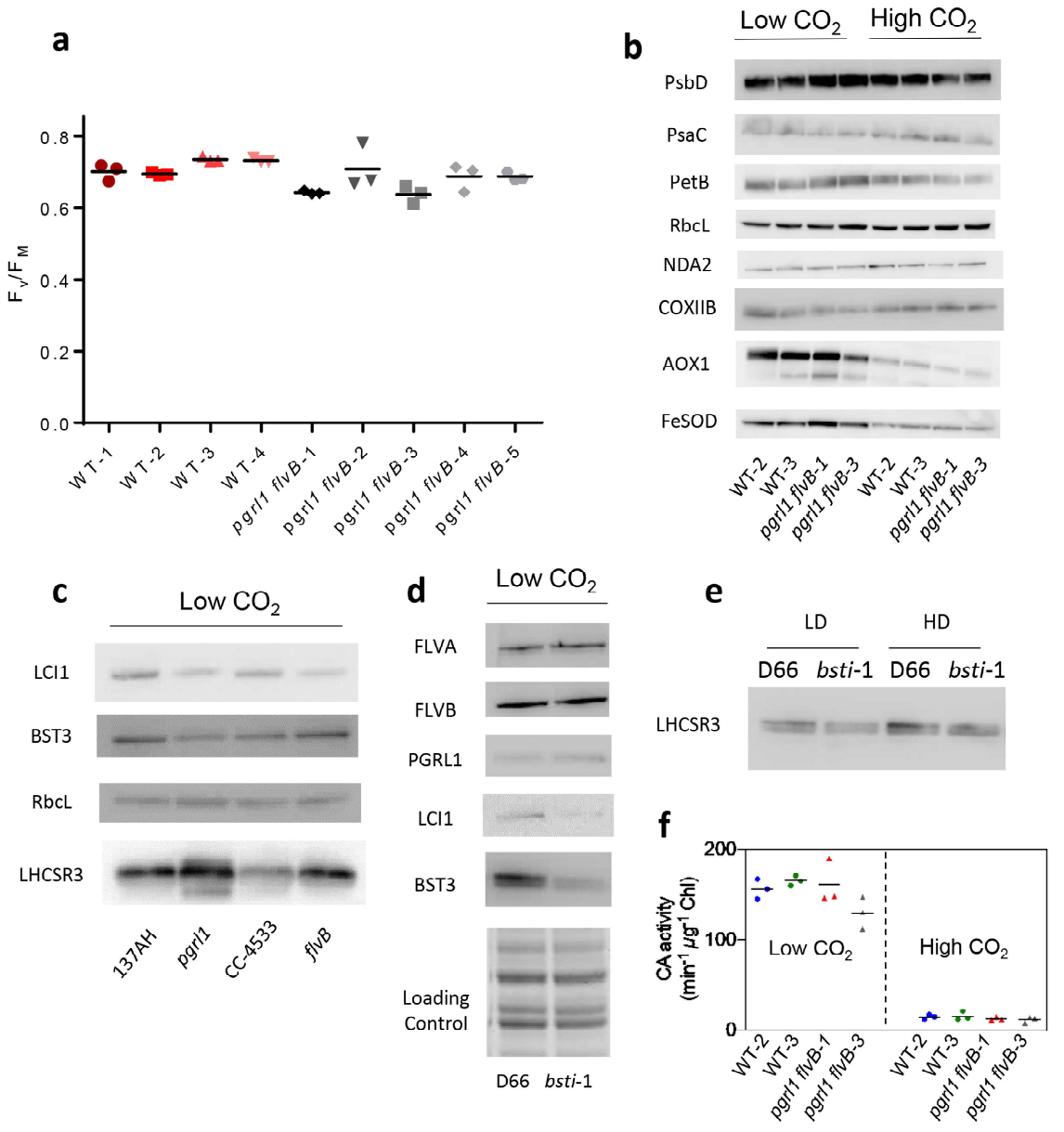

Extended Data Fig. 4 | Photosynthesis and CCM components assessment. **a**, Maximum PSII efficiency (F_V/F_M) of double mutants (*pgrl1 flvB*-1 to -5) and their control strains (WT-1 to -4), measured using a PAM fluorimeter after 15 min dark adaptation. **b**, Immunodetection of the PSII subunit PsbD, the PSI subunit PsaC, the cytochrome b_6f complex subunit PetB, the large Rubisco subunit RbcL, the type II NADH dehydroagenase NDA2, the mitochondrial cytochrome *aa3* oxidase subunit CoxIIB, of the alternative oxidase AOX1, and of the Fe superoxide dismutase FeSOD, in two independent *pgrl1 flvB* double mutants and controls grown under Low CO_2 or High CO_2. **c**, Immunodetection of LCI1, BST3, RbcL and LHCSR3 in *pgrl1*, *flvB*, and their respective control strains (137AH and CC-4533). **d**, Immunodetection of FLVA, FLVB, PGRL1, LCI1, and BST3 in *bsti*-1 and its control strain (D66) at low density. **e**, Immunodetection of LHCSR3 in *bsti-1* and its control strain (D66) cultivated at low (LD, 6 µg chlorophyll. mL^{-1}) or high (LD, 12 µg chlorophyll. mL^{-1}) cell density. When cultivating algae at different cell densities, which affects light and CO_2 availability (two factors known to modulate LHCSR3 accumulation), we observed that *bsti*-1 accumulates lower LHCSR3 levels as compared to D66 at LD, but similar levels at HD. Data shown in **b**–**e** have been reproduced with n = 2 independent experiments. **f**, Carbonic anhydrase (CA) activity was determined *in vivo* by following the unlabelling of ^{18}O-enriched CO_2 in the same strains and conditions as in Fig. 2 **b**. Shown are mean values and replicates (n = 3 biologically independent sample).

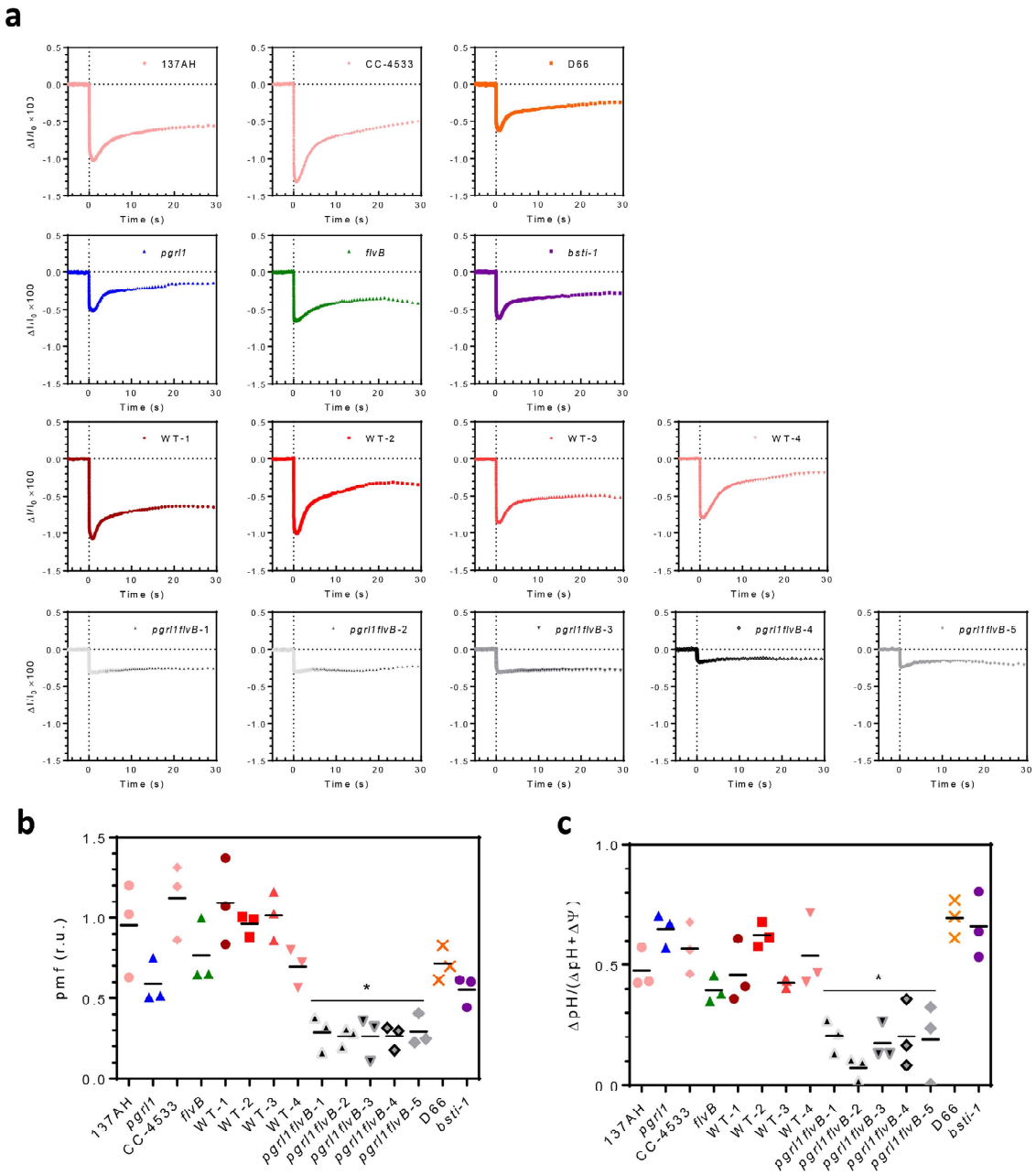

Extended Data Fig. 5| Electrochromic carotenoid absorbance changes measurements and *pmf* size and partitioning between ΔpH and ΔΨ. ECS signal was measured upon light to dark transition after 2 min red light illumination (500 µmol photons $m^2 s^{-1}$) in the presence of 1mM $NaHCO_3$. **a**, Typical ECS traces are shown for single mutants (*pgrl1*, *flvB* and *bsti-1*), their control strains (137AH, CC-4533 and D66 respectively), for double mutants (*pgrl1flvB-1* to -5) and their controls (WT-1 to -4). Light was turned off at t = 0. **b**, relative *pmf* size was determined for each strain. **c**. Proportion of ΔpH in the *pmf* was determined for each strain. Shown are means and replicate values (n = 3 biologically independent sample). *pgrl1flvB* double mutants showed a significantly lower *pmf* and ΔpH as compared to simple mutants and control strains ($p < 0.05$, one way ANOVA).

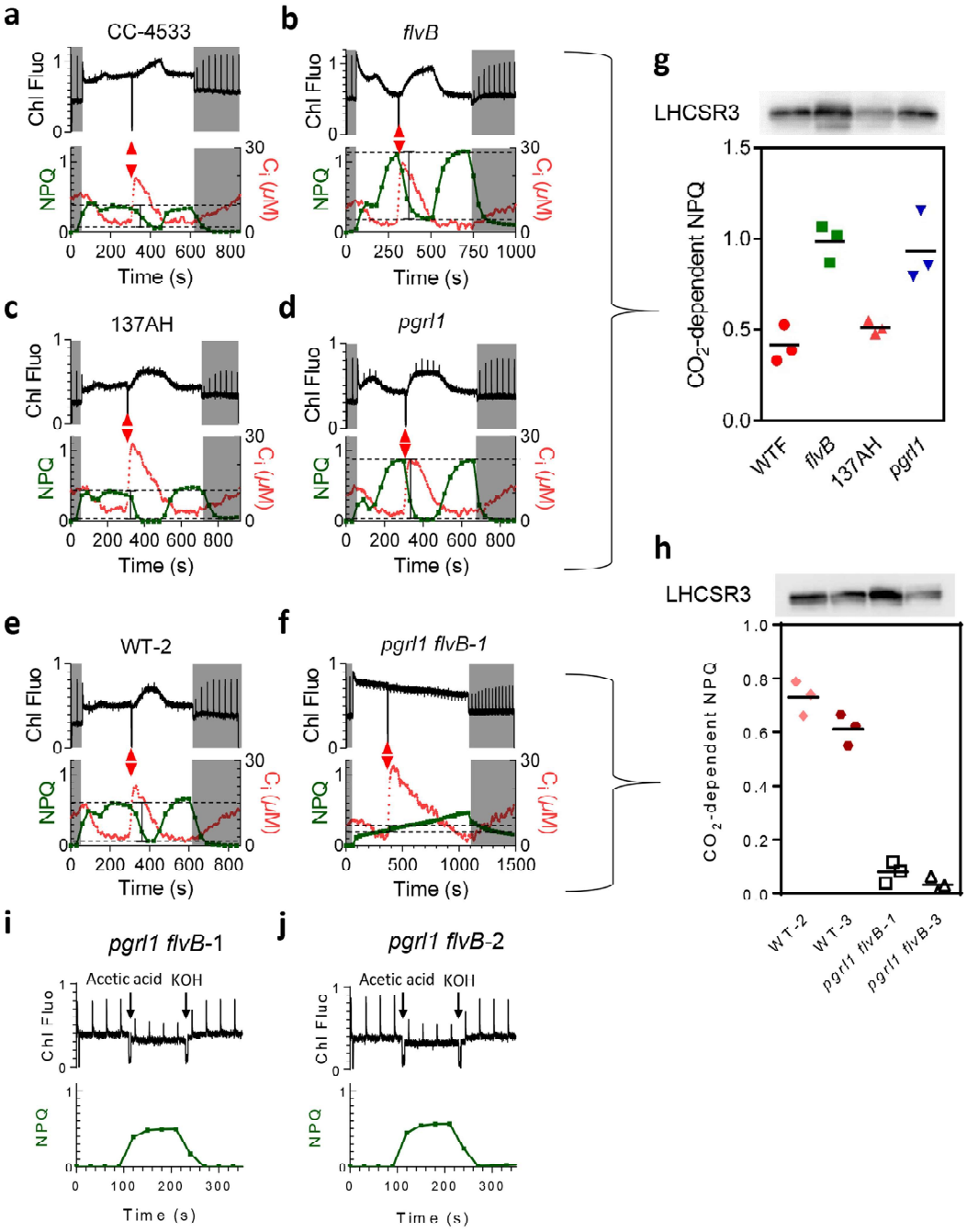

Extended Data Fig. 6 | Chlorophyll fluorescence, NPQ and C_i measured during dark-light-dark transients in *pgrl1*, *flvB*, *pgrl1flvB* and their respective controls. a–f, Chlorophyll fluorescence patterns (upper panels), NPQ and C_i measurements (lower panels). Shown are representative experiments of three biological replicates. **g**, **h**, CO_2-dependent NPQ was determined by subtracting the NPQ value measured after C_i injection from the NPQ value measured upon the initial C_i depletion as indicated by dotted lines (**a–f**). Immunodetection of LHCSR3 is shown on top of each corresponding strain. Shown are mean values and replicates (n = 3 biologically independent sample). All strains were grown as in Fig. 1 under low CO_2. Red arrows indicate addition of bicarbonate. **i**, **j**, *pgrl1flvB* double mutants have maintained a full qE potential. Chlorophyll fluorescence and NPQ were measured in *pgrl1flvB*-1 and *pgrl1flvB*-2 following the addition of acetic acid (13 mM) decreasing the pH to 5.5 and further addition of KOH (13 mM) according to the experimental protocol described in ref. [34] of the main text. Shown are representative experiments of three biological replicates.

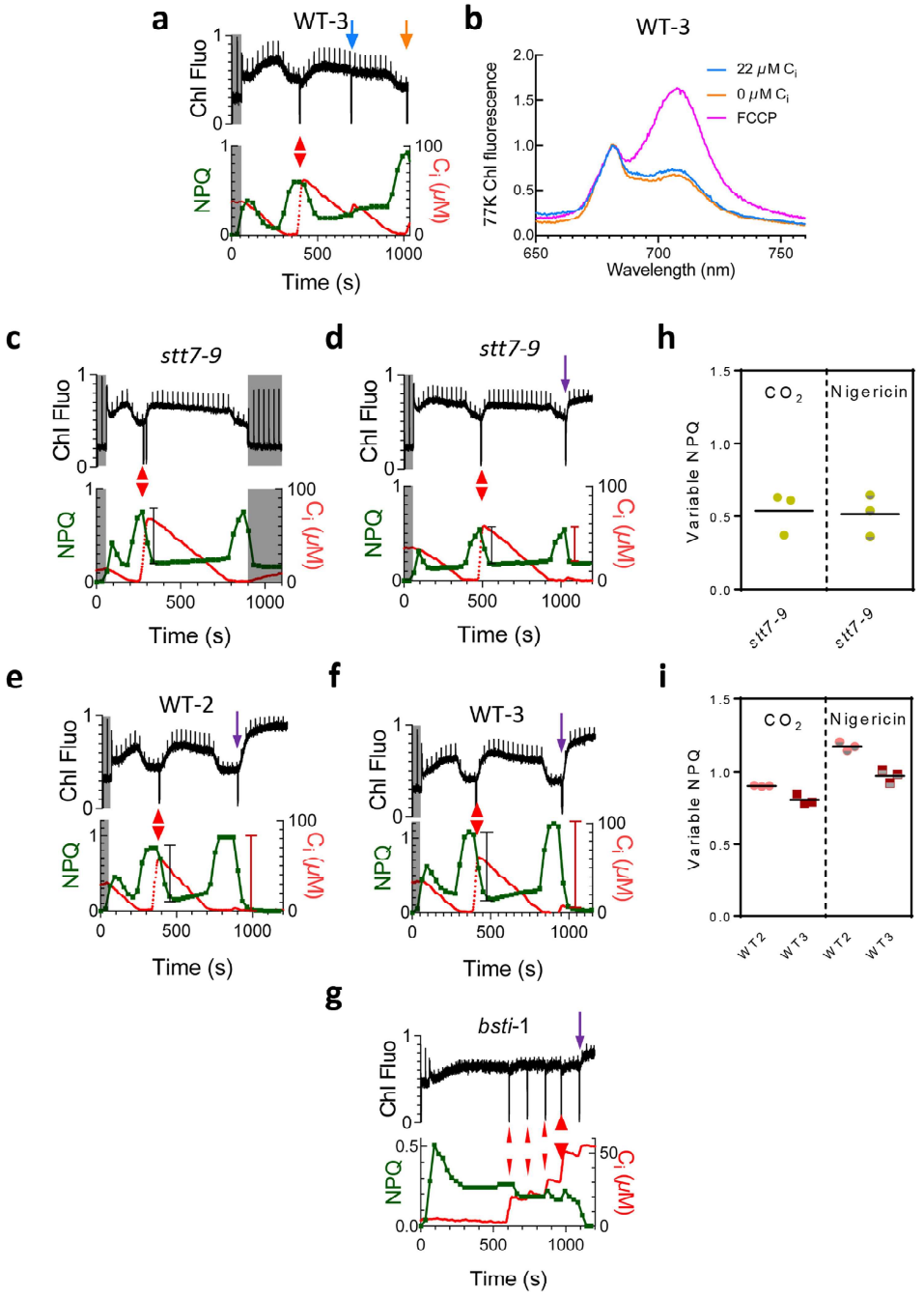

Extended Data Fig. 7 | See next page for caption.

Annex IV

Article

Extended Data Fig. 7 | C_i-dependent NPQ variations are independent of state transition and linked with trans-thylakoidal ΔpH. a, **b**, 77K chlorophyll fluorescence spectra were measured during C_i depletion in the control strain WT3. Samples were taken at 22 µM C_i (blue arrow, **a**) and 0 µM C_i (orange arrow, **a**) and 77K chlorophyll fluorescence spectra were recorded (**b**). Addition of carbonyl cyanide trifluoromethoxy phenylhydrazone (FCCP, 5 µM) was used as a control to induce state 2 (pink curve). Shown are representative experiments of n = 3 biologically independent sample. **a**, **c**–**g**, Chlorophyll fluorescence patterns (upper panels), NPQ and C_i measurements (lower panels) in control strains, the state transition mutant *stt7-9* and *bsti-1* mutant during C_i depletion in the light followed either by a dark period (**a**, **c**) or subsequent addition of the uncoupler nigericin (10 µM, purple arrow) (**d**–**g**). Shown are representative experiments of n = 3 biologically independent sample. (**H, I**) CO_2-dependent NPQ was determined as described in Extended Data Fig. 5 (black bar, **c**–**f**). Nigericin-dependent NPQ was determined from NPQ values measured before and after nigericin addition (red bars, **d**–**f**). All strains were grown as in Fig. 1 under low CO_2. Red arrows indicate addition of bicarbonate.

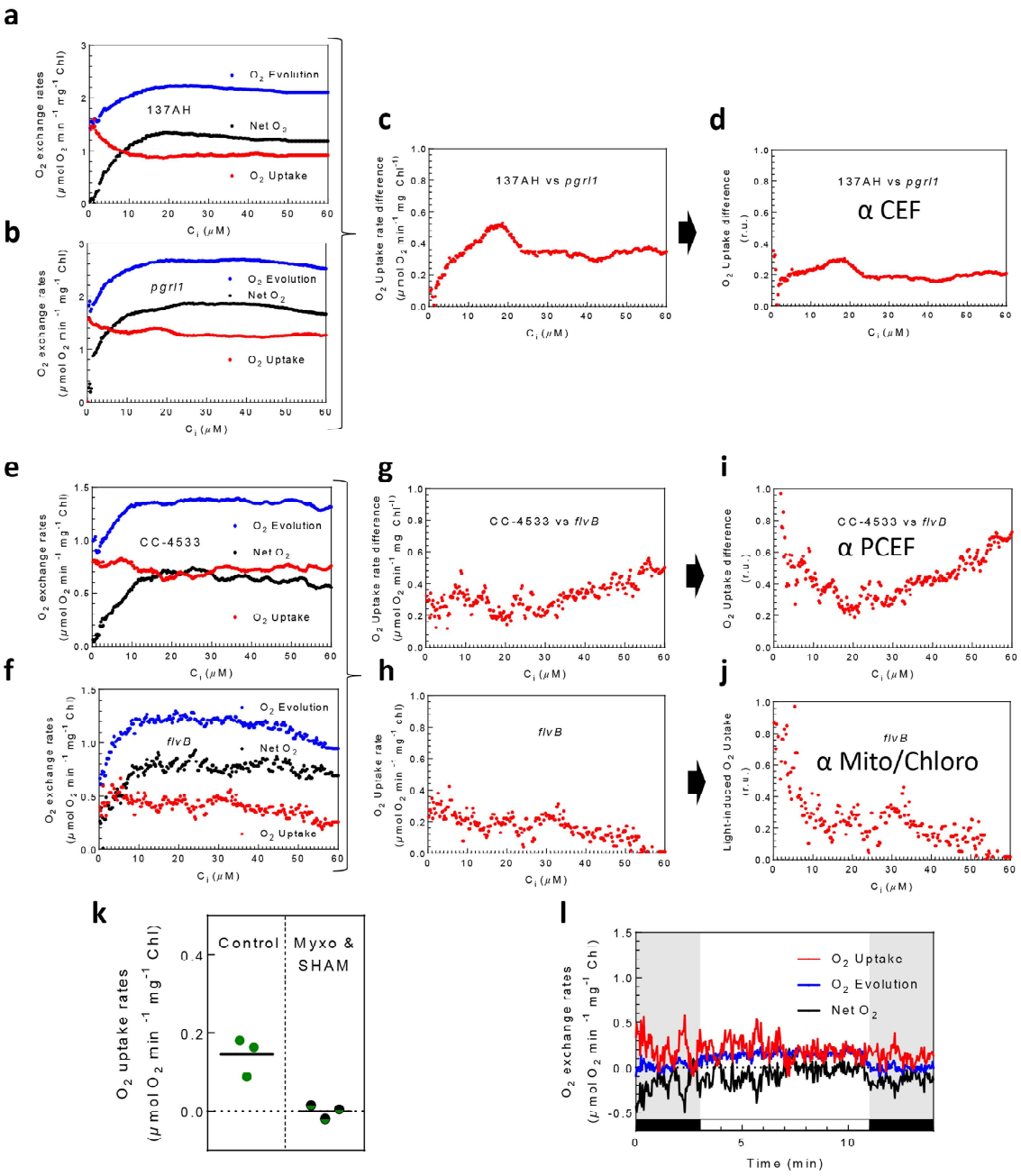

Extended Data Fig. 8 | See next page for caption.

Annex IV

Article

Extended Data Fig. 8 | C_i dependency of O_2 exchange rates measured by using MIMS in the presence of $^{18}O_2$-enriched O_2 in *pgrl1*, *flvB* and their respective controls. Strains were grown under low CO_2 as in Fig. 1. **a**, **b**, O_2 exchange rates in *pgrl1* and its control strain 137AH. **c**, Difference in O_2 uptake rates between 137AH and *pgrl1*. **d**, Difference in O_2 uptake rates as determined in (**c**) normalized to the net O_2 production of *pgrl1* is used to determine the CEF contribution (**e**, **f**) O_2 exchange rates in *flvB* and its control strain (CC-4533). **g**, Difference in O_2 uptake rates between CC-4533 and *flvB*. **h**, Light-induced O_2 uptake in *flvB* mutant. **i**, The difference in O_2 uptake rates as determined in (**g**) normalized to the net O_2 production in *flvB* is used to determine the contribution of PCEF. **j**, the difference in O_2 uptake rates as determined in (**h**) normalized to the net O_2 production in *flvB* is used to determine the contribution of CMEF. **k**, Effect of the mitochondrial respiration inhibitors myxothiazol and SHAM on the light-induced O_2 uptake rate measured in *flvB* mutant at low C_i after 3 min of illumination. Shown are mean values and replicates (n = 3 biologically independent sample). **l**, Effect of myxothiazol and SHAM on O_2 exchange rates in *pgrl1 flvB*-1 double mutant. Shown are representative exchange rates from 3 independent replicates. The full inhibition of photosynthetic O_2 exchange observed in these conditions reflects the requirement of CO_2 fixation for additional ATP supply by CEF, PCEF and CMEF.

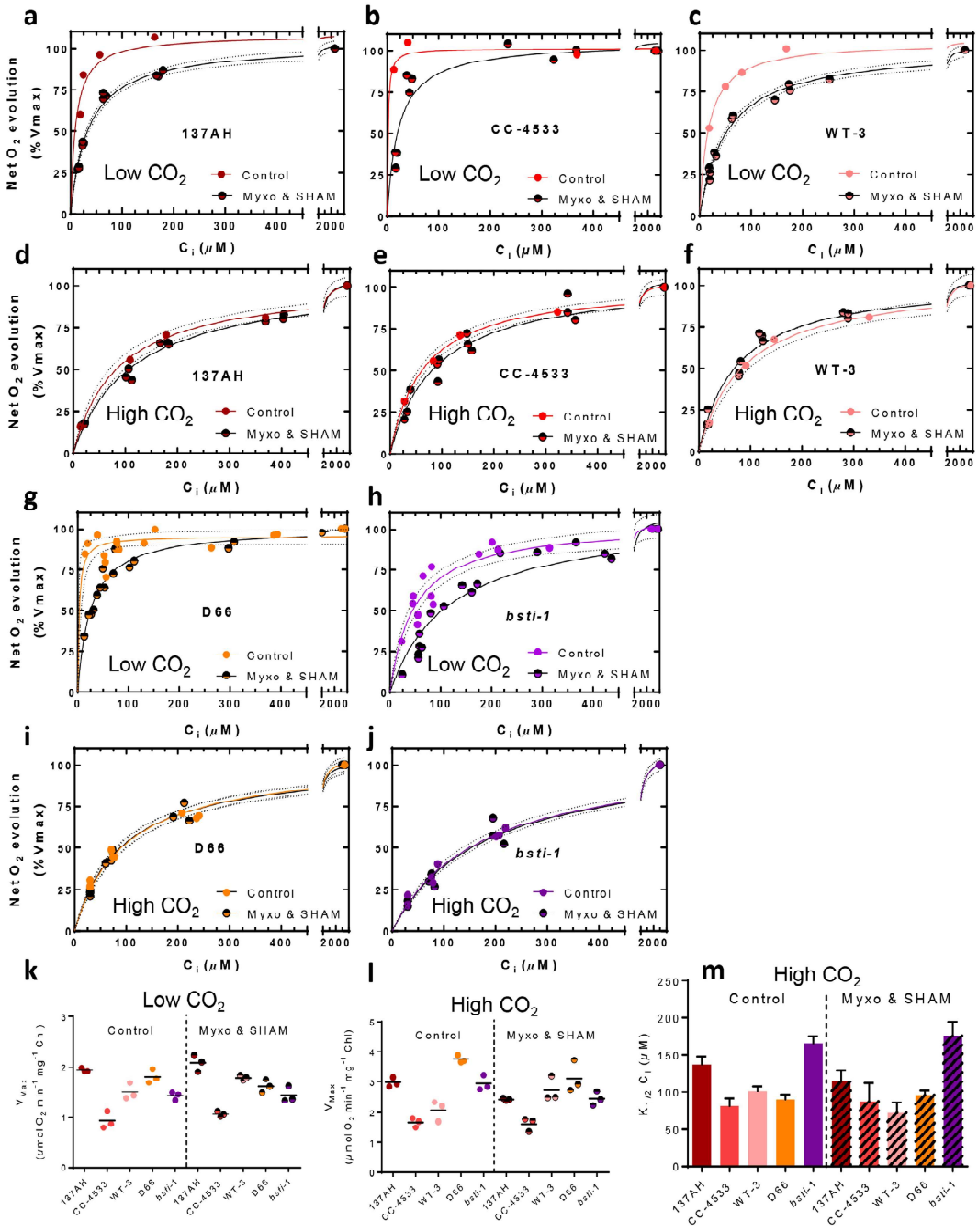

Extended Data Fig. 9 | Effect of mitochondrial respiration inhibitors on the C_i affinity of net O_2 photosynthesis. Photosynthetic net O_2 production was measured as in Fig. 1 in low CO_2 (**a**, **b**, **c**, **g**, **h**, **k**) or high CO_2 (**d**, **e**, **f**, **i**, **j**, **l**) grown cells in the absence or presence of the two mitochondrial respiration inhibitors myxothiazol (Myxo, 2.5 μM) and salicylhydroxamic acid (SHAM, 400 μM). **a–j**, For each replicate, net O_2 production was measured at four different concentrations of C_i and normalized to the maximum photosynthetic net O_2 production. Shown are three replicates for each strain (dots) and hyperbolic fit with variability (plain lines, dotted lines). **k, l**, Maximum net O_2 production rates. Shown are mean values and replicates (n = 3 Shown are mean values and replicates (n = 3 biologically independent sample). **m**, $K_{1/2}$ C_i values of high CO_2 grown cells in the absence or presence of myxothiazol and SHAM. Shown are mean values ±SD of the fit of data shown in Extended Data Fig. 9 d–f, i, j.

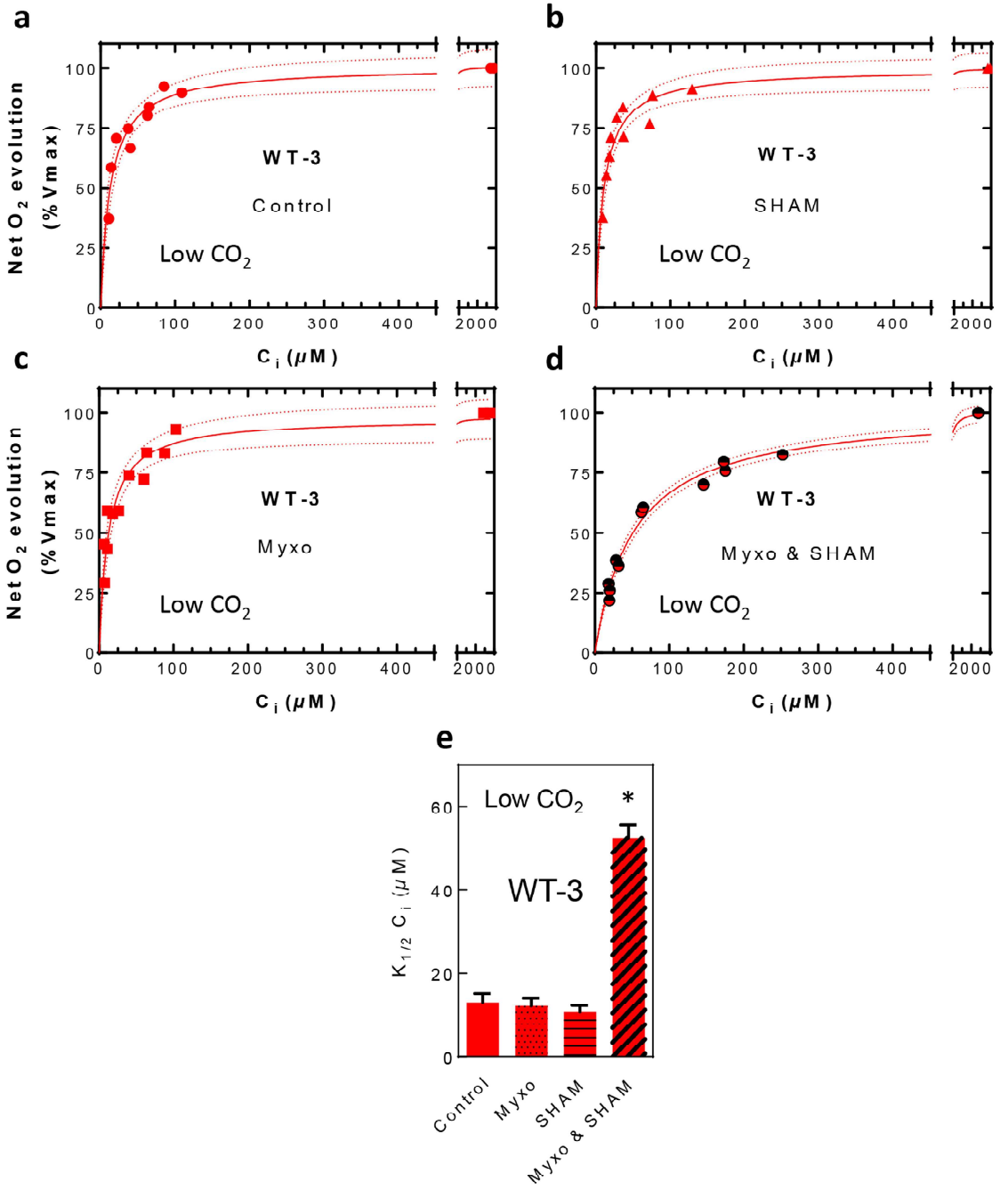

Extended Data Fig. 10 | Effects of respiratory inhibitors myxothiazol and SHAM added separately or simultaneously on the C_i affinity of net O_2 photosynthesis. Photosynthetic net O_2 production was measured as in Fig. 1 in WT-3 low CO_2 grown cells in the absence or in the presence of respiratory inhibitors. **a**, In the absence of inhibitors. **b**, in the presence of 400 μM SHAM. **c**, in the presence of 2.5 μM myxothiazol. **d**, in the presence of both 2.5 μM myxothiazol and 400 μM SHAM. Data shown on **a–d** are from n = 3 biologically independent sample (dots) and hyperbolic fit with variability (plain lines, dotted lines). **e**, $K_{1/2}$ values were determined from hyperbolic fits. Shown are mean ± SD of the fit of experimental data shown in **a–d**. Asterisk represent significant difference ($p < 0.05$, multiple t-test).

Annex IV

nature research

Corresponding author(s): Gilles Peltier

Last updated by author(s): Feb 4, 2022

Reporting Summary

Nature Research wishes to improve the reproducibility of the work that we publish. This form provides structure for consistency and transparency in reporting. For further information on Nature Research policies, see our Editorial Policies and the Editorial Policy Checklist.

Statistics

For all statistical analyses, confirm that the following items are present in the figure legend, table legend, main text, or Methods section.

n/a	Confirmed	
☐	☒	The exact sample size (*n*) for each experimental group/condition, given as a discrete number and unit of measurement
☐	☒	A statement on whether measurements were taken from distinct samples or whether the same sample was measured repeatedly
☐	☒	The statistical test(s) used AND whether they are one- or two-sided *Only common tests should be described solely by name; describe more complex techniques in the Methods section.*
☒	☐	A description of all covariates tested
☐	☒	A description of any assumptions or corrections, such as tests of normality and adjustment for multiple comparisons
☐	☒	A full description of the statistical parameters including central tendency (e.g. means) or other basic estimates (e.g. regression coefficient) AND variation (e.g. standard deviation) or associated estimates of uncertainty (e.g. confidence intervals)
☐	☒	For null hypothesis testing, the test statistic (e.g. *F*, *t*, *r*) with confidence intervals, effect sizes, degrees of freedom and *P* value noted *Give P values as exact values whenever suitable.*
☒	☐	For Bayesian analysis, information on the choice of priors and Markov chain Monte Carlo settings
☒	☐	For hierarchical and complex designs, identification of the appropriate level for tests and full reporting of outcomes
☒	☐	Estimates of effect sizes (e.g. Cohen's *d*, Pearson's *r*), indicating how they were calculated

Our web collection on statistics for biologists contains articles on many of the points above.

Software and code

Policy information about availability of computer code

Data collection	MIMS data was acquired using the Thermo-Fisher commercial software (Gasworks, v1.0) for mass spectrometers.
Data analysis	The software used to treat MIMS data was previsously published (Burlacot et al, 2020, Frontiers in Plant Science) and available at: https://github.com/francoisBurlacot/MIMS_Analysis. Additionally, Prism 6 for windows (v6.07) was used to generate figures, fit curves and perform statistical analysis.

For manuscripts utilizing custom algorithms or software that are central to the research but not yet described in published literature, software must be made available to editors and reviewers. We strongly encourage code deposition in a community repository (e.g. GitHub). See the Nature Research guidelines for submitting code & software for further information.

Data

Policy information about availability of data

All manuscripts must include a data availability statement. This statement should provide the following information, where applicable:

- Accession codes, unique identifiers, or web links for publicly available datasets
- A list of figures that have associated raw data
- A description of any restrictions on data availability

All data needed to evaluate the conclusions in the paper are present in the paper and/or the Supplementary Materials.

Annex IV

Field-specific reporting

Please select the one below that is the best fit for your research. If you are not sure, read the appropriate sections before making your selection.

☒ Life sciences ☐ Behavioural & social sciences ☐ Ecological, evolutionary & environmental sciences

For a reference copy of the document with all sections, see nature.com/documents/nr-reporting-summary-flat.pdf

Life sciences study design

All studies must disclose on these points even when the disclosure is negative.

Sample size	No sample size calculations were performed. The sample size (n) of each experiment is provided in the corresponding figure captions in the main manuscript and supplementary information files. Sample sizes were chosen to support meaningful conclusions based on previous publications of similar experiments including: Gas exchange measurements doi.org/10.1073/pnas.1915276117 Chlorophyll fluorescence measurements doi.org/10.1104/pp.17.00421 Growth test doi.org/10.1104/pp.17.00421 ECS measurements doi.org/10.1016/j.bbabio.2019.01.004
Data exclusions	No data was excluded from the analyses.
Replication	All replicates shown are biological replicates from independent cultures. Each experiment was replicated at least three times independently, each replication was successful. Number of independent replication is state on each corresponding figure.
Randomization	Microalgal cells of different genetic background where analyzed in a random order as for replications of experiments with no formal randomization technique.
Blinding	Investigators were not blinded during experiments as it does not include clinical trials. The research materials being microalgae, the blind design is not applicable in our field. Researchers were not blinded to algal genotypes during experiments but experiments were conducted by different authors, whenever possible.

Reporting for specific materials, systems and methods

We require information from authors about some types of materials, experimental systems and methods used in many studies. Here, indicate whether each material, system or method listed is relevant to your study. If you are not sure if a list item applies to your research, read the appropriate section before selecting a response.

Materials & experimental systems

n/a	Involved in the study
☐	☒ Antibodies
☒	☐ Eukaryotic cell lines
☒	☐ Palaeontology and archaeology
☒	☐ Animals and other organisms
☒	☐ Human research participants
☒	☐ Clinical data
☒	☐ Dual use research of concern

Methods

n/a	Involved in the study
☒	☐ ChIP-seq
☒	☐ Flow cytometry
☒	☐ MRI-based neuroimaging

Antibodies

Antibodies used	Immunodetection was performed using antibodies raised against recombinant PGRL1 (1:1000, dilution), FLVB (1:1000, dilution) and FLVA(1:1000, dilution), NDA2(1:5000, dilution). Other antibodies against PsbD (AS06 146)(1:10000, dilution), PsaC (AS10 939)(1:1000, dilution), Cytb6 (AS03-034)(1:10000, dilution), RbcL (AS03 037)(1:5000, dilution), ATP-B (AS05-085)(1:5000, dilution), COXIIB (AS06 151)(1:5000, dilution), AOX1 (AS06 152)(1:2000, dilution), FeSOD (AS06-125)(1:1000, dilution), EPYC1 (AS09-602)(1:500, dilution), LHCSR3 (AS14-2766)(1:500, dilution), CAH1/ 2 (AS11-1737) (1:1000, dilution) and CAH3 (AS05 073)(1:2000, dilution) were obtained from Agrisera (https://www.agrisera.com/). The LCIC antibody (1:1000, dilution) was generated for this study against a synthetic peptide containing the sequence of 12 amino acids found in the C-terminus of LCIC. Two rabbits were injected with the synthetic peptide for the production of LCIC antibody. BST3 (1:500, dilution) antibody is a kind gift from Pr. Luke Mackinder (University of York, England), LCI1 (1:500, dilution) and LCIA (1:2500, dilution) antibodies are a kind gift of Pr. Hideya Fukuzawa (Kyoto University, Japan).
Validation	Validation of all antibodies has been done in previous studies. In short, the validation of antibodies was performed in vivo for non-commercial antibodies by using mutants of the green microalgae Chlamydomonas reinhardtii for anti PGRL1 (1), FLVA and FLVB (2), NDA2 (3), LCIC (4), BST3 (5), LCI1 (6), LCIA (7). For other antibodies bought from Agrisera (https://www.agrisera.com/), the reactivity of the antibodies have been confirmed on Chlamydomonas whole cell extract.

1 Tolleter, D. et al. Control of hydrogen photoproduction by the proton gradient generated by cyclic electron flow in Chlamydomonas reinhardtii. Plant Cell 23, 2619-2630, doi:10.1105/tpc.111.086876 (2011).
2 Chaux, F. et al. Flavodiiron proteins promote fast and transient O2 photoreduction in Chlamydomonas. Plant Physiol. 174, 1825-1836, doi:10.1104/pp.17.00421 (2017).
3 Desplats, C. et al. Characterization of Nda2, a plastoquinone-reducing type II NAD(P)H dehydrogenase in Chlamydomonas chloroplasts. J. Biol. Chem. 284, 4148-4157, doi:10.1074/jbc.M804546200 (2009).
4 Yamano, T. et al. Light and Low-CO2-Dependent LCIB–LCIC complex localization in the chloroplast supports the carbon-concentrating mechanism in Chlamydomonas reinhardtii. Plant Cell Physiol. 51, 1453-1468, doi:10.1093/pcp/pcq105 (2010).
5 Mukherjee, A. et al. Thylakoid localized bestrophin-like proteins are essential for the CO2 concentrating mechanism of Chlamydomonas reinhardtii. Proc. Nat. Acad. Sci. U. S. A. 116, 16915-16920, doi:10.1073/pnas.1909706116 (2019).
6 Ohnishi, N. et al. Expression of a low CO2–inducible protein, LCI1, increases inorganic carbon uptake in the green alga Chlamydomonas reinhardtii. Plant Cell 22, 3105-3117, doi:10.1105/tpc.109.071811 (2010).
7 Yamano, T., Sato, E., Iguchi, H., Fukuda, Y. & Fukuzawa, H. Characterization of cooperative bicarbonate uptake into chloroplast stroma in the green alga Chlamydomonas reinhardtii. Proc. Nat. Acad. Sci. 112, 7315-7320, doi:10.1073/pnas.1501659112 (2015).

References

Aboelmy MH, Peterhansel C (2014) Enzymatic characterization of Chlamydomonas reinhardtii glycolate dehydrogenase and its nearest proteobacterial homologue. Plant Physiology and Biochemistry **79**: 25–30

Adler L, Díaz-Ramos A, Mao Y, Pukacz KR, Fei C, McCormick AJ (2022) New horizons for building pyrenoid-based CO2-concentrating mechanisms in plants to improve yields. Plant Physiology kiac373

Alberts B, Johnson A, Lewis J, Raff M, Roberts K, Walter P (2002) The Compartmentalization of Cells. Molecular Biology of the Cell. 4th edition

Allen JF (1975) Oxygen reduction and optimum production of ATP in photosynthesis. Nature **256**: 599–600

Allen JF (2002) Photosynthesis of ATP—Electrons, Proton Pumps, Rotors, and Poise. Cell **110**: 273–276

Allen JF (2003) Cyclic, pseudocyclic and noncyclic photophosphorylation: new links in the chain. Trends in Plant Science **8**: 15–19

Alric J (2014) Redox and ATP control of photosynthetic cyclic electron flow in Chlamydomonas reinhardtii: (II) Involvement of the PGR5–PGRL1 pathway under anaerobic conditions. Biochimica et Biophysica Acta (BBA) - Bioenergetics **1837**: 825–834

Alric J, Johnson X (2017) Alternative electron transport pathways in photosynthesis: a confluence of regulation. Current Opinion in Plant Biology **37**: 78–86

Arkblad EL, Betsholtz C, Mandoli D, Rydström J (2001) Characterization of a nicotinamide nucleotide transhydrogenase gene from the green alga Acetabularia acetabulum and comparison of its structure with those of the corresponding genes in mouse and Caenorhabditis elegans1Nucleotide sequences have been submitted to GenBank and assigned the accession numbers AF257137–AF257157, AY007197, AF325205–AF325208.1. Biochimica et Biophysica Acta (BBA) - Gene Structure and Expression **1520**: 115–123

Atkinson N, Feike D, Mackinder LCM, Meyer MT, Griffiths H, Jonikas MC, Smith AM, McCormick AJ (2016) Introducing an algal carbon-concentrating mechanism into higher plants: location and incorporation of key components. Plant Biotechnol J **14**: 1302–1315

Atteia A, Adrait A, Brugière S, Tardif M, van Lis R, Deusch O, Dagan T, Kuhn L, Gontero B, Martin W, et al (2009) A Proteomic Survey of Chlamydomonas reinhardtii Mitochondria Sheds New Light on the Metabolic Plasticity of the Organelle and on the Nature of the α-Proteobacterial Mitochondrial Ancestor. Mol Biol Evol **26**: 1533–1548

Backhausen JE, Scheibe R (1999) Adaptation of tobacco plants to elevated CO2: influence of leaf age on changes in physiology, redox states and NADP-malate dehydrogenase activity. Journal of Experimental Botany **50**: 665–675

Badger MR, von Caemmerer S, Ruuska S, Nakano H (2000) Electron flow to oxygen in higher plants and algae: rates and control of direct photoreduction (Mehler reaction) and rubisco oxygenase. Philos Trans R Soc Lond B Biol Sci **355**: 1433–1446

Baikie TK, Wey LT, Lawrence JM, Medipally H, Reisner E, Nowaczyk MM, Friend RH, Howe CJ, Schnedermann C, Rao A, et al (2023) Photosynthesis re-wired on the pico-second timescale. Nature **615**: 836–840

Bailleul B, Berne N, Murik O, Petroutsos D, Prihoda J, Tanaka A, Villanova V, Bligny R, Flori S, Falconet D, et al (2015) Energetic coupling between plastids and mitochondria drives CO_2 assimilation in diatoms. Nature **524**: 366–369

Basso L, Sakoda K, Kobayashi R, Yamori W, Shikanai T (2022) Flavodiiron proteins enhance the rate of CO2 assimilation in Arabidopsis under fluctuating light intensity. Plant Physiology kiac064

Bauwe H (2023) Photorespiration – Rubisco's repair crew. Journal of Plant Physiology **280**: 153899

Bauwe H, Hagemann M, Fernie AR (2010) Photorespiration: players, partners and origin. Trends in Plant Science **15**: 330–336

Blaby IK, Blaby-Haas CE, Pérez-Pérez ME, Schmollinger S, Fitz-Gibbon S, Lemaire SD, Merchant SS (2015) Genome-wide analysis on Chlamydomonas reinhardtii reveals the impact of hydrogen peroxide on protein stress responses and overlap with other stress transcriptomes. The Plant Journal **84**: 974–988

Blaby IK, Glaesener AG, Mettler T, Fitz-Gibbon ST, Gallaher SD, Liu B, Boyle NR, Kropat J, Stitt M, Johnson S, et al (2013) Systems-level analysis of nitrogen starvation-induced modifications of carbon metabolism in a Chlamydomonas reinhardtii starchless mutant. Plant Cell **25**: 4305–4323

Bonente G, Ballottari M, Truong TB, Morosinotto T, Ahn TK, Fleming GR, Niyogi KK, Bassi R (2011) Analysis of LhcSR3, a Protein Essential for Feedback De-Excitation in the Green Alga Chlamydomonas reinhardtii. PLOS Biology **9**: e1000577

Boschetti A, Schmid K (1998) Energy Supply for ATP-Synthase Deficient Chloroplasts of Chlamydomonas reinhardii. Plant Cell Physiol **39**: 160–168

Boyle NR, Page MD, Liu B, Blaby IK, Casero D, Kropat J, Cokus SJ, Hong-Hermesdorf A, Shaw J, Karpowicz SJ, et al (2012) Three Acyltransferases and Nitrogen-responsive Regulator Are Implicated in Nitrogen Starvation-induced Triacylglycerol Accumulation in Chlamydomonas*. Journal of Biological Chemistry **287**: 15811–15825

Buchert F, Mosebach L, Gäbelein P, Hippler M (2020) PGR5 is required for efficient Q cycle in the cytochrome b6f complex during cyclic electron flow. Biochemical Journal **477**: 1631–1650

Buchert F, Scholz M, Hippler M (2022) Electron transfer via cytochrome b 6 f complex displays sensitivity to Antimycin A upon STT7 kinase activation. Biochemical Journal. doi: 10.1042/BCJ20210802

Burlacot A, Burlacot F, Li-Beisson Y, Peltier G (2020) Membrane Inlet Mass Spectrometry: A Powerful Tool for Algal Research. Front Plant Sci **11**: 1302

Burlacot A, Dao O, Auroy P, Cuiné S, Li-Beisson Y, Peltier G (2022) Alternative photosynthesis pathways drive the algal CO2-concentrating mechanism. Nature 1–6

Burlacot A, Peltier G (2023) Energy crosstalk between photosynthesis and the algal CO2-concentrating mechanisms. Trends in Plant Science. doi: 10.1016/j.tplants.2023.03.018

Burlacot A, Peltier G, Li-Beisson Y (2019) Subcellular Energetics and Carbon Storage in Chlamydomonas. Cells **8**: 1154

Burlacot A, Sawyer A, Cuiné S, Auroy-Tarrago P, Blangy S, Happe T, Peltier G (2018) Flavodiiron-Mediated O2 Photoreduction Links H2 Production with CO2 Fixation during the Anaerobic Induction of Photosynthesis. Plant Physiol **177**: 1639–1649

Busch FA, Sage RF, Farquhar GD (2018) Plants increase CO2 uptake by assimilating nitrogen via the photorespiratory pathway. Nat Plants **4**: 46–54

Calatrava V, Tejada-Jimenez M, Sanz-Luque E, Fernandez E, Galvan A, Llamas A (2023) Chlamydomonas reinhardtii, a Reference Organism to Study Algal–Microbial Interactions: Why Can't They Be Friends? Plants **12**: 788

Canvin DT (1981) Photorespiration and Nitrogen Metabolism. *In* JD Bewley, ed, Nitrogen and Carbon Metabolism: Proceedings of a Symposium on the Physiology and Biochemistry of Plant Productivity, held in Calgary, Canada, July 14–17, 1980. Springer Netherlands, Dordrecht, pp 178–194

Cardol P, Gloire G, Havaux M, Remacle C, Matagne R, Franck F (2003) Photosynthesis and State Transitions in Mitochondrial Mutants of Chlamydomonas reinhardtii Affected in Respiration. Plant Physiology **133**: 2010–2020

Cavanagh AP, South PF, Bernacchi CJ, Ort DR (2022) Alternative pathway to photorespiration protects growth and productivity at elevated temperatures in a model crop. Plant Biotechnology Journal **20**: 711–721

Champigny ML (1995) Integration of photosynthetic carbon and nitrogen metabolism in higher plants. Photosynth Res **46**: 117–127

Chauvin L, Tural B, Moroney JV (2008) Chlamydomonas reinhardtii Has Genes For Both Glycolate Oxidase and Glycolate Dehydrogenase. *In* JF Allen, E Gantt, JH Golbeck, B Osmond, eds, Photosynthesis. Energy from the Sun. Springer Netherlands, Dordrecht, pp 823–827

Chaux F, Burlacot A, Mekhalfi M, Auroy P, Blangy S, Richaud P, Peltier G (2017a) Flavodiiron Proteins Promote Fast and Transient O2 Photoreduction in Chlamydomonas. Plant Physiology **174**: 1825–1836

Chaux F, Johnson X, Auroy P, Beyly-Adriano A, Te I, Cuiné S, Peltier G (2017b) PGRL1 and LHCSR3 Compensate for Each Other in Controlling Photosynthesis and Avoiding Photosystem I Photoinhibition during High Light Acclimation of Chlamydomonas Cells. Mol Plant **10**: 216–218

Chen H, Hu J, Qiao Y, Chen W, Rong J, Zhang Y, He C, Wang Q (2015) Ca(2+)-regulated cyclic electron flow supplies ATP for nitrogen starvation-induced lipid biosynthesis in green alga. Sci Rep **5**: 15117

Chow WS (2003) Photosynthesis: From Natural Towards Artificial. Journal of Biological Physics **29**: 447–459

Costa JAV, Linde GA, Atala DIP, Mibielli GM, Krüger RT (2000) Modelling of growth conditions for cyanobacterium Spirulina platensis in microcosms. World Journal of Microbiology and Biotechnology **16**: 15–18

Cousins AB, Pracharoenwattana I, Zhou W, Smith SM, Badger MR (2008) Peroxisomal Malate Dehydrogenase Is Not Essential for Photorespiration in Arabidopsis But Its Absence Causes an Increase in the Stoichiometry of Photorespiratory CO2 Release. Plant Physiol **148**: 786–795

Cramer WA, Hasan SS, Yamashita E (2011) The Q Cycle of Cytochrome bc Complexes: a Structure Perspective. Biochim Biophys Acta **1807**: 788–802

Crespo JL, Pérez-Pérez ME (2023) Monitoring Autophagic Flux in the Model Single-Celled Microalga Chlamydomonas reinhardtii. *In* LM Lois, M Trujillo, eds, Plant Proteostasis: Methods and Protocols. Springer US, New York, NY, pp 123–134

Criscuolo A, Gribaldo S (2010) BMGE (Block Mapping and Gathering with Entropy): a new software for selection of phylogenetic informative regions from multiple sequence alignments. BMC Evol Biol **10**: 210

Cross FR, Umen JG (2015) The Chlamydomonas cell cycle. The Plant Journal **82**: 370–392

Crozet P, Navarro FJ, Willmund F, Mehrshahi P, Bakowski K, Lauersen KJ, Pérez-Pérez M-E, Auroy P, Gorchs Rovira A, Sauret-Gueto S, et al (2018) Birth of a Photosynthetic Chassis: A MoClo Toolkit Enabling Synthetic Biology in the Microalga Chlamydomonas reinhardtii. ACS Synth Biol **7**: 2074–2086

DalCorso G, Pesaresi P, Masiero S, Aseeva E, Schünemann D, Finazzi G, Joliot P, Barbato R, Leister D (2008) A complex containing PGRL1 and PGR5 is involved in the switch between linear and cyclic electron flow in Arabidopsis. Cell **132**: 273–285

Dang K-V, Plet J, Tolleter D, Jokel M, Cuiné S, Carrier P, Auroy P, Richaud P, Johnson X, Alric J, et al (2014) Combined Increases in Mitochondrial Cooperation and Oxygen Photoreduction Compensate for Deficiency in Cyclic Electron Flow in Chlamydomonas reinhardtii. The Plant Cell **26**: 3036–3050

Dao O, Kuhnert F, Weber APM, Peltier G, Li-Beisson Y (2022) Physiological functions of malate shuttles in plants and algae. Trends in Plant Science **27**: 488–501

De Souza AP, Burgess SJ, Doran L, Hansen J, Manukyan L, Maryn N, Gotarkar D, Leonelli L, Niyogi KK, Long SP (2022) Soybean photosynthesis and crop yield are improved by accelerating recovery from photoprotection. Science **377**: 851–854

Desplats C, Mus F, Cuiné S, Billon E, Cournac L, Peltier G (2009) Characterization of Nda2, a Plastoquinone-reducing Type II NAD(P)H Dehydrogenase in Chlamydomonas Chloroplasts. J Biol Chem **284**: 4148–4157

Doebbe A, Keck M, Russa ML, Mussgnug JH, Hankamer B, Tekçe E, Niehaus K, Kruse O (2010) The Interplay of Proton, Electron, and Metabolite Supply for Photosynthetic H2 Production in Chlamydomonas reinhardtii. J Biol Chem **285**: 30247–30260

Du E, Terrer C, Pellegrini AFA, Ahlström A, van Lissa CJ, Zhao X, Xia N, Wu X, Jackson RB (2020) Global patterns of terrestrial nitrogen and phosphorus limitation. Nat Geosci **13**: 221–226

Du Z-Y, Benning C (2016) Triacylglycerol Accumulation in Photosynthetic Cells in Plants and Algae. Lipids in Plant and Algae Development 179–205

Du Z-Y, Lucker BF, Zienkiewicz K, Miller TE, Zienkiewicz A, Sears BB, Kramer DM, Benning C (2018) Galactoglycerolipid Lipase PGD1 Is Involved in Thylakoid Membrane Remodeling in Response to Adverse Environmental Conditions in Chlamydomonas. The Plant Cell **30**: 447–465

Durán P, Flores-Uribe J, Wippel K, Zhang P, Guan R, Garrido-Oter R (2021) Characterization of the Chlamydomonas reinhardtii phycosphere reveals conserved features of the plant microbiota. 2021.03.04.433956

Eisenhut M, Planchais S, Cabassa C, Guivarc'h A, Justin A-M, Taconnat L, Renou J-P, Linka M, Gagneul D, Timm S, et al (2013) Arabidopsis A BOUT DE SOUFFLE is a putative mitochondrial transporter involved in photorespiratory metabolism and is required for meristem growth at ambient CO2 levels. The Plant Journal **73**: 836–849

Eisenhut M, Roell M-S, Weber APM (2019) Mechanistic understanding of photorespiration paves the way to a new green revolution. New Phytologist **223**: 1762–1769

Eisenhut M, Ruth W, Haimovich M, Bauwe H, Kaplan A, Hagemann M (2008) The photorespiratory glycolate metabolism is essential for cyanobacteria and might

have been conveyed endosymbiontically to plants. Proc Natl Acad Sci U S A **105**: 17199–17204

Elsässer M, Feitosa-Araujo E, Lichtenauer S, Wagner S, Fuchs P, Giese J, Kotnik F, Hippler M, Meyer AJ, Maurino VG, et al (2020) Photosynthetic activity triggers pH and NAD redox signatures across different plant cell compartments. bioRxiv 2020.10.31.363051

Erickson E, Wakao S, Niyogi KK (2015) Light stress and photoprotection in Chlamydomonas reinhardtii. The Plant Journal **82**: 449–465

Facchinelli F, Colleoni C, Ball SG, Weber APM (2013) Chlamydia, cyanobiont, or host: who was on top in the ménage à trois? Trends in Plant Science **18**: 673–679

Falkowski PG, Katz ME, Knoll AH, Quigg A, Raven JA, Schofield O, Taylor FJR (2004) The Evolution of Modern Eukaryotic Phytoplankton. Science **305**: 354–360

Fan J, Yan C, Andre C, Shanklin J, Schwender J, Xu C (2012) Oil accumulation is controlled by carbon precursor supply for fatty acid synthesis in Chlamydomonas reinhardtii. Plant Cell Physiol **53**: 1380–1390

Fang W, Si Y, Douglass S, Casero D, Merchant SS, Pellegrini M, Ladunga I, Liu P, Spalding MH (2012) Transcriptome-Wide Changes in Chlamydomonas reinhardtii Gene Expression Regulated by Carbon Dioxide and the CO2-Concentrating Mechanism Regulator CIA5/CCM1[W][OA]. Plant Cell **24**: 1876–1893

Fernández FGA, Reis A, Wijffels RH, Barbosa M, Verdelho V, Llamas B (2021) The role of microalgae in the bioeconomy. New Biotechnology **61**: 99–107

Fernie AR, Bauwe H (2020) Wasteful, essential, evolutionary stepping stone? The multiple personalities of the photorespiratory pathway. The Plant Journal **102**: 666–677

Field CB, Behrenfeld MJ, Randerson JT, Falkowski P (1998) Primary Production of the Biosphere: Integrating Terrestrial and Oceanic Components. Science **281**: 237–240

Flowers JM, Hazzouri KM, Pham GM, Rosas U, Bahmani T, Khraiwesh B, Nelson DR, Jijakli K, Abdrabu R, Harris EH, et al (2015) Whole-Genome Resequencing Reveals Extensive Natural Variation in the Model Green Alga Chlamydomonas reinhardtii. The Plant Cell **27**: 2353–2369

Foyer C, Furbank R, Harbinson J, Horton P (1990) The mechanisms contributing to photosynthetic control of electron transport by carbon assimilation in leaves. Photosynth Res **25**: 83–100

Fridlyand LE, Backhausen JE, Scheibe R (1998) Flux Control of the Malate Valve in Leaf Cells. Archives of Biochemistry and Biophysics **349**: 290–298

Fuhrmeister R, Streubel J (2023) Functional Analysis of Plant Monosaccharide Transporters Using a Simple Growth Complementation Assay in Yeast. Bio Protoc **13**: e4733

Fukuzawa H, Miura K, Ishizaki K, Kucho K, Saito T, Kohinata T, Ohyama K (2001) Ccm1, a regulatory gene controlling the induction of a carbon-concentrating mechanism in Chlamydomonas reinhardtii by sensing CO2 availability. PNAS **98**: 5347–5352

Gabaldón T, Pittis AA (2015) Origin and evolution of metabolic sub-cellular compartmentalization in eukaryotes. Biochimie **119**: 262–268

Gallaher SD, Fitz-Gibbon ST, Glaesener AG, Pellegrini M, Merchant SS (2015) Chlamydomonas Genome Resource for Laboratory Strains Reveals a Mosaic of

Sequence Variation, Identifies True Strain Histories, and Enables Strain-Specific Studies. Plant Cell **27**: 2335–2352

Gallaher SD, Fitz-Gibbon ST, Strenkert D, Purvine SO, Pellegrini M, Merchant SS (2017) High-throughput sequencing of the chloroplast and mitochondrion of Chlamydomonas reinhardtii to generate improved de novo assemblies, analyze expression patterns and transcript speciation, and evaluate diversity among laboratory strains and wild isolates. Plant J. doi: 10.1111/tpj.13788

Gargouri M, Bates PD, Park J-J, Kirchhoff H, Gang DR (2017) Functional photosystem I maintains proper energy balance during nitrogen depletion in Chlamydomonas reinhardtii, promoting triacylglycerol accumulation. Biotechnology for Biofuels **10**: 89

Geigenberger P, Fernie AR (2014) Metabolic Control of Redox and Redox Control of Metabolism in Plants. Antioxid Redox Signal **21**: 1389–1421

Geigenberger P, Kolbe A, Tiessen A (2005) Redox regulation of carbon storage and partitioning in response to light and sugars. Journal of Experimental Botany **56**: 1469–1479

Gerotto C, Alboresi A, Meneghesso A, Jokel M, Suorsa M, Aro E-M, Morosinotto T (2016) Flavodiiron proteins act as safety valve for electrons in Physcomitrella patens. PNAS **113**: 12322–12327

Gietl C (1992) Malate dehydrogenase isoenzymes: Cellular locations and role in the flow of metabolites between the cytoplasm and cell organelles. Biochimica et Biophysica Acta (BBA) - Bioenergetics **1100**: 217–234

Godaux D, Emonds-Alt B, Berne N, Ghysels B, Alric J, Remacle C, Cardol P (2013) A novel screening method for hydrogenase-deficient mutants in Chlamydomonas reinhardtii based on in vivo chlorophyll fluorescence and photosystem II quantum yield. International Journal of Hydrogen Energy **38**: 1826–1836

Goodenough U, Blaby I, Casero D, Gallaher SD, Goodson C, Johnson S, Lee J-H, Merchant SS, Pellegrini M, Roth R, et al (2014) The path to triacylglyceride obesity in the sta6 strain of Chlamydomonas reinhardtii. Eukaryot Cell **13**: 591–613

Goodson C, Roth R, Wang ZT, Goodenough U (2011) Structural correlates of cytoplasmic and chloroplast lipid body synthesis in Chlamydomonas reinhardtii and stimulation of lipid body production with acetate boost. Eukaryot Cell **10**: 1592–1606

Hagemann M, Kern R, Maurino VG, Hanson DT, Weber APM, Sage RF, Bauwe H (2016) Evolution of photorespiration from cyanobacteria to land plants, considering protein phylogenies and acquisition of carbon concentrating mechanisms. Journal of Experimental Botany **67**: 2963–2976

Hanawa H, Ishizaki K, Nohira K, Takagi D, Shimakawa G, Sejima T, Shaku K, Makino A, Miyake C (2017) Land plants drive photorespiration as higher electron-sink: comparative study of post-illumination transient O2-uptake rates from liverworts to angiosperms through ferns and gymnosperms. Physiologia Plantarum **161**: 138–149

Harris EH (2009) The Chlamydomonas Sourcebook: Introduction to Chlamydomonas and Its Laboratory Use: Volume 1. Academic Press

Hashida S, Kawai-Yamada M (2019) Inter-Organelle NAD Metabolism Underpinning Light Responsive NADP Dynamics in Plants. Front Plant Sci. doi: 10.3389/fpls.2019.00960

Häusler RE, Bailey KJ, Lea PJ, Leegood RC (1996) Control of photosynthesis in barley mutants with reduced activities of glutamine synthetase and glutamate synthase. Planta **200**: 388–396

Hebbelmann I, Selinski J, Wehmeyer C, Goss T, Voss I, Mulo P, Kangasjärvi S, Aro E-M, Oelze M-L, Dietz K-J, et al (2012) Multiple strategies to prevent oxidative stress in Arabidopsis plants lacking the malate valve enzyme NADP-malate dehydrogenase. J Exp Bot **63**: 1445–1459

Hemschemeier A, Happe T (2011) Alternative photosynthetic electron transport pathways during anaerobiosis in the green alga Chlamydomonas reinhardtii. Biochimica et Biophysica Acta (BBA) - Bioenergetics **1807**: 919–926

Hernandez JS, Nägele T (2023) The trade-off function of photorespiration in a changing environment. in silico Plants **5**: diac022

Hertle AP, Blunder T, Wunder T, Pesaresi P, Pribil M, Armbruster U, Leister D (2013) PGRL1 Is the Elusive Ferredoxin-Plastoquinone Reductase in Photosynthetic Cyclic Electron Flow. Molecular Cell **49**: 511–523

Heyno E, Innocenti G, Lemaire SD, Issakidis-Bourguet E, Krieger-Liszkay A (2014) Putative role of the malate valve enzyme NADP–malate dehydrogenase in H2O2 signalling in Arabidopsis. Philosophical Transactions of the Royal Society B: Biological Sciences **369**: 20130228

Hoang DT, Chernomor O, von Haeseler A, Minh BQ, Vinh LS (2018) UFBoot2: Improving the Ultrafast Bootstrap Approximation. Molecular Biology and Evolution **35**: 518–522

Houille-Vernes L, Rappaport F, Wollman F-A, Alric J, Johnson X (2011) Plastid terminal oxidase 2 (PTOX2) is the major oxidase involved in chlororespiration in Chlamydomonas. Proc Natl Acad Sci USA **108**: 20820–20825

Hu Q, Sommerfeld M, Jarvis E, Ghirardi M, Posewitz M, Seibert M, Darzins A (2008) Microalgal triacylglycerols as feedstocks for biofuel production: perspectives and advances. Plant J **54**: 621–639

Huang W, Krishnan A, Plett A, Meagher M, Linka N, Wang Y, Ren B, Findinier J, Redekop P, Fakhimi N, et al (2023) Chlamydomonas mutants lacking chloroplast TRIOSE PHOSPHATE TRANSPORTER3 are metabolically compromised and light sensitive. Plant Cell **35**: 2592–2614

Jackson JB (2012) A review of the binding-change mechanism for proton-translocating transhydrogenase. Biochimica et Biophysica Acta (BBA) - Bioenergetics **1817**: 1839–1846

Jackson JB, Peake SJ, White SA (1999) Structure and mechanism of proton-translocating transhydrogenase. FEBS Letters **464**: 1–8

Johnson JE, Berry JA (2021) The role of Cytochrome b6f in the control of steady-state photosynthesis: a conceptual and quantitative model. Photosynth Res **148**: 101–136

Johnson X, Alric J (2013) Central Carbon Metabolism and Electron Transport in Chlamydomonas reinhardtii: Metabolic Constraints for Carbon Partitioning between Oil and Starch. Eukaryot Cell **12**: 776–793

Johnson X, Alric J (2012) Interaction between Starch Breakdown, Acetate Assimilation, and Photosynthetic Cyclic Electron Flow in Chlamydomonas reinhardtii. J Biol Chem **287**: 26445–26452

Johnson X, Steinbeck J, Dent RM, Takahashi H, Richaud P, Ozawa S-I, Houille-Vernes L, Petroutsos D, Rappaport F, Grossman AR, et al (2014) Proton Gradient Regulation 5-Mediated Cyclic Electron Flow under ATP- or Redox-

Limited Conditions: A Study of ΔATPase pgr5 and ΔrbcL pgr5 Mutants in the Green Alga Chlamydomonas reinhardtii1[C][W]. Plant Physiol **165**: 438–452

Jokel M, Johnson X, Peltier G, Aro E-M, Allahverdiyeva Y (2018) Hunting the main player enabling Chlamydomonas reinhardtii growth under fluctuating light. The Plant Journal **94**: 822–835

Jokel M, Kosourov S, Battchikova N, Tsygankov AA, Aro EM, Allahverdiyeva Y (2015) Chlamydomonas Flavodiiron Proteins Facilitate Acclimation to Anoxia During Sulfur Deprivation. Plant and Cell Physiology **56**: 1598–1607

Jørgensen ME, Crocoll C, Halkier BA, Nour-Eldin HH (2017) Uptake Assays in Xenopus laevis Oocytes Using Liquid Chromatography-mass Spectrometry to Detect Transport Activity. Bio Protoc **7**: e2581

Juergens MT, Deshpande RR, Lucker BF, Park J-J, Wang H, Gargouri M, Holguin FO, Disbrow B, Schaub T, Skepper JN, et al (2015) The Regulation of Photosynthetic Structure and Function during Nitrogen Deprivation in Chlamydomonas reinhardtii. Plant Physiology **167**: 558–573

Jüppner J, Mubeen U, Leisse A, Caldana C, Brust H, Steup M, Herrmann M, Steinhauser D, Giavalisco P (2017) Dynamics of lipids and metabolites during the cell cycle of Chlamydomonas reinhardtii. The Plant Journal **92**: 331–343

Kalyaanamoorthy S, Minh BQ, Wong TKF, von Haeseler A, Jermiin LS (2017) ModelFinder: fast model selection for accurate phylogenetic estimates. Nat Methods **14**: 587–589

Kämäräinen J, Huokko T, Kreula S, Jones PR, Aro E-M, Kallio P (2017) Pyridine nucleotide transhydrogenase PntAB is essential for optimal growth and photosynthetic integrity under low-light mixotrophic conditions in Synechocystis sp. PCC 6803. New Phytologist **214**: 194–204

Karkar S, Facchinelli F, Price DC, Weber APM, Bhattacharya D (2015) Metabolic connectivity as a driver of host and endosymbiont integration. Proceedings of the National Academy of Sciences **112**: 10208–10215

Karpowicz SJ, Prochnik SE, Grossman AR, Merchant SS (2011) The GreenCut2 Resource, a Phylogenomically Derived Inventory of Proteins Specific to the Plant Lineage. J Biol Chem **286**: 21427–21439

Katoh K, Standley DM (2013) MAFFT multiple sequence alignment software version 7: improvements in performance and usability. Mol Biol Evol **30**: 772–780

Kauny J, Sétif P (2014) NADPH fluorescence in the cyanobacterium Synechocystis sp. PCC 6803: A versatile probe for in vivo measurements of rates, yields and pools. Biochimica et Biophysica Acta (BBA) - Bioenergetics **1837**: 792–801

Kaye Y, Huang W, Clowez S, Saroussi S, Idoine A, Sanz-Luque E, Grossman AR (2019) The mitochondrial alternative oxidase from Chlamydomonas reinhardtii enables survival in high light. J Biol Chem **294**: 1380–1395

Kern R, Facchinelli F, Delwiche C, Weber APM, Bauwe H, Hagemann M (2020) Evolution of Photorespiratory Glycolate Oxidase among Archaeplastida. Plants (Basel) **9**: 106

Kinoshita H, Nagasaki J, Yoshikawa N, Yamamoto A, Takito S, Kawasaki M, Sugiyama T, Miyake H, Weber APM, Taniguchi M (2011) The chloroplastic 2-oxoglutarate/malate transporter has dual function as the malate valve and in carbon/nitrogen metabolism. The Plant Journal **65**: 15–26

Klughammer C, Schreiber U (1994) An improved method, using saturating light pulses, for the determination of photosystem I quantum yield via P700+-absorbance changes at 830 nm. Planta **192**: 261–268

Kong F, Burlacot A, Liang Y, Légeret B, Alseekh S, Brotman Y, Fernie AR, Krieger-Liszkay A, Beisson F, Peltier G, et al (2018) Interorganelle Communication: Peroxisomal MALATE DEHYDROGENASE2 Connects Lipid Catabolism to Photosynthesis through Redox Coupling in Chlamydomonas. The Plant Cell **30**: 1824–1847

Kong F, Liang Y, Légeret B, Beyly-Adriano A, Blangy S, Haslam RP, Napier JA, Beisson F, Peltier G, Li-Beisson Y (2017) Chlamydomonas carries out fatty acid β-oxidation in ancestral peroxisomes using a bona fide acyl-CoA oxidase. The Plant Journal **90**: 358–371

Kong F, Yamaoka Y, Ohama T, Lee Y, Li-Beisson Y (2019) Molecular Genetic Tools and Emerging Synthetic Biology Strategies to Increase Cellular Oil Content in Chlamydomonas reinhardtii. Plant Cell Physiol **60**: 1184–1196

Kramer DM, Evans JR (2011) The Importance of Energy Balance in Improving Photosynthetic Productivity. Plant Physiology **155**: 70–78

Krishnan A, Kumaraswamy GK, Vinyard DJ, Gu H, Ananyev G, Posewitz MC, Dismukes GC (2015) Metabolic and photosynthetic consequences of blocking starch biosynthesis in the green alga Chlamydomonas reinhardtii sta6 mutant. The Plant Journal **81**: 947–960

Krömer S, Scheibe R (1996) Function of the chloroplastic malate valve for respiration during photosynthesis. Biochemical Society Transactions **24**: 761–766

Labun K, Montague TG, Krause M, Torres Cleuren YN, Tjeldnes H, Valen E (2019) CHOPCHOP v3: expanding the CRISPR web toolbox beyond genome editing. Nucleic Acids Res **47**: W171–W174

Lamb JJ, Røkke G, Hohmann-Marriott MF (2018) Chlorophyll fluorescence emission spectroscopy of oxygenic organisms at 77 K. Photosynthetica **56**: 105–124

Lauersen KJ, Willamme R, Coosemans N, Joris M, Kruse O, Remacle C (2016) Peroxisomal microbodies are at the crossroads of acetate assimilation in the green microalga Chlamydomonas reinhardtii. Algal Research **16**: 266–274

Launay H, Avilan L, Gérard C, Parsiegla G, Receveur-Brechot V, Gontero B, Carriere F (2023) Location of the photosynthetic carbon metabolism in microcompartments and separated phases in microalgal cells. FEBS Lett. doi: 10.1002/1873-3468.14754

LeBauer DS, Treseder KK (2008) Nitrogen limitation of net primary productivity in terrestrial ecosystems is globally distributed. Ecology **89**: 371–379

Leboulanger C, Descolas-Gros C, Jupin H (1994) HPLC determination of glycolic acid in seawater. An estimation of phytoplankton photorespiration in the Gulf of Lions, western Mediterranean Sea. Journal of Plankton Research **16**: 897–903

Leboulanger C, Martin-Jézéquel V, Descolas-Gros C, Sciandra A, Jupin HJ (1998) Photorespiration in Continuous Culture of Dunaliella Tertiolecta (chlorophyta): Relationships Between Serine, Glycine, and Extracellular Glycolate. Journal of Phycology **34**: 651–654

Leboulanger C, Oriol L, Jupin H, Desolas-gros C (1997) Diel variability of glycolate in the eastern tropical Atlantic Ocean. Deep Sea Research Part I: Oceanographic Research Papers **44**: 2131–2139

Lee CP, Millar AH (2016) The Plant Mitochondrial Transportome: Balancing Metabolic Demands with Energetic Constraints. Trends in Plant Science **21**: 662–676

Lee J, Yamaoka Y, Kong F, Cagnon C, Beyly-Adriano A, Jang S, Gao P, Kang B-H, Li-Beisson Y, Lee Y (2020) The phosphatidylethanolamine-binding protein DTH1 mediates degradation of lipid droplets in *Chlamydomonas reinhardtii*. Proc Natl Acad Sci USA **117**: 23131–23139

Lee RA, Lavoie J-M (2013) From first- to third-generation biofuels: Challenges of producing a commodity from a biomass of increasing complexity. Anim Fron **3**: 6–11

Légeret B, Schulz-Raffelt M, Nguyen HM, Auroy P, Beisson F, Peltier G, Blanc G, Li-Beisson Y (2016) Lipidomic and transcriptomic analyses of Chlamydomonas reinhardtii under heat stress unveil a direct route for the conversion of membrane lipids into storage lipids. Plant, Cell & Environment **39**: 834–847

Lemaire C, Wollman FA, Bennoun P (1988) Restoration of phototrophic growth in a mutant of Chlamydomonas reinhardtii in which the chloroplast atpB gene of the ATP synthase has a deletion: an example of mitochondria-dependent photosynthesis. Proc Natl Acad Sci USA **85**: 1344–1348

Lemaire SD, Quesada A, Merchan F, Corral JM, Igeno MI, Keryer E, Issakidis-Bourguet E, Hirasawa M, Knaff DB, Miginiac-Maslow M (2005) NADP-Malate Dehydrogenase from Unicellular Green Alga Chlamydomonas reinhardtii. A First Step toward Redox Regulation? Plant Physiology **137**: 514–521

Lepori-Bui M, Paight C, Eberhard E, Mertz CM, Moeller HV (2022) Evidence for evolutionary adaptation of mixotrophic nanoflagellates to warmer temperatures. Glob Chang Biol **28**: 7094–7107

Li J, Han D, Wang D, Ning K, Jia J, Wei L, Jing X, Huang S, Chen J, Li Y, et al (2014) Choreography of Transcriptomes and Lipidomes of Nannochloropsis Reveals the Mechanisms of Oil Synthesis in Microalgae. The Plant Cell **26**: 1645–1665

Li X, Moellering ER, Liu B, Johnny C, Fedewa M, Sears BB, Kuo M-H, Benning C (2012) A Galactoglycerolipid Lipase Is Required for Triacylglycerol Accumulation and Survival Following Nitrogen Deprivation in Chlamydomonas reinhardtii. The Plant Cell **24**: 4670–4686

Li X, Zhang R, Patena W, Gang SS, Blum SR, Ivanova N, Yue R, Robertson JM, Lefebvre PA, Fitz-Gibbon ST, et al (2016) An Indexed, Mapped Mutant Library Enables Reverse Genetics Studies of Biological Processes in Chlamydomonas reinhardtii. Plant Cell **28**: 367–387

Li Y, Han D, Hu G, Sommerfeld M, Hu Q (2010) Inhibition of starch synthesis results in overproduction of lipids in Chlamydomonas reinhardtii. Biotechnology and Bioengineering **107**: 258–268

Li-Beisson Y, Beisson F, Riekhof W (2015) Metabolism of acyl-lipids in Chlamydomonas reinhardtii. The Plant Journal **82**: 504–522

Li-Beisson Y, Thelen JJ, Fedosejevs E, Harwood JL (2019) The lipid biochemistry of eukaryotic algae. Progress in Lipid Research **74**: 31–68

Lim S-L, Voon CP, Guan X, Yang Y, Gardeström P, Lim BL (2020) In planta study of photosynthesis and photorespiration using NADPH and NADH/NAD + fluorescent protein sensors. Nature Communications **11**: 3238

Lindén P, Keech O, Stenlund H, Gardeström P, Moritz T (2016) Reduced mitochondrial malate dehydrogenase activity has a strong effect on photorespiratory metabolism as revealed by 13C labelling. Journal of Experimental Botany **67**: 3123–3135

Lisec J, Schauer N, Kopka J, Willmitzer L, Fernie AR (2006) Gas chromatography mass spectrometry–based metabolite profiling in plants. Nature Protocols **1**: 387–396

Lucker B, Kramer DM (2013) Regulation of cyclic electron flow in Chlamydomonas reinhardtii under fluctuating carbon availability. Photosyn Res **117**: 449–459

Mackinder LCM, Chen C, Leib RD, Patena W, Blum SR, Rodman M, Ramundo S, Adams CM, Jonikas MC (2017) A Spatial Interactome Reveals the Protein Organization of the Algal CO2-Concentrating Mechanism. Cell **171**: 133-147.e14

Malone LA, Proctor MS, Hitchcock A, Hunter CN, Johnson MP (2021) Cytochrome b6f – Orchestrator of photosynthetic electron transfer. Biochimica et Biophysica Acta (BBA) - Bioenergetics **1862**: 148380

Mamedov TG, Suzuki K, Miura K, Kucho K, Fukuzawa H (2001) Characteristics and Sequence of Phosphoglycolate Phosphatase from a Eukaryotic Green Alga Chlamydomonas reinhardtii *. Journal of Biological Chemistry **276**: 45573–45579

Mansour JS, Anestis K (2021) Eco-Evolutionary Perspectives on Mixoplankton. Frontiers in Marine Science 8:

Marcus Y, Harel E, Kaplan A (1983) Adaptation of the Cyanobacterium Anabaena variabilis to Low CO2 Concentration in Their Environment. Plant Physiol **71**: 208–210

Marek LF, Spalding MH (1991) Changes in Photorespiratory Enzyme Activity in Response to Limiting CO2 in Chlamydomonas reinhardtii. Plant Physiology **97**: 420–425

Marella TK, Bhattacharjya R, Tiwari A (2021) Impact of organic carbon acquisition on growth and functional biomolecule production in diatoms. Microb Cell Fact **20**: 135

Maxwell K, Johnson GN (2000) Chlorophyll fluorescence—a practical guide. J Exp Bot **51**: 659–668

Mehler AH (1951) Studies on reactions of illuminated chloroplasts: I. Mechanism of the reduction of oxygen and other hill reagents. Archives of Biochemistry and Biophysics **33**: 65–77

Melis A (2009) Solar energy conversion efficiencies in photosynthesis: Minimizing the chlorophyll antennae to maximize efficiency. Plant Science **177**: 272–280

Merchant SS, Prochnik SE, Vallon O, Harris EH, Karpowicz SJ, Witman GB, Terry A, Salamov A, Fritz-Laylin LK, Maréchal-Drouard L, et al (2007) The Chlamydomonas genome reveals the evolution of key animal and plant functions. Science **318**: 245–250

Mettler IJ, Beevers H (1980) Oxidation of NADH in Glyoxysomes by a Malate-Aspartate Shuttle. Plant Physiology **66**: 555–560

Michelet L, Zaffagnini M, Morisse S, Sparla F, Pérez-Pérez ME, Francia F, Danon A, Marchand CH, Fermani S, Trost P, et al (2013) Redox regulation of the Calvin–Benson cycle: something old, something new. Front Plant Sci. doi: 10.3389/fpls.2013.00470

Miller R, Wu G, Deshpande RR, Vieler A, Gärtner K, Li X, Moellering ER, Zäuner S, Cornish AJ, Liu B, et al (2010) Changes in Transcript Abundance in Chlamydomonas reinhardtii following Nitrogen Deprivation Predict Diversion of Metabolism1[W][OA]. Plant Physiol **154**: 1737–1752

Minh BQ, Schmidt HA, Chernomor O, Schrempf D, Woodhams MD, von Haeseler A, Lanfear R (2020) IQ-TREE 2: New Models and Efficient Methods for Phylogenetic Inference in the Genomic Era. Molecular Biology and Evolution **37**: 1530–1534

Miura K, Yamano T, Yoshioka S, Kohinata T, Inoue Y, Taniguchi F, Asamizu E, Nakamura Y, Tabata S, Yamato KT, et al (2004) Expression Profiling-Based Identification of CO2-Responsive Genes Regulated by CCM1 Controlling a

Carbon-Concentrating Mechanism in Chlamydomonas reinhardtii. Plant Physiol **135**: 1595–1607

Moroney JV, Husic HD, Tolbert NE, Kitayama M, Manuel LJ, Togasaki RK (1989) Isolation and Characterization of a Mutant of Chlamydomonas reinhardtii Deficient in the CO(2) Concentrating Mechanism. Plant Physiol **89**: 897–903

Moroney JV, Wilson BJ, Tolbert NE (1986) Glycolate Metabolism and Excretion by Chlamydomonas reinhardtii 1. Plant Physiology **82**: 821–826

Mukherjee A, Lau CS, Walker CE, Rai AK, Prejean CI, Yates G, Emrich-Mills T, Lemoine SG, Vinyard DJ, Mackinder LCM, et al (2019) Thylakoid localized bestrophin-like proteins are essential for the CO_2 concentrating mechanism of *Chlamydomonas reinhardtii*. Proc Natl Acad Sci USA **116**: 16915–16920

Munekage Y, Hojo M, Meurer J, Endo T, Tasaka M, Shikanai T (2002) PGR5 Is Involved in Cyclic Electron Flow around Photosystem I and Is Essential for Photoprotection in Arabidopsis. Cell **110**: 361–371

Munekage Y, Takeda S, Endo T, Jahns P, Hashimoto T, Shikanai T (2001) Cytochrome b6f mutation specifically affects thermal dissipation of absorbed light energy in Arabidopsis. The Plant Journal **28**: 351–359

Nakamura Y, Kanakagiri S, Van K, He W, Spalding MH (2005) Disruption of the glycolate dehydrogenase gene in the high-CO2-requiring mutant HCR89 of Chlamydomonas reinhardtii. Can J Bot **83**: 820–833

Nakamura Y, Tetali S, Van K, He W, Spalding M (2011) Disruption of the glycolate dehydrogenase gene in the high-CO2-requiring mutant HCR89 of Chlamydomonas reinhardtii. Canadian Journal of Botany **83**: 820–833

Neto MCL, Carvalho FEL, Souza GM, Silveira JAG (2021) Understanding photosynthesis in a spatial–temporal multiscale: The need for a systemic view. Theor Exp Plant Physiol **33**: 113–124

Neuhaus HE, Wagner R (2000) Solute pores, ion channels, and metabolite transporters in the outer and inner envelope membranes of higher plant plastids. Biochimica et Biophysica Acta (BBA) - Biomembranes **1465**: 307–323

Nguyen HM, Cuiné S, Beyly-Adriano A, Légeret B, Billon E, Auroy P, Beisson F, Peltier G, Li-Beisson Y (2013) The Green Microalga Chlamydomonas reinhardtii Has a Single ω-3 Fatty Acid Desaturase That Localizes to the Chloroplast and Impacts Both Plastidic and Extraplastidic Membrane Lipids. Plant Physiology **163**: 914–928

Noguchi K, Yoshida K (2008) Interaction between photosynthesis and respiration in illuminated leaves. Mitochondrion **8**: 87–99

Ourbak T, Tubiana L (2017) Changing the game: the Paris Agreement and the role of scientific communities. Climate Policy **17**: 819–824

Park J-J, Wang H, Gargouri M, Deshpande RR, Skepper JN, Holguin FO, Juergens MT, Shachar-Hill Y, Hicks LM, Gang DR (2015) The response of Chlamydomonas reinhardtii to nitrogen deprivation: a systems biology analysis. The Plant Journal **81**: 611–624

Paul JS, Sullivan CW, Volcani BE (1975) Photorespiration in diatoms: Mitochondrial glycolate dehydrogenase in Cylindrotheca fusiformis and Nitzschia alba. Archives of Biochemistry and Biophysics **169**: 152–159

Paul JS, Volcani BE (1976) Photorespiration in diatoms. Arch Microbiol **110**: 247–252

Peers G, Truong TB, Ostendorf E, Busch A, Elrad D, Grossman AR, Hippler M, Niyogi KK (2009) An ancient light-harvesting protein is critical for the regulation of algal photosynthesis. Nature **462**: 518–521

Peltier G, Aro E-M, Shikanai T (2016) NDH-1 and NDH-2 Plastoquinone Reductases in Oxygenic Photosynthesis. Annu Rev Plant Biol **67**: 55–80

Peltier G, Cournac L (2002) Chlororespiration. Annu Rev Plant Biol **53**: 523–550

Peltier G, Schmidt GW (1991) Chlororespiration: an adaptation to nitrogen deficiency in Chlamydomonas reinhardtii. Proceedings of the National Academy of Sciences **88**: 4791–4795

Peltier G, Stoffel C, Findinier J, Madireddi SK, Dao O, Epting V, Grossman A, Li-Beisson Y, Burlacot A (2023) Algal CO2 capture is powered by alternative electron pathways of photosynthesis. 2023.08.08.552514

Peltier G, Thibault P (1985a) O2 Uptake in the Light in Chlamydomonas. Plant Physiol **79**: 225–230

Peltier G, Thibault P (1985b) Light-Dependent Oxygen Uptake, Glycolate, and Ammonia Release in l-Methionine Sulfoximine-Treated Chlamydomonas. Plant Physiol **77**: 281–284

Penzler J-F, Marino G, Reiter B, Kleine T, Naranjo B, Leister D (2022) Commonalities and specialties in photosynthetic functions of PROTON GRADIENT REGULATION5 variants in Arabidopsis. Plant Physiol **190**: 1866–1882

Penzler J-F, Naranjo B, Walz S, Marino G, Kleine T, Leister D (2023) A pgr5 suppressor screen uncovers a distinct mechanism safeguarding the cytochrome b 6 f complex from damage through PGR5. doi: 10.1101/2023.11.28.569138

Petroutsos D, Terauchi AM, Busch A, Hirschmann I, Merchant SS, Finazzi G, Hippler M (2009) PGRL1 Participates in Iron-induced Remodeling of the Photosynthetic Apparatus and in Energy Metabolism in Chlamydomonas reinhardtii*. Journal of Biological Chemistry **284**: 32770–32781

Picariello T, Hou Y, Kubo T, McNeill NA, Yanagisawa H, Oda T, Witman GB (2020) TIM, a targeted insertional mutagenesis method utilizing CRISPR/Cas9 in Chlamydomonas reinhardtii. PLOS ONE **15**: e0232594

Plancke C, Vigeolas H, Höhner R, Roberty S, Emonds-Alt B, Larosa V, Willamme R, Duby F, Dhali DO, Thonart P, et al (2014) Lack of isocitrate lyase in Chlamydomonas leads to changes in carbon metabolism and in the response to oxidative stress under mixotrophic growth. The Plant Journal **77**: 404–417

Polle JEW, Benemann JR, Tanaka A, Melis A (2000) Photosynthetic apparatus organization and function in the wild type and a chlorophyll b-less mutant of Chlamydomonas reinhardtii. Dependence on carbon source. Planta **211**: 335–344

Pollock SV, Prout DL, Godfrey AC, Lemaire SD, Moroney JV (2004) The Chlamydomonas reinhardtii proteins Ccp1 and Ccp2 are required for long-term growth, but are not necessary for efficient photosynthesis, in a low-CO2 environment. Plant Mol Biol **56**: 125–132

Porcelli V, Vozza A, Calcagnile V, Gorgoglione R, Arrigoni R, Fontanesi F, Marobbio CMT, Castegna A, Palmieri F, Palmieri L (2018) Molecular identification and functional characterization of a novel glutamate transporter in yeast and plant mitochondria. Biochimica et Biophysica Acta (BBA) - Bioenergetics **1859**: 1249–1258

Pracharoenwattana I, Cornah JE, Smith SM (2007) Arabidopsis peroxisomal malate dehydrogenase functions in β-oxidation but not in the glyoxylate cycle. The Plant Journal **50**: 381–390

Pröschold T, Harris EH, Coleman AW (2005) Portrait of a Species. Genetics **170**: 1601–1610

Puzanskiy RK, Romanyuk DA, Kirpichnikova AA, Shishova MF (2023) Effects of Trophic Acclimation on Growth and Expression Profiles of Genes Encoding Enzymes of Primary Metabolism and Plastid Transporters of Chlamydomonas reinhardtii. Life (Basel) **13**: 1398

Puzanskiy RK, Romanyuk DA, Shishova MF (2020) Shift in Expression of the Genes of Primary Metabolism and Chloroplast Transporters in Chlamydomonas reinhardtii under Different Trophic Conditions. Russ J Plant Physiol **67**: 867–878

Raghavendra AS, Padmasree K (2003) Beneficial interactions of mitochondrial metabolism with photosynthetic carbon assimilation. Trends Plant Sci **8**: 546–553

Ral J-P, Colleoni C, Wattebled F, Dauvillée D, Nempont C, Deschamps P, Li Z, Morell MK, Chibbar R, Purton S, et al (2006) Circadian Clock Regulation of Starch Metabolism Establishes GBSSI as a Major Contributor to Amylopectin Synthesis in Chlamydomonas reinhardtii. Plant Physiology **142**: 305–317

Reinhold T, Alawady A, Grimm B, Beran KC, Jahns P, Conrath U, Bauer J, Reiser J, Melzer M, Jeblick W, et al (2007) Limitation of nocturnal import of ATP into Arabidopsis chloroplasts leads to photooxidative damage†. The Plant Journal **50**: 293–304

Reiser J, Linka N, Lemke L, Jeblick W, Neuhaus HE (2004) Molecular Physiological Analysis of the Two Plastidic ATP/ADP Transporters from Arabidopsis. Plant Physiology **136**: 3524–3536

Reisoglu Ş, Aydin S, Reisoglu Ş, Aydin S (2023) Microalgae as a promising candidate for fighting climate change and biodiversity loss. doi: 10.5772/intechopen.1002414

Renberg L, Johansson AI, Shutova T, Stenlund H, Aksmann A, Raven JA, Gardeström P, Moritz T, Samuelsson G (2010) A metabolomic approach to study major metabolite changes during acclimation to limiting CO2 in Chlamydomonas reinhardtii. Plant Physiol **154**: 187–196

Renné P, Dreßen U, Hebbeker U, Hille D, Flügge U-I, Westhoff P, Weber APM (2003) The Arabidopsis mutant dct is deficient in the plastidic glutamate/malate translocator DiT2. The Plant Journal **35**: 316–331

Riebesell U, Wolf-Gladrow DA, Smetacek V (1993) Carbon dioxide limitation of marine phytoplankton growth rates. Nature **361**: 249–251

Roach T, Sedoud A, Krieger-Liszkay A (2013) Acetate in mixotrophic growth medium affects photosystem II in Chlamydomonas reinhardtii and protects against photoinhibition. Biochimica et Biophysica Acta (BBA) - Bioenergetics **1827**: 1183–1190

Rochaix JD (1995) Chlamydomonas reinhardtii as the photosynthetic yeast. Annu Rev Genet **29**: 209–230

van Roermund CWT, Schroers MG, Wiese J, Facchinelli F, Kurz S, Wilkinson S, Charton L, Wanders RJA, Waterham HR, Weber APM, et al (2016) The Peroxisomal NAD Carrier from Arabidopsis Imports NAD in Exchange with AMP1[OPEN]. Plant Physiol **171**: 2127–2139

Rühle T, Dann M, Reiter B, Schünemann D, Naranjo B, Penzler J-F, Kleine T, Leister D (2021) PGRL2 triggers degradation of PGR5 in the absence of PGRL1. Nat Commun **12**: 3941

Sacksteder CA, Kanazawa A, Jacoby ME, Kramer DM (2000) The proton to electron stoichiometry of steady-state photosynthesis in living plants: A proton-pumping Q cycle is continuously engaged. Proc Natl Acad Sci U S A **97**: 14283–14288

Saint-Sorny M, Brzezowski P, Arrivault S, Alric J, Johnson X (2022) Interactions Between Carbon Metabolism and Photosynthetic Electron Transport in a

Chlamydomonas reinhardtii Mutant Without CO2 Fixation by RuBisCO. Frontiers in Plant Science 13:

Salomé PA, Merchant SS (2019) A Series of Fortunate Events: Introducing Chlamydomonas as a Reference Organism. The Plant Cell **31**: 1682–1707

Santhanagopalan I, Wong R, Mathur T, Griffiths H (2021) Orchestral manoeuvres in the light: crosstalk needed for regulation of the Chlamydomonas carbon concentration mechanism. J Exp Bot **72**: 4604–4624

Saroussi S, Karns DAJ, Thomas DC, Bloszies C, Fiehn O, Posewitz MC, Grossman AR (2019) Alternative outlets for sustaining photosynthetic electron transport during dark-to-light transitions. PNAS **116**: 11518–11527

Saroussi S, Redekop P, Karns DAJ, Thomas DC, Wittkopp TM, Posewitz MC, Grossman AR (2023) Restricting electron flow at cytochrome b6f when downstream electron acceptors are severely limited. Plant Physiology kiad185

Saroussi S, Sanz-Luque E, Kim RG, Grossman AR (2017) Nutrient scavenging and energy management: acclimation responses in nitrogen and sulfur deprived Chlamydomonas. Current Opinion in Plant Biology **39**: 114–122

Saroussi SI, Wittkopp TM, Grossman AR (2016) The Type II NADPH Dehydrogenase Facilitates Cyclic Electron Flow, Energy-Dependent Quenching, and Chlororespiratory Metabolism during Acclimation of Chlamydomonas reinhardtii to Nitrogen Deprivation. Plant Physiology **170**: 1975–1988

Sasso S, Stibor H, Mittag M, Grossman AR (2018) From molecular manipulation of domesticated Chlamydomonas reinhardtii to survival in nature. eLife **7**: e39233

Schada von Borzyskowski L, Severi F, Krüger K, Hermann L, Gilardet A, Sippel F, Pommerenke B, Claus P, Cortina NS, Glatter T, et al (2019) Marine Proteobacteria metabolize glycolate via the β-hydroxyaspartate cycle. Nature **575**: 500–504

Scheibe R (2004) Malate valves to balance cellular energy supply. Physiologia Plantarum **120**: 21–26

Scheibe R (2019) Maintaining homeostasis by controlled alternatives for energy distribution in plant cells under changing conditions of supply and demand. Photosynth Res **139**: 81–91

Scheibe R, Backhausen JE, Emmerlich V, Holtgrefe S (2005) Strategies to maintain redox homeostasis during photosynthesis under changing conditions. J Exp Bot **56**: 1481–1489

Scheibe R, Jacquot J-P (1983) NADP regulates the light activation of NADP-dependent malate dehydrogenase. Planta **157**: 548–553

Schlüter U, Weber APM (2020) Regulation and Evolution of C4 Photosynthesis. Annual Review of Plant Biology **71**: 183–215

Schmollinger S, Mühlhaus T, Boyle NR, Blaby IK, Casero D, Mettler T, Moseley JL, Kropat J, Sommer F, Strenkert D, et al (2014) Nitrogen-Sparing Mechanisms in Chlamydomonas Affect the Transcriptome, the Proteome, and Photosynthetic Metabolism. The Plant Cell **26**: 1410–1435

Schneidereit J, Häusler RE, Fiene G, Kaiser WM, Weber APM (2006) Antisense repression reveals a crucial role of the plastidic 2-oxoglutarate/malate translocator DiT1 at the interface between carbon and nitrogen metabolism. The Plant Journal **45**: 206–224

Schnitzler Parker M, Armbrust EV, Piovia-Scott J, Keil RG (2004) Induction of Photorespiration by Light in the Centric Diatom Thalassiosira Weissflogii (bacillariophyceae): Molecular Characterization and Physiological Consequences1. Journal of Phycology **40**: 557–567

Schroda M (2019) Good News for Nuclear Transgene Expression in Chlamydomonas. Cells **8**: 1534

Schulz-Raffelt M, Chochois V, Auroy P, Cuiné S, Billon E, Dauvillée D, Li-Beisson Y, Peltier G (2016) Hyper-accumulation of starch and oil in a Chlamydomonas mutant affected in a plant-specific DYRK kinase. Biotechnology for Biofuels **9**: 55

Segura Broncano L, Pukacz KR, Reichel-Deland V, Schlüter U, Triesch S, Weber APM (2023) Photorespiration is the solution, not the problem. Journal of Plant Physiology **282**: 153928

Selinski J, Scheibe R (2019) Malate valves: old shuttles with new perspectives. Plant Biol (Stuttg) **21**: 21–30

Selinski J, Scheibe R (2014) Lack of malate valve capacities lead to improved N-assimilation and growth in transgenic A. thaliana plants. Plant Signaling & Behavior **9**: e29057

Selosse M-A, Charpin M, Not F (2017) Mixotrophy everywhere on land and in water: the grand écart hypothesis. Ecology Letters **20**: 246–263

Sharkey TD (2001) Photorespiration. Encyclopedia of Life Sciences. doi: 10.1038/npg.els.0001292

Shen B-R, Wang L-M, Lin X-L, Yao Z, Xu H-W, Zhu C-H, Teng H-Y, Cui L-L, Liu E-E, Zhang J-J, et al (2019) Engineering a New Chloroplastic Photorespiratory Bypass to Increase Photosynthetic Efficiency and Productivity in Rice. Molecular Plant **12**: 199–214

Shi M, Ge T, Wang Y, Zhao L (2022) Photorespiration is essential for acclimation to salt stress under high carbon availability in Chlamydomonas. Algal Research **64**: 102687

Shi M, Zhao L, Wang Y (2021) Identification and Characterization of Genes Encoding the Hydroxypyruvate Reductases in Chlamydomonas Reveal Their Distinct Roles in Photorespiration. Front Plant Sci **12**: 690296

Shi X, Bloom A (2021) Photorespiration: The Futile Cycle? Plants **10**: 908

Shinkawa H, Kajikawa M, Nomura Y, Ogura M, Sawaragi Y, Yamano T, Nakagami H, Sugiyama N, Ishihama Y, Kanesaki Y, et al (2019) Algal Protein Kinase, Triacylglycerol Accumulation Regulator 1, Modulates Cell Viability and Gametogenesis in Carbon/Nitrogen-Imbalanced Conditions. Plant and Cell Physiology **60**: 916–930

Siaut M, Cuiné S, Cagnon C, Fessler B, Nguyen M, Carrier P, Beyly A, Beisson F, Triantaphylidès C, Li-Beisson Y, et al (2011) Oil accumulation in the model green alga Chlamydomonas reinhardtii: characterization, variability between common laboratory strains and relationship with starch reserves. BMC Biotechnology **11**: 7

Sinclair T, Specht J, Cassman K, Purcell L, Rufty T (2023) Comment on "Soybean photosynthesis and crop yield are improved by accelerating recovery from photoprotection." Science **379**: eade8506

Smetacek V (1999) Diatoms and the Ocean Carbon Cycle. Protist **150**: 25–32

Smith K, Strand DD, Kramer DM, Walker BJ (2023) The role of photorespiration in preventing feedback regulation via ATP synthase in Nicotiana tabacum. Plant, Cell & Environment. doi: 10.1111/pce.14759

Somerville SC, Ogren WL (1983) An Arabidopsis thaliana mutant defective in chloroplast dicarboxylate transport. Proceedings of the National Academy of Sciences **80**: 1290–1294

Spalding H, Ogren L (1982) Photosynthesis is required for induction of the C@-concentrating system in. FEBS LETTERS 145:

Spalding M, Van K, Wang Y, Nakamura Y (2002) Acclimation of Chlamydomonas to changing carbon availability. Functional Plant Biology **29**: 221–230

Spalding MH, Spritzer RJ, Ogren WL (1985) Use of Mutants in Analysis of the CO2-Concentrating Pathway of Chlamydomonas Reinhardtii.

Steinbeck J, Nikolova D, Weingarten R, Johnson X, Richaud P, Peltier G, Hermann M, Magneschi L, Hippler M (2015) Deletion of Proton Gradient Regulation 5 (PGR5) and PGR5-Like 1 (PGRL1) proteins promote sustainable light-driven hydrogen production in Chlamydomonas reinhardtii due to increased PSII activity under sulfur deprivation. Front Plant Sci **6**: 892

Stiehl HH, Witt HT (1969) Quantitative treatment of the function of plastoquinone in phostosynthesis. Z Naturforsch B **24**: 1588–1598

Sun J-Z, Wang T, Huang R, Yi X, Zhang D, Beardall J, Hutchins DA, Liu X, Wang X, Deng Z, et al (2022) Enhancement of diatom growth and phytoplankton productivity with reduced O2 availability is moderated by rising CO2. Commun Biol **5**: 1–12

Suzuki K, Mamedov TG, Ikawa T (1999) A Mutant of Chlamydomonas reinhardtii with Reduced Rate of Photorespiration. Plant and Cell Physiology **40**: 792–799

Suzuki K, Marek LF, Spalding MH (1990) A Photorespiratory Mutant of Chlamydomonas reinhardtii. Plant Physiology **93**: 231–237

Tagawa K, Tsujimoto HY, Arnon DI (1963) ROLE OF CHLOROPLAST FERREDOXIN IN THE ENERGY CONVERSION PROCESS OF PHOTOSYNTHESIS. Proc Natl Acad Sci U S A **49**: 567–572

Takahashi S, Bauwe H, Badger M (2007) Impairment of the Photorespiratory Pathway Accelerates Photoinhibition of Photosystem II by Suppression of Repair But Not Acceleration of Damage Processes in Arabidopsis. Plant Physiology **144**: 487–494

Takeuchi T, Benning C (2019) Nitrogen-dependent coordination of cell cycle, quiescence and TAG accumulation in Chlamydomonas. Biotechnology for Biofuels **12**: 292

Taniguchi M, Taniguchi Y, Kawasaki M, Takeda S, Kato T, Sato S, Tabata S, Miyake H, Sugiyama T (2002) Identifying and Characterizing Plastidic 2-Oxoglutarate/Malate and Dicarboxylate Transporters in Arabidopsis thaliana. Plant Cell Physiol **43**: 706–717

Tardif M, Atteia A, Specht M, Cogne G, Rolland N, Brugière S, Hippler M, Ferro M, Bruley C, Peltier G, et al (2012) PredAlgo: A New Subcellular Localization Prediction Tool Dedicated to Green Algae. Mol Biol Evol **29**: 3625–3639

Taubert A, Jakob T, Wilhelm C (2019) Glycolate from microalgae: an efficient carbon source for biotechnological applications. Plant Biotechnology Journal **17**: 1538–1546

Terashima M, Specht M, Hippler M (2011) The chloroplast proteome: a survey from the Chlamydomonas reinhardtii perspective with a focus on distinctive features. Curr Genet **57**: 151–168

Tiwari A, Kiran T (2018) Biofuels from Microalgae. Advances in Biofuels and Bioenergy. doi: 10.5772/intechopen.73012

Tolleter D, Ghysels B, Alric J, Petroutsos D, Tolstygina I, Krawietz D, Happe T, Auroy P, Adriano J-M, Beyly A, et al (2011) Control of Hydrogen Photoproduction by the Proton Gradient Generated by Cyclic Electron Flow in Chlamydomonas reinhardtii[W]. Plant Cell **23**: 2619–2630

Torres-Romero I, Légeret B, Huleux M, Sorigue D, Damm A, Cuiné S, Veillet F, Blot C, Brugière S, Couté Y, et al (2023) The α/β hydrolase domain-containing protein 1 (ABHD1) acts as a lysolipid lipase and is involved in lipid droplet formation. 2023.12.17.572040

Tran Q-G, Cho K, Park S-B, Kim U, Lee YJ, Kim H-S (2019) Impairment of starch biosynthesis results in elevated oxidative stress and autophagy activity in Chlamydomonas reinhardtii. Sci Rep **9**: 9856

Tyra HM, Linka M, Weber AP, Bhattacharya D (2007) Host origin of plastid solute transporters in the first photosynthetic eukaryotes. Genome Biology **8**: R212

Ullmann J, Grimm D (2021) Algae and their potential for a future bioeconomy, landless food production, and the socio-economic impact of an algae industry. Org Agr **11**: 261–267

Upadhyaya S, Agrawal S, Gorakshakar A, Rao BJ (2020) TOR kinase activity in Chlamydomonas reinhardtii is modulated by cellular metabolic states. FEBS Letters **594**: 3122–3141

Van Aken O, Whelan J (2012) Comparison of transcriptional changes to chloroplast and mitochondrial perturbations reveals common and specific responses in Arabidopsis. Front Plant Sci **3**: 281

Van K, Wang Y, Nakamura Y, Spalding MH (2001) Insertional Mutants of Chlamydomonas reinhardtii That Require Elevated CO2 for Survival. Plant Physiol **127**: 607–614

Villanova V, Singh D, Pagliardini J, Fell D, Le Monnier A, Finazzi G, Poolman M (2021) Boosting Biomass Quantity and Quality by Improved Mixotrophic Culture of the Diatom Phaeodactylum tricornutum. Front Plant Sci **12**: 642199

Villanova V, Spetea C (2021) Mixotrophy in diatoms: Molecular mechanism and industrial potential. Physiologia Plantarum **173**: 603–611

Vitousek PM, Howarth RW (1991) Nitrogen limitation on land and in the sea: How can it occur? Biogeochemistry **13**: 87–115

Wada S, Yamamoto H, Suzuki Y, Yamori W, Shikanai T, Makino A (2018) Flavodiiron Protein Substitutes for Cyclic Electron Flow without Competing CO2 Assimilation in Rice. Plant Physiology **176**: 1509–1518

Wallsgrove RM, Kendall AC, Hall NP, Turner JC, Lea PJ (1986) Carbon and nitrogen metabolism in a barley (Hordeum vulgare L.) mutant with impaired chloroplast dicarboxylate transport. Planta **168**: 324–329

Wang Y, Spalding MH (2014a) LCIB in the Chlamydomonas CO2-concentrating mechanism. Photosynth Res **121**: 185–192

Wang Y, Spalding MH (2014b) Acclimation to Very Low CO2: Contribution of Limiting CO2 Inducible Proteins, LCIB and LCIA, to Inorganic Carbon Uptake in Chlamydomonas reinhardtii. Plant Physiology **166**: 2040–2050

Wang Y, Stessman DJ, Spalding MH (2015) The CO2 concentrating mechanism and photosynthetic carbon assimilation in limiting CO2: how Chlamydomonas works against the gradient. The Plant Journal **82**: 429–448

Weber A, Flügge U (2002) Interaction of cytosolic and plastidic nitrogen metabolism in plants. Journal of Experimental Botany **53**: 865–874

Weber A, Menzlaff E, Arbinger B, Gutensohn M, Eckerskorn C, Fluegge U-I (1995) The 2-oxoglutarate/malate translocator of chloroplast envelope membranes: molecular cloning of a transporter containing a 12-helix motif and expression of the functional protein in yeast cells. Biochemistry **34**: 2621–2627

Weber APM, Linka N (2011) Connecting the Plastid: Transporters of the Plastid Envelope and Their Role in Linking Plastidial with Cytosolic Metabolism. Annu Rev Plant Biol **62**: 53–77

White S, Anandraj A, Trois C (2014) NADPH fluorescence as an indicator of hydrogen production in the green algae Chlamydomonas reinhardtii. International Journal of Hydrogen Energy **39**: 1640–1647

Wu S, Gu W, Huang A, Li Y, Kumar M, Lim PE, Huan L, Gao S, Wang G (2019) Elevated CO2 improves both lipid accumulation and growth rate in the glucose-6-phosphate dehydrogenase engineered Phaeodactylum tricornutum. Microb Cell Fact. doi: 10.1186/s12934-019-1214-x

Wuebbles DJ, Jain AK (2001) Concerns about climate change and the role of fossil fuel use. Fuel Processing Technology **71**: 99–119

Xie X, Huang A, Gu W, Zang Z, Pan G, Gao S, He L, Zhang B, Niu J, Lin A, et al (2016) Photorespiration participates in the assimilation of acetate in Chlorella sorokiniana under high light. New Phytologist **209**: 987–998

Yamamoto H, Shikanai T (2019) PGR5-Dependent Cyclic Electron Flow Protects Photosystem I under Fluctuating Light at Donor and Acceptor Sides. Plant Physiology **179**: 588–600

Yamamoto H, Takahashi S, Badger MR, Shikanai T (2016) Artificial remodelling of alternative electron flow by flavodiiron proteins in Arabidopsis. Nat Plants **2**: 16012

Yamano T, Miura K, Fukuzawa H (2008) Expression Analysis of Genes Associated with the Induction of the Carbon-Concentrating Mechanism in Chlamydomonas reinhardtii. Plant Physiol **147**: 340–354

Yokochi Y, Yoshida K, Hahn F, Miyagi A, Wakabayashi K, Kawai-Yamada M, Weber APM, Hisabori T (2021) Redox regulation of NADP-malate dehydrogenase is vital for land plants under fluctuating light environment. PNAS. doi: 10.1073/pnas.2016903118

Yun EJ, Zhang G-C, Atkinson C, Lane S, Liu J-J, Ort DR, Jin Y-S (2021) Glycolate production by a Chlamydomonas reinhardtii mutant lacking carbon-concentrating mechanism. Journal of Biotechnology **335**: 39–46

Zhang N, Pazouki L, Nguyen H, Jacobshagen S, Bigge BM, Xia M, Mattoon EM, Klebanovych A, Sorkin M, Nusinow DA, et al (2022) Comparative Phenotyping of Two Commonly Used Chlamydomonas reinhardtii Background Strains: CC-1690 (21gr) and CC-5325 (The CLiP Mutant Library Background). Plants (Basel) **11**: 585

Zhang Y-M, Chen H, He C-L, Wang Q (2013) Nitrogen Starvation Induced Oxidative Stress in an Oil-Producing Green Alga Chlorella sorokiniana C3. PLOS ONE **8**: e69225

Zhao Y, Luo L, Xu J, Xin P, Guo H, Wu J, Bai L, Wang G, Chu J, Zuo J, et al (2018) Malate transported from chloroplast to mitochondrion triggers production of ROS and PCD in Arabidopsis thaliana. Cell Research **28**: 448–461

Zhao Y, Yu H, Zhou J-M, Smith SM, Li J (2020) Malate Circulation: Linking Chloroplast Metabolism to Mitochondrial ROS. Trends in Plant Science **25**: 446–454

Zhou Q, Yamamoto H, Shikanai T (2023) Distinct contribution of two cyclic electron transport pathways to P700 oxidation. Plant Physiology **192**: 326–341

Zienkiewicz K, Du Z-Y, Ma W, Vollheyde K, Benning C (2016) Stress-induced neutral lipid biosynthesis in microalgae — Molecular, cellular and physiological insights.

Biochimica et Biophysica Acta (BBA) - Molecular and Cell Biology of Lipids **1861**: 1269–1281

Zones JM, Blaby IK, Merchant SS, Umen JG (2015) High-Resolution Profiling of a Synchronized Diurnal Transcriptome from Chlamydomonas reinhardtii Reveals Continuous Cell and Metabolic Differentiation. Plant Cell **27**: 2743–2769

Zuccaro G, Steyer J-P, Van Lis R (2019) The algal trophic mode affects the interaction and oil production of a synergistic microalga-yeast consortium. Bioresource Technology **273**: 608–617